THE EFFECTS OF FOOD PROCESSING ON FOOD COMPONENTS AND THEIR HEALTH FUNCTIONS, VOLUME II

EDITED BY: Jinkai Zheng and Hang Xiao
PUBLISHED IN: Frontiers in Nutrition

frontiers Research Topics

ISSN 1664-8714
ISBN 978-2-83250-833-6
DOI 10.3389/978-2-83250-833-6

About Frontiers

Frontiers is more than just an open-access publisher of scholarly articles: it is a pioneering approach to the world of academia, radically improving the way scholarly research is managed. The grand vision of Frontiers is a world where all people have an equal opportunity to seek, share and generate knowledge. Frontiers provides immediate and permanent online open access to all its publications, but this alone is not enough to realize our grand goals.

Frontiers Journal Series

The Frontiers Journal Series is a multi-tier and interdisciplinary set of open-access, online journals, promising a paradigm shift from the current review, selection and dissemination processes in academic publishing. All Frontiers journals are driven by researchers for researchers; therefore, they constitute a service to the scholarly community. At the same time, the Frontiers Journal Series operates on a revolutionary invention, the tiered publishing system, initially addressing specific communities of scholars, and gradually climbing up to broader public understanding, thus serving the interests of the lay society, too.

Dedication to Quality

Each Frontiers article is a landmark of the highest quality, thanks to genuinely collaborative interactions between authors and review editors, who include some of the world's best academicians. Research must be certified by peers before entering a stream of knowledge that may eventually reach the public - and shape society; therefore, Frontiers only applies the most rigorous and unbiased reviews.
Frontiers revolutionizes research publishing by freely delivering the most outstanding research, evaluated with no bias from both the academic and social point of view. By applying the most advanced information technologies, Frontiers is catapulting scholarly publishing into a new generation.

What are Frontiers Research Topics?

Frontiers Research Topics are very popular trademarks of the Frontiers Journals Series: they are collections of at least ten articles, all centered on a particular subject. With their unique mix of varied contributions from Original Research to Review Articles, Frontiers Research Topics unify the most influential researchers, the latest key findings and historical advances in a hot research area! Find out more on how to host your own Frontiers Research Topic or contribute to one as an author by contacting the Frontiers Editorial Office: frontiersin.org/about/contact

THE EFFECTS OF FOOD PROCESSING ON FOOD COMPONENTS AND THEIR HEALTH FUNCTIONS, VOLUME II

Topic Editors:
Jinkai Zheng, Institute of Food Science and Technology, Chinese Academy of Agricultural Sciences, China
Hang Xiao, University of Massachusetts Amherst, United States

The authors declare that the research was conducted in the absence of any commercial or financial relationships that could be construed as a potential conflict of interest.

Citation: Zheng, J., Xiao, H., eds. (2022). The Effects of Food Processing on Food Components and Their Health Functions, Volume II.
Lausanne: Frontiers Media SA. doi: 10.3389/978-2-83250-833-6

Table of Contents

frontiers | Frontiers in Nutrition

TYPE Editorial
PUBLISHED 07 November 2022
DOI 10.3389/fnut.2022.1051869

OPEN ACCESS

EDITED AND REVIEWED BY
Fuguo Liu,
Northwest A&F University, China

*CORRESPONDENCE
Jinkai Zheng
zhengjinkai@caas.cn
Hang Xiao
hangxiao@foodsci.umass.edu

SPECIALTY SECTION
This article was submitted to Food Chemistry, a section of the journal Frontiers in Nutrition

RECEIVED 23 September 2022
ACCEPTED 12 October 2022
PUBLISHED 07 November 2022

CITATION
Zheng J and Xiao H (2022) Editorial: The effects of food processing on food components and their health functions, Volume II. *Front. Nutr.* 9:1051869. doi: 10.3389/fnut.2022.1051869

Editorial: The effects of food processing on food components and their health functions, Volume II

Jinkai Zheng[1,2]* and Hang Xiao[3]*

[1]Institute of Food Science and Technology, Chinese Academy of Agricultural Sciences, Beijing, China, [2]College of Food Science and Engineering, Qingdao Agricultural University, Qingdao, China, [3]Department of Food Science, University of Massachusetts, Amherst, MA, United States

KEYWORDS

food, components, processing, properties, health functions

Editorial on the Research Topic
The effects of food processing on food components and their health functions, Volume II

Food processing plays an important role in our food supply and can significantly influence the properties of food components and their impact on health (1, 2). This Research Topic is focused on the effects of food processing on food components, and their physicochemical properties and health functions (Figure 1). The studies demonstrated that various processing methods (e.g., drying, extraction, ultra-high pressure treatment, hydroxylation, backing, and dehydration) significantly influenced the non-volatile and volatile chemical components in foods, which further affected their health-promoting effects. Processing parameters such as temperature, enzymes, pressure, and treatment time are also important and should be considered carefully.

Liu, Meng, et al. investigated the transformation of non-volatile taste components in Stropharia rugosoannulata subjected to hot air drying, vacuum freeze drying, and microwave vacuum drying. The diversity of metabolites in the samples changed little in response to the three drying methods tested, but their relative abundance and metabolic pathways differed significantly. This study also showed that the metabolite differences caused by different drying methods are modulated by temperature (higher temperatures may cause protein degradation), Strecker degradation, and the Maillard reaction. Liu, Mao, et al. also showed that high pressure treatment significantly increased the ordered structure content such as α-helices, inhibited the formation of disulfide bonds, and decreased the surface hydrophobicity of myofibrillar proteins (MP). Moreover, MP had the optimal solubility and *in vitro* digestibility at 200 MPa due to the minimum particle size and turbidity, and relatively dense and uniform microstructure. The ultrahigh pressure treatment effectively improved the digestibility of MP from scallop mantle. Processing facilitated the inter-conversion of components, and components with high value could be obtained by modulating the processing parameters. Li, Shao, et al. studied the effects of amino acids and processing methods on the conversion of ginsenosides

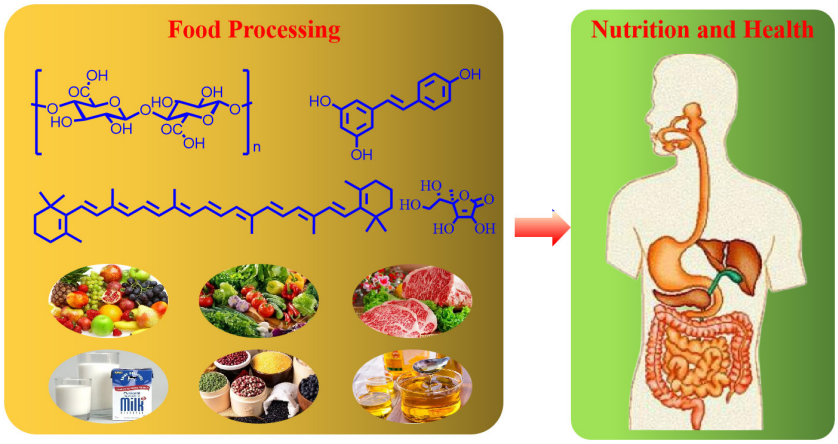

FIGURE 1
Food processing affecting food components and their health functions.

in American ginseng into rare ginsenosides. The results showed that aspartic acid was the best catalyst, and thermal extraction had the best effect. Qiao, et al. obtained a novel angiotensin I-converting enzyme inhibitory peptide by hydrolyzing goat milk casein. Feng, et al. developed two-step vacuum-mediated conversion from fatty acid ethyl esters and fatty acids into a lipid-lowering diacylglycerol-enriched functional oil derived from soy sauce by-product oil. Lipase loading, temperature, substrate molar ratio, and initial vacuum combination significantly affected the reaction efficiency. Wang, Nie, et al. demonstrated that the flavonoid, phenolic acid, γ-GABA, and polysaccharide contents and antioxidant activity during the germination of buckwheat gradually trended upward, and the antioxidant properties of buckwheat sprouts might be related to the phenolic acid and polysaccharide contents, which were improved by plasma-activated water treatment.

In addition to non-volatiles, significant variation in volatiles was detected during processing. Wang, Yu, et al. characterized the transformation and formation of volatile metabolites during green tea processing. They showed that volatile compounds underwent different changes during various procedures, with the greatest transformation occurring during fixation, followed by pan-frying and second drying. During the fixation process, high temperature promoted the degradation of lipids to generate free fatty acids, which led to the formation of volatile alcohols and aldehydes. Glycosides were also degraded into multiple volatiles. Baking significantly affected the chemical composition, sensory quality, and bioactivity of Tie Guan Yin Oolong Tea (Gao, et al.). Baking promoted the formation of colored macromolecules (e.g., theabrownins), which affected the color of the tea infusion. Floral and fresh volatiles were remarkably reduced, while multiple new volatiles were produced, resulting in a typical baked aroma. The antioxidant and antibacterial activities were reduced after baking, which might be associated with the decrease in monomeric catechins. Dehydration increased the food shelf life and affected the composition and physicochemical properties of food. For example, most aldehydes and alcohols were increased when Pugionium is subject to different dehydration procedures, whereas esters were decreased, and the dehydrated Pugionium has a more harmonious, less pungent aroma compared with the fresh Pugionium (Li, Wu, et al.).

In summary, processing significantly affects food properties, especially their chemical compositions, physicochemical properties, and health effects. Targeted modulation of foods could be achieved by regulating processing. Due to their nutritional and health properties, the development and application of functional foods is attracting increasing attention. Since individuals respond differently to the same foods and their bioactive compounds (3), precision nutrition is regarded as a promising strategy for maintaining human health and preventing disease. Precise targets of foods based on the systematic study of the health-promoting effects of various foods and their components is the basis for precision nutrition. Precise manufacture of foods based on the development of novel techniques is a critical part of precision nutrition. Precise detection techniques for real-time dynamic monitoring of *in vivo* biomarkers is also important to the realization of precision nutrition (4). Notably, traditional precision nutrition emphasizes the final function of food. However, foods are a complex mixture of components that interact with each other and influence the health-promoting effects of foods generally. There is complex variation in food chemical compositions during processing, as well as in the human body (3, 5). Therefore, to achieve precise nutrition, the molecular targets of food components need to be identified and the food composition needs to be precisely regulated. Such information would provide critical scientific basis for the design and

manufacture of innovative health-promoting foods, which in turn promote the realization of precision nutrition.

Author contributions

JZ and HX prepared, checked and revised the manuscript, and approved the submitted version.

Acknowledgments

The authors would like to acknowledge the financial support provided by National Natural Science Foundation of China (No. 32072181). We also appreciate the National Elite Youth Program and Leading Scientist Program of Chinese Academy of Agricultural Sciences.

Conflict of interest

The authors declare that the research was conducted in the absence of any commercial or financial relationships that could be construed as a potential conflict of interest.

Publisher's note

References

1. Cui JF, Zhao CY, Feng LP, Han YH, Du HJ, Xiao H, Zheng JK. Pectins from fruits: Relationships between extraction methods, structural characteristics, and functional properties. *Trends Food Sci Tech.* (2021) 110:39–54. doi: 10.1016/j.tifs.2021.01.077

2. Azeredo HMC, Tonon RV, McClements DJ. Designing healthier foods: reducing the content or digestibility of key nutrients. *Trends Food Sci Tech*. (2021) 118:459–70. doi: 10.1016/j.tifs.2021.10.023

3. Karn A, Zhao CY, Yang FL, Cui JF, Gao ZL, Wang MQ, et al. *In-vivo* biotransformation of citrus functional components and their effects on health. *Crit Rev Food Sci.* (2021) 61:756–76. doi: 10.1080/10408398.2020.1746234

4. Lu C, Zhou S, Gao F, Lin J, Liu J, Zheng J. DNA-mediated growth of noble metal nanomaterials for biosensing applications. *Trac-Trend Anal Chem.* (2022) 148:116533. doi: 10.1016/j.trac.2022.116533

5. Ding Y, Ban Q, Wu Y, Sun Y, Zhou Z, Wang Q, et al. Effect of high hydrostatic pressure on the edible quality, health and safety attributes of plant-based foods represented by cereals and legumes: a review. *Crit Rev Food Sci.* (2021). doi: 10.1080/10408398.2021.2005531

frontiers in Nutrition

ORIGINAL RESEARCH
published: 24 February 2022
doi: 10.3389/fnut.2022.849615

The Effects of Plasma-Activated Water Treatment on the Growth of Tartary Buckwheat Sprouts

*Ya Wang, Zihan Nie and Tingjun Ma**

School of Food Science and Engineering, Beijing University of Agriculture, Beijing, China

The aim was to investigate the effects of buckwheat sprout treated with plasma-activated water (PAW) and their quality, nutrients (protein, amino acids, fat, and carbohydrates), functional active ingredients (total flavonoids, total phenolic acids, γ-gamma aminobutyric acid (GABA), and polysaccharides), and antioxidant activity during germination. PAW had no negative effects on the germination rate, but promoted the stem growth instead, which indicated 1.12-fold higher germination rate compared with the control group. The results of sensory evaluation demonstrated that the obtained sprouts were bright green, shinning, crisp and smooth, with sufficient moisture, and easy to chew. During germination (1–9 days), the water content, amino acids, and reducing sugars of sprouts showed an increasing trend and were basically higher in the PAW group than in the control group, while protein, carbohydrate, and crude fat presented a decreasing trend. The results were that the flavonoid, phenolic acid, γ-GABA, polysaccharides content, and antioxidant activity during germination showed a gradual upward trend but with slight differences, and the antioxidant properties of buckwheat sprouts might be related to the phenolic acid and polysaccharides content. These data show that the PAW treatment on buckwheat sprout have great potential as a dietary source of antioxidant function with health benefits.

Keywords: buckwheat, germination, plasma-activated water, nutrients, functional activity, antioxidant activity

OPEN ACCESS

Edited by:
Jinkai Zheng,
Institute of Food Science and Technology (CAAS), China

Reviewed by:
Ivan Kreft,
University of Ljubljana, Slovenia
Moyang Liu,
Shanghai Jiao Tong University, China

****Correspondence:***
Tingjun Ma
mtingjun@163.com

Specialty section:
This article was submitted to Food Chemistry, a section of the journal Frontiers in Nutrition

Received: *06 January 2022*
Accepted: *24 January 2022*
Published: *24 February 2022*

Citation:
Wang Y, Nie Z and Ma T (2022) The Effects of Plasma-Activated Water Treatment on the Growth of Tartary Buckwheat Sprouts. Front. Nutr. 9:849615. doi: 10.3389/fnut.2022.849615

INTRODUCTION

Tartary buckwheat (*Fagopyrum tataricum* (L.) Gaertn.) is a dicotyledonous plant that belongs to the *Polygonaceae* family, which is a traditionally edible and medicinal plant (1). Buckwheat is a nutritionally balanced gluten-free crop that has been in the cultivation for 4,000 years and is now grown globally (2). Buckwheat grains are mainly composed of high-quality starch and dietary fiber, protein, lipids, vitamins, amino acids, etc. (3, 4). It is rich in flavonoids (5), phenols (6), proteins and peptides (7), sugar alcohols, D-Chiral inositol (8), polysaccharides (9), steroids, and other bioactive substances, which has a high antioxidant effect by inhibiting the oxidative stress, beneficial to the prevention and treatment of cardiovascular disease, and reduce triglycerides (10), total cholesterol, so it has a very good healthcare, medicinal value (11). However, there is fagopyrin substance in buckwheat, which is a phototoxic naftodianthrone related to hypericin (12). The phototoxic dose of fagopyrin for humans is still unknown (13), some researchers have estimated the recommended daily intake of buckwheat sprouts to be less than 40 g, based on a comparison to hypericin toxicity (14).

Buckwheat has been made into a series of consumer foods, such as bread (15), noodles (16), and honey (17). In addition, buckwheat sprouts are used as functional vegetables which are healthy and unpolluted (18). Buckwheat germination can make phenolic acids, flavonoids, and other active substances content increase significantly, while the antioxidant activity is increased and the taste is also improved (19, 20). Besides, the production process of buckwheat sprouts is simple and convenient with a short reproductive cycle. All this makes the research of buckwheat product worthwhile. The use of some new technologies to promote germination can result in higher quality sprouts, increase active substance content, and promote the sprout growth, such as plasma.

Plasma is an ionized gas consisting of electrons, atoms, ions, radicals, and other molecules (21). The non-thermal (cold) plasma technology is an emerging non-thermal food preservation approach for fresh production. It is investigated as an alternative for the safe and residual-free antimicrobial food treatment, drawing considerable interest in the last decade, and becoming an important factor widely (22). The plasma treatment of water, termed as plasma-activated water (PAW), results in changes of the redox potential, conductivity, and in the formation of reactive oxygen species (ROS) and reactive nitrogen species (RNS) (23). A number of studies have shown that plasma is effective in improving the seed quality, inactivating bacteria (24), and has the potential to be used for the activation of germination and seedling growth (25, 26). It was found that plasma treatments on mung bean seeds could induce significantly more water absorption and lead to a higher rate of germination (27).

The study of buckwheat sprouts becomes very significant. The objective was to investigate the effect of PAW on the germination of buckwheat seeds. Furthermore, the influences of PAW treatment on germination, sensory properties, nutrients, and active substances, and antioxidant properties of buckwheat seeds were also evaluated.

MATERIALS AND METHODS

Materials

Tartary buckwheat seeds (Hefeng No. 1) were cultivated in Datong, Shanxi Province, China, and were acquired from Beijing Green Valley Sprout Co., Ltd. (Beijing, China). Rutin, gallic acid, and γ-Amino butyric acid standard were purchased from Shanghai solarbio Bioscience & Technology Co., Ltd. (Shanghai, China). The analytical grade chemicals, such as Folin-Ciocalteu reagent, gallic acid (GA), sodium carbonate, sodium hypochlorite, potassium dihydrogen phosphate, dipotassium hydrogen phosphate, phosphoric acid, glucose anhydrous, aluminum chloride, potassium acetate, o-phthalaldehyde, copper sulfate, potassium sulfate, sulfuric acid, boric acid, ethanol, ethyl acetate, hydrochloric acid, trichloroacetic acid, sodium acetate, phenol, potassium persulfate, sodium hydroxide, and aluminum chloride were purchased from Shanghai Macklin Biochemical Co., Ltd. (Shanghai, China). In addition, 2,2-diphenyl picryl hydrazyl (DPPH), acetone, and methanol (HPLC grade) were purchased from Shanghai Aladdin Biochemical Technology Co., Ltd. (Shanghai, China). Total antioxidant capacity (T-AOC) kit was purchased from Nanjing Jiancheng Bioengineering Institute (Nanjing, China).

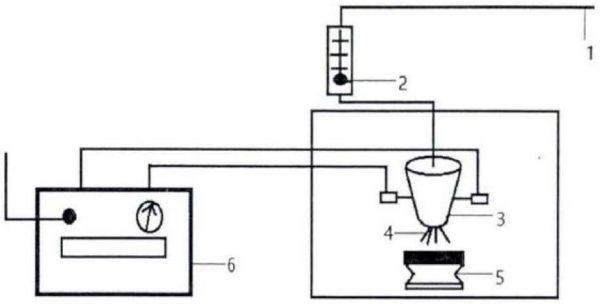

FIGURE 1 | Schematic diagram of experimental set-up for plasma-activated water (PAW) generation. 1. Gas source; 2. Gas flow tester; 3. Reactor; 4. Sliding arc discharge; 5. Sample stage; 6. Power supply.

Preparation of PAW

According to previous studies in the laboratory, PAW was prepared by using a discharge time of 20 min, an action spacing of 0.3 cm, a gas flow rate of 40 L/min, and a discharge power of 450 W (the plasma device is shown in **Figure 1**). The treated PAW was sprayed on the buckwheat seeds instantly.

PAW Treatment for Tartary Buckwheat Seeds

Full buckwheat seeds of uniform size and free from mold were selected, washed 3 times, and then activated with water at 65°C. After that, the seeds were soaked with deionized water in a water bath at 30° for 4 h and then removed from water, disinfected with 1% NaClO solution for 15 min, wrapped in a moist breathable soft cloth, and placed in a dark place for germination. Germinated seeds were poured with the appropriate PAW two times a day during germination, until the seeds sprouted.

The germinated seeds were evenly placed in the perforated sprout culture tray and covered with a sheet of paper wetted with PAW, and then placed in the back shade for the germination and growth.

Plasma-activated water was sprayed daily until the buckwheat on the shoot axis reached 1–2 cm, and then the top of the paper was removed. The germinated seeds were grown in a low-light condition (30 $\mu mol/m^2/s$), sprayed with PAW 4 times every day. After 4 days, the sprouts were put into the place with high light (100 $\mu mol/m^2/s$) for growth.

Buckwheat Sprouts Quality Analysis

Germination Rate

The germination rate was determined according to the method proposed by Cao et al. (27). The germinated buckwheat seeds were put into a constant temperature incubator, and a certain temperature to germinate was set for daily observation and recording. The buckwheat was considered to be germinated when the radicle reached 2.0 mm. One hundred grains were taken out randomly after 72 h of germination, and the number of

buckwheat sprouts which reached the standard of germination were counted. The germination rate was calculated based on the total 100 buckwheat seeds. Each sample was counted three times and the mean was calculated as the result.

$$Germination\ rate/\% = \frac{Germinated\ seeds}{Total\ seeds} \times 100\%$$

Seed Size and Thousand Seed Weight

A total of 100 full seeds were randomly selected, measured their total particle size, and calculated the average single grain size; a total of 1,000 buckwheat seeds were randomly selected and their weight was measured.

Root and Stem Lengths

The buds and seedlings on the 10th day were selected and their root and stem lengths were measured by using a ruler. The average value was chosen for data analysis.

Sprout Weight

Fifty buckwheat sprouts of the same growth were selected randomly for weight measurement.

Moisture Content

Sprouts moisture content was determined gravimetrically, using an oven at 130°C for 3 h. The assay was carried out in triplicate.

Sensory Evaluation

Sensory evaluation was determined according to the method proposed by Li et al. (28). The sensory evaluation was made by 40 untrained volunteers. They were staff and students from the Beijing University of Agriculture who were regular sprouts consumers from various socioeconomic backgrounds between the ages of 18 and 50 years. The samples of freshly-made sprouts were evaluated. Panelists were asked to evaluate the brittleness, glossiness, flavor, juiciness, and overall liking using a 9-point hedonic scale ranging from 4 (dislike extremely) to 20 (like extremely). Water was provided to rinse the mouth between evaluations. Finally, panelists were encouraged to write down additional comments.

Material Treatment

Preparation of Buckwheat Sprout Powder

Buckwheat sprouts were treated with a lyophilizer for 24 h, crushed and sieved through 60 mesh, and then stored in a 4°C refrigerator for backup.

Crude Extract

Furthermore, 0.5 g of Tartary buckwheat sprout powder was weighed, 35 ml of 70% ethanol was added accurately, and an ultrasonic extraction was applied at 700 W, 40 Hz, and 50°C for 20 min. In addition, the sample was centrifuged at 4,000 r/min for 10 min to obtain the buckwheat crude extract (BCE).

Polysaccharides Crude Extract

For this, 20 ml of deionized water was added to 1 g of Tartary buckwheat sprout powder, an ultrasonic extraction was applied for 30 min, 4,000 r/min centrifugation was conducted for 10 min. Then, 2 ml of the deionized water was taken to be dissolved in water and transferred to a 50 ml centrifuge tube. Then, 20 ml of anhydrous ethanol was added and mixed well. After that, the mixture was let stand for 2 h, centrifuged at 4,000 r/min for 10 min. It then followed that the supernatant was discarded and 20 ml of anhydrous ethanol was added. The mixture was then centrifuged at 4,000 r/min for 10 min and washed two times repeatedly. The residue was dissolved in water and transferred to a 10 ml colorimetric tube, diluted to the scale with water, and mixed to obtain the crude extract of buckwheat polysaccharides.

Nutrients of Buckwheat Sprouts

The amounts of protein, amino acids, carbohydrates, crude fat, and reducing sugar in the Tartary buckwheat flour samples were determined according to the Chinese National Standard method (Standard No. GB 5009.5-2016, GB/T 5009.9-2016, GB5009.6-2016, and GB 5009.7-2016; Standards Press of China, Beijing, China).

Active Substances of Buckwheat Sprouts

Flavonoid Content

The content of total flavonoids was estimated by the method of Gabr et al. (29). Briefly, 1 ml of ethanolic solution $AlCl_3$ (0.1 mM) was combined with 1 ml of BCE, after which 1.5 ml of 1 mol/L CH_3COONa solution, and 1.5 ml 70% ethanol solution were added. The mixture was kept for 1 h at room temperature. The absorbance was measured at 420 nm. The content of total flavonoids was expressed as rutin (RE) [mg RE/g dry weight (DW)].

Total Phenolics Content

Total phenolics content of the extract was determined by the method of Park et al. (30) with a slight modification. The BCE (1 ml) was mixed with 6 ml water, 1 ml 5% Folin-Ciocalteu reagent, and 2 ml 5% (w/v) sodium carbonate solution. The mixture reacted for 30 min at 40°C. Absorbance was measured at 765 nm. Total phenolics content was expressed as gallic acid equivalent.

Gamma Aminobutyric Acid Content

The freeze-dried powder sample (0.500 g) was mixed with 5 ml 10% trichloroacetic acid, and the samples extracts were shaken on an oscillator for 1 min and then held at 40°C for 2 h to extract the gamma aminobutyric acid (GABA). The extracts were centrifuged at 13,000 ×g for 15 min (31). Then, 0.6 ml of centrifugation supernatant was transferred to standard solution, 0.5 ml of 0.1 mol/L sodium tetraborate solution (pH = 10), 0.4 ml of 6% phenol, and 0.6 ml of sodium hypochlorite (effective chlorine 8%) were added, and 20 min of reaction was applied. Then, 2 ml of 60% ethanol solution was added after it turned blue-green, and the absorbance value was measured at 650 nm.

Polysaccharides Content

The total content of polysaccharides was determined using the modified phenol-sulfuric acid method. Briefly, 1 ml of deionized water was added to 1 ml buckwheat polysaccharides crude extract, then 1 ml of 6% phenol solution was added, shaken well, and 5.0 ml of concentrated sulfuric acid was added quickly. After being placed for 5 min, it was heated in a boiling water bath for 15 min, cooled to room temperature, and the absorbance was measured at 490 nm.

In vitro Antioxidant Assays

Total Antioxidant

The determination of T-AOC was performed according to the assay kit method, with the absorbance measured at 520 nm.

1-Diphenyl-2-Picrylhydrazyl (DPPH) Radical-Scavenging Activity

The radical scavenging activity of polysaccharides was measured by 1-diphenyl-2-picrylhydrazyl (DPPH) method (32). Briefly, 2 ml of crude extract was mixed with of 0.5 mM DPPH, mixtures were shaken, and left in the dark for 30 min, and absorbance was measured at 517 nm. DPPH free radical scavenging activity (%) was calculated as follows:

$$DPPH\ free\ radical\ scavenging\ activity/\% = \left[1 - \frac{k\left(sample\right)}{k\left(control\right)}\right] \times 100\%$$

Where the solution without the sample was the control.

2,2-Azino-Bis (3-Ethylbenzothiazoline-6-Sulfonic Acid) (ABTS) Radical-Scavenging Activity

The 2,2-azino-bis (3-ethylbenzothiazoline-6-sulfonic acid) (ABTS) free radical scavenging activity was determined by the method of Edziri et al. (33). To make ABTS solution, 7 mM ABTS solution, and 2.45 mM potassium persulfate solution were mixed at a ratio of 1:1 and kept overnight at room temperature. The ABTS solution was diluted with water to an absorbance of less than 0.70 at 734 nm before use. Then, 40 μl of BCE was mixed with 1 ml of the diluted ABTS solution. The mixture was shaken for 30 s, and the reaction was carried out for 30 min with protection from light. Absorbance was measured at 734 nm. The ABTS free radical scavenging activity (%) was calculated as follows:

$$ABTS\ free\ radical\ scavenging\ activity/\% = \left[1 - \frac{k\left(sample\right)}{k\left(control\right)}\right] \times 100\%$$

Where the solution without the sample was the control.

Superoxide Anion Radical Scavenging Ability

The scavenging activity was assessed by the autoxidation of pyragallol in alkaline solution in accordance with the protocol by Mtetwa (34) with slight alterations. Briefly, 200 μl of BCE was added with 5.7 ml of Tris-HCl buffer (50 mM, pH 8.2). Thereafter, 100 μl BCE was added and vortexed for 15 s, subsequently incubated at 25°C for 10 min. The absorbance was measured at 420 nm. The superoxide anion radical scavenging ability was calculated as follows:

$$Superoxide\ anion\ radical\ scavenging\ ability/\% = \left[1 - \frac{k\left(sample\right) - k\left(blank\right)}{k\left(control\right)}\right] \times 100\%$$

Where the solution without the sample was the control and the solution without the sample was the blank. Vitamin C was used as the positive control.

Statistical Analysis

All results are expressed as mean ± SD. Statistical data of three independent replicates were analyzed using the SPSS statistical package 22.0 (SPSS Inc, USA). Data were subjected to two-way ANOVA. Mean comparison was performed using the Duncan's test at a significance level of 0.05 ($p < 0.05$).

RESULTS

Growth Indicators of Buckwheat Seeds

As shown in **Table 1**, the seeds [the weight and size of which were not significantly different ($p > 0.05$)] were treated for germination. The stem length, shoot weight, and germination rate of buckwheat sprouts in the PAW group increased significantly ($p < 0.05$) compared with the control group, and the germination rate reached 93 ± 0.66%, the control group was only 83 ± 0.67%, indicating that the PAW treatment has a positive effect on buckwheat germination, which can promote the growth of roots and facilitate the uptake of water during the seed reproduction.

Moisture Content

The effect of PAW treatment on buckwheat sprouts moisture content is shown in **Figure 2A**. Both the control and PAW groups showed a flat increase followed by a steep increase, but the moisture content of PAW group is higher than that of the control group consistently. The fastest growing period of moisture content of sprouts is from the 2nd to the 6th day. The increase in moisture content for the reproductive process of water absorption has a positive effect, and is also beneficial to the root growth, indicating that the treatment of PAW can promote seed germination and growth of buckwheat sprouts, which means a better hydration of the plants (35).

Sensory Evaluation

The sensory evaluation scores of sprouts are shown in **Figure 2B**. Taste panelists could not differentiate between the control and PAW samples (data not shown). There was no significant difference ($p < 0.05$) in brittleness, glossiness, flavor, juiciness, or overall liking of the PAW samples as compared with control. Taste panelists generally agreed that the sprouts were bright green, shinning, crisp and smooth, with sufficient moisture, and easy to chew. The PAW group of sprouts on the 8th day had the highest score and the best overall quality.

Nutrients of Buckwheat Sprouts

Compared with the seed group, sprouts grown to the 9th day had a significant increase in 16 kinds of amino acids in the control group and a significant increase in 17 kinds of amino acids in the PAW group (18 kinds of amino acids in total). The PAW group had a significant increase of 13 amino acids compared with the control group and the total amount was also higher than the control group (**Table 2**). Both the PAW and control groups showed an overall balance between a continuous increase in total amino acid content and a continuous decrease in protein content during

TABLE 1 | Growth index of Tartary buckwheat seeds.

Group	Seed size (mm)	Weight of 1,000 seeds (g)	Root length (mm)	Stem length (mm)	Sprout weight (g)	Germination rate (%)
Control	3.87 ± 0.15[a]	27.63 ± 0.17[a]	122.86 ± 0.52[a]	30.58 ± 0.43[a]	1.82 ± 0.80[a]	83 ± 0.67[a]
PAW	3.86 ± 0.20[a]	27.49 ± 0.21[a]	155.52 ± 0.48[b]	45.56 ± 0.68[b]	2.11 ± 0.69[b]	93 ± 0.66[b]

Values are given as the mean ± SD (n = 3). Different lowercase letters in the same column indicate significant differences (p < 0.05).

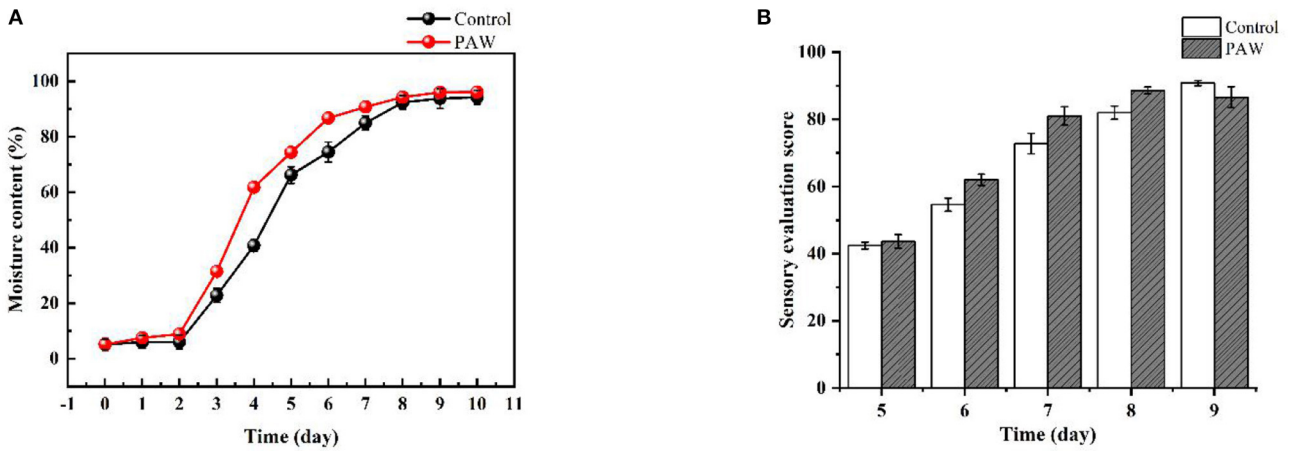

FIGURE 2 | Effects of PAW on moisture content **(A)**, sensory evaluation scores of sprouts in different periods **(B)**.

TABLE 2 | Amino acid analysis of buckwheat sprouts on the 9th day.

	Seed (ng/g)	Control (ng/g)	PAW (ng/g)
Aspartic Acid	1,516.858 ± 0.1[a]	1,711.999 ± 0.21[b]	1,783.864 ± 0.1[c]
L-Threonine	424.853 ± 0.13[a]	721.111 ± 0.1[b]	739.156 ± 0.21[c]
Serine	830.508 ± 0.2[a]	999.492 ± 0.12[b]	1,046.447 ± 0.21[c]
Glutamic acid	3,777.001 ± 0.15[a]	4,470.853 ± 0.11[b]	4,633.509 ± 0.13[c]
Glycine	1,003.99 ± 0.1[a]	1,112.563 ± 0.13[b]	1,191.033 ± 0.16[c]
Alanine	546.349 ± 0.2[a]	1,066.239 ± 0.20[b]	1,132.401 ± 0.16[c]
L (+)-Cysteine	279.687 ± 0.2[c]	89.208 ± 0.11[b]	82.579 ± 0.13[a]
Valine	987.194 ± 0.2[a]	1,588.843 ± 0.14[b]	1,685.827 ± 0.12[c]
DL-Methionine	88.646 ± 0.2[c]	68.001 ± 0.13[a]	81.785 ± 0.12[b]
L-isoleucine	592.34 ± 0.1[a]	908.701 ± 0.16[b]	964.818 ± 0.15[c]
Leucine	278.23 ± 0.21[a]	352.278 ± 0.12[c]	344.863 ± 0.15[b]
Tyrosine	312.456 ± 0.14[a]	582.69 ± 0.20[b]	623.533 ± 0.13[c]
Phenylalanine	95.9 ± 0.21[a]	122.995 ± 0.13[c]	109.9 ± 0.15[b]
Lysine	1,229.383 ± 0.11[a]	1,914.7 ± 0.13[b]	2,036.545 ± 0.13[c]
Histidine	379.366 ± 0.12[a]	632.662 ± 0.15[b]	678.406 ± 0.15[c]
Arginine	1,907.837 ± 0.11[c]	1,593.887 ± 0.11[a]	1,697.259 ± 0.24[b]
Hydroxyproline	12.56 ± 0.13[a]	539.837 ± 0.22[b]	572.122 ± 0.21[c]
Proline	177.081 ± 0.13[a]	327.739 ± 0.31[b]	346.411 ± 0.21[c]
Total	14,440.239	18,803.798	19,750.458

Values are given as the mean ± SD (n = 3). Different lowercase letters in the same line indicate significant differences (p < 0.05).

germination, which was due to the breakdown of protein into small molecule peptides and amino acids during the germination process.

As shown in **Figure 3A**, the protein content of the control group (during 0–7 days) and the PAW group (during 0–6 days) decreased rapidly, in the last 3 days, the protein content decreased at a slower rate because of the impact of proteases during germination. The protein content on 9th day was 8.56 ± 0.121% in the PAW group and 8.83 ± 0.123% in the control group. As shown in **Figure 3B**, the carbohydrate content of buckwheat germination on the first day basically did not change, which decreased gradually from 1–9 days after germination, during which the starch was decomposed to provide available energy for plant growth. The content of reducing sugar in Tartary buckwheat seeds was 8.42 ± 0.19%, which was as high as 12.29 ± 0.1% on the 9th day after germination. There was no significant difference in the changes of carbohydrates and reducing sugars between the PAW group and the control group. The decrease and increase of carbohydrates and reducing sugars in the PAW group would be more obvious. The crude fat content of buckwheat is shown in **Figure 4**. During buckwheat seed germination, crude fat declined continuously. Photosynthesis was weak at the beginning of germination and the carbon source was insufficient to be utilized as an energy source, so crude fat was used for energy supplementation and the content started to decrease.

Active Substances of Buckwheat Sprouts

As shown in **Figure 5A**, with the increase of germination time, the content of total flavonoids gradually increased, and the growth rate of flavonoids was relatively fast in the early stage of germination (0–6 days in the PAW group and 0–7 days in the

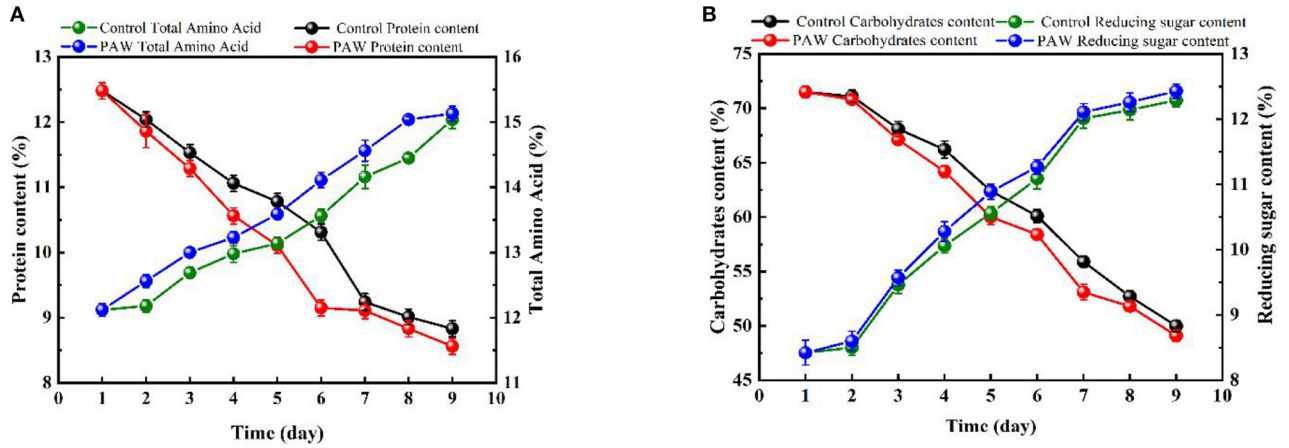

FIGURE 3 | Changes of nutrients during the germination of buckwheat: protein and total amino acid content **(A)**, carbohydrate and reducing sugar **(B)**.

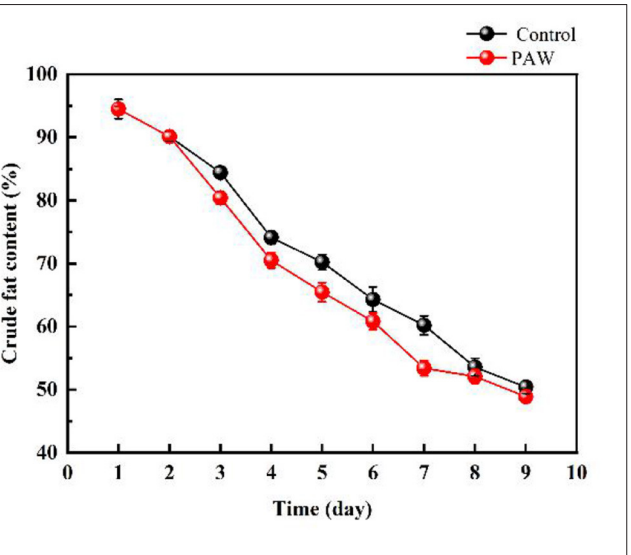

FIGURE 4 | Changes of crude fat during the germination of buckwheat.

control group). The flavonoid content of Tartary buckwheat seeds was 5.25 ± 0.23 mg/g, and the flavonoid content of dry weight of Tartary buckwheat sprouts in the PAW group reached 15.81 ± 0.21 mg/g on the 6th day of germination, which was three times that of the original seeds and there was a significant difference between the flavonoid content of Tartary buckwheat sprouts and seeds 6 days before germination ($p < 0.05$). The change of total phenolic acid content during the Tartary buckwheat germination is shown in **Figure 5B**. During 0–9 days of germination, the total phenolic acid content showed an overall gradual increasing trend. On the 8th day of germination, the total phenolic acid content (2.151 ± 0.044 mg/g in the PAW group, and 2.09 ± 0.023 mg/g in the control group) was about 2.1 times that of total phenolic of Tartary buckwheat seed dry weight (1.02 mg/g).

The change of γ-GABA content during the Tartary buckwheat germination is shown in **Figure 5C**. With the increase of germination time, γ- GABA content raised as well. The maximum amount was reached on the 9th day of germination (0.30 ± 0.009 mg/g in the PAW group and 0.31 ± 0.008 mg/g in the control group), which was nearly three times that of seeds. With the increase of germination time, the content of polysaccharides also increased (**Figure 5D**). The maximum polysaccharides content of the control group was 2.88 ± 0.082 mg/g on the 9th day of germination, and that of PAW group was 2.98 ± 0.070 mg/g on the 8th day, which was 2.7 times that of seeds. Then, the polysaccharides content of the PAW group started to decrease, which was consistent with the trend of flavonoid content in the PAW group.

In vitro Antioxidant Assays

The changes in antioxidant values during germination in the control and PAW groups are shown in **Figure 6**, and overall both increased with time, because for both the control and PAW groups, the germination significantly increased the antioxidant activity. The total antioxidant capacity was not significantly different between the control and PAW groups from 0–6 days. However, the PAW group increased rapidly on the 7th day, reaching a maximum value of 59 ± 1.9 mg/g on the 9th day. The DPPH scavenging capacity of PAW group reached a maximum (150 ± 3.1 mg/g) at the 8th day of germination, which was 5 times higher than that of buckwheat seeds, with the same trend of total phenolic acids and polysaccharides.

The changing trend of ABTS radical scavenging ability in the control group and the PAW group was similar. The scavenging rate of sprouts cultivated on 9th day reached 55.95 ± 1.2 mg/g, which was 13.36 mg/g higher than that of control and 4.1 times higher than that of seeds. The superoxide anion radical scavenging capacity also increased with germination time, reaching the maximum amount in both groups at the 9th day of germination (96.4 ± 0.79 mg/g in the PAW group and 96.1 ± 0.77 mg/g in the control group), but there was no significant change in both during the germination process.

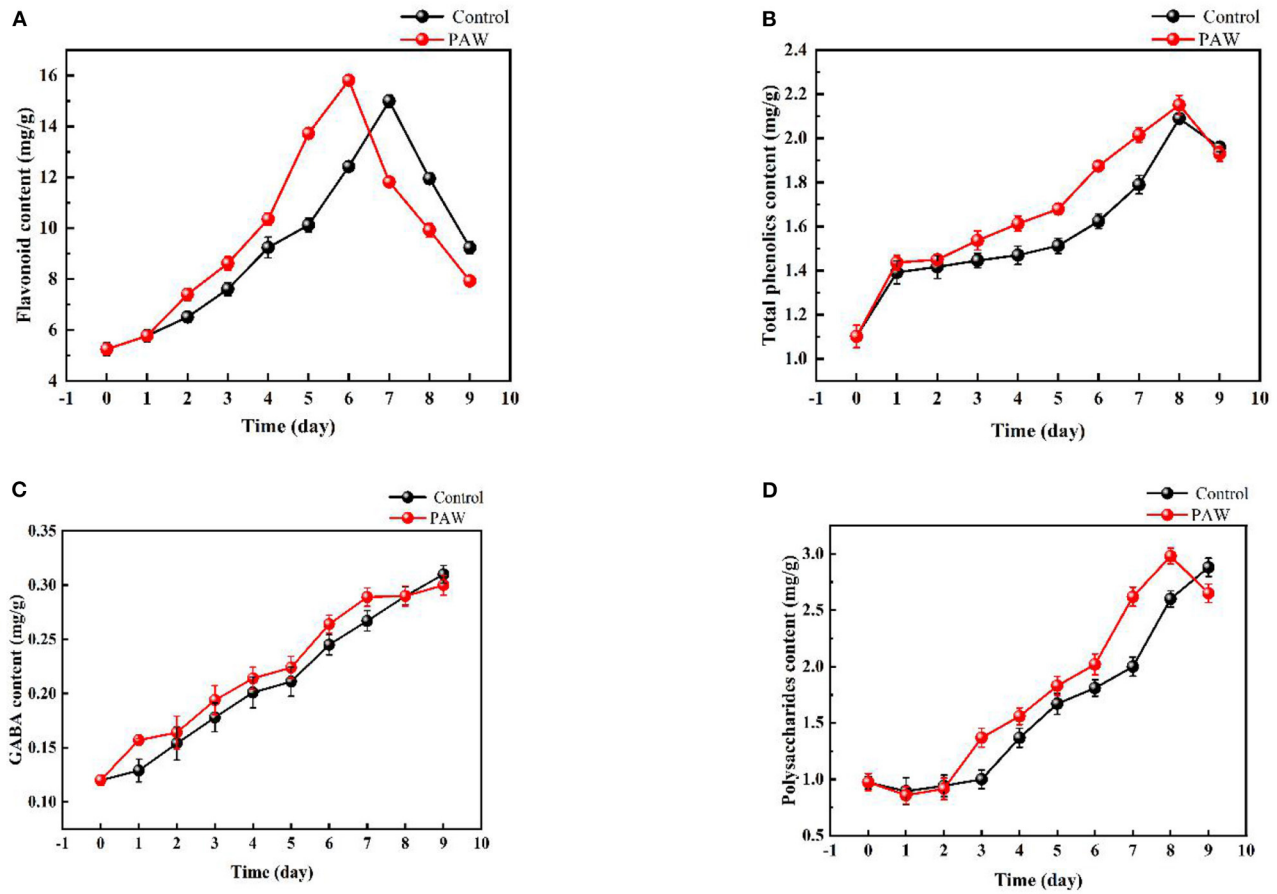

FIGURE 5 | Changes of active substances during the germination of Tartary buckwheat: total flavonoids **(A)**, total phenolic **(B)**, gamma aminobutyric acid (GABA) **(C)**, polysaccharides **(D)**.

DISCUSSION

The root length, stem length, sprout weight, and germination rate of PAW-treated sprouts were higher than those of the control group, this may be attributed to the fact that the cold plasma treatment increased the activity of metabolic enzymes associated, and reduced the impact of oxidative reactions caused by ROS in plant cells, thus improving root vigor (36, 37). Filatova's research showed that the plasma treatment causes cracks on the seed surface and this "erosive" effect can increase the total surface energy and hydrophilicity, thus promoting the root growth (38). It also has been reported that PAW could significantly stimulate mung bean seeds germination and growth, which might be related to the active components in PAW (39). Hence, we can observe that the PAW treatment has a promotional effect on the growth of buckwheat sprouts. The results of the sensory evaluation revealed that taste panelists were unable to distinguish the taste of PAW and control samples and they liked the PAW samples and the controls equally. Thus, PAW did not affect the overall acceptability of the sprouts. During germination, the reducing sugar content of sprouts increased, which might improve the taste of sprouts.

In the process of buckwheat germination, protein, crude fat, and carbohydrate content follow a downtrend, while amino acids and reducing sugars are the opposite. Protein content decreases rapidly in the early stages of seed germination, which is consumed as the most important source of energy during buckwheat germination, germination also leads to increase the *in vitro* digestibility of proteins (40). As buckwheat contains some amino acids, these decompositions are dispersed to the germ, at which time the germ is activated to synthesize new proteins, so the rate of change in protein content slows down in the later stages. Ishikawa (41) found that the proteolysis reaction and metabolic reactions of amino acids might coexist in sprouts, which explains the increased amino acid content. Carbohydrates are used as the main source of energy for plants, which includes numerous components, such as starch and complex polysaccharides. Amylase is able to breakdown starch into monosaccharides and oligosaccharides. The taste and digestibility of buckwheat could be improved because of the increase of reducing sugar.

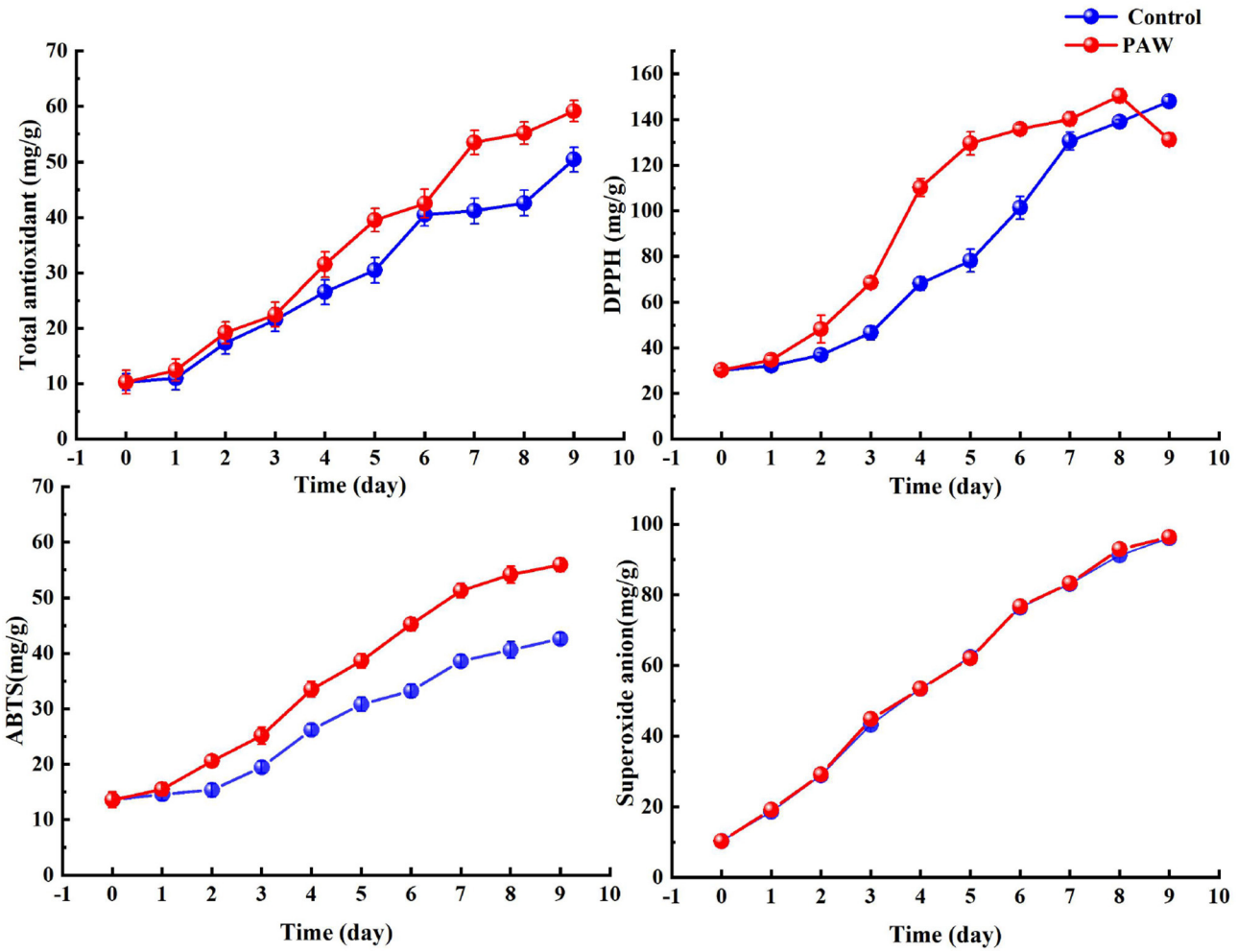

FIGURE 6 | Changes of the antioxidant activity during the germination of Tartary buckwheat.

In our study, the trend in carbohydrate content was gradually decreasing, while some studies have shown that the flavonoids in buckwheat (rutin, quercetin, and kaempferol) inhibit the activity of α-amylase, which leads to a slower rate of starch breakdown (5). Therefore, whether the increase in flavonoid content of buckwheat sprouts obtained by the PAW treatment decreases the rate of carbohydrate decomposition remains to be studied subsequently.

A growing amount of evidence for the role of PAW in the promotion of sprout germination. The experimental results indicated that PAW has been proved to be effective in promoting the growth of buckwheat sprouts, but also in increasing the content of bioactive compounds and enhancing the antioxidant capacity. Scholars have found that the accumulation of flavonoids might be closely linked to the increase in FtFLS2 (one flavonol synthetase isoform gene) expression (20). Their study demonstrated that the flavonoid content showed an increasing trend followed by a decreasing trend during germination. The increases in total phenolic acid might be due to the increase in phenylalanine ammonialyase (PAL) catalyst during germination (42). GABA is a central nervous system (CNS) transmitter that exhibits hypolipidemic and hypocholesterolemic effects. The persistent increase in GABA content suggests that buckwheat sprouts may have the potential as a therapeutic food for the dietary intervention in patients with hyperlipidemia. Earlier studies have shown that the DPPH radical-scavenging activity may be attributed to the fact that the amount of flavonoid ingredients and phenolic acid significantly increased during common buckwheat germination (43), the DPPH assay were strongly correlated to the content of total phenolic acids and proanthocyanidins level in the cotyledons (44). The results of ABTS radical-scavenging activity were essentially the same as those obtained by Živković Andrej's study (45), compared with phenolic content, the antioxidant activity (DPPH and ABTS) measures showed similar trends during the course of germination. However, the changes in flavonoids and phenolic acid monomers and the relevance to the antioxidant properties of sprouts were not studied, so in future studies, the effect

of PAW on antioxidant activity in buckwheat sprouts can be considered by targeted metabolomics and analyze the intrinsic mechanism, and improve the study of changes in relevant enzymes in parallel with a view to provide a basis for their nutrient changes.

CONCLUSIONS

The data obtained showed that the PAW treatment had no negative impact on buckwheat germination, but instead promoted the growth of sprouts, improved the germination rate, increased the content of active substance, and enhanced their antioxidant activity. These results indicated that PAW could significantly stimulate buckwheat seeds germination and growth, which might be considered as a promising technology to improve the seeds germination and seedling growth. The PAW treatment provides ideas for the preparation of functional foods made from buckwheat, but the mechanisms involved still need to be studied.

DATA AVAILABILITY STATEMENT

The original contributions presented in the study are included in the article/supplementary material, further inquiries can be directed to the corresponding author/s.

AUTHOR CONTRIBUTIONS

YW, ZN, and TM: conceptualization, methodology, software, validation, formal analysis, investigation, resources, data curation, and visualization. YW and ZN: writing—original draft preparation. YW and TM: writing—review and editing. TM: supervision. All authors contributed to the article and approved the submitted version.

REFERENCES

1. Zou L, Wu DT, Ren GX, Hu YC, Peng LX, Zhao JL, et al. Bioactive compounds, health benefits, and industrial applications of Tartary buckwheat (*Fagopyrum tataricum*). *Crit Rev Food Sci Nutr*. (2021). doi: 10.1080/10408398.2021.1952161. [Epub ahead of print].
2. Liu YX, Cai CZ, Yao YL, Xu BJ. Alteration of phenolic profiles and antioxidant capacities of common buckwheat and Tartary buckwheat produced in China upon thermal processing. *J Sci Food Agric*. (2019) 99:5565–76. doi: 10.1002/jsfa.9825
3. Liu F, He CA, Wang LJ, Wang M. Effect of milling method on the chemical composition and antioxidant capacity of Tartary buckwheat flour. *Int J Food Sci Tech*. (2018) 53:2457–64. doi: 10.1111/ijfs.13837
4. Saeed F, Afzaal M, Ikram A, Imran A, Hussain S, Mohamed AA, et al. Exploring the amino acid composition and vitamin-B profile of buckwheat varieties. *J Food Process Pres*. (2021) 45:1–8. doi: 10.1111/jfpp.15743
5. Peng LX, Wei LJ Yi Q, Chen GH, Yao ZD, Yan ZY, et al. In vitro potential of flavonoids from Tartary buckwheat on antioxidants activity and starch digestibility. *Int J Food Sci Tech*. (2019) 54:2209–18. doi: 10.1111/ijfs.14131
6. Rachman A, Chen LJ, Brennan M, Brennan C. Effects of addition of buckwheat bran on physicochemical, pasting properties and starch digestion of buckwheat gels. *Eur Food Res Technol*. (2020) 246:2111–7. doi: 10.1007/s00217-020-03560-6
7. Zhu F. Buckwheat proteins and peptides: biological functions and food applications. *Trends Food Sci Tech*. (2021) 110:155–67. doi: 10.1016/j.tifs.2021.01.081
8. Cheng FE, Ge XH, Gao CF Li YL, Wang M. The distribution of D-chiro-inositol in buckwheat and its antioxidative effect in HepG2. *J Cereal Sci*. (2019) 89:1–29. doi: 10.1016/j.jcs.2019.102808
9. Wu SC, Lee BH. Buckwheat polysaccharide exerts antiproliferative effects in THP-1 human leukemia cells by inducing differentiation. *J Med Food*. (2011) 14:26–33. doi: 10.1089/jmf.2010.1252
10. Kayashita J, Shimaoka I, Nakajoh M, Kato N. Feeding of buckwheat protein extract reduces hepatic triglyceride concentration, adipose tissue weight, and hepatic lipogenesis in rats. *J Nutr Biochem*. (1996) 7:555–9. doi: 10.1016/S0955-2863(96)00110-6
11. Skrabanja V, Elmsthl HGML, Kreft I, Björck IME. Nutritional properties of starch in buckwheat products: studies in vitro and in vivo. *J Agric Food Chem*. (2001) 49:490–6. doi: 10.1021/jf000779w
12. Brockmann H, Weber E, Pampus G. Protofagopyrin und Fagopyrin, die photodynamisch wirksamen Farbstoffe des Buchweizens (*Fagopyrum esculentum*). *Eur J Org Chem*. (2010) 575:53–83. doi: 10.1002/jlac.19525750106
13. Glavač NK, Stojilkovski K, Kreft S, Park CH, Kreft I. Determination of fagopyrins, rutin, and quercetin in Tartary buckwheat products. *LWT-Food Sci Technol*. (2017) 79:423–7. doi: 10.1016/j.lwt.2017.01.068
14. Kreft S, Janes D, Kreft I. The content of fagopyrin and polyphenols in common and tartary buckwheat sprouts. *Acta Pharm*. (2013) 63:553–60. doi: 10.2478/acph-2013-0031
15. Lin LY, Hsieh YJ, Liu HM, Lee CC, Mau JL. Flavor Components in Buckwheat Bread. *J Food Process Pres*. (2009) 33:814–26. doi: 10.1111/j.1745-4549.2008.00313.x
16. Johnson SK, Kaur G, Luitel S, Hoang LAP, Bhattarai RR. Replacement of buckwheat by black sorghum flour on soba-type noodles. *Int J Food Sci Tech*. (2021) 56:5861–70. doi: 10.1111/ijfs.15326
17. Deng JL, Liu R, Lu Q, Hao PY, Xu AQ, Zhang JL, et al. Biochemical properties, antibacterial and cellular antioxidant activities of buckwheat honey in comparison to manuka honey. *Food Chem*. (2018) 252:243–9. doi: 10.1016/j.foodchem.2018.01.115
18. Sun LK, Young KS, Jong JH, Sung KK, Han SH, Cheol HP. Development and utilization of buckwheat sprouts as functional vegetables. *Fagopyrum*. (2001) 18:49–54.
19. Koyama M, Nakamura C, Nakamura K. Changes in phenols contents from buckwheat sprouts during growth stage. *J Food Sci Tech*. (2011) 50:86–93. doi: 10.1007/s13197-011-0316-1
20. Zhang G, Xu ZC, Gao YY, Huang XX, Zou YP, Yang TG. Effects of germination on the nutritional properties, phenolic profiles, and antioxidant activities of buckwheat. *J Food Sci*. (2015) 80:H1111–9. doi: 10.1111/1750-3841.12830
21. Mravlje J, Regvar M, Staric P, Mozetic M, Vogel-Mikus K. Cold plasma affects germination and fungal community structure of buckwheat seeds. *Plants (Basel)*. (2021) 10:851–69. doi: 10.3390/plants10050851
22. Niedzwiedz I, Waśko A, Pawłat J, Polak-Berecka M. The state of research on antimicrobial activity of cold plasma. *Pol J Microbiol*. (2019) 68:153–64. doi: 10.33073/pjm-2019-028
23. Thirumdas R, Kothakota A, Annapure U, Siliveru K, Blundell R, Gatt R, et al. Plasma activated water (PAW): chemistry, physico-chemical properties, applications in food and agriculture. *Trends Food Sci Tech*. (2018) 77:21–31. doi: 10.1016/j.tifs.2018.05.007
24. Butscher D, Loon HV, Waskow A, Rohr PR, Schuppler M. Plasma inactivation of microorganisms on sprout seeds in a dielectric barrier discharge. *Int J Food Microbiol*. (2016) 238:222–32. doi: 10.1016/j.ijfoodmicro.2016.09.006
25. MildaŽiene V, Aleknavičiute V, Žukiene R, PauŽaite G, Naučiene Z, Filatova I, et al. Treatment of common sunflower (*Helianthus annus L*) seeds with radio-frequency electromagnetic field and cold plasma induces changes in seed phytohormone balance, seedling development and leaf protein expression. *Sci Rep*. (2019) 9:6437–49. doi: 10.1038/s41598-019-42893-5

26. Xiang QS, Liu XF, Liu SG, Ma YF, Xu CQ, Bai YH. Effect of plasma-activated water on microbial quality and physicochemical characteristics of mung bean sprouts. *Innov Food Sci Emerg.* (2019) 52:49–56. doi: 10.1016/j.ifset.2018.11.012
27. Chou YJ, Cheng CY, Hsu FC, Wu JSB, Ting YW. Producing high quality mung bean sprout using atmospheric cold plasma treatment: better physical appearance and higher γ-aminobutyric acid (GABA) content. *J Sci Food Agr.* (2021) 101:6463–71. doi: 10.1002/jsfa.11317
28. Li Y, Sun YF, Zhong MM, Xie FY, Wang H, Li L, et al. Digestibility, textural and sensory characteristics of cookies made from residues of enzyme-assisted aqueous extraction of soybeans. *Sci Rep.* (2020) 10:4222–30. doi: 10.1038/s41598-020-61179-9
29. Gabr AMM, Sytar O, Ghareeb H, Brestic M. Accumulation of amino acids and flavonoids in hairy root cultures of common buckwheat (*Fagopyrum esculentum*). *Physiol Mol Biol Plants.* (2019) 25:787–97. doi: 10.1007/s12298-019-00669-1
30. Park BI, Kim J, Lee K, Lim T, Hwang KT. Flavonoids in common and Tartary buckwheat hull extracts and antioxidant activity of the extracts against lipids in mayonnaise. *J Food Sci Technol.* (2019) 56:2712–20. doi: 10.1007/s13197-019-03761-2
31. Cao YP, Jia FG, Han YL, Liu Y, Zhang, Q. Study on the optimal moisture adding rate of brown rice during germination by using segmented moisture conditioning method. *J Food Sci Technol.* (2015) 52:6599–606. doi: 10.1007/s13197-015-1722-6
32. Hao JX, Wu TJ Li HY, Wang W, Liu HJ. Dual effects of slightly acidic electrolyzed water (SAEW) treatment on the accumulation of γ-aminobutyric acid (GABA) and rutin in germinated buckwheat. *Food Chem.* (2016) 201:87–93. doi: 10.1016/j.foodchem.2016.01.037
33. Edziri H, Haddad O, Saidana D, Chouchen S, Skhiri F, Mastouri M, et al. *Ruscus hypophyllum* L. extracts: chemical composition, antioxidant, anticoagulant, and antimicrobial activity against a wide range of sensitive and multi-resistant bacteria. *Environ Sci Pollut R.* (2020) 27:17063–71. doi: 10.1007/s11356-020-08159-8
34. Mtetwa MD, Qian LS, Zhu HA, Cui FJ, Zan XY, Sun WJ, et al. Ultrasound-assisted extraction and antioxidant activity of polysaccharides from Acanthus ilicifolius. *J Food Meas Charact.* (2020) 14:1223–35. doi: 10.1007/s11694-019-00371-6
35. Fan LM, Liu XF, Ma YF, Xiang QS. Effects of plasma-activated water treatment on seed germination and growth of mung bean sprouts. *J Taibah Univ Sci.* (2020) 14:823–30. doi: 10.1080/16583655.2020.1778326
36. Lemmens E, Deleu L, Brier N, Man W, Proft M, Prinsen E, et al. The impact of hydro-priming and osmo-priming on seedling characteristics, plant hormone concentrations, activity of selected hydrolytic enzymes, and cell wall and phytate hydrolysis in sprouted wheat (Triticum aestivum L). *ACS omega.* (2019) 4:22089–100. doi: 10.1021/acsomega.9b03210
37. Zhang F, Yu JL, Johnston CR, Wang YQ, Zhu K, Lu F, et al. Seed priming with polyethylene glycol induces physiological changes in sorghum (*Sorghum bicolor* L. *Moench*) seedlings under suboptimal soil moisture environments. *PLoS ONE.* (2015) 10:e0140620. doi: 10.1371/journal.pone.0140620
38. Filatova I, Azharonok V, Kadyrov M, Beljavsky V, Sera B, Hruskova I, et al. Rf and microvawe plasma application for pre-sowing caryopsis treatments. *Publications De Lobservatoire Astronomique De Beograd.* (2010) 89:289–92.
39. Lo Porto C, Ziuzina D, Los A, Boehm D, Palumbo F, Favia P, et al. Plasma activated water and airborne ultrasound treatments for enhanced germination and growth of soybean. *Innov Food Sci Emerg.* (2018) 49:13–9. doi: 10.1016/j.ifset.2018.07.013
40. Savelkoul F, Poel A, Tamminga S. The presence and inactivation of trypsin inhibitors, tannins, lectins and amylase inhibitors in legume seeds during germination. *Plant Food Hum Nutr.* (1992) 42:71–85. doi: 10.1007/BF02196074
41. Ishikawa D, Shigihara I, Nakai R, Tamate H, Tsukada Y, Fujii T. High pressure induced effects on free amino acid generation in mung bean sprouts during preservation after trigger pressurization. *Food Sci Technol Res.* (2019) 25:49–55. doi: 10.3136/fstr.25.49
42. Ma H, Xu XM, Wang SM Wang JZ, Peng WP. Effects of microwave irradiation on the expression of key flavonoid biosynthetic enzyme genes and the accumulation of flavonoid products in Fagopyrum tataricum sprouts. *J Cereal Sci.* (2021) 101:1–7. doi: 10.1016/j.jcs.2021.103275
43. Ren SC, Sun JT. Changes in phenolic content, phenylalanine ammonia-lyase (PAL) activity, and antioxidant capacity of two buckwheat sprouts in relation to germination. *J Funct Foods.* (2014) 7:298–304. doi: 10.1016/j.jff.2014.01.031
44. Wiczkowski W, Szawara-Nowak D, Sawicki T, Mitrus J, Kasprzykowski Z, Horbowicz M. Profile of phenolic acids and antioxidant capacity in organs of commom buckwheat sprout. *Acta Alimentaria.* (2016) 45:250–7. doi: 10.1556/066.2016.45.2.12
45. Živković A, Polak T, Cigic B, Pozrl T. Germinated buckwheat: effects of dehulling on phenolics profile and antioxidant activity of buckwheat seeds. *Foods.* (2021) 10:740–56. doi: 10.3390/foods10040740

Conflict of Interest: The authors declare that the research was conducted in the absence of any commercial or financial relationships that could be construed as a potential conflict of interest.

Publisher's Note: All claims expressed in this article are solely those of the authors and do not necessarily represent those of their affiliated organizations, or those of the publisher, the editors and the reviewers. Any product that may be evaluated in this article, or claim that may be made by its manufacturer, is not guaranteed or endorsed by the publisher.

frontiers | Frontiers in Nutrition

ORIGINAL RESEARCH
published: 04 April 2022
doi: 10.3389/fnut.2022.833859

Transformation Mechanism of Rare Ginsenosides in American Ginseng by Different Processing Methods and Antitumour Effects

Zhi-man Li[1†], Zi-jun Shao[1†], Di Qu[1], Xiao-hui Huo[1], Mei Hua[1], Jian-bo Chen[1], Yu-shun Lu[1], Ji-Yue Sha[1], Shan-shan Li[2] and Yin-shi Sun[1*]*

[1] Institute of Special Animal and Plant Sciences, Chinese Academy of Agricultural Sciences, Changchun, China, [2] Institute of Biological and Pharmaceutical Engineering, Jilin Agricultural Science and Technology University, Jilin, China

OPEN ACCESS

Edited by:
Jinkai Zheng,
Institute of Food Science and Technology (CAAS), China

Reviewed by:
Biao Yuan,
China Pharmaceutical University, China
Kefeng Zhai,
Suzhou University, China

***Correspondence:**
Yin-shi Sun
sunyinshi2015@163.com
Shan-shan Li
shanshanli123456@163.com

†These authors have contributed equally to this work

Specialty section:
This article was submitted to Food Chemistry, a section of the journal Frontiers in Nutrition

Received: 12 December 2021
Accepted: 24 January 2022
Published: 04 April 2022

Citation:
Li Z-m, Shao Z-j, Qu D, Huo X-h, Hua M, Chen J-b, Lu Y-s, Sha J-Y, Li S-s and Sun Y-s (2022) Transformation Mechanism of Rare Ginsenosides in American Ginseng by Different Processing Methods and Antitumour Effects. Front. Nutr. 9:833859. doi: 10.3389/fnut.2022.833859

The mechanism by which ginsenosides from *Panax quinquefolium* L. transform into rare saponins by different processing methods and their antitumour effects have yet to be fully elucidated. Our study aimed to detect the effect of amino acids and processing methods on the conversion of ginsenosides in American ginseng to rare ginsenosides, using 8 monomeric ginsenosides as substrates to discuss the reaction pathway and mechanism. S180 tumour-bearing mice were established to study the antitumour effects of American ginseng total saponins (AGS-Q) or American ginseng total saponins after transformation (AGS-H) synergistic CTX. The results showed that aspartic acid was the best catalyst, and the thermal extraction method had the best effect. Under the optimal conditions, including a reaction temperature of 110°C, an aspartic acid concentration of 5%, a reaction time of 2.5 h and a liquid-solid ratio of 30 mL/g, the highest conversion of Rk_1 and Rg_5 was 6.58 ± 0.11 mg/g and 3.74 ± 0.05 mg/g, respectively. In the reaction pathway, the diol group saponins participated in the transformation process, and the triol group saponins basically did not participate in the transformation process. AGS-Q or AGS-H synergistic CTX, or AGS-H synergistic CTX/2 could significantly increase the tumour inhibition rate, spleen index and white blood cell count, had a significant upregulation effect on IL-2 and IL-10 immune cytokines; significantly restored the ratio of $CD4^+/CD8^+$; and significantly inhibited the level of $CD4^+CD25^+$. AGS-Q or AGS-H synergistic with CTX or CTX/2 can significantly upregulate the expression of Bax and cleaved-Caspase-3 and inhibit the expression of antiapoptotic protein Bcl-2. AGS synergistic CTX in the treatment of S180 tumour-bearing mice can improve the efficacy and reduce toxicity.

Keywords: ***Panax quinquefolium*** **L., rare ginsenosides, transformation, S180 tumour-bearing mice, processing methods**

INTRODUCTION

Panax quinquefolium L. is an herbaceous plant of the genus, also called American ginseng, which originates from the United States and Canada (1). Shandong, Jilin, and Heilongjiang in China are now the main areas producing this plant. Ginsenoside is the main active component of American ginseng and can be divided into dammarane type and oleanolic acid type according to

structure. Among dammarane ginsenosides, tetracyclic triterpenoids can be further divided into protopanaxadiol (PPD) types, such as Rb_1, Rb_2, Rc, Rd, and protoparitol (PPT) types, such as Re and Rg_1 (2, 3). In addition, there are some ginsenosides in American ginseng that have a low content of raw materials, such as 20(S)-Rg_3, 20(R)-Rg_3, Rk_1 and Rg_5. Natural ginsenosides have the characteristics of high polarity and large molecular weight, and are not easily absorbed through the intestinal mucosa. Instead, they are converted into rare ginsenosides under the action of enzymes secreted by specific flora in the intestinal tract, which are absorbed and utilized by the body, and then exert medicinal effect. Therefore, that obtains rare ginsenosides with better activity through *in vitro* biotransformation of natural ginsenosides is also one of the directions pursued by researchers in the industry.

Some studies have shown that rare ginsenosides, Rk_1 and Rg_5, have significant effects on some diseases, such as depression (4), diabetes (5), and anti-septicaemia (6), and they have an obvious effect on promoting apoptosis of cancer cells such as liver cancer, lung cancer and gastric cancer (7–10). Shenyi capsules are the first to contain rare ginsenoside monomers, and 20(S)-Rg_3 prescription drugs are used in clinical anticancer therapy. Due to the beneficial effects of rare saponins Rk_1 and Rg_5, researchers have paid more attention to Rk_1 and Rg_5, and the market demand has also increased. Therefore, it is important to explore an efficient enrichment method. In some reports, the rare ginsenosides, Rk_1 and Rg_5 have been shown to be enriched by cooking and drying processes (11–13). These methods are complicated and time-consuming. In addition, rare ginsenosides Rk_1 and Rg_5 can also be increased by acid hydrolysis, microbial degradation, and metal ion catalysis (14–16). However, these methods require high specificity and reaction conditions and cause environmental pollution. Therefore, it is very important to screen environmentally friendly, safe, and efficient catalysts. It has been reported that aspartic acid can degrade the total saponins of purified protopanaxadiol in ginseng by steaming to obtain the rare ginsenosides 20(S)-Rg_3, 20(R)-Rg_3, Rk_1 and Rg_5 (17). Amino acids are biologically active macromolecules used by organisms to construct and repair tissues. Amino acids also provide energy to the body and brain. Therefore, the selection of a suitable amino acid as a catalyst is of great significance for the safe and efficient conversion of rare ginsenosides. Our study for the first time reported the preparation method of tramforming ginsenosides from American ginseng natural ginsenosides into rare saponins Rk_1 and Rg_5, aiming to develop a low-polluting, simple and low-cost conversion route, and verify the anticancer mechanism of the AGS-H. This will have potential value for the development of high-efficiency preparations based on rare ginsenosides, and the large-scale industrial production of rare ginsenosides is of great significance.

Cyclophosphamide (CTX) is an effective anticancer alkylating agent that also has a broad spectrum of cytotoxicity to normal cells. Its metabolites, such as phosphamide mustard (PM) and acrolein (Acr), can interact with DNA to induce the formation of DNA admixtures, resulting in oxidative damage to DNA (18). Many studies have shown that Chinese herbal medicines have great potential in reducing the toxicity of chemotherapy. American ginseng, a well-known traditional Chinese herbal medicine with nourishing effects, contains bioactive ingredients such as saponins, polysaccharides and peptides. In this study, based on the pharmacological effects of ginsenosides on immune regulation, antitumour activity, and anti-inflammatory activity, we investigated the effect of American ginseng total saponins (AGS-Q) or American ginseng total saponins after transformation (AGS-H) on CTX mediated immunosuppression and its antitumour mechanism.

MATERIALS AND METHODS

Materials and Reagents

Aspartic acid (Asp), glutamic acid (Glu), arginine (Arg), histidine (His), and lysine (Lys) were purchased from Soledad Bao (Beijing, China). Ginsenosides Re, Rg_1, Rb_1, Rb_2, Rc, Rd, 20(S)-Rg_3, 20(R)-Rg_3, Rk_1 and Rg_5 were purchased from Shanghai Yuanye Biotechnology Co., Ltd., China, purity ≥98%. Chromatographic grade acetonitrile and methanol were purchased from Fisher (Waltham, MA, USA) and C_{18} Sep-Pak® SPE was purchased from Race Point Technology (Saifen Technology Co., Ltd., Ireland). An Ultrapure Water System (Water Purifier Co., Ltd., Chengdu, China) was used to obtain ultrapure water. The mouse S180 sarcoma cell line was obtained from Shanghai Institute of Biochemistry and Cell Biology, China. RPMI-1640 medium, fetal bovine serum (FBS), benzylpenicillin, and streptomycin were provided by Gibco (Grand Island, NY, USA). CTX was purchased from Shengdi Pharmaceutical Co., Ltd. (Jiangsu, China). Antibodies against T subpopulations, including fluorescein isothiocyanate (FITC)-conjugated rat anti-mouse CD4, allophycocyanin (APC)-conjugated rat anti-mouse CD8, and phycoerythrin (PE)-conjugated rat anti-mouse CD25, were obtained from BioLegend (San Diego, CA, USA). Anti-Caspase-3 (sc7272) antibody was purchased from Santa Cruz Biotechnology Inc. (Santa Cruz, CA, USA). Anti-Bcl-2 (ab182858), anti-Bax (ab32563), anti-GAPDH (ab8245) and horseradish peroxidase (HRP)- conjugated secondary antibodies were purchased from Abcam (Cambridge, MA, USA).

Source and Treatment of American Ginseng

The dried samples were purchased from Wanliang Ginseng Market in Fusong County, Jilin Province, China, and identified as American ginseng (4 years old) by Professor Li Wei for Jilin Agricultural University. The medicinal material was pulverized into a powder by a pulverizer (Dingli Medical Instrument Co., Ltd., Wenzhou, China), further processed through a 60-mesh stainless steel mesh and then stored in a cool dry place.

Amino Acid Screening

Five amino acids, including two acidic amino acids, Asp and Glu, and three basic amino acids, Arg, His, and Lys were chosen. The reaction conditions were a concentration of 5% amino acids, reaction time of 1 h, liquid-solid ratio of 20 mL/g, and a temperature of 120 °C. The extract was collected and filtered through a 0.22-μm filter. The analysis was performed using an Acquity Ultra High-Performance Liquid Chromatography

(UPLC) (Waters, Manchester, UK). The process was repeated three times for all samples.

Optimization of Reaction Conditions

First, four factors were investigated: reaction temperature (70–120 °C), concentration of amino acids (1–20%), liquid-solid ratio (5–50 mL/g), and reaction time (0.5–3 h). Second, according to the results of the above single factor experiments, orthogonal experiments were designed to optimize the conversion parameters (factors). The orthogonal experiments consisted of nine independent factors. The order of the experiments was random to ensure that the results were valid in this study. The process was repeated three times for all samples.

Optimization of Extraction Method

Four extraction methods were examined: reflux extraction (RE), heat extraction (HE), soak extraction (ME), and ultrasonic extraction (USE) for optimization of the extraction method. All extraction methods involved 2 g of American ginseng powder being accurately weighed. RE (19) involved American ginseng powder, 5% amino acid, and 100 mL of 70% ethanol solution left to react for 1.5 h. The supernatant was collected by filtration and the residue was extracted once, combined with the supernatant, and passed through a 0.22 μm filter. UPLC analysis was then repeated three times. HE (16) involved American ginseng powder and 5% amino acid added to 40 mL of distilled water and left to react at 110 °C for 2 h. The supernatant was collected and filtered through a 0.22-μm filter, and UPLC analysis was repeated three times. ME involved American ginseng powder and 5% amino acid extracted three times in 40 mL of distilled water for 6 h. The supernatant was collected and filtered through a 0.22-μm filter, and UPLC analysis was repeated three times. USE (20) involved American ginseng powder and 5% amino acid in triplicate added to 100 mL of 50% ethanol solution and left to react in a 250-W ultrasonic wave (Hubei Dingtai Biochemical Technology Equipment Manufacturing Co., Ltd.) for 1 h. The supernatant was collected and filtered through a 0.22-μm filter, and UPLC analysis was repeated three times.

Verification of the Transformation Pathway

Eight pure ginsenosides were selected, including two common PPT types: Re and Rg_1, four common PPD types: Rb_1, Rb_2, Rc, Rd, and two rare ginsenosides 20(S)-Rg_3 and 20(R)-Rg_3. The reaction conditions of the optimized ginsenosides Rk_1 and Rg_5 were used to simulate and verify their transformation pathways.

UPLC Analysis

Chromatographic Conditions

Columns ACQUITY UPLC® BEH C_{18} (2.1 mm × 50 mm, 1.7 μm); mobile phase of water (A)-acetonitrile (B), elution program (0∼5.80 min, 87%∼78% A; 5.80∼18.75 min, 78%∼62% A; 18.75∼22.05 min, 62%-60% A; 22.05∼23.55 min, 60%∼55% A; 23.55∼24.25 min, 55%∼42% A; 24.25∼30.00 min, 42%∼38% A; 30.00∼30.75 min, 38%∼20% A; 30.75∼37.75 min, 20%∼0% A; 37.75∼40 min, 0%∼87% A); column temperature was 35 °C; flow rate was 0.4 mL/min; injection volume was 3 μL; detection wavelength was 203 nm.

Preparation of the Drawing Standard Curves

First, 5 mg of ginsenosides Rk_1 and Rg_5 were weighed and dissolved in methanol in a 5 mL volumetric flask. A mixed standard of 0.1, 0.2, 0.4, 0.8, and 1.6 mL into a 5 mL volumetric flask chromatography methanol solution was prepared. The standard curve was drawn with the concentration as the abscissa and the peak area as the ordinate. The regression equation of ginsenoside Rk_1 was $Y = 2.63e + 6X\text{-}2.38e + 4$, $R2 = 0.9996$, linear range was 0.0208–0.3328 mg/mL; the regression equation of ginsenoside Rg_5 was $Y = 9.36e + 6X\text{–}8.19e + 4$, $R^2 = 0.9998$, and linear range was 0.0206–0.3296 mg/mL.

Preparation of Total Saponins From American Ginseng

According to the method of amino acid transforming rare saponins in American ginseng, the optimal transformation conditions were selected. The rare saponins in American ginseng were transformed to obtain the transformed extract. Purification of D101 macroporous resin was performed. Ethanol gradient elution was used to obtain the eluted total saponin solution, which was concentrated and freeze-dried to obtain freeze-dried powder of the total saponin of *Panax quinquefolium* before (AGS-Q) and after the transformation (AGS-H).

Animals Treatment and Experimental Procedure

SPF ICR mice (18–22 g) were provided by Changsheng Biotechnology Co., Ltd. (Liaoning, China) were raised in a 12 h light/dark cycle at 23 ± 1°C, relative humidity of 50 ± 5% environment. Mice had a free access to water and foods during the adaptation period. All experiments were executed strictly according to the Principle of Laboratory Animal Care and the guidelines prescribed by the Animal Research Committee of the Institute of Special Animals and

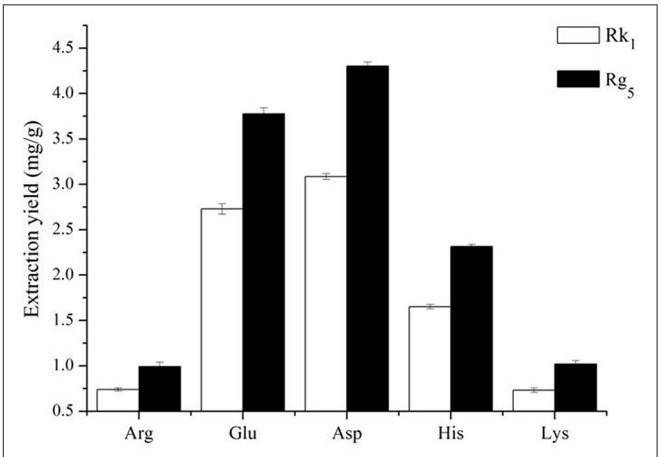

FIGURE 1 | Effect of different amino acids on the contents of ginsenosides Rk_1 and Rg_5 ($n = 3$).

Plants Sciences, Chinese Academy of Agricultural Sciences (Permit No.: ECLA-ISAP-18079). Each mouse was injected with 0.2 mL S180 cell suspension at a concentration of 1×10^5 cells/mL in the right axilla to establish the S180 tumour-bearing mouse model.

After 24 h, these mice were randomly divided into: the model group, CTX (25 mg/kg), CTX + AGS-QL (25 mg/kg + 100 mg/kg), CTX + AGS-QM (25 mg/kg+200 mg/kg), CTX+AGS-QH (25 mg/kg + 400 mg/kg), CTX + AGS-HL (25 mg/kg + 100 mg/kg), CTX + AGS-HM (25 mg/kg + 200 mg/kg), and CTX + AGS-HH (25 mg/kg + 400 mg/kg).

After inoculation, the mice were divided into the model group, CTX group (25 mg/kg), AGS-HL and AGS-HH groups (200 and 400 mg/kg), and CTX/2 + AGS-HL group (12.5 mg/kg + 200 mg/kg), CTX/2 + AGS-HH (12.5 mg/kg + 400 mg/kg).

Mice were given AGS daily by gavage and intraperitoneal injection of CTX for 14 consecutive days. Mice in the normal group were intragastrically injected with normal saline. After the last administration, the mice were fasted for 12 h. The mice were anesthetized and sacrificed after blood collection. The tumor and spleen were stripped and weighed, fixed with 10% formalin and stored at−80 °C.

ELISA Analysis

After the tests, blood were isolated immediately. The serum was separated by centrifugation at 3000 rpm for 30 min at 4 °C. Serum and tissue samples were frozen at −80 °C for subsequent analysis. Mouse IL-2 and IL-10 levels in serum were measured by enzyme-linked immunosorbent assay (ELISA) kits of Ebioscience (California, USA).

Mouse Leukocyte Assay and Splenic T-Lymphocyte Subpopulation Assay

For the splenic T-lymphocyte subpopulation assay, the splenocyte suspension was adjusted to 1×10^6 cells/mL and subjected to flow cytometry to measure the splenocyte lymphocyte subpopulations. The splenocyte surface markers were labeled with fluorescein isothiocyanate (FITC)-conjugated anti-mouse CD4, APC-conjugated anti-mouse CD8, and PE-conjugated anti-mouse CD25. The labeled cells were washed twice, resuspended in staining buffer (BioLegend), and analyzed using a FACSCalibur (BD Medical Technologies, Franklin Lakes, NJ, USA) and CellQuest software. For comparison, the cells stained with isotype-matched antibodies were used to calibrate the FACSCalibur instrument settings.

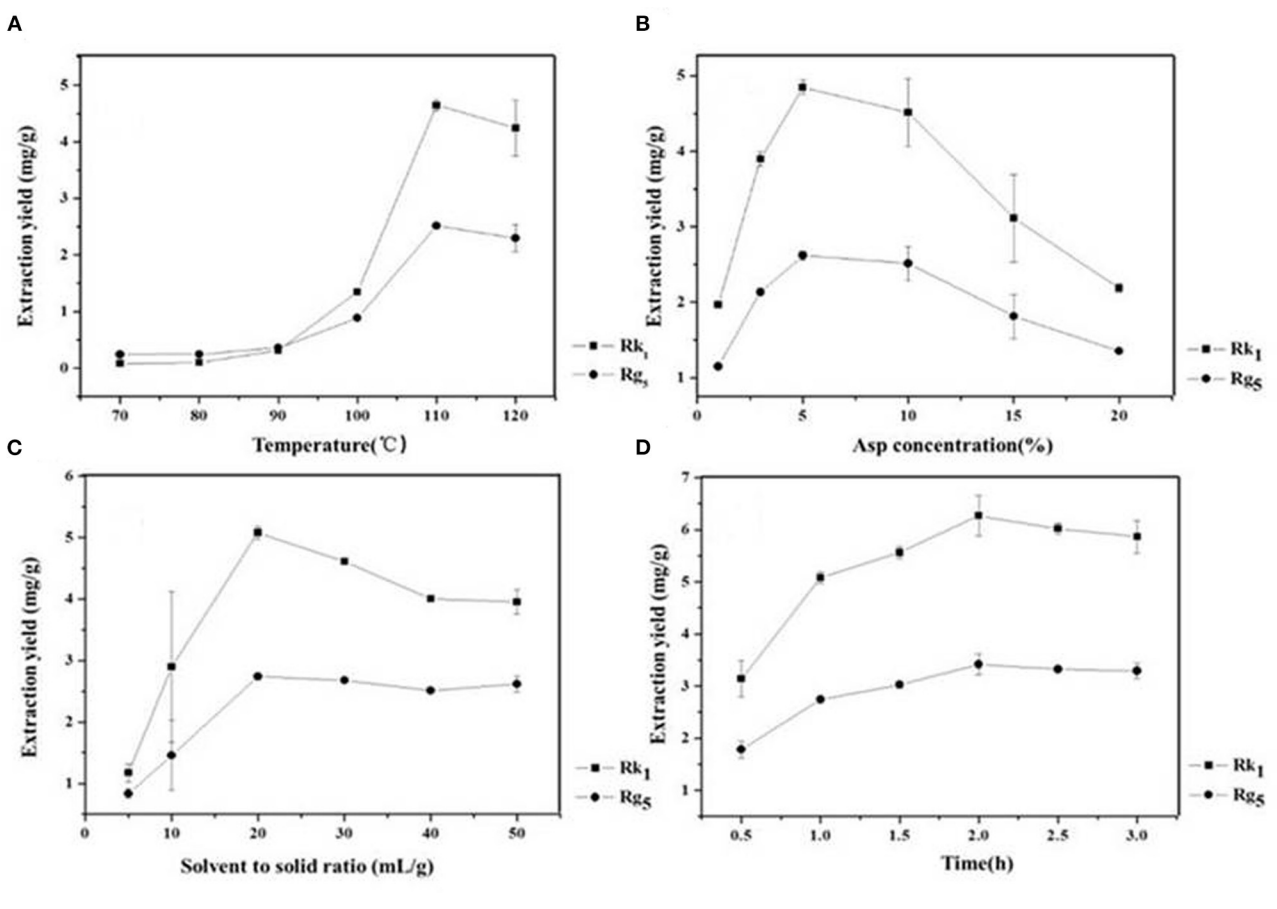

FIGURE 2 | Effect of reaction **(A)** temperature **(B)** Asp concentration **(C)** liquid-solid ratio and **(D)** reaction time on the conversion content of rare ginsenosides Rk_1 and Rg_5 ($n = 3$).

Western Blotting

The protein extracted from tumor with lysis buffer. SDS-PAGE (8–12%) gels were used to separate equal amounts of the protein, and then proteins were transferred onto PVDF membranes. The membranes were incubated with blocking solution (5% skim milk) for 1 h and then specific primary antibodies, including Bax, Bcl-2, cleaved-Caspase-3 and GAPDH antibodies, followed by an HRP-conjugated secondary antibody. Finally, the target proteins were visualized using a BeyoECL Plus Kit (Beyotime Biotechnology, Shanghai, China), and analyzed by densitometry with Image-Pro Plus 6.0 (Media Cybernetics Inc., Rockville, MD, USA).

Statistical Analysis

Data are represented as the mean±SD. All data's were analyzed using one-way ANOVA and Tukey's multiple comparisons test. Statistically significant differences in p values between groups were considered as < 0.05. All statistical analyses were performed using GraphPad Prism version 5 (GraphPad Software, San Diego, CA, USA).

RESULTS

Effect of Amino Acids on the Conversion Rates

The effect of different amino acids on the conversion rates of Rk_1 and Rg_5 is shown in **Figure 1**. The conversion rates of Rk_1 and Rg_5 using five different amino acids were significant ($P < 0.05$). The transformation effects of Asp, Glu, His, Lys and Arg on Rk_1 and Rg_5 were successively weakened. The transformation of Rk_1 and Rg_5 by acidic amino acids was significantly higher than that by alkaline amino acids ($P < 0.05$). The effect of Glu on the conversion rates of Rk_1 and Rg_5 was 2.73 ± 0.06 mg/g and 3.78 ± 0.07 mg/g, respectively. The effect of Asp on the conversion rates of Rk_1 and Rg_5 was 3.08 ± 0.03 mg/g and 4.30 ± 0.04 mg/g, respectively, with the best conversion rate. This was consistent with results from Xia Juan (21). Compared with strong acids, the conversion rates of rare ginsenosides can be increased by 1.28 times, so Asp was selected as the best catalyst (22).

Effect of Temperature, Asp Concentration, Liquid to Solid Ratio and Time on the Conversion Rates

Temperature is an important factor that affects the formation of rare ginsenosides. The results show that the conversion rates of the rare ginsenosides Rk_1 and Rg_5 increased gradually and tended to be stable (**Figure 2A**). At 110 °C, the conversion rates of Rk_1 and Rg_5 were the highest, 4.65 ± 0.10 mg/g and 2.52 ± 0.05 mg/g, respectively, which were significantly different from those of the first 4 groups ($P < 0.05$). Although the conversion rates at 110°C were higher than those achieved at 120°C, there was no significant difference between the two groups. Considering large-scale production, 110°C is easier to achieve with less energy consumption and a higher conversion rate. Therefore, 110°C was finally selected as the reaction temperature (**Figure 2A**). The concentration of the amino acid has a direct effect on the conversion rates of ginsenosides. The results showed that as the concentration of Asp increased (1–5%), the conversion rates of the rare ginsenosides Rk_1 and Rg_5 also increased, as shown in **Figure 2B**. With 5% Asp, the highest conversion rates of Rk_1 and Rg_5 were reached, 4.84 ± 0.09 mg/g and 2.62

TABLE 1 | Comparison of extraction methods.

Method	Extraction yield (mg/g)	
	Ginsenoside Rk_1	Ginsenoside Rg_5
RE	2.89 ± 1.22	1.45 ± 0.57
HE	6.27 ± 0.39	3.42 ± 0.19
ME	0.10 ± 0.02	0.24 ± 0.01
USE	1.35 ± 0.02	0.88 ± 0.01

TABLE 2 | Orthogonal test design and results.

Desgin ID number	Factor				Extraction yield (mg/g)	
	(A) Temperature (°C)	(B) Asp concentration (%)	(C) Solvent to solid ratio (mL/g)	(D) Time (h)	Rk_1	Rg_5
1	$A_1 = 100$	$B_1 = 3$	$C_1 = 10$	$D_1 = 2$	2.37	1.65
2	$A_1 = 100$	$B_2 = 5$	$C_2 = 20$	$D_2 = 2.5$	3.94	2.88
3	$A_1 = 100$	$B_3 = 10$	$C_3 = 30$	$D_3 = 3$	3.22	2.49
4	$A_2 = 110$	$B_1 = 3$	$C_2 = 20$	$D_3 = 3$	4.35	2.85
5	$A_2 = 110$	$B_2 = 5$	$C_3 = 30$	$D_1 = 2$	5.84	4.08
6	$A_2 = 110$	$B_3 = 10$	$C_1 = 10$	$D_2 = 2.5$	4.83	3.07
7	$A_3 = 120$	$B_1 = 3$	$C_3 = 30$	$D_2 = 2.5$	4.07	2.79
8	$A_3 = 120$	$B_2 = 5$	$C_1 = 10$	$D_3 = 3$	5.14	3.45
9	$A_3 = 120$	$B_3 = 10$	$C_2 = 20$	$D_1 = 2$	2.85	2.37
K_1	5.52	6.04	6.84	6.39		
K_2	8.34	8.44	6.42	7.19		
K_3	6.89	6.27	7.49	7.18		
R	2.82	2.40	1.07	0.80		

TABLE 3 | Analysis of variance of orthogonal test.

Factors	SS	df	MS	F	P	Significant
A	11.960	2	5.9800	7.928	0.0406	*
B	10.509	2	5.2545	6.967	0.0497	*
C	1.747	2	0.8735	1.158	0.401	
D	1.270	2	0.6350	0.842	0.495	
Erro	3.02	4				
Total	25.486	8				

$F_{0.05}$ (2,4) = 6.940

SS, Sum of square; df, Degree of freedom; MS, Mean of square; F, F-value.

**P<0.05 (F >$F_{0.05}$ (2,4), (A) Temperature (B) Asp Concentration (C) Solvent to solid ratio (D) Time.*

± 0.05 mg/g, respectively, and were significantly higher than those of the other groups ($P < 0.05$). When the concentration of the amino acid exceeded 5%, the conversion rates of the rare ginsenosides gradually decreased. Therefore, the optimum concentration of Asp was finally selected to be 5% (**Figure 2B**). The effect of the liquid-solid ratio on the conversion rates of the rare ginsenosides Rk_1 and Rg_5 is shown in **Figure 2C**. With an increase in the liquid-solid ratio, the conversion rates of Rk_1 and Rg_5 initially increased and then decreased. The conversion rates of Rk_1 and Rg_5 reached their highest values at 20 mL/g, 5.08 ± 0.11 mg/g and 2.74 ± 0.05 mg/g, respectively, and were significantly higher than those of other five groups ($P < 0.05$). The optimum liquid to solid ratio was finally selected to be 20 mL/g (**Figure 2C**). The effect of reaction time on the conversion rates of Rk_1 and Rg_5 is shown in **Figure 2D**. Rare ginsenosides, Rk_1 and Rg_5, gradually increased with increasing reaction time. The conversion rates of Rk_1 and Rg_5 reached their highest values at 2 h, 6.27 ± 0.39 mg/g and 3.42 ± 0.19 mg/g, respectively, and were significantly higher than those of the first three groups ($P < 0.05$). When the reaction time exceeded 2 h, the conversion rate of Rk_1 and Rg_5 did not continue to increase, and there was no significant difference between the conversion content obtained at 2 h ($P < 0.05$). This may be because as the reaction time increases, the substrate is continuously consumed, and the effective collision decreases after the active ingredient reaches the maximum value, so the content changes tend to remain the same. Considering the principle of large-scale production in the future, low energy consumption and high yield, 2 h was selected as the best reaction time (**Figure 2D**).

Effect of Extraction Methods on the Conversion Rates

The choice of extraction method depends mainly on the advantages and disadvantages of each extraction technique and its impact on the extraction rate. The traditional extraction methods of ginsenosides mainly include decocting, dipping and reflow. In the Chinese pharmacopeia, ginsenosides are mainly treated by ultrasound, so we chose the above four methods RE, HE, ME, and USE for comparison. The results were are shown in **Table 1**. After adding the amino acids, HE produced the highest conversion rates of Rk_1 and Rg_5, which were 6.27 ± 0.39 mg/g and 3.42 ± 0.19 mg/g, respectively, RE was second best, and the conversion rates of USE were not ideal. The conversion of Rk_1 and Rg_5 by HE was twice as high as that by RE and four times as high as that by USE. This may be because temperature was an important factor in the conversion of rare ginsenosides by amino acids (23). Therefore, HE was more suitable for the conversion of Rk_1 and Rg_5, and HE was simple and easy to mass produce.

Orthogonal Test Results

Due to a number of factors needed for the conversion of rare ginsenosides, there are certain factors used to optimize the extraction process. Through the results of the previous single factor test, the final selection was based on the reaction temperature (°C), reaction time (h), amino acid concentration (%), and liquid-solid ratio (mL/g) as the investigation factors, and each factor was set at three levels. The L_9 (3^4) orthogonal test design table was carried out for nine tests. The orthogonal design and measurement results are shown in **Tables 2**, **3**. Variance analysis results showed that the concentration of Asp and the

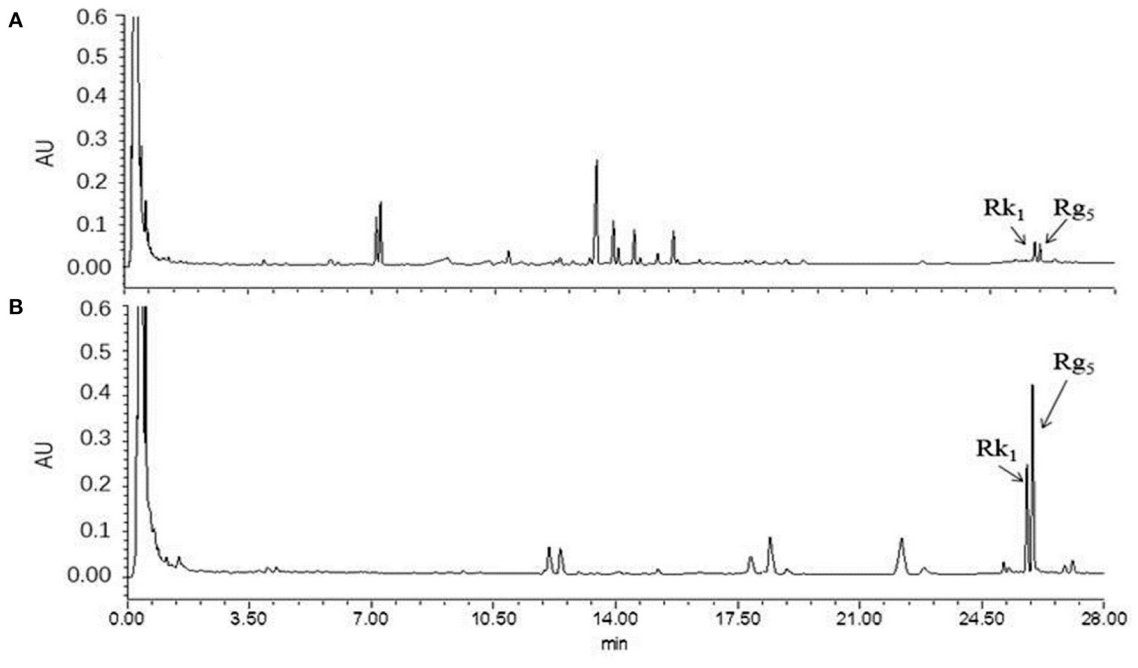

FIGURE 3 | UPLC diagram before and after the reaction of American ginseng. **(A)** before reaction, **(B)** after reaction ($n = 3$).

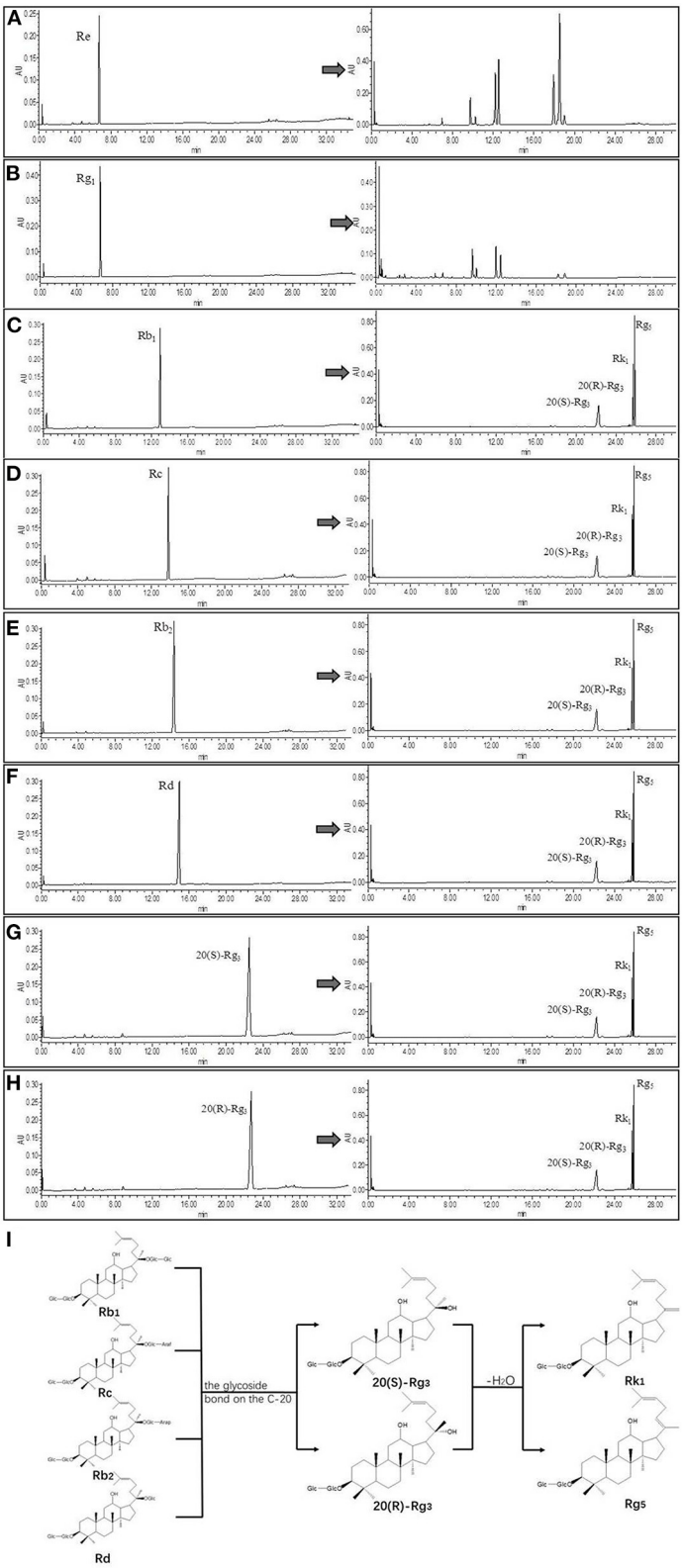

FIGURE 4 | UPLC comparison chart before and after monomeric saponin conversion ($n = 3$). **(A–H)** is a comparison of UPLC before and after transformation of ginsenoside Re, ginsenoside Rg_1, ginsenoside Rb_1, ginsenoside Rc, ginsenoside Rb_2, ginsenoside Rd, ginsenoside 20(S)-Rg_3, and ginsenoside 20(R)-Rg_3. **(I)** Transformation pathway of ginsenosides Rk_1 and Rg_5 in protopanaxadiol saponins.

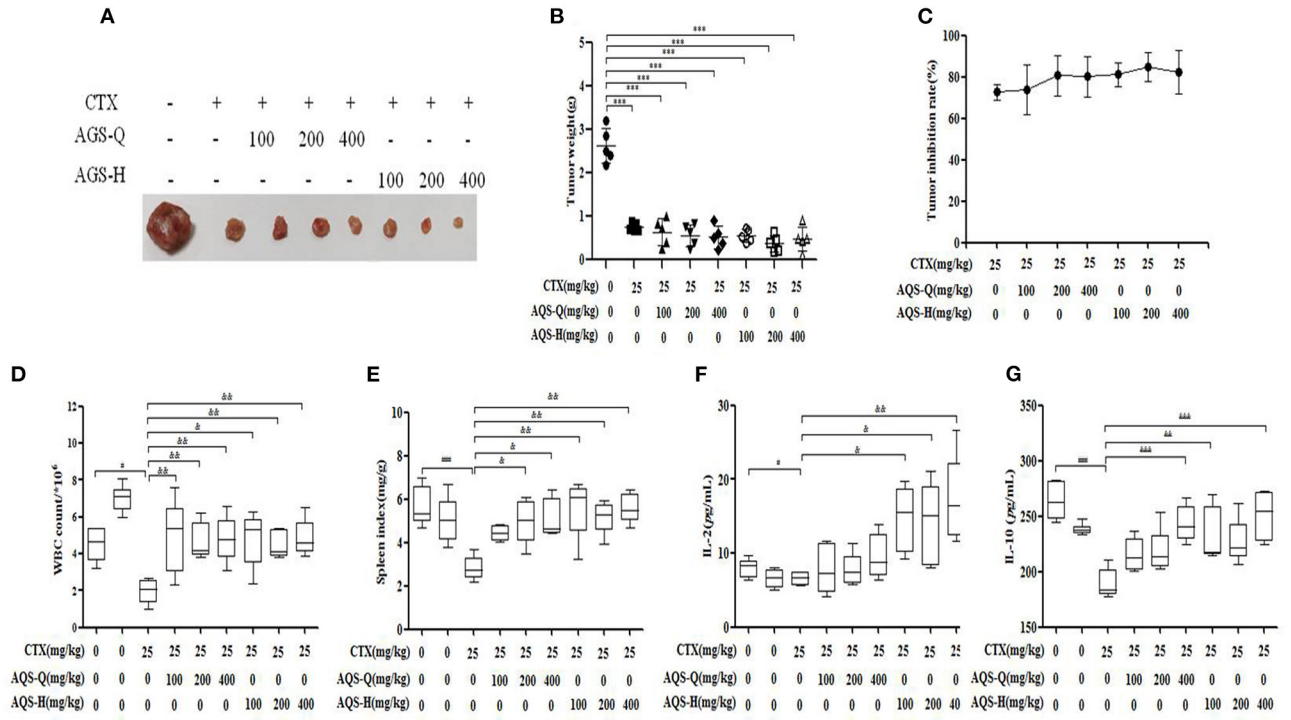

FIGURE 5 | Effects of AGS-Q or AGS-H synergistic CTX on tumor inhibition and immune indexes ($n = 8$). **(A)** Tumor image. **(B)** Tumor weight. **(C)** Tumor inhibition rate. **(D)** The white blood cells count. **(E)** Spleen index. **(F)** The content of IL-2. **(G)** The content of IL-2. Values are presented as mean ± SD. vs. normal group, $^{\#\#}P < 0.01$; vs. model group, $^{***}P < 0.001$; vs. CTX group, $^{\&}P < 0.05$, $^{\&\&}P < 0.01$, $^{\&\&\&}P < 0.001$.

reaction temperature had significant effects on the conversion rates of the rare ginsenosides Rk_1 and Rg_5 ($P < 0.05$) and the liquid-solid ratio and reaction time had no significant effect on the conversion rates. Range analysis was used to show that the effect of the four factors on Rk_1 and Rg_5. The results were Asp concentration>reaction temperature>solid-liquid ratio>time, and the *F value* result was consistent with the variance analysis. The optimal transformation conditions for amino acid hydrolysis of American ginseng to transform to the rare ginsenosides Rk_1 and Rg_5, are as follows: 5% Asp, 110°C reaction temperature, 30 mL/g solid-liquid ratio, and 2.5 h reaction time. The optimal conversion process was verified and the total content of Rk_1 and Rg_5 was 10.25 ± 0.32 mg/g. The UPLC comparison chart of American ginseng before and after the reaction is shown in **Figure 3**.

Confirmation of Transformation Pathway

Referring to the experimental results of Liu Z (16, 24), we selected eight pure ginsenosides to confirm the transformation pathway of the rare ginsenosides Rk_1 and Rg_5. The UPLC comparison before and after the conversion of pure ginsenosides is shown in **Figure 4**. The PPD types, Rc, Rd, Rb_1, and Rb_2 were completely converted into the rare ginsenosides 20(S)-Rg_3, 20(R)-Rg_3, Rk_1, and Rg_5 under the optimal conditions of this experiment. Under these conditions, ginsenosides 20(S)-Rg_3 and 20(R)-Rg_3 were partially converted to Rk_1 and Rg_5; the PPT types Rg_1 and Re did not generate Rk_1 and Rg_5. This is consistent with the possible reaction pathway of ginsenosides as explained in the ginseng pyrolysis study (20). The reaction pathway is shown in **Figure 4**. The PPD types cleave at the C-20 position to form the intermediate products 20(S)-Rg_3 and 20(R)-Rg_3, and further dehydration and hydrolysis occur to transform them to Rk_1 and Rg_5. In this paper, the addition of Asp increased the yield of rare ginsenosides. This may be due to the fact Asp is an acidic amino acid and H^+ promotes the hydrolysis reaction (25). Moreover, the content of PPD types is high in American ginseng, which provides the necessary conditions for the conversion of rare ginsenosides.

Effect of AGS Synergistic CTX on S180 Tumor-Bearing Mice on Tumor Inhibition and Immune Indices

CTX is a broad-spectrum anticancer drug that has a good inhibitory effect on malignant tumors, but has obvious toxic side effects. It can cause loss of appetite, nausea, weight loss and adverse reactions such as decreased white blood cells (23). IL-2 and IL-10 are a type of cell growth factor in the immune system that can regulate the cell activity of white blood cells in the immune system, promote the proliferation of Th0 cells and CTLs, and also participate in the antibody response, haematopoiesis and tumor surveillance (26). Compared with the model group, mice treated with CTX, American ginseng total saponins (AGS-Q)

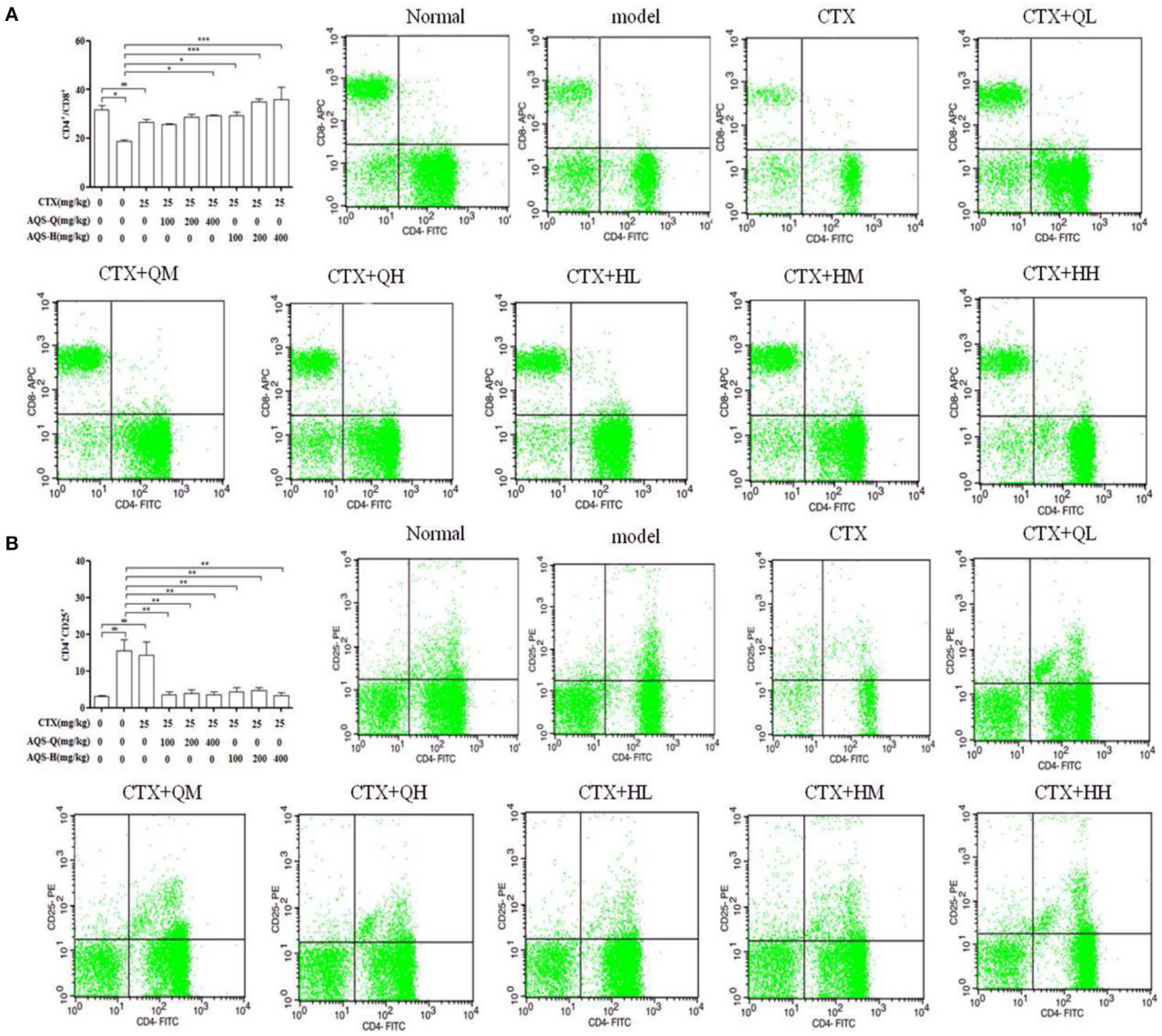

FIGURE 6 | Flow scatter plot of T lymphocyte subsets ($n = 8$). Percentage of T lymphocyte subsets and **(A)** $CD4^+/CD8^+$, **(B)** $CD4^+CD25^+$ T lymphocyte ratio. Values are presented as mean ± SD. vs. normal group, $^{\#\#}P < 0.01$, $^{\#\#\#}P < 0.001$; vs. model group, $^{*}P < 0.05$, $^{***}P < 0.001$.

or American ginseng total saponins after transformation (AGS-H) synergistic CTX can significantly reduced tumor weights, as shown in **Figure 5B** ($P < 0.001$). Compared with the normal group, CTX significantly reduced the white blood cell count, spleen index and IL-2 and IL-10 content ($P < 0.05$, $P < 0.001$), which showed obvious immunosuppressive side effects. AGS-Q synergistic CTX enhanced the spleen index, white blood cell count and IL-10 content compared with the CTX group ($P < 0.05$, $P < 0.001$). AGS-H synergistic CTX enhanced the spleen index, white blood cell count, and IL-2 and IL-10 contents compared with the CTX group ($P < 0.05$, $P < 0.001$). The AGS-H synergistic CTX group improved the immune indices better than the AGS-Q group.

Effect of AGS Synergistic CTX on Splenic T-Lymphocyte Subpopulations

Splenocytes consist of various immune cells, including T or B lymphocytes, macrophages, and dendritic cells. T cell subpopulations have a great importance in T cell homeostasis and immune regulation, and the T lymphocyte phenotype is mainly divided into $CD3^+$, $CD4^+$ and $CD8^+$ T cells (27). Compared with the normal group in **Figure 6**, CTX significantly decreased the $CD4^+/CD8^+$ ratio, and enhanced the $CD4^+CD25^+$ content ($P < 0.001$). Compared with the model group in **Figure 6**, AGS-Q synergistic CTX can significantly restored the ratio of $CD4^+/CD8^+$ cells and significantly inhibited the level of $CD4^+CD25^+$ ($P < 0.001$). AGS-H synergistic CTX

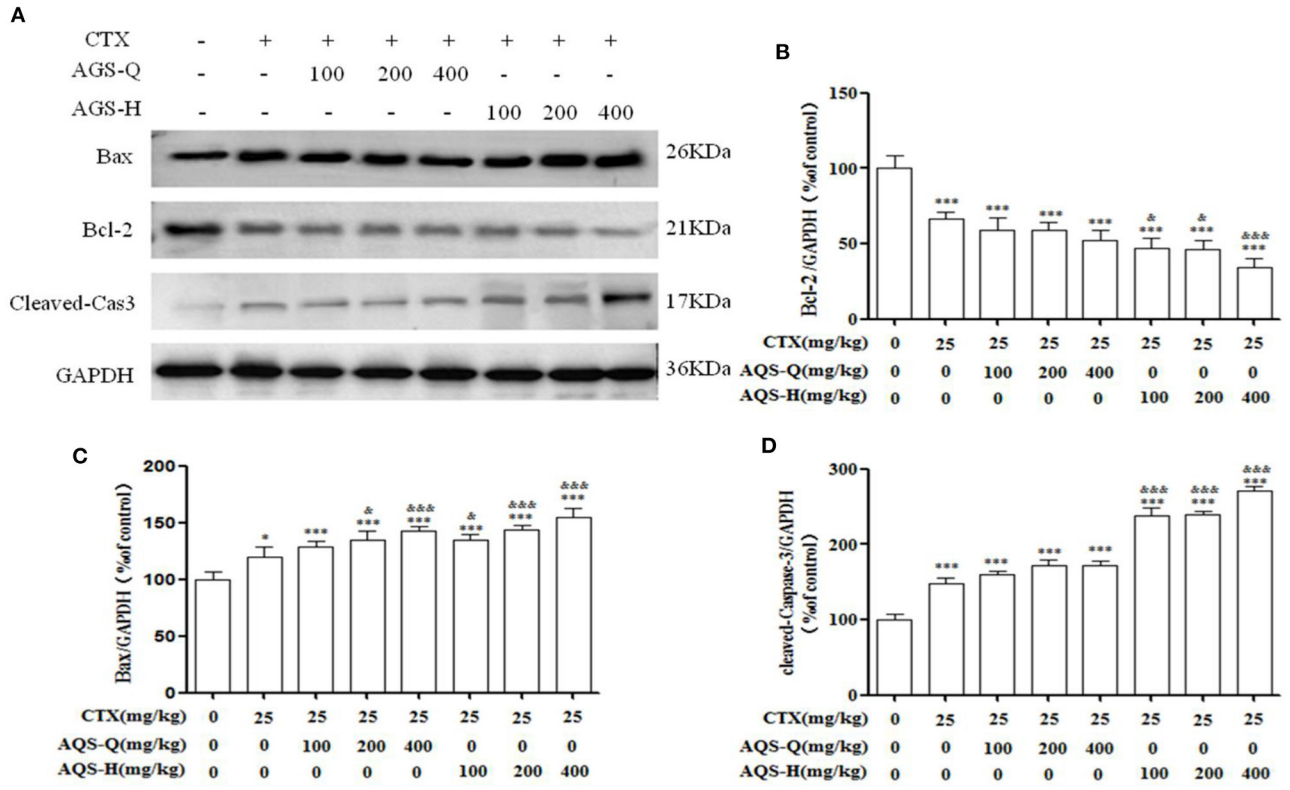

FIGURE 7 | Effects of AGS synergistic CTX on Bcl-2, Bax and cleaved-Caspase-3 in S180 tumor-bearing mice ($n = 8$). **(A)** The protein expression levels of Bcl-2, Bax and cleaved-Caspase-3 were detected by Western blotting. **(B)** The relative Bcl-2 expression level. **(C)** The relative Bax expression level. **(D)** The relative cleaved-Caspase-3 expression level. Values are presented as mean ± SD. vs. model group, $^{*}P < 0.05$, $^{**}P < 0.01$, $^{***}P < 0.001$; vs. CTX group, $^{\&}P < 0.05$, $^{\&\&}P < 0.01$, $^{\&\&\&}P < 0.001$.

can significantly restored the ratio of $CD4^{+}/CD8^{+}$ cells and significantly inhibited the level of $CD4^{+}CD25^{+}$ ($P < 0.001$). The results indicated that the AGS can restore the damaged splenic T lymphocyte subsets.

Effect of AGS Synergistic With CTX on Tumor Apoptosis in S180 Tumor-Bearing Mice

In order to explore the effect of AGS synergistic with CTX on the tumor apoptosis. We detected the effects of AGS-Q and AGS-H on Bax, Bcl-2 and cleaved-Caspase-3 proteins in tumor tissue (**Figure 7**). Compared with the model group, CTX significantly upregulated the expression of Bax and cleaved-Caspase-3, and inhibited the expression of antiapoptotic protein Bcl-2 ($P < 0.05$, $P < 0.001$). AGS-Q or AGS-H synergistic with CTX significantly upregulated the expression of Bax and cleaved-Caspase-3, and inhibited the expression of antiapoptotic protein Bcl-2 in a dose-dependent manner ($P < 0.001$). In comparison with CTX, AGS-Q synergistic with CTX increased the expression of Bax. AGS-H synergistic with CTX significantly inhibited the expression of Bcl-2 and promoted Bax and cleaved-Caspase-3 in tumor tissues ($P < 0.05$, $P < 0.001$). The AGS-H synergistic CTX group had a higher level of promoting tumor apoptosis protein expression than the AGS-Q synergistic CTX group.

Effect of AGS-H Synergistic CTX/2 on Tumor Inhibition and Immune Indices

The tumor weight in the model group was more than 1 g, indicating that S180 tumor-bearing mice were successfully inoculated. Compared with the model group, the CTX, AGS-L and AGS-H groups had significantly reduced tumor weight and inhibited tumor growth ($P < 0.05$, $P < 0.001$). CTX/2 + AGS-HL or AGS-HH significantly reduced tumor weight (**Figures 8A,B**). The spleen and white blood cells are an important part of the immune system and protect the body from infectious diseases and pathogens. Compared with the normal group, the number of white blood cells significantly increased, and the levels of the immune factors IL-2 and IL-10 were significantly decreased in the model group ($P < 0.05$, $P < 0.01$, $P < 0.001$). CTX significantly reduced white blood cell counts, spleen index and IL-10 levels in mice ($P < 0.01$). Compared with the CTX group, AGS-HL, AGS-HH and CTX/2 + AGS-HL or HH significantly increased the white blood cell count and serum IL-10 content ($P < 0.05$, $P < 0.01$, $P < 0.001$). AGS-HL, AGS-HH and CTX/2 + AGS-HH increased the spleen index ($P < 0.05$, $P < 0.01$). AGS-HH

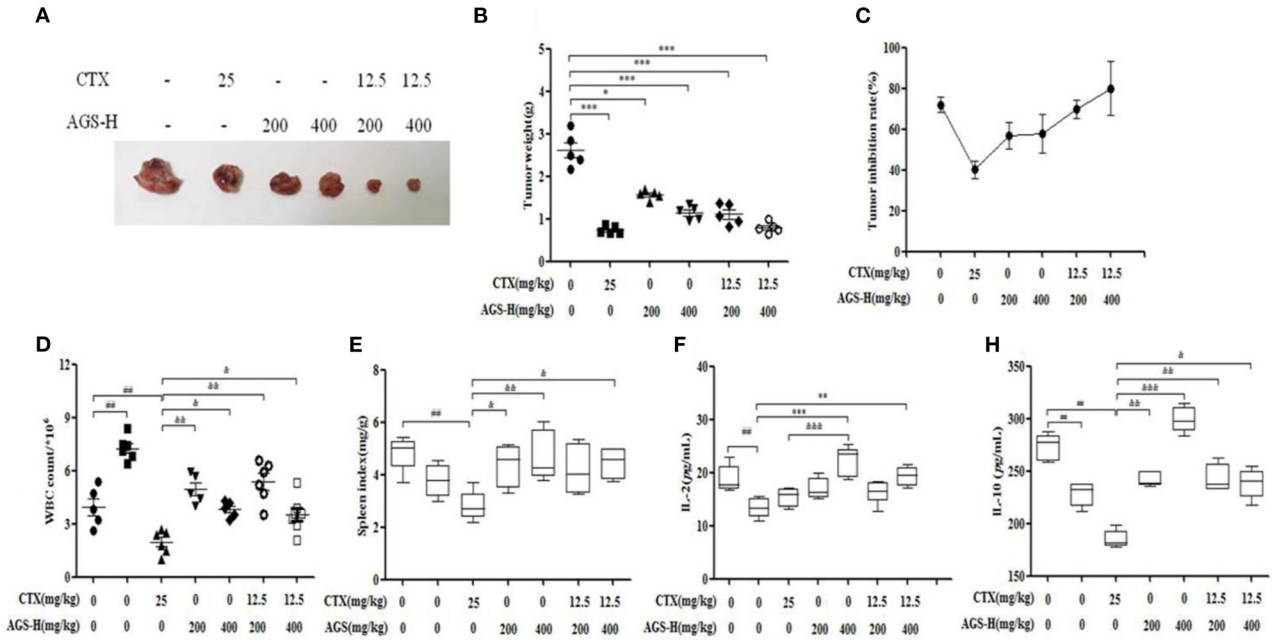

FIGURE 8 | Effects of CTX/2 + AGS-H on tumor inhibition and immune indexes ($n = 8$). **(A)** Tumor image. **(B)** Tumor weight. **(C)** Tumor inhibition rate. **(D)** The white blood cells count. **(E)** Spleen index. **(F)** The content of IL-2. **(G)** The content of IL-10. Values are presented as mean ± SD. vs. normal group, $^{\#\#}P < 0.01$; vs. model group, $^{*}P < 0.05$, $^{**}P < 0.01$, $^{***}P < 0.001$; vs. CTX group, $^{\&}P < 0.05$ $^{\&\&}P < 0.01$, $^{\&\&\&}P < 0.001$.

significantly increased IL-2 levels ($P < 0.001$). These results suggest that AGS-H can improve the development of immune organs in tumor-bearing mice, upregulate the number of white blood cells to enhance cellular immunity, and regulate the effects of the immune factors IL-2 and IL-10.

Effects of AGS-H Synergistic CTX/2 on Lymphocyte Subsets of S180 Tumor-Bearing Mice

In **Figure 9**, compared with the normal group, we observed that the $CD4^+/CD8^+$ T cell ratio was significantly decreased, and the content of $CD4^+CD25^+$ T cells was significantly increased in the model and CTX groups ($P < 0.05$, $P < 0.001$). Compared with the CTX group, AGS-HH and AGS-HH synergistic CTX/2 treatment slightly enhanced $CD4^+/CD8^+$ ($P < 0.05$). Treatment with AGS-HL and AGS-HH caused a significant decrease of $CD4^+CD25^+$ ($P < 0.001$). Treatment with AGS-HL or AGS-HH synergistic CTX/2 caused a significant decrease in $CD4^+CD25^+$ ($P < 0.001$). These results indicated that the AGS-H synergistic with CTX/2 administration group could restore the damaged T lymphocyte subsets of the spleen.

Effects of AGS-H Synergistic CTX/2 on Apoptotic Proteins in S180 Tumor-Bearing Mice

As shown in **Figure 10**, compared with the S180 tumor-bearing mice model group, the expression of the antiapoptotic factor Bcl-2 was decreased in the AGS-H and AGS-H synergistic with CTX/2 groups ($P < 0.05$, $P < 0.001$), which significantly increased the expression of the apoptosis factors Bax and cleaved-Caspase-3 ($P < 0.05$, $P < 0.001$) in a dose-dependent manner. Compared with the CTX group, AGS-H and AGS-H synergistic CTX/2 treatment significantly inhibited the level of Bcl-2 in tumor tissues. AGS-HL synergistic CTX/2 significantly promoted the expression of Bax ($P < 0.01$). AGS-HH synergistic with CTX/2 increased the content of cleaved-Caspase-3 ($P < 0.05$). The results showed that AGS-H synergistic CTX/2 administration induced apoptosis in S180 tumor tissue.

DISCUSSION

Ginsenosides are the main active components in *Panax* ginseng and *Panax quinquefolium* L. With different processing methods, the contents and types of ginsenosides in ginseng also changed, and new ginsenosides were generated. Studies have shown that cooking ginseng at high temperature can change the species of ginsenosides and transform them into less polar ginsenosides. In acidic environments, ginsenosides are usually transformed by deglycosylation (24, 28). Therefore, temperature and pH value are the key factors for the transformation of ginsenosides. Liu discussed that aspartic acid could effectively degrade ginsenosides into rare ginsenosides, and the concentration of ginsenoside Rg5 increased with temperature, which also proved that ginsenosides could be transformed into rare ginsenosides by heating and adding aspartic acid (16).

In our study, the effects of the types of amino acids and extraction methods on the conversion of common ginsenosides

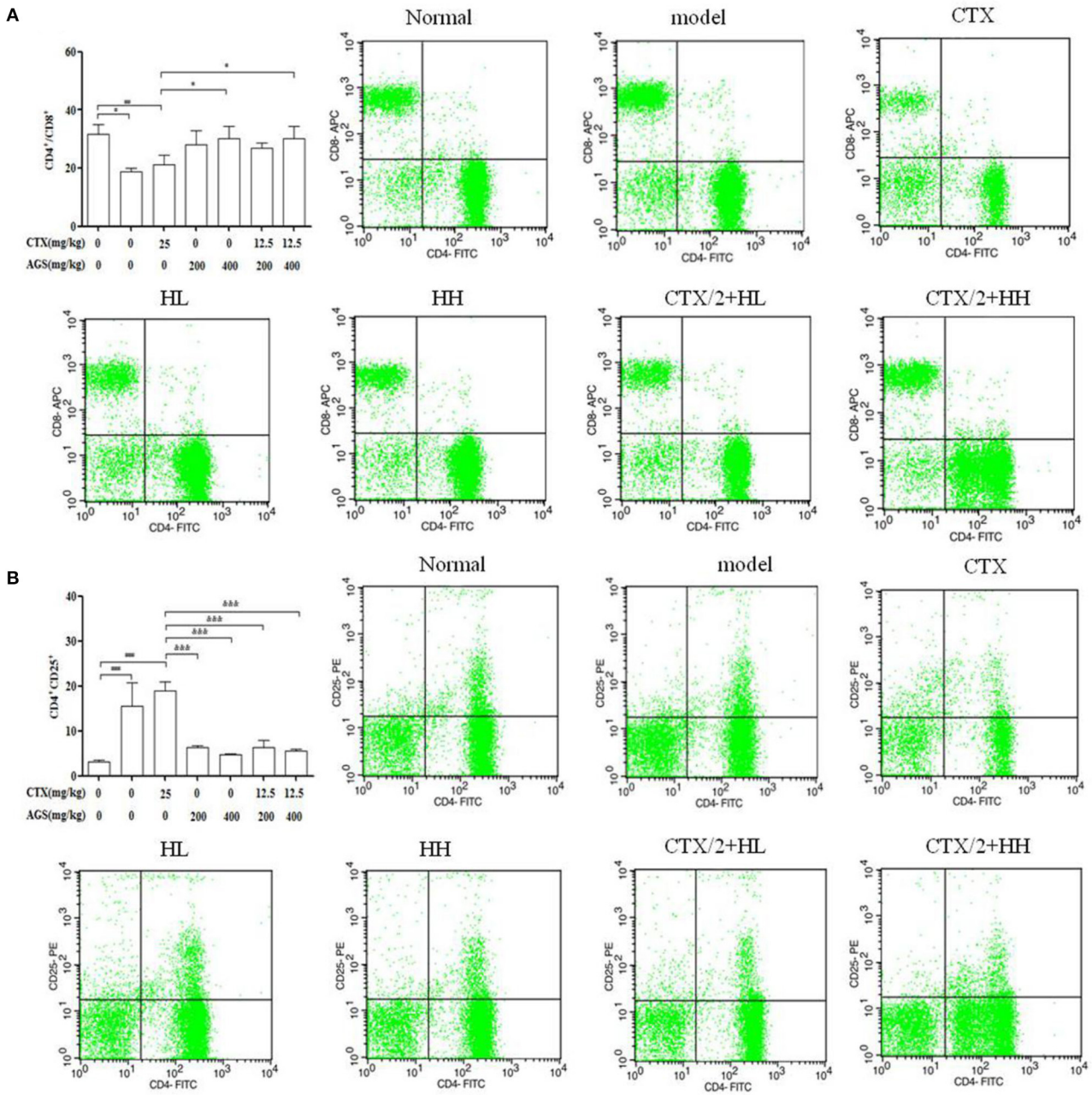

FIGURE 9 | Effects of AGS-H synergistic CTX/2 on lymphocyte subsets in S180 tumor-bearing mice ($n = 8$). **(A)** $CD4^+/CD8^+$. **(B)** $CD4^+CD25^+$. Values are presented as mean ± SD. vs. normal group, $^{\#}P < 0.05$, $^{\#\#\#}P < 0.001$; vs. model group, $^{*}P < 0.05$, $^{**}P < 0.01$, $^{***}P < 0.001$; vs. CTX group, $^{\&}P < 0.05$, $^{\&\&}P < 0.01$, $^{\&\&\&}P <$'0.001.

into rare ginsenosides Rk_1 and Rg_5 were investigated, and the reaction temperature (°C), amino acid concentration (%), reaction time (h) and liquid-solid ratio were further discussed using orthogonal experiments (mL/g). The effect of its conversion rate, the reaction pathway and mechanism are preliminarily discussed using monomeric ginsenoside as the substrate. In variance analysis, we found that temperature and the amount of amino acids had the most important influence on the transformation of rare ginsenosides. The results show that Asp is the best catalyst, and thermal extraction has the best effect. The addition of aspartic acid makes the solution weakly acidic, which is also the reason for the transformation of a large number of rare ginsenosides. Under the optimal conversion conditions (110°C, 5% Asp, 2.5 h reaction time, 30 mL/g), the highest conversion rates of rare ginsenosides Rk_1 and Rg_5 were 6.58 ± 0.11 mg/g and 3.74 ± 0.05 mg/g, respectively. In the

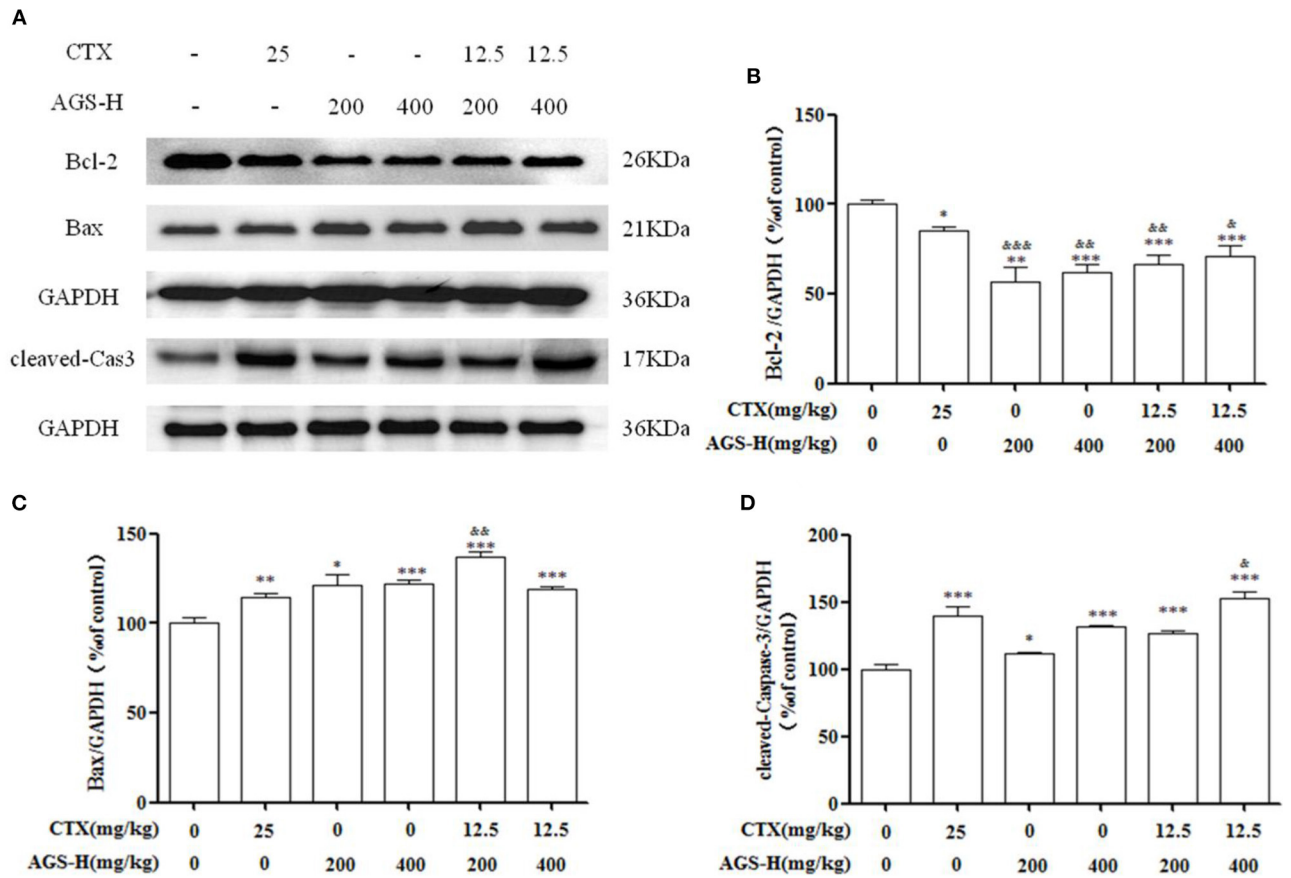

FIGURE 10 | Effects of AGS-H synergistic CTX/2 on Bcl-2, Bax and cleaved Caspase-3 in S180 tumor-bearing mice ($n = 8$). **(A)** The protein expression levels of Bcl-2, Bax and cleaved-Caspase-3 were detected by Western blotting. **(B)** The relative Bcl-2 expression level. **(C)** The relative Bax expression level. **(D)** The relative cleaved-Caspase-3 expression level. Values are presented as mean ±SD. vs. model group, $^{*}P < 0.05$, $^{***}P < 0.001$; vs. CTX group, $^{\&}P < 0.05$, $^{\&\&}P < 0.01$, $^{\&\&\&}P < 0.001$.

reaction pathway, the saponins of the ginsengdiol group mainly participate in the transformation process, and the saponins of the ginsengtriol group basically do not participate in the transformation process. Compared with existing transformation methods such as enzymatic acid hydrolysis, the food-grade amino acid transformation method is simpler, more feasible, safe and effective, and provides the possibility for the large-scale production and preparation of rare ginsenosides Rk_1 and Rg_5. Therefore, the use of Asp will improve American ginseng transformation of rare ginsenosides and is of great significance.

Ginsenosides have a good immunomodulatory and anticancer effects. CTX is a broad-spectrum anticancer drug that has a good inhibitory effect on malignant tumors, but has obvious toxicity and side effects, including immunosuppression, and adverse reactions such as loss of appetite, nausea, weight loss and leukopenia (29). In this study, combined with the deficiency of CTX in tumor treatment and the advantages of AGS-Q and AGS-H in antitumour and immune regulation, CTX combined with AGS-Q and AGS-H was used to treat S180 tumor-bearing mice, giving full play to the advantages of chemotherapy and Chinese herbal medicine. We conducted experiments on the effect of AGS-Q or AGS-H synergistic CTX on S180 tumor-bearing mice. The results showed that AGS-Q or AGS-H synergistic CTX in each dose group can significantly inhibit tumor-bearing growth, and upregulate white blood cells and spleen index in comparison with CTX. Additionally, AGS-H synergistic CTX/2 treatment of S180 tumor-bearing mice was found to inhibit tumor growth and restore the immune organ index and white blood cell number.

The imbalance of T lymphocyte subsets may lead to immune dysfunction, leading to a series of immune responses and immunopathological changes (30). During tumor immunity, the function of helper $CD4^+$ T cells is weakened, while the immunosuppressive function of regulatory T cells is enhanced (31). $CD4^+$ is a marker on the surface of helper T cells (Th cells), which play an important role in enhancing humoral and cellular immunity. $CD8^+$ T cells are a marker of inhibitory T cells (Ts cells) that specifically kill infected and dysfunctional cells (27). The increase in the $CD4^+/CD8^+$ ratio indicates that Th cells are higher than inhibitory T cells, indicating that the immune capacity of the body is improved. Treg cells, as the main immunosuppressive cells in mouse and human tumors, are T cell subsets with phenotypic characteristics of

$CD4^+CD25^+Foxp3^+$, which play an important role in regulating the tumor microenvironment and promoting tumor immune avoidance (32). Cytokines are small active molecules produced by immune cells. Cytokines have strong immunomodulatory effects and play an important role in tumor immunity (33). The cytokine IL-2 is a growth factor of T cells and plays an important role in the activation and proliferation of T cells, the activation of B cells and macrophages, and the secretion of IL-2 by T cells. IL-2 mainly plays an immune promotion role *in vivo* and can promote the antitumour immunity of immune cells (34, 35). Interleukin-10 (IL-10) is a cytokine widely expressed in T cells, B lymphocytes, mononuclear macrophages and keratin cells, and has both promoting and inhibiting effects on tumors (36). In this study, AGS-Q or AGS-H synergistic with CTX and AGS-H synergistic with CTX/2 combined activated the immune system of S180 mice, increased the ratio of $CD4^+/CD8^+$ and reduced the number of $CD4^+CD25^+$ cells. Activated $CD4^+$ T cells secrete IL-2. IL-10 release catalyses an immune response that inhibits tumor growth. AGS-H synergistic CTX showed better tumor suppression than AGS-Q synergistic with CTX and reduced the immunosuppression induced by CTX. AGS-H synergistic with CTX/2 treatment of S180 tumor-bearing mice has an equivalent tumor suppressive effect to CTX and meanwhile can reduce the immunosuppressive effect of CTX.

The occurrence of tumor diseases is a sign of the unregulation of cell apoptosis, which makes some abnormal or senescent cells immune escape and enter a state of immortal proliferation. Changes in cell apoptosis are related to the occurrence and development of tumors. Members of the Bcl-2 family are important regulators of the mitochondrial apoptosis pathway (37). According to their different functions, they can be divided into the antiapoptotic protein family and the proapoptotic protein family. Bcl-2 is the main representative member of the antiapoptotic protein family, and Bax is one of the main representative proteins of the proapoptotic protein family (38, 39). Studies have shown that the Bcl-2 protein is highly expressed in many tumor cells, is the main antiapoptotic protein for sudden mitochondrial apoptosis, and plays an important role in the regulation of tumor cell apoptosis (40). In this study, compared with the CTX alone group, AGS synergistic with CTX or CTX/2 significantly upregulated the expression of Bax and cleaved-Caspase-3 and inhibited the expression of the antiapoptotic protein Bcl-2.

CONCLUSION

This study provides a safe, green and effective transformation method for the enrichment of rare ginsenosides and provides a new idea for the development and utilization of American ginseng. AGS can not only play an antitumour role, but also reduce the side effects of immunosuppression caused by CTX, improve the immune activity of S180 tumor-bearing mice and promote the apoptosis of tumor cells. AGS-H is more effective in enhancing anticancer activity and immunity may be closely related to the increase in rare ginsenosides Rk_1 and Rg_5.

DATA AVAILABILITY STATEMENT

The original contributions presented in the study are included in the article/**Supplementary Material**, further inquiries can be directed to the corresponding authors.

ETHICS STATEMENT

All experiments were executed strictly according with the Principle of Laboratory Animal Care and the guidelines prescribed by the Animal Research Committee of the Institute of Special Animals and Plants Sciences, Chinese Academy of Agricultural Sciences (Permit No.: ECLA-ISAP-18079).

AUTHOR CONTRIBUTIONS

Z-mL and Z-jS performed the implementation of animal experiments and wrote the manuscript. DQ, J-YS, and X-hH analyzed the data. MH and J-bC guided the transformation conditions. Y-sL supervised HPLC conditions and results. Y-sS and S-sL participated in the overall design guidance and manuscript review. All authors contributed to the article and approved the submitted version.

FUNDING

This work was supported by National Natural Science Foundation of China (Grant No. 31200261), Jilin province science and technology development project (Grant No. 20200708070YY), and Central Public-interest Scientific Institution Basal Research Fund (Grant Nos. 1610342019008, 1610342020005, and CAAS-ASTIP-ISAPS-2021-010).

SUPPLEMENTARY MATERIAL

The Supplementary Material for this article can be found online at: https://www.frontiersin.org/articles/10.3389/fnut.2022.833859/full#supplementary-material

REFERENCES

1. Li TSC, Mazza G, Cottrell AC, Gao L. Ginsenosides in roots and leaves of American ginseng. *J Agric Food Chem*. (1996) 44:717–20. doi: 10.1021/jf950309f
2. Qi L W, Wang C Z, Yuan C S. American ginseng: potential structure-function relationship in cancer chemoprevention. *Biochem Pharmacol*. (2010) 80:947–54.023. doi: 10.1016/j.bcp.2010.06.023
3. Zhai K F, Duan H, Wang W, Zhao S Y, Khan G J, Wang M T, et al. Ginsenoside Rg[[sb]]1[[/s]] ameliorates blood-brain barrier disruption and traumatic brain injury via attenuating macrophages derived exosomes miR-21 release. *Acta Pharm Sin B*. (2021) 11:3493–507. doi: 10.1016/j.apsb.2021.03.032

4. Li ZM, Zhao LJ, Chen JB, Liu C, Li SS, Hua M, et al. Ginsenoside Rk1 alleviates LPS-induced depression-like behavior in mice by promoting BDNF and suppressing the neuroinflammatory response. *Biochem Biophys Res Commun.* (2020) 530:658–64. doi: 10.1016/j.bbrc.2020.07.098
5. Xiao N, Lou MD, Lu YT, Yang LL, Liu Q, Liu B, et al. Ginsenoside Rg5 attenuates hepatic glucagon response via suppression of succinate-associated HIF-1α induction in HFD-fed mice. *Diabetologia.* (2017) 60:1084–93. doi: 10.1007/s00125-017-4238-y
6. Kim J E, Lee W, Yang S, Cho S H, Baek M C, Song G Y, et al. Suppressive effects of rare ginsenosides, Rk1 and Rg5, on HMGB1-mediated septic responses. *Food Chem Toxicol.* (2019) 124:45–53. doi: 10.1016/j.fct.2018.11.057
7. Zhang P. Ginsenoside-Rg5 treatment inhibits apoptosis of chondrocytes and degradation of cartilage matrix in a rat model of osteoarthritis. *Oncol Rep.* (2017) 37:1497–502. doi: 10.3892/or.2017.5392
8. Choi P, Park JY, Kim T, Park SH, Kim HK, Kang KS, et al. Improved anticancer effect of ginseng extract by microwave-assisted processing through the generation of ginsenosides Rg3, Rg5, and Rk1. *J Funct Foods*. (2015) 14:613–22. doi: 10.1016/j.jff.2015.02.038
9. Yao CJ, Chow JM, Chuang SE, Chang CL, Yan MD, Lee HL, et al. Induction of forkhead class box O3a and apoptosis by a standardized ginsenoside formulation, KG-135, is potentiated by autophagy blockade in A549 human lung cancer cells. *J Ginseng Res.* (2017) 41:247–56. doi: 10.1016/j.jgr.2016.04.003
10. Kim H, Choi P, Kim T, Kim T, Song B G, Park YT, et al. Ginsenosides Rk1 and Rg5 inhibit transforming growth factor-β1-induced epithelial-mesenchymal transition and suppress migration, invasion, anoikis resistance, and development of stem-like features in lung cancer. *J Ginseng Res.* (2021) 45:134–48. doi: 10.1016/j.jgr.2020.02.005
11. Jo SK, Kim IS, Yoon K S, Yoon HH, Yoo HH. Preparation of ginsenosides Rg3, Rk1, and Rg5-selectively enriched ginsengs by a simple steaming process. *Eur Food Res Technol.* (2015) 240:251–6. doi: 10.1007/s00217-014-2370-1
12. Wang YT, You JY, Yu Y, Qu C L, Zhang H R. Ding L, et al. Analysis of ginsenosides in Panax ginseng in high pressure microwave-assisted extraction. *Food Chem.* (2008) 110:161–7. 01.028. doi: 10.1016/j.foodchem.2008.01.028
13. Lee M R, Yun B S, Sung C K. Comparative study of white and steamed black *Panax ginseng*, P. quinquefolium, and P notoginseng on cholinesterase inhibitory and antioxidative activity. *J Ginseng Res.* (2012) 36:93–101. doi: 10.5142/jgr.2012.36.1.93
14. Sun CP, Gao WP, Zhao BZ, Cheng LQ. Preliminary study on the preparation of ginsenoside Rg5 by lemon-catalyzed conversion of protopanaxadiol saponins. *Chinese Patent Med.* (2013) 35:2694–8.
15. Bao HY, Li L, Zan LF, Wang CL. Suriguge. biotransformation of ginsenoside Re by *Rhizopus arrhizus*. *Mycosystema.* (2010) 29:548–54. doi: 10.13346/j.mycosystema.2010.04.013
16. Liu Z, Xia J, Li W, Zhang J, Sun GZ, Ruan CC. Degradation of protopanaxadiol-type ginsenosides with aspartic acid and antioxidant activity of maillard reaction products. *Food Sci.* (2018) 572:20–6. doi: 10.7506/spkx102-6630-201807004
17. Kim M H, Lee Y C, Choi S Y, Cho C W, Rho J, Lee K W. The changes of ginsenoside patterns in red ginseng processed by organic acid impregnation pretreatment. *J Ginseng Res.* (2011) 35:497–503. doi: 10.5142/jgr.2011.35.4.497
18. Yong MH, Burns KE, de Zoysa J, Helsby NA. Intracellular activation of 4-hydroxycyclophosphamide into a DNA-alkylating agent in human leucocytes. *Xenobiotica*. (2021) 51:1188–98. doi: 10.1080/00498254.2021.1975060
19. Shi LX, Gen WL. Screening of extraction process of ginsenosides by orthogonal test. *Specialty Res.* (2006) 28:18–21. doi: 10.16720/j.cnki.tcyj.2006.02.007
20. Zhang J, Chen QC, Gong XJ, Zheng YN, Liu WX. Effects of different extraction methods on the extraction rate of ginsenosides. *J Jilin Agric Univ.* (2003) 25:71–2. doi: 10.13327/j.jjlau.2003.01.019
21. Xia J. *Study on the Preparation of Rare Ginsenoside by Hydrolysis With Acidic Amino Acid*. Jilin Agric Univ. (2017). Available online at: https://kns.cnki.net/KCMS/detail/detail.aspx?dbname=CMFD201801& filename=1017842625.nh.
22. Li X G, Fu L, Lu Q, Li X. Study on hydrolysis reaction of ginsenoside and products in red ginseng processing. *J Jilin Agric Univ.* (2000) 22:64–70. doi: 10.13327/j.jjlau.2000.04.017
23. Wang YJ, Qi QC, Li A, Yang M, Huang WZ, Xu HY, et al. Immuno-enhancement effects of yifei tongluo granules on cyclophosphamide-induced immunosuppression in Balb/c mice. *J Ethnopharmacol.* (2016) 194:72–82. doi: 10.1016/j.jep.2016.08.046
24. Liu Z, Xia J, Wang CZ, Zhang JQ, Ruan CC, Sun GZ, et al. Remarkable impact of acidic ginsenosides and organic acids on ginsenoside transformation from fresh ginseng to red ginseng. *J Agric Food Chem.* (2016) 64:5389–99. doi: 10.1021/acs.jafc.6b00963
25. Xie YY, Luo D, Cheng YJ, Ma JF, Wang YM, Liang QL, et al. Steaming-induced chemical transformations and holistic quality assessment of red ginseng derived from *Panax ginseng* by means of HPLC-ESI-MS/MSn-based multicomponent quantification fingerprint. *J Agric Food Chem.* (2012) 60:8213–24. doi: 10.1021/jf301116x
26. Qi Z, Chen L X, Li Z, Shao Z J, Qi Y L, Gao K, et al. Immunomodulatory effects of (24R)-Pseudo-Ginsenoside HQ and (24S)-Pseudo-Ginsenoside HQ on cyclophosphamide-induced immunosuppression and their anti-tumor effects study. *Inter J Mol Sci.* (2019) 20:1–16. doi: 10.3390/ijms20040836
27. Wang JX, Tong X, Li PB, Cao H, Su WW. Immuno-enhancement effects of shenqi fuzheng injection on cyclophosphamide-induced immunosuppression in Balb/c mice. *J Ethnopharmacol.* (2012) 139:788–95. doi: 10.1016/j.jep.2011.12.019
28. Guan DP, Wang H, Li W, Liu WC, Wang YP, Wang J, et al. Optimization of preparation process of ginsenosides Rk1 and Rg5 by high temperature pyrolysis. *Shanghai J of Traditional Chinese Med.* (2015) 49:91–5. doi: 10.16305/j.1007-1334.2015.01.031
29. Qi Y, Hu X, Cui J, Chen J, Wu Q, Sun X, et al. Combined use of insoluble β-glucan from the cell wall of candida albicans and cyclophosphamide: Validation in S180 tumor-bearing mice. *Biomed Pharmacother.* (2018) 97:1366–72. doi: 10.1016/j.biopha.2017.11.049
30. Pist G, Trisciuoglio D, Ceci C, Garufi A, D'Orazi G. Apoptosis as anti-cancer mechanism: function and dysfunction of its modulators and targeted therapeutic strategies. *Aging (Albany NY).* (2016) 8:603–19. doi: 10.1111/ceo.12397
31. Li Q, Rao RR, Araki K, Pollizzi K, Odunsi K, Powell JD, et al. A central role for mTOR kinase in homeostatic proliferation induced $CD8^+$ T cell memory and tumor immunity. *Immunity.* (2011) 34:541–53. doi: 10.1016/j.immuni.2011.04.006
32. Li X, Ye F, Chen HZ, Lu WG, Wan XY, Xie X. Human ovarian carcinoma cells generate $CD4^+CD25^+$ regulatory T cells from peripheral $CD4^+CD25^-$ T cells through secreting TGF-beta. *Cancer Lett.* (2007) 253:144–53. doi: 10.1016/j.canlet.2007.01.024
33. Pellegrini M, Mak T W, Ohashi PS. Fighting cancers from within: augmenting tumor immunity with cytokine therapy. *Trends Pharmacol Sci.* (2010) 31:356–63. doi: 10.1016/j.tips.2010.05.003
34. Wong HS, Park K, Gola A, Baptista AP, Miller CH, Deep D, et al. A local regulatory T cell feedback circuit maintains immune homeostasis by pruning self-activated T cells. *Cell.* (2021) 184:3981–97. doi: 10.101/j.cell.2021.05.028
35. Chinen T, Kannan AK, Levine AG, Fan XY, Klein U, Zheng Y, et al. An essential role for the IL-2 receptor in Treg cell function. *Nat Immunol.* (2016) 17:1322–33. doi: 10.1038/ni.3540
36. Islam H, Neudorf H, Mui AL, Little JP. Interpreting 'anti-inflammatory' cytokine responses to exercise: focus on interleukin-10. *J Physiol.* (2021) 599:5163–77. doi: 10.1113/JP281356
37. Pentimalli F. Bcl-2: a 30-year tale of life, death and much more to come. *Cell Death Diff.* (2018) 25:7–9. doi: 10.1038/cdd.2017.189
38. Zhai KF, Duan H, Chen Y, Khan GJ, Cao WG, Gao GZ, et al. Apoptosis effects of imperatorin on synoviocytes in rheumatoid arthritis through mitochondrial/caspase-mediated pathways. *Food Funct.* (2018) 9:2070–9. doi: 10.1039/c7fo01748k
39. Zhai KF, Duan H, Cui CY, Cao YY, Si JL, Yang HJ, et al. Liquiritin from glycyrrhiza uralensis attenuating rheumatoid arthritis via reducing inflammation, suppressing angiogenesis, and inhibiting MAPK signaling pathway. *J Agric Food Chem.* (2019) 67:2856–64. doi: 10.1021/acs.jafc.9b00185
40. Yu S, Gong LS, Li NF, Pan YF, Zhang L. Galangin (GG) combined with cispla-tin (DDP) to suppress human lung cancer by inhibition of STAT3-regulated NF-κB and Bcl-2/Bax signaling pathways. *Biomed Pharmacother.* (2018) 97:213–24. doi: 10.1016/j.biopha.2017.10.059

Conflict of Interest: The authors declare that the research was conducted in the absence of any commercial or financial relationships that could be construed as a potential conflict of interest.

The handling editor declared a shared affiliation with the authors at time of review.

Publisher's Note: All claims expressed in this article are solely those of the authors and do not necessarily represent those of their affiliated organizations, or those of the publisher, the editors and the reviewers. Any product that may be evaluated in this article, or claim that may be made by its manufacturer, is not guaranteed or endorsed by the publisher.

frontiers | Frontiers in Nutrition

ORIGINAL RESEARCH
published: 11 April 2022
doi: 10.3389/fnut.2022.878768

A Novel Angiotensin I-Converting Enzyme Inhibitory Peptide Derived From Goat Milk Casein Hydrolysate Modulates Angiotensin II-Stimulated Effects on Vascular Smooth Muscle Cells

Zijiao Qiao[1], Jiaqi Wang[2], Zeqi He[1], Lina Pan[2], Konglong Feng[1], Xiaoyu Peng[2], Qianru Lin[1], Yu Gao[2], Mingyue Song[1], Sufang Cao[2], Yunjiao Chen[1], Yong Cao[1] and Guo Liu[1,3]**

[1] Guangdong Provincial Key Laboratory of Nutraceuticals and Functional Foods, College of Food Sciences, South China Agricultural University, Guangzhou, China, [2] Ausnutria Dairy (China) Co., Ltd., Changsha, China, [3] College of Horticulture, South China Agricultural University, Guangzhou, China

OPEN ACCESS

Edited by:
Jinkai Zheng,
Institute of Food Science and Technology (CAAS), China

Reviewed by:
Mouming Zhao,
South China University of Technology, China
Pengjie Wang,
China Agricultural University, China

***Correspondence:**
Yong Cao
caoyong2181@scau.edu.cn
Guo Liu
liuguo@scau.edu.cn

Specialty section:
This article was submitted to Food Chemistry, a section of the journal Frontiers in Nutrition

Received: *18 February 2022*
Accepted: *14 March 2022*
Published: *11 April 2022*

Citation:
Qiao Z, Wang J, He Z, Pan L, Feng K, Peng X, Lin Q, Gao Y, Song M, Cao S, Chen Y, Cao Y and Liu G (2022) A Novel Angiotensin I-Converting Enzyme Inhibitory Peptide Derived From Goat Milk Casein Hydrolysate Modulates Angiotensin II-Stimulated Effects on Vascular Smooth Muscle Cells. Front. Nutr. 9:878768. doi: 10.3389/fnut.2022.878768

Hypertension is a major risk factor leading to cardiovascular disease, and is frequently treated with angiotensin I-converting enzyme (ACE) inhibitory peptides. The objective of this study was to separate and identify an ACE-inhibitory peptide from goat milk casein hydrolysates, and to evaluate its potential for improving angiotensin II (Ang II)-mediated adverse effects on vascular smooth muscle cells (VSMCs). A novel ACE-inhibitory peptide with the highest activity from the goat milk casein hydrolysates as determined by four steps of RP-HPLC was purified and identified as Phe-Pro-Gln-Tyr-Leu-Gln-Tyr-Pro-Tyr (FPQYLQYPY). The results of inhibitory kinetics studies indicated that the peptide was a non-competitive inhibitor against ACE. Gastrointestinal digest *in vitro* analysis showed that the hydrolysate of FPQYLQYPY was still active after digestion with gastrointestinal proteases. Moreover, we found that the peptide could significantly inhibit the proliferation and migration of Ang II-stimulated VSMCs. Further transcriptomic analysis revealed that differentially expressed genes (DEGs) were enriched in the cardiovascular disease-related pathways, and that the peptide may have the ability to regulate vascular remodeling. Our findings indicate the potential anti-hypertensive effects of FPQYLQYPY, as well-implicate its role in regulating vascular dysfunction.

Keywords: goat milk casein hydrolysates, Angiotensin I-converting enzyme inhibitory peptide, amino acid sequence, hypertensive, vascular smooth muscle cells, Angiotensin II

INTRODUCTION

Hypertension is a major preventable risk factor for cardiovascular disease and all-cause mortality globally. The prevalence of hypertension is increasing worldwide due to unhealthy diet and lack of exercise (1), and in China, hypertension was highly prevalent but remained undertreated and uncontrolled (2). Serious health implications coupled with pervasiveness, make the prevention and treatment of high blood pressure is an onus to society.

Angiotensin I-Converting enzyme (ACE) is a key enzyme in the regulation of blood pressure and is the subject of most research (3). It can cleave Angiotensin II (Ang II) to form Angiotensin II (Ang II) in the renin-angiotensin system (RAS) pathway (4, 5). Ang II is a key active vasoconstrictor component of RAS and is harmful to vascular health (6). Vascular smooth muscle cells (VSMCs) are an important cellular component of the blood vessel wall that not only protect the structure of blood vessels, but also play a role in regulating the diameter and blood flow of the blood vessel. Ang II overstimulates VSMCs, resulting in abnormal cell proliferation, migration, oxidative stress, and inflammation (6). These processes promote vascular remodeling, leading to hypertension and atherosclerosis (7). Therefore, vascular smooth muscle cells are used as a cell model to evaluate the mechanism of antihypertensive peptides, and angiotensin II is used to construct the cell model *in vitro* (8).

The current standard care for the treatment of hypertension includes drugs which are mostly synthetic ACE-inhibitors, such as captopril and enalapril, to name a few. But, regardless of their anti-hypertensive effects, synthetic ACE-inhibitors are accompanied by undesirable side effects, including headache, cough, dizziness, fatigue, and diarrhea (9). Therefore, patients are encouraged to consider the use of bioactive peptides from functional foods to avoid side-effects.

It has been shown that bioactive peptides from milk proteins have potential health benefits for humans and are used in health-promoting food as well as drug applications (10). Based on their activity, these peptides can be divided into categories based on their properties, such as ACE-inhibition, anti-oxidation, antibacterial, mineral-binding, opioid, and immunomodulation, etc. (11). Studies have shown that peptides with antihypertensive ability may exert antihypertensive effects through a variety of mechanisms (5), and amongst the polypeptides with antihypertensive effects that have been confirmed, ACE-inhibition is the main mechanism. In recent decades, biologically active peptides with ACE inhibitory effects have been extensively studied.

Milk protein is one of the good sources of ACE-inhibitory peptides, and various ACE-inhibitory peptides have been purified and identified from it using enzymatic hydrolysis or fermentation (12). The beneficial effects of ACE-inhibitory peptides on hypertension are not limited to ACE inhibition, but also can improve vascular function disorder (13). So far, research on milk-derived bioactive peptides has focused mainly on bovine milk protein and products (14). To the best of our knowledge, the bioactive peptides isolated from goat milk casein hydrolysates have not been studied in depth, especially the ACE-inhibitory peptide (15).

Research on the separation and *in vitro* activity of ACE-inhibitory peptides in goat milk remains insufficient (16–18), and the need for more research is obvious.

In this study, we separated the ACE-inhibitory peptide from goat milk casein hydrolysates using RP-HPLC and identified the amino acid sequence of a novel peptide using MALDI TOF-MSMS and Protein Sequencer. We evaluated the ability of the purified peptide to improve the Ang II-mediated adverse effects on VSMCs and assessed its potential to improve vascular dysfunction.

MATERIALS AND METHODS

Materials

Goat micellar casein (gMCC60) was provided by Ausnutria (Netherlands) and contained 63% protein and 22% lactose.

Trypsin (10–20% activity protein) was purchased from Novozymes (Bagsvaerd, Denmark). Pepsin (10000 NFU mg^{-1}) was purchased from China Pangbo Biological Engineering Co., Ltd. (Nanning, China). Angiotensin Converting Enzyme from rabbit lung, hippuryl-L-histidyl-L-leucine (HHL), and α-amylase (109.8 U mg^{-1}) were purchased from Sigma-Aldrich (USA). The Dulbecco's modified Eagle's medium (DMEM), phosphate-buffered saline (PBS), 0.25% trypsin-EDTA, penicillin-streptomycin solution, and Fetal bovine serum (FBS) were purchased from Gibco Life Technologies (Grand Island, NY, USA). Angiotensin II (Ang II) and the Cell Counting Kit-8 were purchased from MedChemExpress (MEC, NJ, USA).

Preparation of Goat Milk Casein Hydrolysates

The hydrolysis process parameters were according to the reported method with some modifications (12). The specific process was to first dissolve the goat milk casein in distilled water until its concentration was 10%. When the solution was heated to 40°C, the pH was adjusted to 8.0 by adding 6 M NaOH. Then, trypsin was added to the reaction mixture at the ratio of 0.4% (enzyme: substrate, w/w, protein basis). The pH of the reaction mixture was maintained by continuous addition of 6 M NaOH during enzymatic hydrolysis. After enzymolysis for 2.5 h, the enzyme was inactivated by heating for 30 min at 90°C, and the hydrolysates were then freeze-dried and stored at −20°C.

ACE-Inhibitory Activity Assay

ACE inhibitory activity was measured using an RP-HPLC method with Hippuryl-His-Leu (HHL) as a substrate, which generated hippuric acid (HA) under enzymatic hydrolysis (19). The sample was dissolved in a borax-boric acid buffer containing 0.15 M NaCl (pH = 8.3). Firstly, add 10 μL ACE (0.2 U) to the sample tube and blank tube, respectively. At the same time, add 10 μL of sample to the sample tube, and add 10 μL of buffer and 80 μL of 1 M HCl to the blank tube, then pre-incubate at 37°C for 5 min. The reaction was initiated by adding 30 μL HHL (6.5 mM) and incubated for 60 min at the same temperature until 80 μL 1 M HCl was added to terminate the reaction.

ACE inhibitory activity (%) was confirmed by monitoring the formation of HA at 228 nm as detected by RP-HPLC on a C18 column (250 × 4.6 mm, 5 μm, Ecosil). The mobile phase was 25% acetonitrile and 75% water with 0.01% trifluoroacetic acid with

a flow rate of 1 mL/min. The inhibition activity was calculated using the following equation:

$$Inhibition\ activity(\%) = \frac{A - B - A_0}{A - A_0} \times 100\%$$

Where, A = the HA peak area of the control; B = the HA peak area of the sample; A_0 = the HA peak area of control with HCL before pre-incubated.

The inhibitory activity of the hydrolysates or collected fractions was expressed as percentage of ACE inhibition at a given protein concentration (20).

Separation and Purification of ACE-Inhibitory Peptides

The hydrolysate was subjected to a four-step separation process. First, the hydrolysate was separated by a reverse-phase (RP) C18 column (20 × 450 mm, 10 μm, Macherey Nagel, France). Elution was performed with mobile phase A (0.1% trifluoroacetic acid in water) and mobile phase B (0.1% trifluoroacetic acid in acetonitrile) with a gradient of 10–48% B at a rate of 10 mL min^{-1} for 66 min, and 90% B in the next 5 min. Second, the active fraction was further purified by a RP Shim-pack PRC-ODS(K) column (30 × 250 mm, 15 μm, Shimadzu), and the elution was performed with 25–60% solvent B for 70 min. Third, the active fraction peptide was further purified by a RP ECOSIL C18 column (300 × 20 mm,10 μm, Germany), and the elution was performed with 30–43% solvent B for 60 min. Last, the fraction solution with the highest ACE-inhibitory activity was further separated using an analytical HPLC equipped with a C18 column (5 μm, 4.6 × 250 mm, Ecosil), and the elution was performed with 25 to 30% solvent B for 60 min. The peak of highest activity was further analyzed using an analytical RP-HPLC equipped with the same C18 column, and the elution was performed with 10–60% solvent B for 40 min, 90% B for the next 10 min, and 10% B in the last 10 min.

The absorption peaks of every step were fractionated, collected and lyophilized in order to measure the ACE-inhibitory activity. The eluted samples were monitored at a dual wavelength of 214 and 280 nm.

Identification of the ACE Inhibitory Peptides

The molecular mass of the peptide with the highest ACE-inhibitory activity was determined using an ABI 4800 MALDI-TOF-MS/MS (Bruker Daltonik GmbH, Bremen, Germany). The N-terminal sequence of the purified peptides was identified by Protein Sequencer using the Edman degradation procedure (PPSQ-53A, Shimadzu, Japan).

Peptide Syntheses

The peptide (FPQYLQYPY) was synthesized by Synpeptide Co., Ltd (Nanjing, China). The purity of the synthesized peptide was 98%, as evaluated by HPLC and the molecular mass was determined by LC/ESI–MS.

Inhibitory Kinetics Study

To clarify the inhibitory mechanism of the most potent purified peptide on ACE, different concentrations of the ACE inhibitory peptide were added to each reaction mixture, according to a previously reported method (21). Briefly, the enzyme activities were measured with different concentrations of the substrate (HHL) and the ACE inhibitory pattern in the presence of the inhibitor was determined with a Lineweaver–Burk plot.

Stability of the Purified Peptide Against *in vitro* Gastrointestinal Digest

In vitro digestion of the potent purified ACE inhibitory peptide was carried out according to the reported method, with some adjustments (22, 23). Peptide (0.4 mL, 1.5 mg mL^{-1}) was incubated with 2% (w/w) α-amylase, pepsin, or trypsin at 37°C.

In successive digestion tests, the peptide was first dissolved in buffer solution (pH 6.8) to 2 mg mL^{-1} and incubated with α-amylase for 5 min. Then the pH was decreased to pH 2 with the addition of 1 M HCl. Subsequently, the gastric digestion was initiated by adding pepsin at an enzyme-substrate ratio of 2:100 (w/w). The reaction was stopped after 2 h by raising the pH to 8.0 with 1 M NaOH, and trypsin was added to the reactor to continue gastrointestinal digestion for 4 h. Last, the reaction mixture was heated for 15 min in boiling water to inactivate the enzyme.

Purified Peptide Modulates Angiotensin II Effects on Vascular Smooth Muscle Cells

Cell Culture

The rat aortic vascular smooth muscle cell line A7r5, was purchased from Cell bank of Chinese Academy of Sciences (Shanghai, China). A7r5 cells between passage 8 and 20 were grown in DMEM supplemented with 10% FBS and antibiotics until they reached confluence. For experiments, the confluent cells were placed in a quiescing medium (DMEM + 1% FBS + antibiotics) (24) for 24 h, before treatment with different concentrations of FPQYLQYPY and Ang II for different time periods.

Cell Cytotoxicity Test

The cytotoxic effects of FPQYLQYPY in cell culture were evaluated using the Cell Counting Kit-8. First, A7r5 cells were seeded at 1 × 104 cells per well into 96-well plates (Costar, Corning, NY, USA) and cultured in a 5% CO_2 incubator at 37°C for 24 h. Then, the medium of each well was replaced by 100 μL of fresh medium with different concentrations of FPQYLQYPY (0, 1, 5, 10, 50, 100, or 200 μg mL^{-1}). After further incubation for 24 h, 10 μL CCK-8 solution was added to each well. Then, the plate was incubated for another 2 h. The absorbance of samples at a wavelength of 450 nm was measured using a microplate reader. The cell survival rate (%) was determined by the percentage of living cells in the test wells compared to the control wells.

Cell Proliferation Assay

Cell proliferation was measured by the Cell Counting Kit-8. A7r5 cells were seeded at 5 × 10^3 cells per well into 96-well plates and grown in DMEM with 10% of FBS for 24 h, then the medium

was replaced by quiescing medium overnight. The cells were co-treated with different concentrations of FPQYLQYPY (0, 10, 50, 100 $\mu g\ mL^{-1}$) and Ang II (0.1 μM) for 24 h. The absorbance of samples at a wavelength of 450 nm was measured using a microplate reader. The cell survival rate (%) was determined by the percentage of living cells in the test wells compared to the control wells.

Wound Healing Assay

Migration of A7r5 cells was evaluated using the wound healing assay (25). Three lines were drawn horizontally on the back of each hole on the 6-well plate with a marker. Cells in logarithmic growth phase were evenly seeded into 6-well plates with 2×10^5 cells per well, and grown in complete medium until the cells covered the bottom of the plate, then the medium was replaced by quiescing medium for overnight.

Afterwards, a sterile 200 μL spear head was used to quickly delimit at an average equal distance in the vertical direction according to the marking line, and washed with PBS to remove the floating cells. Quiescing medium with FPQYLQYPY (0, 10, 50, 100 $\mu g\ mL^{-1}$) and Ang II (1 μM) was added, then the cells were cultured in an incubator at 37°C and 5% CO_2 for 24 h. The degree of cell migration was observed with inverted microscope and photographs were taken at 0 and 24 h. The migration distance was analyzed by ImageJ software.

Transwell Cell Migration Assay

A7r5 cells were collected and suspended in DMEM (1% FBS), and then the density was adjusted to 2×10^5 cells ml^{-1}. In each group, cell suspensions with or without FPQYLQYPY were cultured in the upper chamber of a Transwell (8.0 μm, Corning, NY, USA) (26), and at the same time, the lower chamber was filled with or without Ang II for 48 h. The superior layer cells of the upper chamber were washed with PBS for 3 times, the cells were then fixed with 4% paraformaldehyde, and stained with 0.1% crystal violet. After rinsing with PBS, a cotton swab was used to remove the upper unmigrated cells. The migratory cells were observed and photographed under an inverted microscope. Last, a 33% acetic acid solution was added to quantify the crystal violet, and the absorbance of samples was measured at a wavelength of 570 nm using a microplate reader.

RNA Extraction and RNA-Seq Transcriptomics

A7r5 cells were incubated with FPQYLQYPY and Ang II for 24 h. Then, total RNA was extracted using the TRIzol reagent (Thermo Scientific, USA), according to the manufacturer's protocol. After the quality test, the libraries were constructed using the TruSeq Stranded mRNA LT Sample Prep Kit (Illumina, San Diego, CA, USA) following the manufacturer's instructions. The transcriptome sequencing and analysis were conducted by OE Biotech Co., Ltd. (Shanghai, China).

Real Time Quantitative RT-PCR

Total RNA was extracted from A7r5 cells using TRIzol reagent, according to the manufacturer's specifications. The information of primer sequences is shown in **Supplementary Table 1**. RT reactions were performed in a GeneAmp® PCR System 9700 (Applied Biosystems, USA). Then, Real-time PCR was performed using the LightCycler® 480 II Real-time PCR Instrument (Roche, Swiss). The relative expression level was calculated using the $2^{-\Delta\Delta Ct}$.

Statistics

All data are expressed as means ± standard deviation (SD). Statistical significance among multiple experimental groups was analyzed by ANOVA coupled with Tukey's *post-hoc* test using SPSS (version 22). $P < 0.05$ were considered statistically significant.

RESULTS

Separation and Purification of ACE-Inhibitory Peptide

Before separating the enzymatic hydrolysate, the ACE-inhibitory activity of goat milk casein and its enzymatic hydrolysate was first compared. It was found that the casein had no ACE-inhibitory ability, but the product after trypsin enzymolysis of casein had certain activity (**Figure 1A**), indicating that the effective fragments in the protein were released by hydrolysis. RP-HPLC is commonly used to isolate a bioactive peptide (27–29). It has been successfully applied in the separation of ACE-inhibitory peptides from whey protein hydrolysate and casein hydrolysates. Still, the composition of goat casein hydrolysate is complicated. In order to filtrate out the highest active peptides, this study adopted a four-step separation method to purify the monomer peptides with the best ACE-inhibitory activity.

In this study, the ACE-inhibitory activity of the hydrolysate was determined before the separation process. The hydrolysate was divided into six fractions by preparative reversed-phase C18 column, and fraction Y3 showed a highest inhibition which was notably higher than the hydrolysate (**Figures 1B,C**). Then, Y3 was further separated with a RP Shim-pack PRC-ODS(K) column and divided into 5 fractions, and Y3-3 had the highest inhibition rate of 63.58 ± 1.91% (**Figures 1D,E**). Next, Y3-3 was divided into six fractions further purified by a RP ECOSIL C18 column (**Figures 1F,G**). Finally, in order to improve the level of purity in the M4 fraction with the highest inhibition in the previous step, RP-HPLC equipped with a C-18 column was used to purify M4 with a gradient elution. Seven peaks were obtained based on differences in polarity, F3 exhibited the best ACE-inhibitory ability (71.19 ± 0.71%) (**Figures 1H,I**) and was regarded as a monomer. F3 was further analyzed by analytical HPLC with the same C18 column, and it was shown that the fraction was single peak with high purity (**Figure 2A**).

Identification of the ACE Inhibitory Peptide

In order to obtain the exact sequence of the purified peptide, MALDI-TOF-MS/MS combined with Protein Sequencer (PPSQ) was used. According to MALDI-TOF-MS/MS analysis, the molecular mass of ACE inhibitory peptide F3 was 1218.552 Da (**Figure 2B**). As shown in **Figure 2C**, the N-terminal amino acid sequence of F3 was analyzed by Protein Sequencer, and

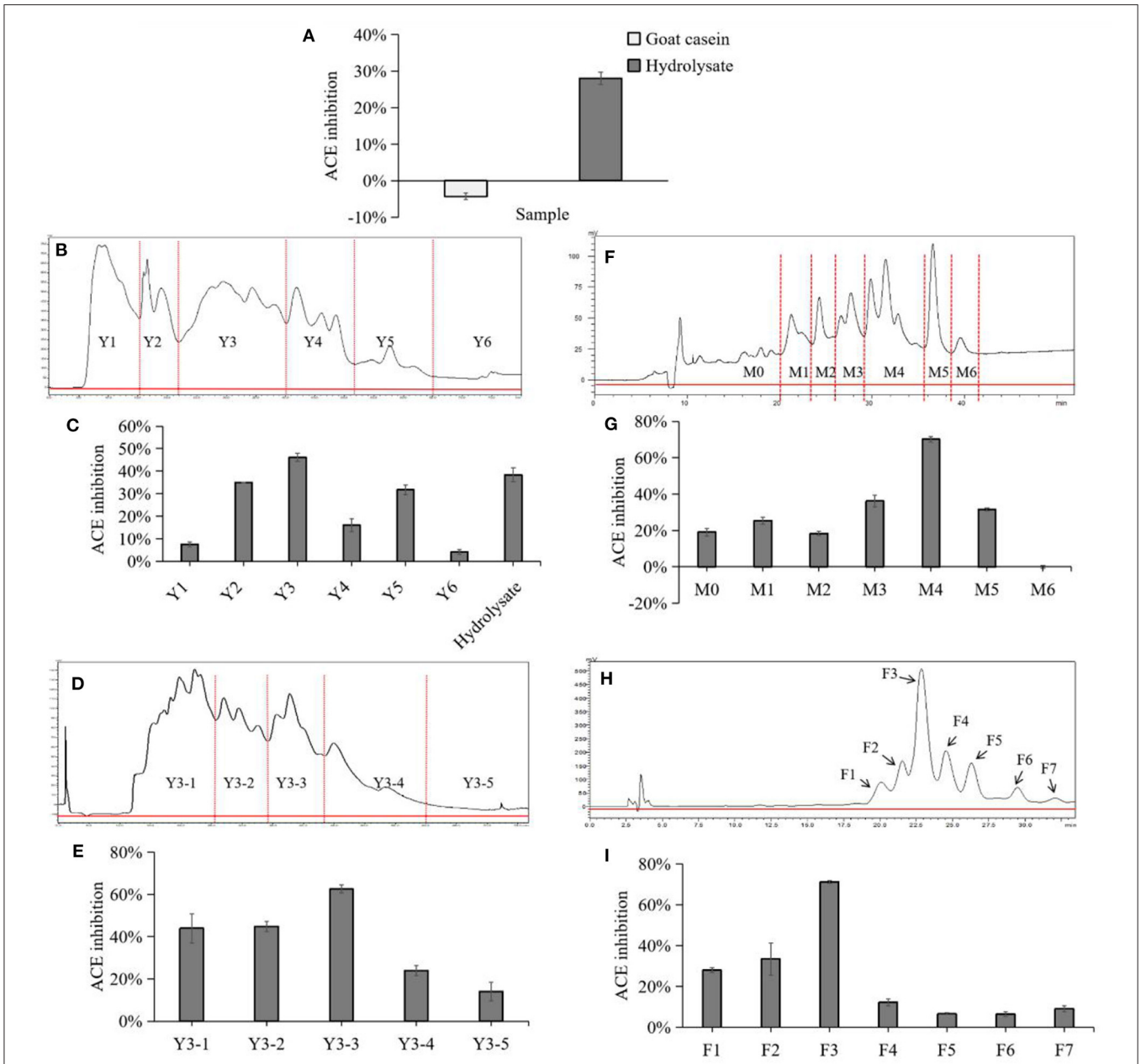

FIGURE 1 | Chromatogram and ACE inhibitory activity of each fraction in separation and purification. **(A)** Comparison of ACE-inhibitory activity before and after casein hydrolysis. **(B)** Preparative HPLC chromatograph of goat milk casein hydrolysates in the first fractionation. Fractions were termed with Y1 to Y6 followed by a number. **(C)** ACE-inhibitory ratios of the collected fractions after the first fractionation and hydrolysate. **(D)** Preparative HPLC chromatograph of goat milk casein hydrolysates in the second fractionation. **(E)** ACE-inhibitory ratios of the collected fractions by the second fractionation. Fractions were termed with Y3-1 to Y3-5 followed by a number. **(F)** Preparative HPLC chromatograph of goat milk casein hydrolysates in the third fractionation. **(G)** ACE-inhibitory ratios of the collected fractions by the third fractionation. Fractions were termed with M0 to M6 followed by a number. **(H)** Separation of the active fraction M4 by analytical RP-HPLC. **(I)** ACE-inhibitory ratios of the collected peaks, and peaks were numbered sequentially from F1 to F7.

peptide F3 was composed of nine amino acids with the sequence identified as Phe-Pro-Gln-Tyr-Leu-Gln-Tyr-Pro-Tyr (FPQYLQYPY). The peptide of this sequence was derived from α-casein, as determined by a search of the protein database of UniProt. The results were consistent with those reported previously that most ACE inhibitory peptides have amino acid residues between 2 and 12 (30) and molecular weight below 3 kDa (31).

Inhibition Pattern of FPQYLQYPY

To clarify the type of inhibition, the peptide was co-incubated with various substrate (HHL) concentrations and an ACE

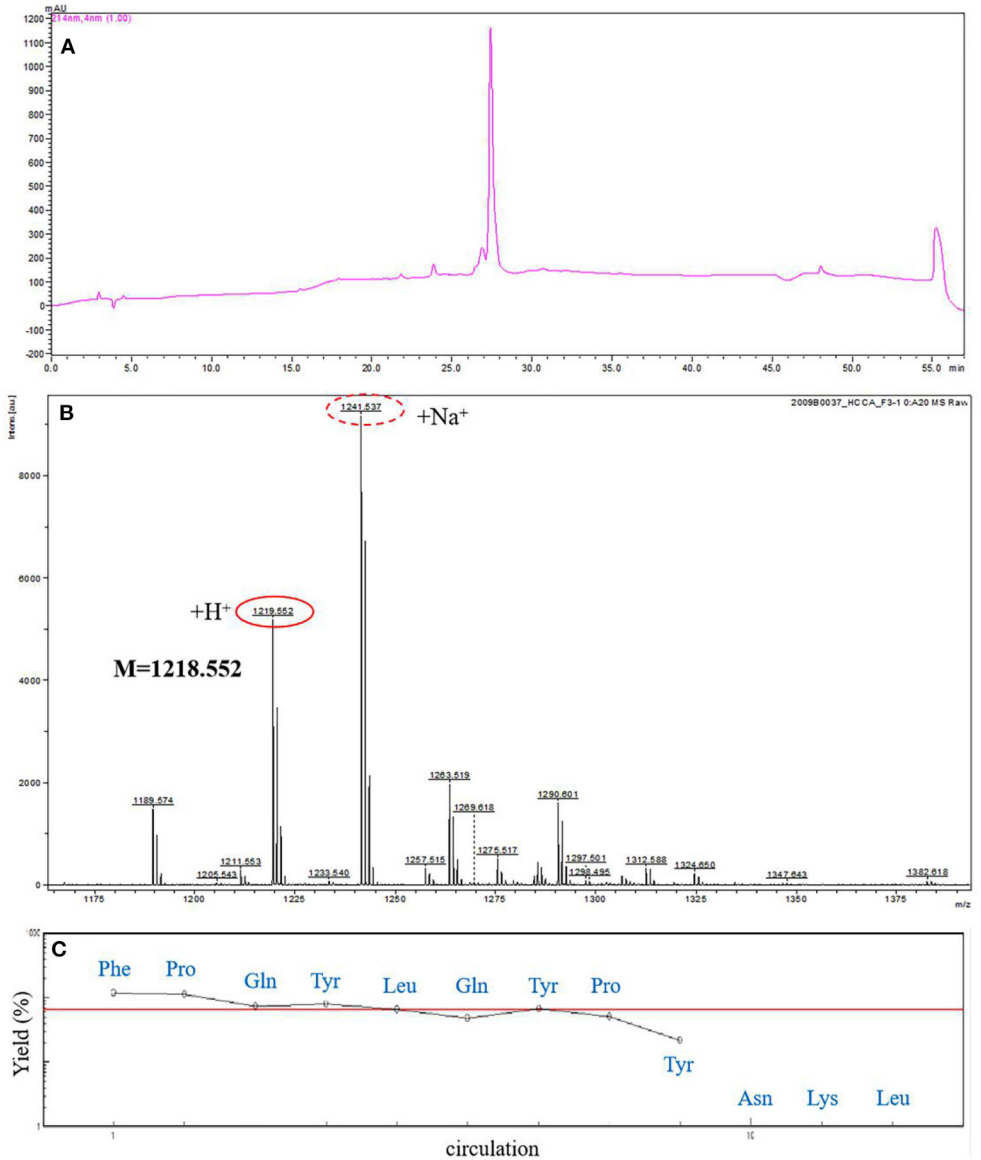

FIGURE 2 | Amino acid sequence analysis of F3. **(A)** Further analysis of F3 by analytical RP-HPLC. **(B)** The molecular mass analysis of the ACE-inhibitory peptide F3 by MALDI-TOF-MS/MS. **(C)** The N-terminal sequence analysis of F3 by PPSQ.

solution, and the double reciprocal velocity-substrate is shown in **Figure 3**. The Michaelis-Menten equation can reflect the relationship between the initial velocity and the substrate concentration in an enzymatic reaction. Usually, the K_m and V_{max} for the reaction at different concentrations of the peptide were determined according to Lineweaver–Burk plots. As Km and Vm are important parameters of enzymatic reactions, the inhibition types of ACE-inhibitory peptides can be determined by them. There are two common inhibition types of ACE-inhibitory peptides, competitive inhibition and non-competitive inhibition. As shown in **Figure 3**, the lines intersected at similar x-intercepts, so the inhibition method of the peptide to ACE was determined to be non-competitive, suggesting that the peptide could bind to the enzyme at a site other than the active site without competition between the substrate and the enzyme.

Stability of the FPQYLQYPY Against *in vitro* Gastrointestinal Digest

The stability of the peptide against gastrointestinal digest was assessed *in vitro*. FPQYLQYPY was progressively incubated with various digestive enzymes, including α-amylase, pepsin, and trypsin. Then, the ACE inhibitory activity was assessed, and we observed that peptide digestion by α-amylase and pepsin promoted ACE inhibitory activity slightly when compared with the original (with inactivation of enzymes at every stage).

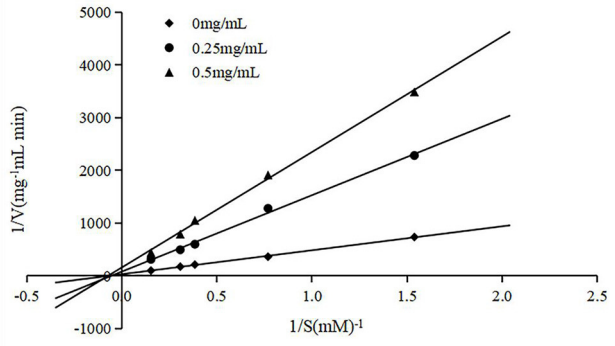

FIGURE 3 | Lineweaver-Burk plots of ACE inhibition by F3.

TABLE 1 | ACE inhibitory activity of FPQYLQYPY after *in vitro* gastrointestinal digest.

Digestion step	Sample	ACE inhibitory (%)
Oral digestion (α-Amylase)	Original	53.47 ± 7.32
	Digested	57.95 ± 0.22
Gastric digestion (Pepsin)	Original	54.12 ± 1.56
	Digested	56.41 ± 1.91
Intestinal digestion (Trypsin)	Original	49.86 ± 1.68
	Digested	45.76 ± 0.42

However, peptide digestion by trypsin after 4 h reduced the ACE inhibitory activity a bit (**Table 1**). Despite these trends, there was no significant difference in activity after incubation with the digestive enzyme. These results suggested that the bioactivity of FPQYLQYPY may be resistant to digestion in the gastrointestinal tract.

Cytotoxicity Test of FPQYLQYPY in VSMCs

The cytotoxicity test result (**Figure 4A**) showed that FPQYLQYPY in the concentration range of 1–200 μg mL^{-1} exhibited no obvious cytotoxic effect on A7r5 cells ($P > 0.05$). And this test results provided a reference for the selection of the peptide concentration in the subsequent experiments.

FPQYLQYPY Inhibited Ang II-Stimulated Proliferation of VSMCs

The proliferation of cultured A7r5 cells was determined by CCK-8 assay. As expected, stimulation with Ang II for 24 h significantly increased the proliferation of VSMCs (**Figure 4B**). Treatment with FPQYLQYPY significantly decreased the percentage of proliferating cells, indicating the potential ability of this peptide for inhibiting excessive proliferation of Ang II-stimulated VSMCs.

The Inhibition of Ang II-Stimulated Migration of VSMCs by FPQYLQYPY

The migration of VSMCs was measured by wound healing assay and Transwell assay. Stimulation of Ang II could promote the migration of A7r5 cells (**Figure 5**), while co-treatment with FPQYLQYPY could adjust the migration ability of Ang II-stimulated A7r5 cells. FPQYLQYPY at a concentration of 100 μg mL^{-1} could restore the distance of the wound healing area to the level of the control group (**Figures 5A,B**).

Furthermore, Transwell experiments further revealed that Ang II caused a significant increase in the number of cells passing through the chamber ($P < 0.01$). However, after 48 h treatment with FPQYLQYPY, the decrease in the level of cell migration was noteworthy (**Figures 5C,D**). These two experiments show that FPQYLQYPY can adjust the migration of Ang II -stimulated VSMCs.

Transcriptomics Responses of FPQYLQYPY to Ang II-Stimulated VSMCs

Transcriptome sequencing was performed using RNA from A7r5 cells. The typically changed genes were identified and shown in the heatmaps and volcano maps (**Figure 6**). The results showed that 342 differentially expressed genes (DEGs) ($P < 0.05$) were detected between the FPQYLQYPY treated group and the Ang II-treated group, and 797 genes between the Ang II-treated group and the control group.

After obtaining the differentially expressed genes, GO enrichment analysis was performed in order to describe their functions, covered biological processes, cellular components, and molecular functions. There were 212 significantly upregulated and 117 significantly downregulated genes in the comparison of the FPQYLQYPY and Ang II-treated groups. The top 30 GO-terms of significantly differential genes were mainly involved in stress fiber, actin cytoskeleton organization, positive regulation of cell migration, wound healing, and actin binding. These enriched GO terms may be related to vascular remodeling. Furthermore, the top 30 GO-terms of DEGs in the Ang II-treated group and the control group are shown in **Figure 7**. The DEGs were mainly involved in cytosolic ribosome, cytoplasmic translation, structural constituent of ribosome, and actin filament binding.

Pathway analysis using KEGG can further appreciate the function of genes and their interactions. Differential genes were enriched in cardiovascular disease-related pathways between the FPQYLQYPY-treated group and the Ang II-treated group, and between the Ang II-treated group and the control group. The top 20 enriched pathways in the FPQYLQYPY-treated group and the Ang II-treated group are presented in **Figure 8** and were involved in diabetic cardiomyopathy, dilated cardiomyopathy, hypertrophic cardiomyopathy, regulation of actin cytoskeleton, cardiac muscle contraction, MAPK signaling pathway, and vascular smooth muscle contraction. However, the KEGG pathway enrichment analysis of the DEGs in the Ang II-treated group and the control group revealed diabetic cardiomyopathy, pathways of neurodegeneration, multiple diseases, cardiac muscle contraction, and the ribosome.

Overall, the analysis of pathways showed that the ACE inhibitory peptide may have a regulatory effect on Ang II -induced changes in cardiovascular-related pathways at the cellular level.

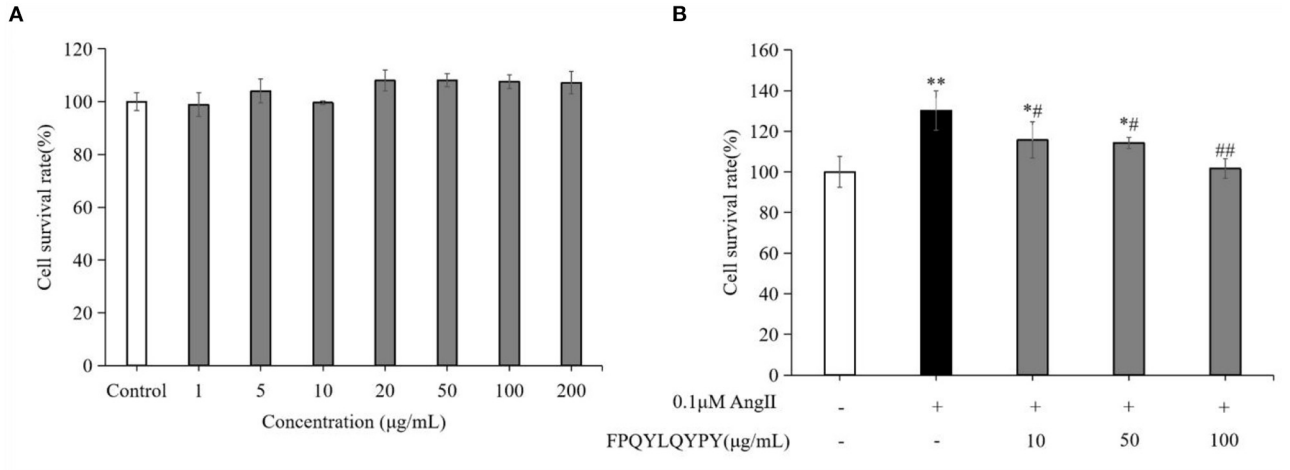

FIGURE 4 | FPQYLQYPY inhibited proliferation of Ang II-stimulated VSMCs. **(A)** Cytotoxicity of FPQYLQYPY in VSMCs cells measured by CCK-8. **(B)** FPQYLQYPY inhibited Ang II-stimulated proliferation of VSMCs. Data are expressed as mean ± SD. $^{*}P < 0.05$ and $^{**}P < 0.01$, respectively, as compared to the control group. $^{\#}P < 0.05$ and $^{\#\#}P < 0.01$, respectively, as compared to the Ang II-treated group.

Verification of Differentially Expressed Genes by RT-PCR

Based on the GO and pathway results, we selected 9 genes among all identified DEGs for verification by RT-PCR. As shown in **Figure 9**. Efna4, Igf1r, Itga3, Plcb3, Cox5b, and Taok3 were downregulated, whereas Shc4, Tgfb1, and Myl4 were upregulated in the comparison of FPQYLQYPY-treated group and the Ang II-treated group. Although, in the comparison of the Ang II-treated group and the control group, Shc4, Itga3, Tgfb1, and Cox5b were downregulated, but Efna4, Igf1r, Plcb3, Taok3, and Myl4 were upregulated. These results are consistent with transcriptome sequencing.

DISCUSSION

Enzyme hydrolysis is a commonly used method to obtain biologically active peptides from milk proteins (32). Compared with unhydrolyzed proteins, these soluble hydrolysates exhibited stronger ACE inhibition. In the present work, ACE inhibitory peptides were produced *in vitro* using gastrointestinal enzymes (usually pepsin, trypsin, or α-chymotrypsin). In previous studies, the effective ACE inhibitory peptides released from goat whey protein and casein by pepsin hydrolysis, PEQSLACQCL of β-lactoglobulin (f 113-122), QSLVYPFTGPI of β-casein (residue 56-66), and ARHPHLSFM of κ-casein (f 96-106), were first introduced by Ibrahim et al. (33). In this study, we used trypsin to hydrolyze goat milk caseins to release the peptides with ACE-inhibitory activity, and used RP-HPLC to gradually separate hydrolysates based on difference in polarity. The ACE inhibitory peptide F3 showed the strongest ACE inhibitory activity and was obtained after separation for four times (**Figure 1I**).

The *in vivo* antihypertensive effects of most ACE-inhibitory peptides have been attributed to their low molecular weight, and short amino acid sequences. For example, after fermenting goat milk with *Lactobacillus casei*, the supernatant was ultrafiltered with 3, 5, and 10 kDa ultrafiltration membranes to obtain different permeate and retentate samples, of which the 3 kDa sample showed the highest ACE-inhibitory activity (34). Aslam et al. (35) used ultrafiltration to separate five peptides with a higher concentration and a molecular weight <3 kDa in fermented goat milk. Among them, VLPVPQKAVPQ and VLPVPQKVVPQ had good ACE-inhibitory activity, and they were composed of <12 amino acids (35). Furthermore, the ACE-inhibitory activity of peptides seemed to rely on their amino acid composition and hydrophobicity. The somatic-ACE consisted of two homologous domains, N- and C-domains (36), which seemed to play an important role in blood pressure regulation (37). Most of the ACE-binding peptides were strongly influenced by the residues in the three positions closest to the C-terminal. In particular, the peptides with hydrophobic amino acids at the C-terminal showed prominent ACE-inhibitory activity, including Phe, Trp, Tyr, Val, Leu, Ile, and Pro, were more favorable for binding with ACE. Besides, amino acid sequences with higher Pro content could enhance the ACE inhibition effect and as well as intensify the strong digestive resistance of the gastrointestinal tract (7). VPP and IPP conformed to these characteristics, and they are the most widely studied ACE inhibitory peptides. They are highly resistant to digestion in the gastrointestinal tract, can reach the small intestine in complete form (38), and have been shown to improve blood pressure in hypertensive patients (39).

In this study, we identified that the peptide with the highest ACE inhibitory activity was Phe-Pro-Gln-Tyr-Leu-Gln-Tyr-Pro-Tyr (FPQYLQYPY), which was derived from α-casein of goat milk (**Figure 2**). Based on currently available information, this peptide has not been previously reported. This peptide had a low molecular weight with many hydrophobic residues, was rich in proline, and ended with the hydrophobic amino acid

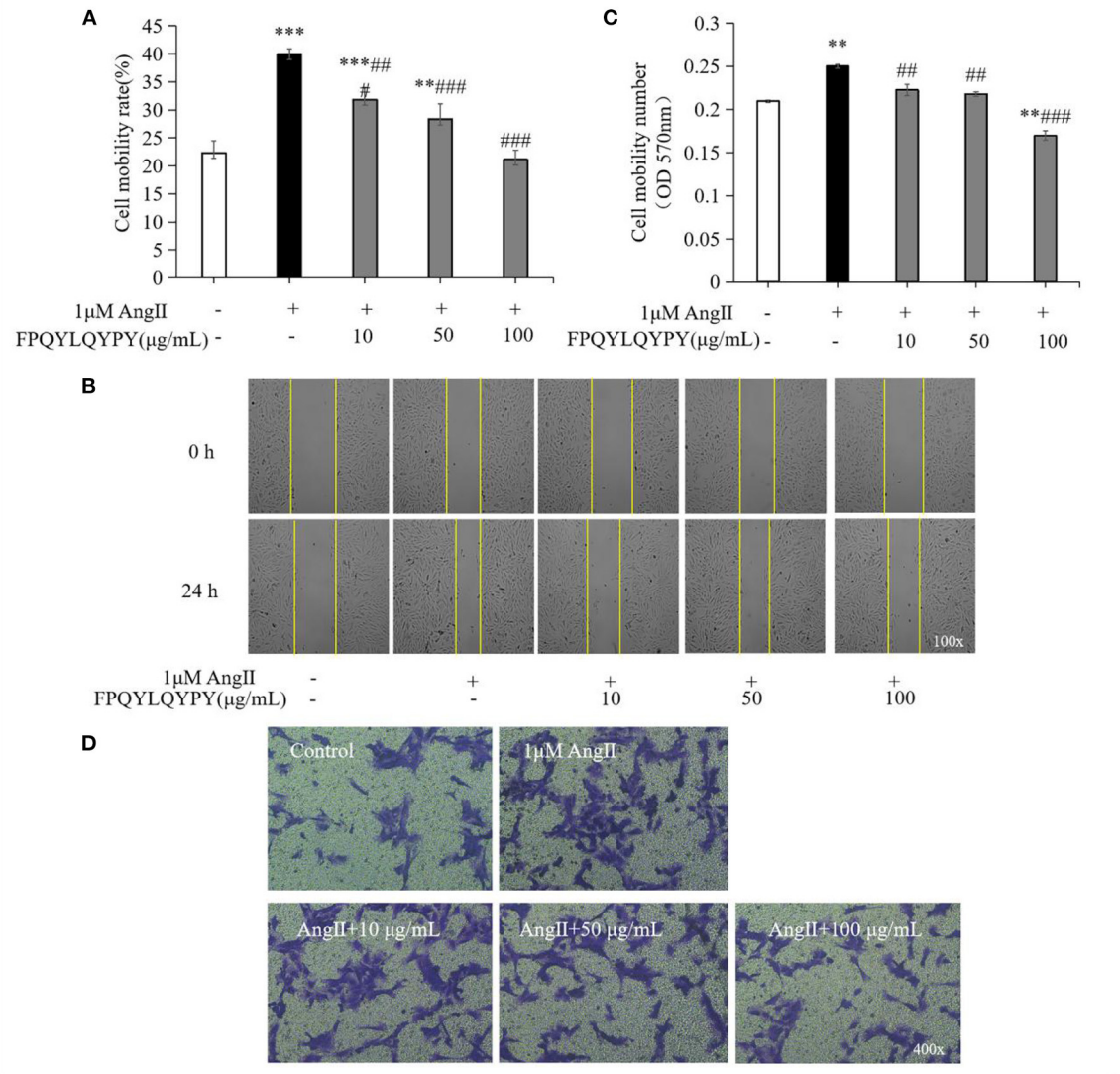

FIGURE 5 | FPQYLQYPY inhibited migration of Ang II-stimulated VSMCs. **(A,B)** Cell migration was evaluated by wound healing assay, and the distance of the wound healing area was measured by ImageJ software. **(C,D)** Cell migration was evaluated by Transwell experiments. All the data are represented as the mean ± SD. $^{**}P < 0.01$ and $^{***}P < 0.001$, respectively, as compared to the control group. $^{\#\#}P < 0.01$ and $^{\#\#\#}P < 0.001$, respectively, as compared to the Ang II-treated group.

Tyr at its C-terminal. Furthermore, it was consistent with the characteristics of high ACE-inhibitory activity sequence as described above, and this may indicate a structure-activity relationship, although more research is needed.

In vitro gastrointestinal enzyme simulation can simply describe the changes of a peptide during oral administration (40). After the digestion, we found that the hydrolysate still had ACE inhibitory activity (**Table 1**), however, we were still unclear whether the peptide was hydrolyzed to the active fragment, or changed to the fragment in this digestive process. These topics will be the focus of future study. We also investigated the inhibition pattern of FPQYLQYPY and confirmed the inhibitory model of the peptide as non-competitive (**Figure 3**), which was found to be the common inhibition pattern of ACE inhibitory peptides in previous reports (41, 42).

Due to the important role of ACE in hydrolyzing angiotensin I into angiotensin II under the condition of strong vasoconstriction, ACE-inhibition has always been a key target of anti-hypertensive research (43, 44). It has been stated that ACE-inhibitory peptides have a variety of blood pressure-lowering effects other than ACE inhibition (8). Previous reports indicate that the effect of angiotensin II on VSMCs is widely used to explore the mechanism of cardiovascular disease (45). Therefore, in this study, the anti-hypertension effects of the

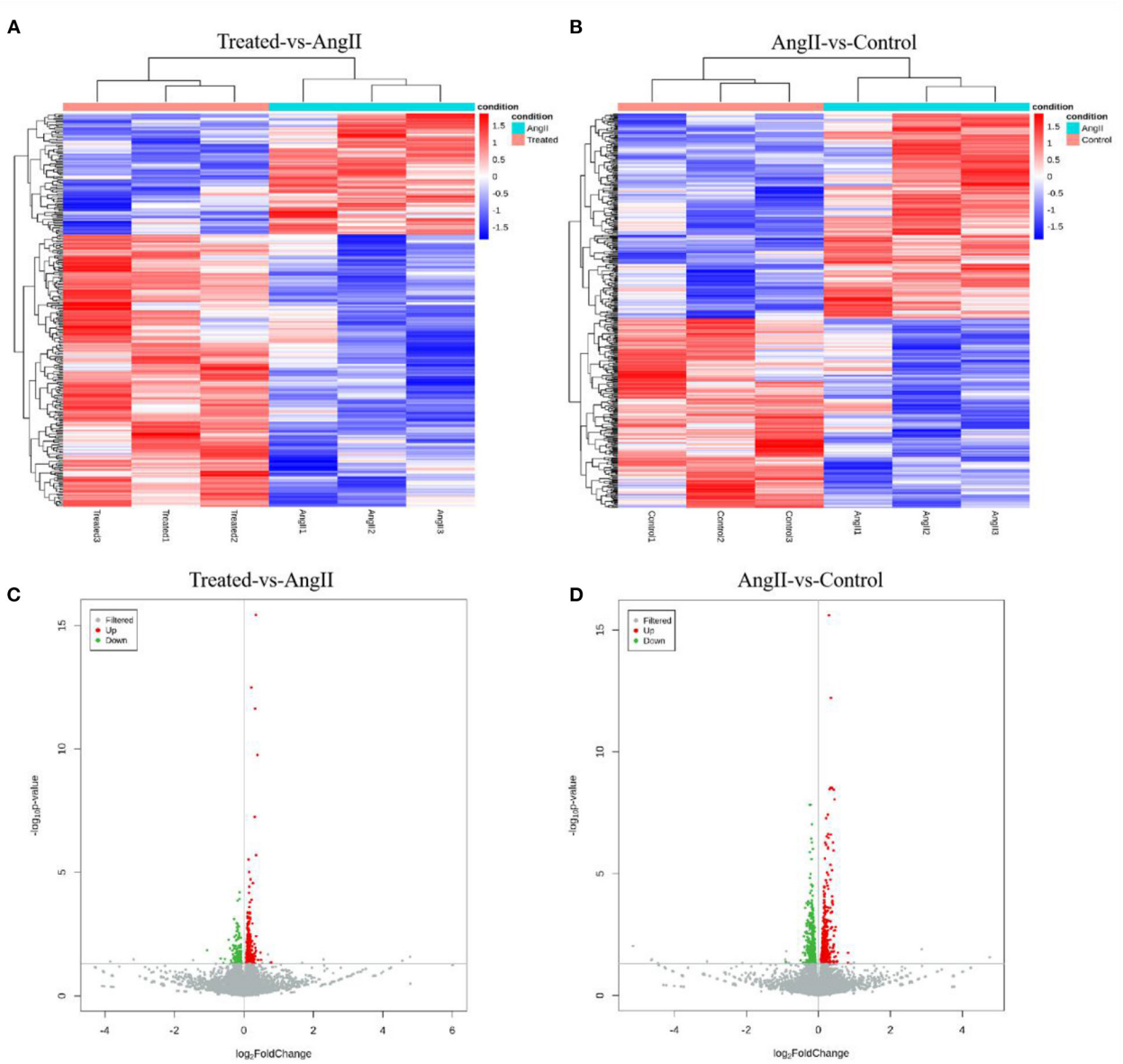

FIGURE 6 | Transcriptome gene expression altered in the VSMCs. **(A)** Hierarchal clustering of differentially expressed genes (DEGs) in FPQYLQYPY treated group and Ang II-treated group. **(B)** Hierarchal clustering of differentially expressed genes (DEGs) in Ang II-treated group and control group. **(C)** The volcano map of differentially expressed genes (DEGs) in FPQYLQYPY treated group and Ang II-treated group. **(D)** The volcano map of differentially expressed genes (DEGs) in Ang II-treated group and control group.

purified peptide *in vitro* were investigated by studying its modulation of the effects on angiotensin II-stimulated vascular smooth muscle cells.

Dysfunction of VSMCs can be induced by Ang II and results in adverse events like increased oxidative stress, inflammation, migration, and hyperplasia, and therefore plays a key role in the pathogenesis of hypertension, restenosis, and atherosclerosis (46, 47). The pathological proliferation and migration of VSMCs induced by Ang II are the dominative factor of vascular remodeling (43). Studies have found that antihypertensive peptides derived from egg white can inhibit migration and regulate Ang II-stimulated VSMCs (48, 49). Aberrant proliferation and migration of vascular smooth muscle cells are a major pathological phenomenon in hypertension (45). In this study, we found that co-incubation with FPQYLQYPY could significantly inhibition the excessive proliferation and migration of Ang II-stimulated VSMCs (**Figures 4B**, **5**). These result indicated that FPQYLQYPY or other ACE inhibitory peptides may improve the vascular remodeling induced by Ang II.

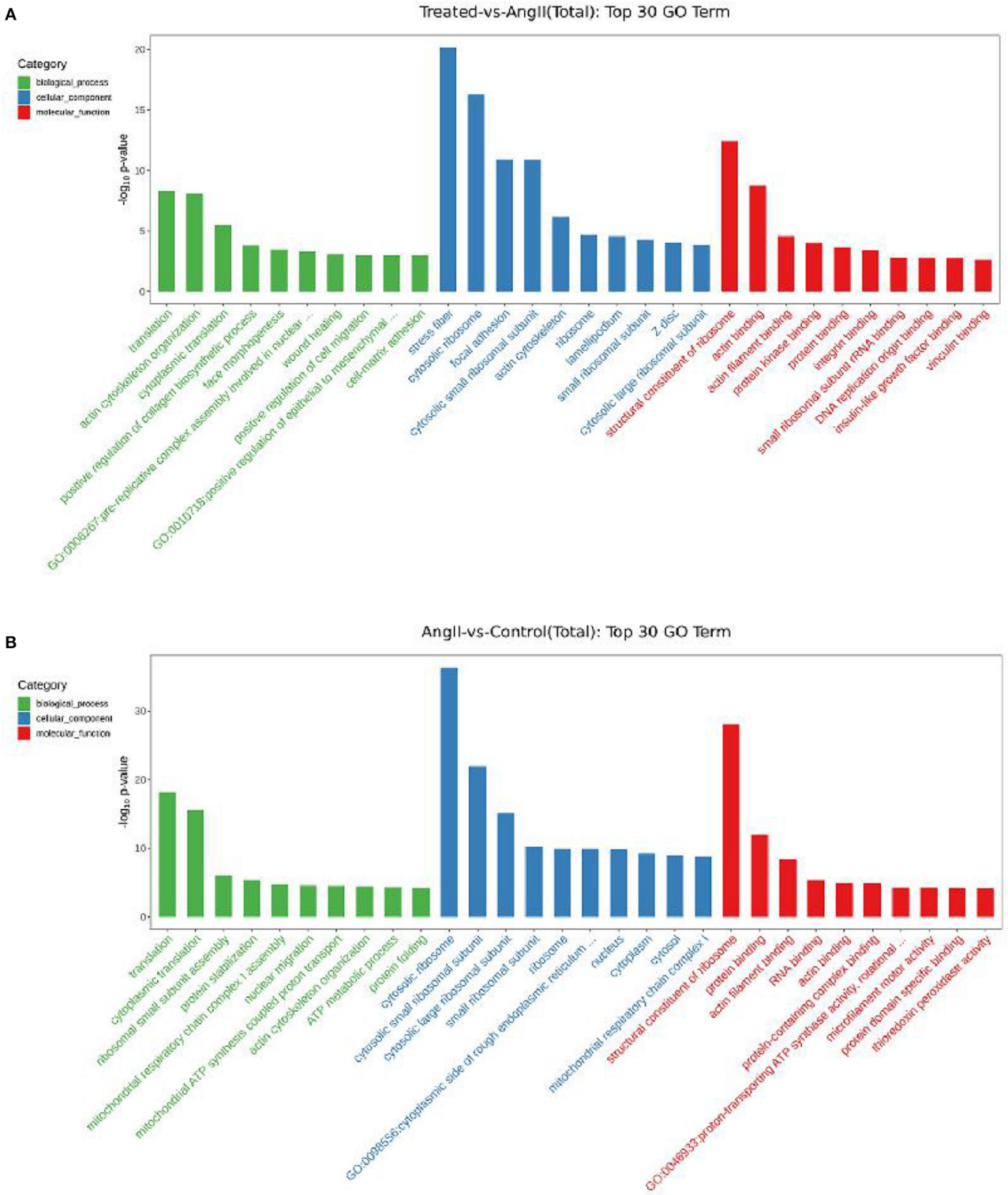

FIGURE 7 | Gene Ontology (GO) enrichment analysis for differentially expressed genes (DEGs). **(A)** Top 30 GO-terms of DEGs in FPQYLQYPY treated group and Ang II-treated group. **(B)** Top 30 GO-terms of DEGs in the Ang II-treated group and control group.

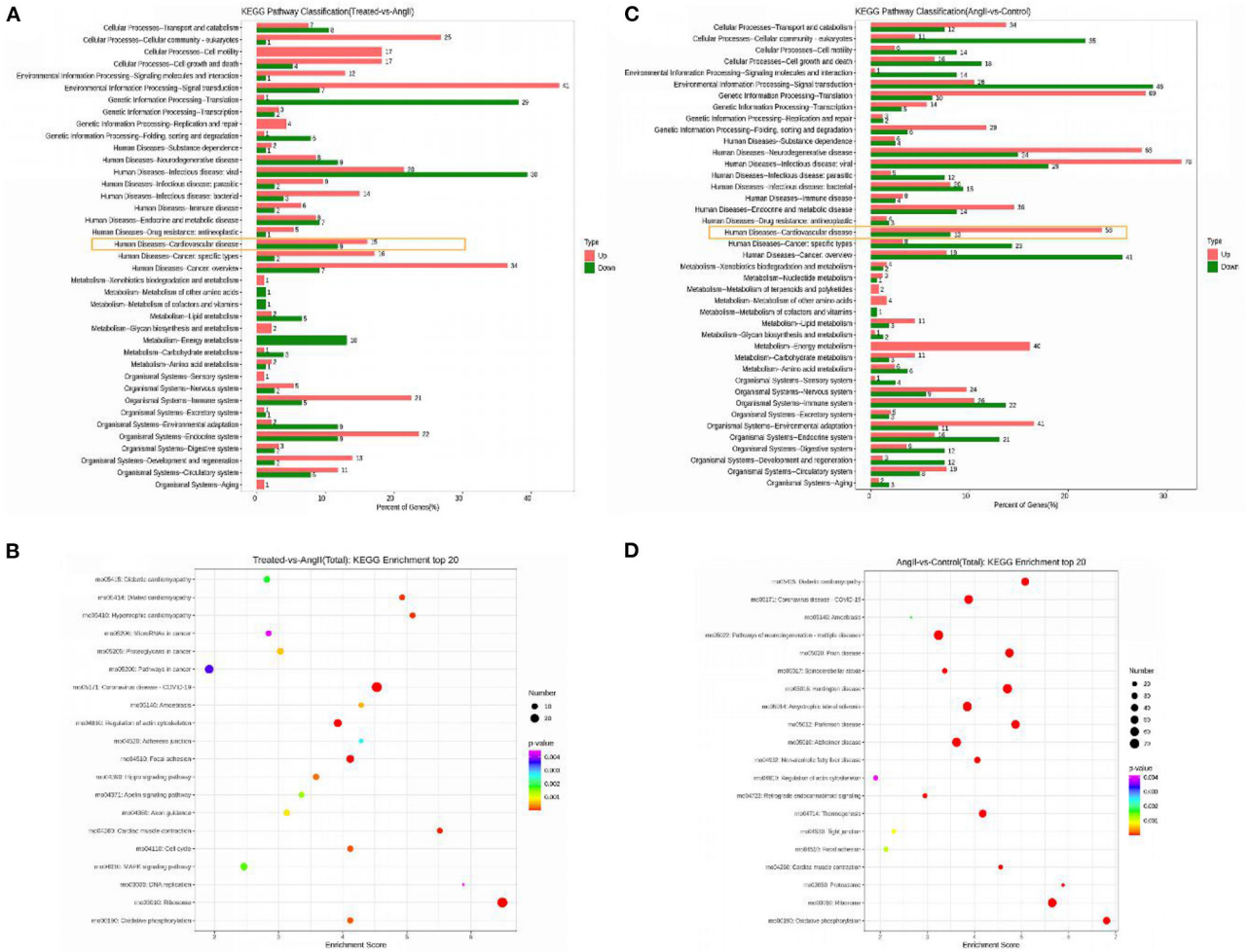

FIGURE 8 | Kyoto Encyclopedia of Genes and Genomes (KEGG) enrichment analysis for differentially expressed genes (DEGs). **(A)** KEGG pathway classification of DEGs in the FPQYLQYPY treated group and Ang II-treated group. **(B)** Bubble chart of the top 20 significantly enriched pathways for DEGs in the FPQYLQYPY treated group and Ang II-treated group. **(C)** KEGG pathway classification of DEGs in the Ang II-treated group and control group. **(D)** Bubble chart of the top 20 significantly enriched pathways for DEGs in the Ang II-treated group and control group.

Transcriptome sequencing analysis revealed the mechanism of the peptide effects on Ang II-stimulated VSMCs, the differentially expressed genes were analysis by GO and KEGG enrichment to determine their mainly biological functions or pathways. The results showed that, the differentially expressed genes were enriched in cardiovascular disease-related pathways, mainly involved in cardiomyopathy, cardiac muscle contraction, and vascular smooth muscle contraction. The differentially expressed genes, such as Itga3 of the integrin family and transforming growth factor beta-1 (Tgfb-1) and insulin-like growth factor 1 receptor (Igf-1R) of the growth factor family, and these genes tend to affect cell proliferation and migration, they are likely to cause fibrotic effects on vascular tissue or angiogenesis (50, 51). At the same time, the peptide also regulated the expression of the Efna4 and Taok3 genes in the MAPK signaling pathway, which has important functions in cardiovascular disease, can repair vascular injury, and is involved in cardiac remodeling (52). Moreover, Pcb3, Cox5b, and Myl4 are involved in atherosclerosis, diabetic cardiomyopathy, and cardiac muscle contraction, respectively. Furthermore, changes in insulin signaling mediated by Shc4 may be involved in the process of cardiac development (53, 54).

The pathways in which these DEGs are involved suggest that the peptide had the ability to modulate cellular dysfunction caused by Ang II on VSMCs. And the regulatory effects of this peptide were manifested in vascular remodeling, cardiac remodeling, and cardiomyopathy. These results correspond to the inhibitory ability of the peptide on excessive proliferation and migration of the Ang II-stimulated VSMCs shown in experiments. Simultaneously, our findings illustrated other antihypertensive mechanisms of this peptide *in vitro*.

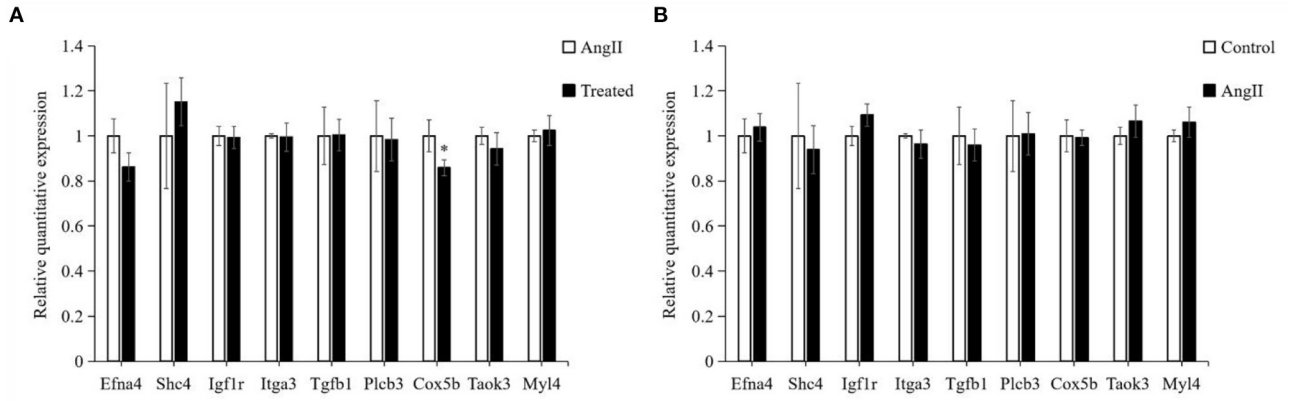

FIGURE 9 | Verification of identified differentially expressed genes (DEGs) in VSMCs by RT-PCR. **(A)** mRNA expression of identified DEGs in the FPQYLQYPY treated group and Ang II-treated group. **(B)** mRNA expression of identified DEGs in the Ang II-treated group and control group. All the data are represented as the mean ± SD. $^*P < 0.05$.

CONCLUSION

In conclusion, a novel ACE-inhibitory peptide was separated and purified from goat milk casein hydrolysates, and the amino acid sequence was identified as FPQYLQYPY. The bioactivity of the hydrolysate persisted against *in vitro* gastrointestinal digest, and the ACE-inhibitory model of the peptide was confirmed as non-competitive. The anti-hypertension of FPQYLQYPY was evaluated by Ang II-stimulated VSMCs *in vitro*. This peptide could inhibit the excessive proliferation and migration of VSMCs. Besides, transcriptome sequencing analysis revealed that DEGs were enriched in cardiovascular disease-related pathways and implicated the regulatory effects of the peptide on vascular remodeling. The results of this study show that, in addition to inhibiting ACE, this peptide also regulates vascular dysfunction, which may broaden the application of the ACE-inhibitory peptides as functional food ingredients. However, the precise antihypertensive mechanism of this peptide remain unclear, and more studies are needed in the future to fully understand this process.

DATA AVAILABILITY STATEMENT

The datasets presented in this study can be found in online repositories. The names of the repository/repositories and accession number(s) can be found below: NCBI; PRJNA809493

AUTHOR CONTRIBUTIONS

ZQ: data curation, formal analysis, investigation, writing—review and editing, and validation. JW, LP, XP, YG, and SC: funding acquisition, resources, and validation. ZH and QL: data curation, formal analysis, and investigation. KF: investigation and writing—review and editing. MS: methodology, writing—reviewing and editing, and investigation. YCh: investigation, writing—review and editing, and supervision. YCa: project administration, funding acquisition, writing—reviewing and editing, investigation, supervision, and resources. GL: project administration, funding acquisition, writing—reviewing and editing, investigation, and supervision. All authors contributed to the article and approved the submitted version.

FUNDING

The authors express their gratitude to the Guangdong Province Engineering Research Center for Bioactive Natural Products (2016B090920093), Guangdong Provincial Key Laboratory of Nutraceuticals and Functional Foods (2018B030322010), the Program for Guangdong Introducing Innovative and Entrepreneurial Teams (2019ZT08N291), the Project funded by China Postdoctoral Science Foundation (2020M672651), and the Innovation Platform and Talent Plan of Hunan Engineering and Technology Research Center for Nutrition and Health Products (2019TP2066).

SUPPLEMENTARY MATERIAL

The Supplementary Material for this article can be found online at: https://www.frontiersin.org/articles/10.3389/fnut.2022.878768/full#supplementary-material

REFERENCES

1. Mills KT, Stefanescu A, He J. The global epidemiology of hypertension. *Nat Rev Nephrol.* (2020) 16:223–37. doi: 10.1038/s41581-019-0244-2

2. Lu J, Lu Y, Wang X, Li X, Linderman GC, Wu C, et al. Prevalence, awareness, treatment, and control of hypertension in China: data from 1·7 million adults in a population-based screening study (China PEACE Million Persons Project). *Lancet.* (2017) 390:2549–58. doi: 10.1016/S0140-6736(17)32478-9

3. Wang JG, Staessen JA. Genetic polymorphisms in the renin-angiotensin system: relevance for susceptibility to cardiovascular disease. *Eur J Pharmacol.* (2000) 410:289–302. doi: 10.1016/S0014-2999(00)00822-0
4. Belova LA. Angiotensin II-generating enzymes. *Biochemistry.* (2000) 65:1337–45. doi: 10.1023/A:1002848402911
5. Marques C, Amorim MM, Pereira JO, Pintado ME, Moura D, Calhau C, et al. Bioactive peptides: are there more antihypertensive mechanisms beyond ACE inhi-bition? *Curr Pharm Design.* (2012) 18:4706. doi: 10.2174/138161212802651670
6. Duprez DA. Role of the renin-angiotensin-aldosterone system in vascular remodeling and inflammation: a clinical review. *J Hypertens.* (2006) 24:983–91. doi: 10.1097/01.hjh.0000226182.60321.69
7. Basatemur GL, Jørgensen HF, Clarke MCH, Bennett MR, Mallat Z. Vascular smooth muscle cells in atherosclerosis. *Nat Rev Cardiol.* (2019) 16:727–44. doi: 10.1038/s41569-019-0227-9
8. Fan H, Liao W, Wu J. Molecular interactions, bioavailability, and cellular mechanisms of angiotensin-converting enzyme inhibitory peptides. *J Food Biochem.* (2019) 43:e12572. doi: 10.1111/jfbc.12572
9. Lin S, Lin S, Chen C, Fu Y, Weng C. Exploring a new natural treating agent for primary hypertension: recent findings and forthcoming perspectives. *J Clin Med.* (2019) 8:2003. doi: 10.3390/jcm8112003
10. Xu Q, Yan X, Zhang Y, Wu J. Current understanding of transport and bioavailability of bioactive peptides derived from dairy proteins: a review. *Int J Food Sci Tech.* (2019) 54:1930–41. doi: 10.1111/ijfs.14055
11. Hartmann R, Meisel H. Food-derived peptides with biological activity: from research to food applications. *Curr Opin Biotech.* (2007) 18:163–9. doi: 10.1016/j.copbio.2007.01.013
12. Geerlings A, Villar IC, Zarco FH, Sánchez M, Vera R, Gomez AZ, et al. Identification and characterization of novel angiotensin-converting enzyme inhibitors obtained from goat milk. *J Dairy Sci.* (2006) 89:3326–35. doi: 10.3168/jds.S0022-0302(06)72369-4
13. Chakrabarti S, Liao W, Davidge ST, Wu J. Milk-derived tripeptides IPP (Ile-Pro-Pro) and VPP (Val-Pro-Pro) differentially modulate angiotensin II effects on vascular smooth muscle cells. *J Funct Foods.* (2017) 30:151–8. doi: 10.1016/j.jff.2016.12.022
14. Claeys WL, Verraes C, Cardoen S, De Block J, Huyghebaert A, Raes K, et al. Consumption of raw or heated milk from different species: an evaluation of the nutritional and potential health benefits. *Food Control.* (2014) 42:188–201. doi: 10.1016/j.foodcont.2014.01.045
15. Lee KJ, Kim SB, Ryu JS, Shin HS, Lim JW. Separation and purification of angiotensin converting enzyme inhibitory peptides derived from goat's milk casein hydrolysates. *Asian-Australas J Anim Sci.* (2005) 18:741–6. doi: 10.5713/ajas.2005.741
16. Gómez-Ruiz JÁ, Taborda G, Amigo L, Recio I, Ramos M. Identification of ACE-inhibitory peptides in different Spanish cheeses by tandem mass spectrometry. *Eur Food Res Technol.* (2006) 223:595–601. doi: 10.1007/s00217-005-0238-0
17. Espejo-Carpio FJ, De Gobba C, Guadix A, Guadix EM, Otte J. Angiotensin I-converting enzyme inhibitory activity of enzymatic hydrolysates of goat milk protein fractions. *Int Dairy J.* (2013) 32:175–83. doi: 10.1016/j.idairyj.2013.04.002
18. Üstün Aytekin Ö, Seker A, Arisoy S. The effect of *in vitro* gastrointestinal simulation on bioactivities of kefir. *Int J Food Sci Tech.* (2019) 55:283–92. doi: 10.1111/ijfs.14274
19. Zhang Y, Zhang Y, Chen P, Shu F, Li K, Qiao L, et al. A novel angiotensin-I converting enzyme inhibitory peptide derived from the glutelin of vinegar soaked black soybean and its antihypertensive effect in spontaneously hypertensive rats. *J Biochem.* (2019) 166:223–30. doi: 10.1093/jb/mvz029
20. Hernández-Ledesma B, Recio I, Ramos M, Amigo L. Preparation of ovine and caprine β-lactoglobulin hydrolysates with ACE-inhibitory activity. identification of active peptides from caprine β-lactoglobulin hydrolysed with thermolysin. *Int Dairy J.* (2002) 12:805–12. doi: 10.1016/S0958-6946(02)00080-8
21. Chen Y, Gao X, Wei Y, Liu Q, Jiang Y, Zhao L, et al. Isolation, purification and the anti-hypertensive effect of a novel angiotensin I-converting enzyme (ACE) inhibitory peptide from ruditapes philippinarum fermented with bacillus natto. *Food Funct.* (2018) 9:5230–7. doi: 10.1039/C8FO01146J
22. Simsek S, Sánchez-Rivera L, El SN, Karakaya S, Recio I. Characterisation of *in vitro* gastrointestinal digests from low fat caprine kefir enriched with inulin. *Int Dairy J.* (2017) 75:68–74. doi: 10.1016/j.idairyj.2017.07.004
23. Lo WMY, Li-Chan ECY. Angiotensin I converting enzyme inhibitory peptides from *in vitro* pepsin-pancreatin digestion of soy protein. *J Agr Food Chem.* (2005) 53:3369–76. doi: 10.1021/jf048174d
24. Lin Q, Liao W, Bai J, Wu W, Wu J. Soy protein-derived ACE-inhibitory peptide LSW (Leu-Ser-Trp) shows anti-inflammatory activity on vascular smooth muscle cells. *J Funct Foods.* (2017) 34:248–53. doi: 10.1016/j.jff.2017.04.029
25. Seo H, Kim SW, Lee CY, Lim KH, Lee J, Choi E, et al. A spleen tyrosine kinase inhibitor attenuates the proliferation and migration of vascular smooth muscle cells. *Biol Res.* (2017) 50. doi: 10.1186/s40659-016-0106-3
26. Wang Y, Zhang X, Gao L, Li J, Chen W, Chi J, et al. Cortistatin exerts antiproliferation and antimigration effects in vascular smooth muscle cells stimulated by Ang II through suppressing ERK1/2, p38 MAPK, JNK and ERK5 signaling pathways. *Ann Trans Med.* (2019) 7:561. doi: 10.21037/atm.2019.09.45
27. Cao Y, Miao J, Liu G, Luo Z, Xia Z, Liu F, et al. Bioactive peptides isolated from casein phosphope-ptides enhance calcium and magnesium uptake in Caco-2 cell monolayers. *J Agr Food Chem.* (2017) 65:2307–14. doi: 10.1021/acs.jafc.6b05711
28. Bravo FI, Mas Capdevila A, Margalef M, Arola Arnal A, Muguerza B. Novel antihypertensive peptides derived from chicken foot proteins. *Mol Nutr Food Res.* (2019) 63:1801176. doi: 10.1002/mnfr.201801176
29. Sultan S, Huma N, Butt MS, Shahid M. Antihypertensive and antioxidative potential of water soluble peptide fraction from different yoghurts. *J Food Process Pres.* (2017) 41:e12979. doi: 10.1111/jfpp.12979
30. Byun HG, Kim SK. Structure and activity of angiotensin I converting enzyme inhibitory peptides derived from Alaskan pollack skin. *J Biochem Mol Biol.* (2002) 35:239–43. doi: 10.5483/BMBRep.2002.35.2.239
31. Moreno-Montoro M, Olalla-Herrera M, Rufián-Henares JÁ, et al. Antioxidant, ACE-inhibitory and antimicrobial activity of fermented goat milk: activity and physicochemical property relationship of the peptide components. *Food Funct.* (2017) 8:2783–91. doi: 10.1039/C7FO00666G
32. Espejo-Carpio FJ, Pérez-Gálvez R, Guadix EM, Guadix A. Optimisation of the hydrolysis of goat milk protein for the production of ACE-inhibitory peptides. *J. Dairy Res.* (2013) 80:214–22. doi: 10.1017/S0022029913000083
33. Ibrahim HR, Ahmed AS, Miyata T. Novel angiotensin-converting enzyme inhibitory peptides from caseins and whey proteins of goat milk. *J Adv, Res.* (2017) 8:63–71. doi: 10.1016/j.jare.2016.12.002
34. Parmar H, Hati S, Sakure A. In vitro and in silico analysis of novel ACE-inhibitory bioactive peptides derived from fermented goat milk. *Int J Pept Res Ther.* (2018) 24:441–53. doi: 10.1007/s10989-017-9630-4
35. Aslam MZ, Shoukat S, Hongfei Z, Bolin Z. Peptidomic analysis of ACE inhibitory peptides extracted from fermented goat milk. *Int J Pept Res Ther.* (2019) 25:1259–70. doi: 10.1007/s10989-018-9771-0
36. Soubrier F, Alhenc-Gelas F, Hubert C, Allegrini J, John M, Tregear G, et al. Two putative active centers in human angiotensin I-converting enzyme revealed by molecular cloning. *Proc Natl Acad Sci USA.* (1988) 85:9386–0. doi: 10.1073/pnas.85.24.9386
37. Natesh R, Schwager SLU, Sturrock ED, Acharya KR. Crystal structure of the human angiotensin-converting enzyme–lisinopril complex. *Nature.* (2003) 421:551–4. doi: 10.1038/nature01370
38. Meyer J, Bütikofer U, Walther B, Wechsler D, Sieber R. Hot topic: changes in angiotensin-converting enzyme inhibition and concentrations of the tripeptides Val-Pro-Pro and Ile-Pro-Pro during ripening of different Swiss cheese varieties. *J Dairy Sci.* (2009) 92:826–36. doi: 10.3168/jds.2008-1531
39. Cicero AFG, Fogacci F, Colletti A. Potential role of bioactive peptides in prevention and treatment of chronic diseases: a narrative review. *Brit J Pharmacol.* (2017) 174:1378–94. doi: 10.1111/bph.13608
40. Brodkorb A, Egger L, Alminger M, Alvito P, Assunção R, Ballance S, et al. INFOGEST static *in vitro* simulation of gastrointestinal food digestion. *Nat Protoc.* (2019) 14:991–1014. doi: 10.1038/s41596-018-0119-1
41. Jung W, Mendis E, Je J, Park PJ, Son BW, Kim HC, et al. Angiotensin I-converting enzyme inhibitory peptide from yellowfin sole (Limanda aspera) frame protein and its antihypertensive effect in spontaneously hypertensive rats. *Food Chem.* (2006) 94:26–32. doi: 10.1016/j.foodchem.2004.09.048

42. Kuba M, Tanaka K, Tawata S, Takead Y, Yasuda M. Angiotensin I-converting enzyme inhibitory peptides isolated from tofuyo fermented soybean food. *Biosci Biotechnol Biochem.* (2003) 67:1278–83. doi: 10.1271/bbb.67.1278
43. Song T, Lv M, Sun B, Zheng L, Zhao M. Tripeptides Val-Pro-Pro (VPP) and Ile-Pro-Pro (IPP) regulate the proliferation and migration of vascular Smooth muscle cells by interfering Ang II-induced human umbilical vein endothelial cells derived EVs delivering RNAs to VSMCs in the co-culture model. *J Agric Food Chem.* (2020) 68:6628–37. doi: 10.1021/acs.jafc.0c02060
44. Chappell MC, Iyer SN, Diz DI, Ferrario CM. Antihypertensive effects of angiotensin-(1-7). *Braz J Med Biol Re.* (1998) 31:1205–12. doi: 10.1590/S0100-879X1998000900014
45. Tian L, Cai D, Zhuang D, Wang W, Wang X, Bian X, et al. miR-96-5p regulates proliferation, migration, and apoptosis of vascular smooth muscle cell induced by angiotensin II via targeting NFAT5. *J Vasc Res.* (2020) 57:86–96. doi: 10.1159/000505457
46. Das S, Zhang E, Senapati P, Amaram V, Reddy MA, Stapleton K, et al. A novel angiotensin II–induced long noncoding RNAGiver regulates oxidative stress, inflammation, and proliferation in vascular smooth muscle cells. *Circ Res.* (2018) 123:1298–312. doi: 10.1161/CIRCRESAHA.118.313207
47. Simões E Silva AC, Teixeira MM. ACE inhibition, ACE2 and angiotensin-(1-7) axis in kidney and cardiac inflammation and fibrosis. *Pharmacol Res.* (2016) 107:154–62. doi: 10.1016/j.phrs.2016.03.018
48. Liao W, Fan H, Wu J. Egg white-derived antihypertensive peptide IRW (Ile-Arg-Trp) inhibits angiotensin II-stimulated migration of vascular smooth muscle cells via angiotensin type I receptor. *J Agr Food Chem.* (2017) 66:5133–8. doi: 10.1021/acs.jafc.8b00483
49. Liao W, Chakrabarti S, Davidge ST, Wu J. Modulatory effects of egg white ovotransferrin-derived tripeptide IRW (Ile-Arg-Trp) on vascular smooth muscle cells against angiotensin II stimulation. *J Agr Food Chem.* (2016) 64:7342–7. doi: 10.1021/acs.jafc.6b03513
50. Piard C, Jeyaram A, Liu Y, Caccamese J, Jay SM, Chen Y, et al. 3D printed HUVECs/MSCs cocultures impact cellular interactions and angiogenesis depending on cell-cell distance. *Biomaterials.* (2019) 222:119423. doi: 10.1016/j.biomaterials.2019.119423
51. Lee S, Chun JN, Lee H, Park HH, So I, Jeon J, et al. Transcriptome analysis of the Anti-TGFβ effect of *Schisandra chinensis* fruit extract and Schisandrin B in A7r5 vascular smooth muscle cells. *Life.* (2021) 11:163. doi: 10.3390/life11020163
52. Muslin AJ. MAPK signalling in cardiovascular health and disease: molecular mechanisms and therapeutic targets. *Clin. Sci.* (2008) 115:203–18. doi: 10.1042/CS20070430
53. Luo Z, Xu L, Lu J, Shen Y, Tang Y, Wang X, et al. Down-regulation of the insulin signaling pathway by SHC may correlate with congenital heart disease in Chinese populations. *Clin Sci.* (2020) 134:349–58. doi: 10.1042/CS20190255
54. Obreztchikova M, Elouardighi H, Ho M, Wilson BA, Gertsberg Z, Steinberg SF. Distinct signaling functions for Shc isoforms in the heart. *J Biol Chem.* (2006) 281:20197–204. doi: 10.1074/jbc.M601859200

Conflict of Interest: JW, LP, XP, YG, and SC were employed by Ausnutria Dairy (China) Co., Ltd.

The remaining authors declare that the research was conducted in the absence of any commercial or financial relationships that could be construed as a potential conflict of interest.

Publisher's Note: All claims expressed in this article are solely those of the authors and do not necessarily represent those of their affiliated organizations, or those of the publisher, the editors and the reviewers. Any product that may be evaluated in this article, or claim that may be made by its manufacturer, is not guaranteed or endorsed by the publisher.

frontiers | Frontiers in Nutrition

ORIGINAL RESEARCH
published: 11 April 2022
doi: 10.3389/fnut.2022.873578

Physicochemical Properties and *in vitro* Digestibility of Myofibrillar Proteins From the Scallop Mantle (*Patinopecten yessoensis*) Based on Ultrahigh Pressure Treatment

Xiaohan Liu†, Kemin Mao†, Yaxin Sang‡, Guifang Tian*‡, Qiuyue Ding and Wenyi Deng*

College of Food Science and Technology, Hebei Agricultural University, Baoding, China

OPEN ACCESS

Edited by:
Hang Xiao,
University of Massachusetts Amherst, United States

Reviewed by:
Dawei Yu,
Jiangnan University, China
Zhenjun Zhu,
Jinan University, China
Jiarun Han,
Zhejiang Gongshang University, China

***Correspondence:**
Yaxin Sang
yxsang1418@163.com
Guifang Tian
fengxinzi.812@163.com

†*These authors have contributed equally to this work and share first authorship*
‡*These authors have contributed equally to this work*

Specialty section:
This article was submitted to Food Chemistry, a section of the journal Frontiers in Nutrition

Received: *11 February 2022*
Accepted: *04 March 2022*
Published: *11 April 2022*

Citation:
Liu X, Mao K, Sang Y, Tian G, Ding Q and Deng W (2022) Physicochemical Properties and in vitro Digestibility of Myofibrillar Proteins From the Scallop Mantle (Patinopecten yessoensis) Based on Ultrahigh Pressure Treatment. Front. Nutr. 9:873578. doi: 10.3389/fnut.2022.873578

The utilization of myofibrillar proteins (MPs) from the scallop mantle was limited due to its poor digestibility *in vitro*. In this study, structural properties and *in vitro* digestibility of MP were evaluated after modified by ultra-high pressure (UHP) at different pressures (0.1, 100, 200, 300, 400, and 500 MPa). The results showed that high pressure could significantly increase the ordered structure content like α-helix, inhibit the formation of disulfide bonds, and decrease surface hydrophobicity. Moreover, MP possessed the optimal solubility and *in vitro* digestibility properties at 200 MPa due to the minimum particle size and turbidity, relatively dense and uniform microstructure. The results indicated that the UHP treatment was an effective method to improve the digestibility of MP from scallop mantle and lay a theoretical basis for the functional foods development of poor digestion people and comprehensive utilization of scallop mantles.

Keywords: ultrahigh pressure, myofibrillar protein, scallop mantle, *in vitro* digestibility, structural properties

INTRODUCTION

In recent years, the annual output of the highly economical scallops (*Patinopecten yessoensis*) has reached nearly 2 million tons in China. As the main byproduct of scallop processing, the annual production of scallop mantle is also on the increase, which was good resource for lowering blood lipids, anti-aging, and resisting atherosclerosis due to its abundant nutrients such as proteins, polysaccharides, taurine, essential amino acids, and mineral elements (1). Myofibrillar protein (MP) is salt-soluble and accounts for 55–65% of the total protein content of scallop mantle, which directly affects the characteristics of solubility, *in vitro* digestibility properties, and emulsification properties of scallop byproducts (2). However, most scallop mantles were randomly discarded and wasted (3), and only a small portion was reprocessed partly due to poor solubility and low utilization rate of MP. Therefore, it is particularly necessary to improve the solubility and *in vitro* digestibility of MP to explore function foods for poor digestion people and increase the utilization rate of the scallop mantle (4).

The ultra-high pressure (UHP) treatment is an alternative to usual thermal processes (5), which is related to flavor, structural, and functional modification of food-derived components like protein. During UHP (100–1,000 MPa), the hydration of the protein chains might be formed through the liquid pressure transmission medium followed by the behavior changes of protein like denaturation, unfolding, and aggregation. Therefore, the UHP treatment was applied to reduce

particle size, increase solubility, improve texture, and functional properties of food-derived proteins (6). UHP treatment might cause variable alterations in MP structure by protein unfolding and aggregation. It is bound up with the exposure of protein side chain amino acids like Phe, Tyr, Trp, Lys, and Arg, which were the target cleavage sites of pepsin or trypsin determining the extents of protein digestion. The solubility of MP from pork meat increased when it was treated under appropriate UHP treatment (≤400 MPa) but decreased under over high pressure (>400 MPa). It could be attributed to the fact that the water amount of MP might increase after proper UHP treatment while the water of MP might be redistributed to the outer compartment of MP under high pressure (7). UHP treatment could modify the secondary structure of oyster protein and enhance its solubility and digestibility. Compared with the untreated one, the digestibility of the treated samples (500 MPa) increased from 26.3 to 39.5% in the stomach and from 62.1 to 83.7% in the total digestion process (8). Zhang et al. stated that MP from chicken breast meat had maximum solubility and gel hardness, minimum particle size, as well as dense and uniform microstructure after the UHP treatment at 200 MPa due to the massive solubilization of myosin heavy chain and actin, and the exposure of both tyrosine and tryptophan residues (6). Previous study showed that high-pressure processing caused MP from bovine *longissimus dorsi* muscle meat disorganization, affected protein digestion kinetics *in vitro*, and changed muscle structure, which correspondingly improved its solubility and *in vitro* digestibility at 600 MPa (9). Although relevant research has focused on the modification of MP structure and function under UHP treatment, knowledge of the effect of UHP treatment on MP from scallop mantle was limited especially for the relationship between the structure and *in vitro* digestibility. Therefore, it is necessary to explore the change mechanism of physicochemical properties and *in vitro* digestibility of MP from the scallop mantle (*Patinopecten yessoensis*) during the UHP treatment.

The aim of the study was to explore the effect of UHP treatment on the solubility and *in vitro* digestibility of MP from scallop mantle by clarifying the relationship between the structure and function. After treated at different pressures (100, 200, 300, 400, and 500 MPa), respectively, the size, zeta potential, surface hydrophobicity, sulfhydryl groups, and microstructure of MP from scallop mantles were detected. Moreover, the influences of the structure change on solubility and *in vitro* digestion were elucidated. The results of this study would broaden the application of MP from the scallop mantle, improve the utilization rate of the scallop mantle, and lay the theoretical foundation for the further development of easily digestible products.

MATERIALS AND METHODS

Materials

Scallop (*Patinopecten yessoensis*) was purchased from an aquatic product market (Qinhuangdao, Hebei, China). All samples were immediately transported on ice to the laboratory. And then they were stored at 4°C and used within 48 h. Protein marker (PR 10–250 kDa) and 5 × Sodium dodecyl sulfate-polyacrylamide gel electrophoresis (SDS-PAGE) loading buffer were obtained from Sevenbio Co. Ltd. (Sevenbio, Beijing, China). Disodium hydrogen phosphate, sodium dihydrogen phosphate, ethylenediaminetetraacetic acid (EDTA), sodium chloride, urea, 5,5'-dithiobis-(2-nitrobenzoic acid) (DTNB), sodium dodecyl sulfate (SDS), 1-anilino naphthalene-8-sulfonate (ANS), Coomassie Brilliant Blue G-250, and bovine serum albumin (BSA) were purchased from the Sigma Reagent Co. Ltd. (St. Louis, MO, USA). All chemical reagents used in this study were analytical or chromatographic grade.

Extraction of MPs From Scallop Mantle

Myofibrillar protein was extracted from the scallop mantle as described by Zhang et al. with few modifications (10). Buffer A was 20 mmol/L phosphate buffer at PH 7.0 containing 100 mmol/L NaCl and 1 mmol/L EDTA while Buffer B was 25 mmol/L phosphate buffer at PH 7.0 containing 0.6 mmol/L NaCl. The scallop mantle was cut into small pieces, added to buffer A at a ratio of 1:10 (W/V), homogenized in ice bath at 10,000 rpm for 90 s, centrifuged (4°C) at 6,790 *g* for 20 min to collect the precipitates, and extracted the precipitate again with buffer A. The entire process was repeated twice. The precipitates were added to a certain amount of buffer B, homogenized at 10,000 rpm for 20 s and centrifuged (4°C) at 6,790 *g* for 20 min. Finally, the supernatant (i.e., MP) was collected after centrifugation. The MP contents were determined by the Biuret method using BSA as standard (11).

Ultra-High Pressure Treatment of MP

The MP solutions sealed in polyethylene bags at 6°C were placed in the chamber of ultra-high pressure processor (HPP.L2-600-2, Hua tai Ltd., Tianjin, China). The high pressure increased to the designed pressure (100, 200, 300, 400, and 500 MPa) at a rate of 3.5 MPa/s and maintained for 10 min, respectively.

Sodium Dodecyl Sulfate-Polyacrylamide Gel Electrophoresis

The SDS-PAGE experiment was carried out according to the method of Laemmli (12) with a few modifications. Diluted MP solutions (1 mg/ml) were mixed with 5 μl SDS-PAGE loading buffer (5×) and heated for 5 min at 100°C. Then, 20 μl MP solutions were electrophoresed on a 10% separating gel and a 5% stacking gel. Finally, a constant current of 80 V was employed for the separation gel until all samples were input into the stacking gel while 120 V was used for the stacking gel until the indicator was about 5 mm above the gel edge. After electrophoresis, the gels were stained by Coomassie brilliant Blue for 1 h and subsequently de-stained with 5% methanol and 7.5% acetic acid. The gels were scanned and analyzed on a gel imager (Tanon-4600SF, Tanon Ltd., Shanghai, China) after decolorizing. MP was identified with standard (Protein Ladder 10–250 kDa).

Circular Dichroism

The secondary structure proportion of MP solutions was recorded according to the method of Wu et al. using CD spectrometer (Applied Photophysics Ltd, JASCO810, UK) with

a quartz cell of 1 cm optical path in the wavelength range of 195–260 nm (**13**). The step size of MP (0.2 mg/ml) measurement was 1 nm, and the scanning speed was 50 nm/min. Protein secondary structures were determined as percentages of α-helix, β-sheet, β-turn, and random coil using the Alix's method.

Endogenous Fluorescence Spectra

The endogenous fluorescence spectrum was obtained by the method described by Jia et al., with few modifications (14). MP (0.5 mg/ml) was detected using the fluorescence spectrophotometer (F-320, Gangdong Instruments Ltd., Tianjin, China) at an excitation wavelength of 295 nm and emission wavelength of 300–420 nm. The constant crack width between excitation and emission wavelength was 10.0 nm.

Surface Hydrophobicity

The surface hydrophobicity was obtained by the method described by Jiang et al., and with slight modifications (15). After mixing 5 ml MP containing 0, 0.2, 0.4, 0.6, 0.8, and 1.0 mg/ml protein with 25 μl ANS solution (8 mmol/L ANS in 20 mmol/L phosphate buffer, pH 7.5), the mixtures were placed in the dark at room temperature for 25 min. The relative fluorescence intensity at the excitation wavelength of 374 nm and the emission wavelength of 485 nm was recorded with the fluorescence spectrophotometer. The slope between the fluorescence intensity and the protein concentration was represented the surface hydrophobicity of MP.

Total and Reactive Sulfhydryl Contents

The total sulfhydryl contents of the MP were determined according to the previous report with slight modifications (16). A total of 0.5 ml MP (1 mg/ml) was mixed with 4.5 ml of solution containing 8 mol/L urea and 10 mmol/L EDTA (pH 6.0), and 100 μl Ellman's reagent (10 mmol/L DTNB in 0.1 mol/L NaH_2PO_4 buffer). Then it was set in the dark at room temperature for 25 min and measured at 412 nm with ultraviolet-visible spectrophotometer (N5000, Yoke Analysis Instrument Co., Shanghai, China). The supernatants without DTNB were used as the control.

The reactive sulfhydryl contents were obtained by the method described of Guo et al., and with slight modifications (17). A total of 5 ml of MP (1 mg/ml) was mixed with 20 μl of DTNB. Then, the solutions were kept at room temperature for 1 h and measured at 412 nm with ultraviolet-visible spectrophotometer. Sulfhydryl concentration was calculated using the following equation:

$$\begin{aligned} &Sulfhydryl\ concentration\ \left(\mu\ mol/g\ protein\right) \\ &= \frac{A412 - A412r}{k \times c} \times 1,000 \end{aligned} \quad (1)$$

where A_{412r} and A_{412} are the absorbance of reagent blank and sample at 412 nm, k is the extinction coefficient (13,600 M^{-1} cm^{-1}), and c is the protein concentration of samples.

Particle Size and Zeta Potential

Malvern Zeta sizer Nano ZS90 instrument (Malvern Instruments Ltd., Malvern, England) was applied to determine the particle size distribution and zeta potential of the MP solutions (0.5 mg/ml).

Atomic Force Microscopy Measurements

The morphology of the MP was monitored by the atomic force microscopy instrument (MFP-3D infinity, Oxford Instruments Ltd., UK) through a previously described method with slight modifications (18). MP was diluted to 10 ppm, then placed on glass slide and air-dried at room temperature.

Solubility and Turbidity Measurements

Solubility was measured using the method with slight modifications (19). MP (3 mg/ml) was centrifuged at 6,790 *g* for 15 min. The supernatant was collected and measured by the biuret method, using BSA as a standard. The formula of the protein solubility was using the following equation:

$$\begin{aligned} &Protein\ solubility\ (\%) \\ &= \frac{protein\ content\ of\ supernatant\ (mg)}{total\ protein\ content\ in\ solution\ (mg)} \times 100\% \end{aligned} \quad (2)$$

Turbidity was measured using the modified protocol with slight modifications (20). MP (1 mg/ml) was incubated for 30 min at room temperature and measured at 340 nm with an ultraviolet-visible spectrophotometer with buffer B as the blank.

In vitro Digestion

In vitro digestion was measured using the method with slight modifications (21). Due to the short residence in the oral cavity, the samples were mainly subjected to gastric and small intestinal stages to simulating digestion *in vitro*.

Statistical Analysis

In this study, statistical analyses of the data were performed by using SPSS 22.0 (SPSS 22.0, Chicago, USA) and *post-hoc* Duncan's test of ANOVA test (significant differences). All experiments were measured in triplicate and data were expressed as the average ± standard deviation (*SD*). Results were considered significantly different for $p \leq 0.05$ (22).

RESULTS AND DISCUSSION

Effect of UHP Treatment on Molecular Structures of MP From Scallop Mantle

Primary Structure

The SDS-PAGE was performed to visualize the change of primary structure in different MP from the scallop mantle. As shown in **Figure 1**, all samples showed the typical molecular pattern distribution for MP with, myosin heavy chain (MHC, 220 kDa), M-protein (97 kDa), actin (44 kDa), and tropomyosin (37 kDa), which was similar to Peng et al. (7). There was no significant difference in the bands between different samples, which demonstrated that the UHP treatment could not change the molecular weight of the protein and degrade the MP molecules.

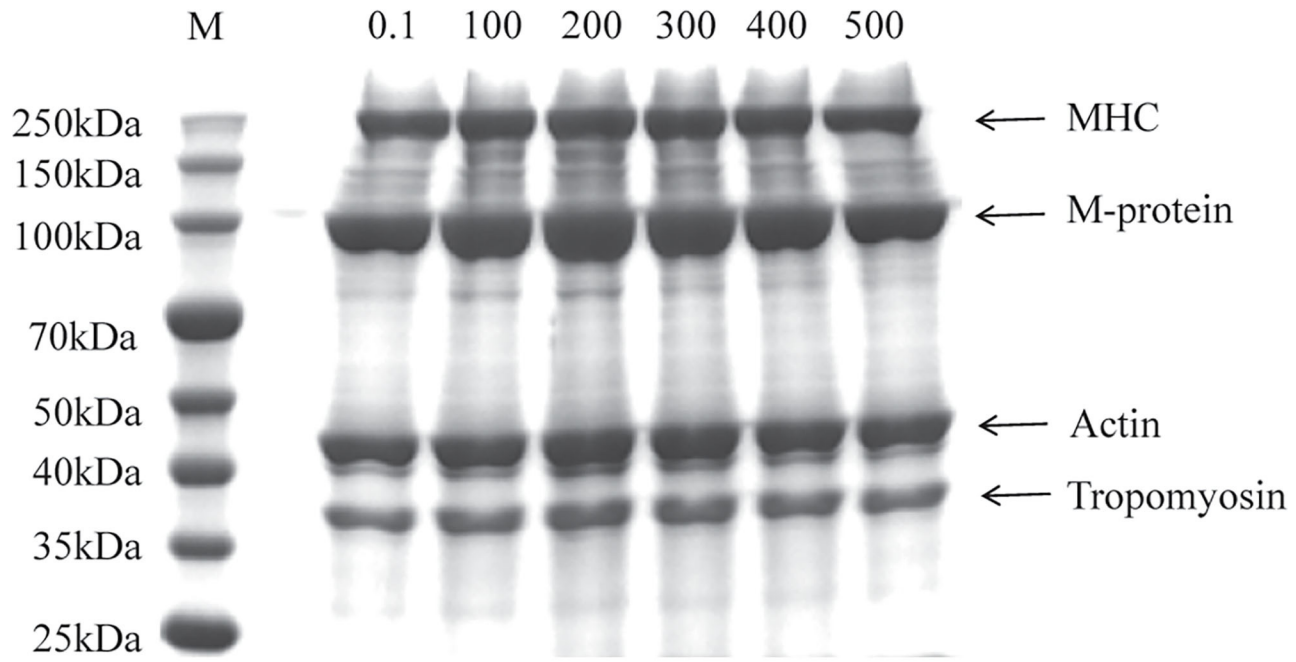

FIGURE 1 | Sodium dodecyl sulfate-polyacrylamide gel electrophoresis (SDS-PAGE) profile of myofibrillar protein (MP) from the scallop mantle at different pressures (Lane M: protein marker, MHC: myosin heavy chain).

Secondary Structure

Circular dichroism was used to assess the change of secondary structure in different samples. As shown in **Table 1**, the relative content of α-helix, β-turn, and random coil significantly increased after the UHP treatment, while the β-sheet content significantly decreased. The β-sheet relies on the hydrogen bonds between peptide bonds. That's probably because the hydrogen bonding was weakened with the increase of the pressure resulting from the unfolding of protein (23). Inter hydrogen bonds of the peptide chain were exhibited the stability capacity of α-helium and were relied on by β-plates. It can be attributed to the fact that the cavitation force produced by the UHP treatment, could disrupt the interaction between protein molecules. It could be concluded that UHP treatment was an effective method to significantly increase the ordered structure contents and stable conformation of MP.

Tertiary Structure

The fluorescence spectrum was applied to reflect the tertiary structure information of MP. The 295 nm was selected as the excitation wavelength to detect the fluorescence intensity caused by the conformational changes from the tryptophan, phenylalanine, and tyrosine residues (24). Higher the pressure, lower the intrinsic fluorescence emission spectra as shown in **Figure 2A**, indicating that the tertiary structure of the protein was changed by UHP-treatment. Tryptophan, phenylalanine, and tyrosine residues were exposed to the external polar environment under strong mechanical forces and the cavitation produced by the UHP-treatment, therefore, reducing the endogenous fluorescence (15).

Total and Reactive Sulfhydryl Contents

Protein sulfhydryl existed in the form of free sulfhydryl and disulfide bonds. The protein structure and interactions were affected by conformation changes between free sulfhydryl and disulfide bonds. Proteins would aggregate if disulfide bonds were formed during the UHP treatment, which was related to the increase of surface hydrophobicity (25). As shown in **Figure 2B**, the total sulfide contents of MP solution decreased with the increase of pressure. The disulfide bonds were liable to form owing to the exposure of sulfhydryl from the protein interior and the shortened distances between intermolecular sulfhydryl contents (2). Proper UHP treatment (150–300 MPa) would facilitate to the formation of disulfide bonds and the decrease of sulfhydryl contents (26). As seen in **Figure 2B**, the contents of reactive sulfhydryl increased with the increase of pressure. It might be ascribed to the exposure of the internal sulfhydryl, resulting from the separation of subunits and breakage of the disulfide bonds. In addition, it might be due to the stretching and unfolding of protein molecules that exposed the interior sulfhydryl under UHP treatment (27).

Surface Hydrophobicity

Besides directly related to the solubility and *in vitro* digestion of proteins, the surface hydrophobicity was a key index to show the extent of surface hydrophobic residues on the surface of protein molecules (14). Compared with the control (0.1 MPa), the surface hydrophobicity of the treated samples decreased significantly as shown in **Figure 2C**. Hydrophobic amino acid residues generally appear obscured deep in the folded structure

TABLE 1 | Secondary structure contents of myofibrillar protein (MP) from the scallop mantle treated by ultra-high pressure (UHP).

UHP–treatment (MPa)	Secondary structure (%)			
	α-helix	β-sheet	β-turn	Random coil
0.1	9.80 ± 0.15 [a]	40.60 ± 0.19 [a]	19.28 ± 0.14 [a]	33.20 ± 0.17 [a]
100	10.49 ± 0.13 [b]	38.73 ± 0.20 [b]	19.52 ± 0.21 [ab]	33.28 ± 0.18 [ab]
200	11.02 ± 0.29 [c]	38.40 ± 0.15 [c]	19.27 ± 0.13 [a]	33.43 ± 0.20 [ab]
300	12.20 ± 0.15 [d]	36.29 ± 0.15 [d]	19.67 ± 0.20 [b]	33.57 ± 0.19 [b]
400	11.77 ± 0.19 [d]	35.70 ± 0.17 [e]	19.50 ± 0.15 [ab]	33.91 ± 0.08 [c]
500	11.71 ± 0.17 [d]	35.30 ± 0.15 [f]	20.08 ± 0.15 [c]	34.21 ± 0.20 [c]

Different letters (a–f) in the same column means significant differences ($p < 0.05$) among samples treated under different pressures.

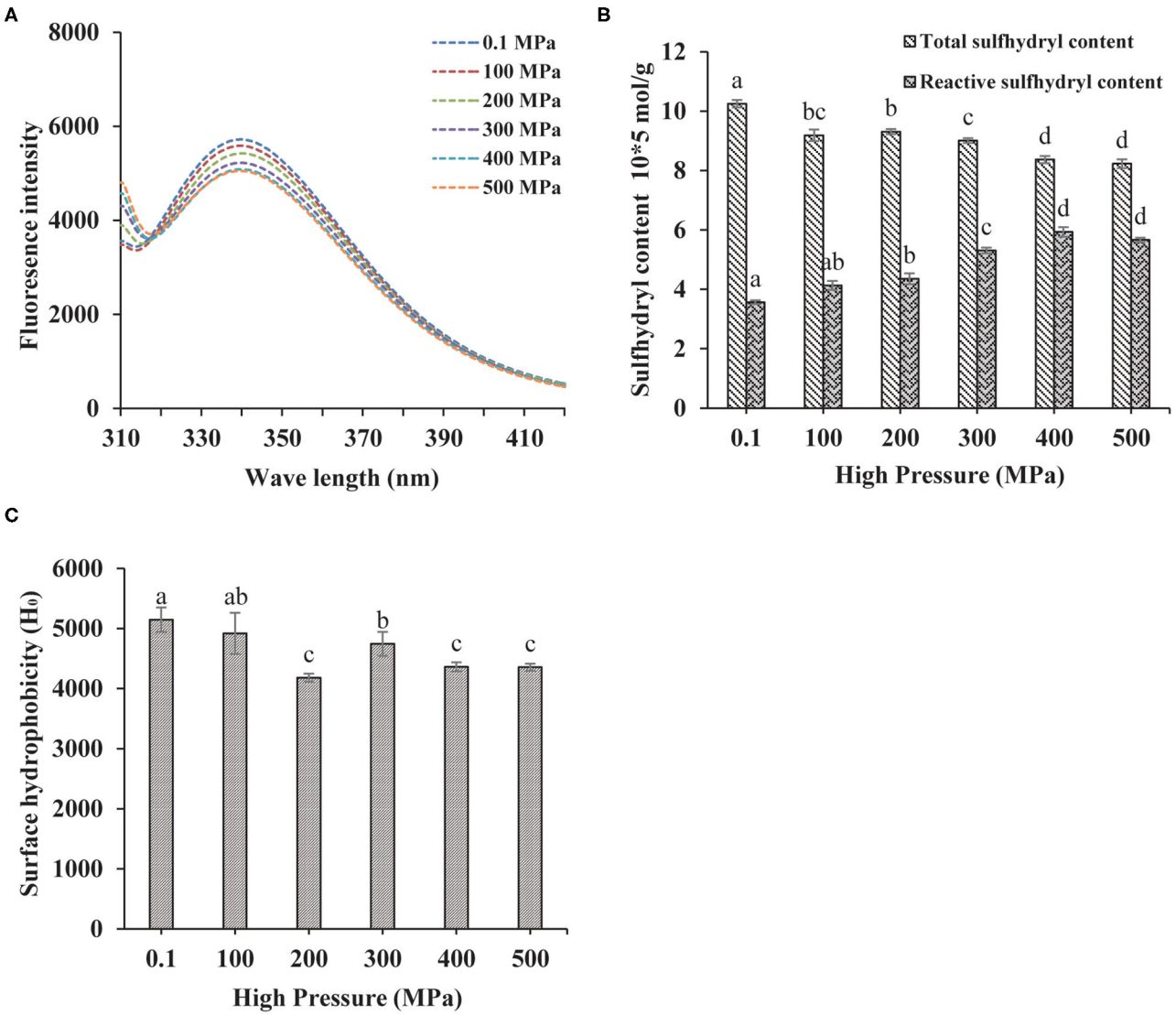

FIGURE 2 | Changes in the endogenous fluorescence **(A)**, sulfhydryl contents **(B)**, and surface hydrophobicity **(C)** of MP from the scallop mantle under the ultra-high pressure (UHP) treatment.

of proteins. After the UHP treatment, the protein conformation structure became loose and destabilized due to the stretching and unfolding of MP, which was detrimental to the hydrophobic interactions between hydrophobic ANS probes and proteins (28). Surface hydrophobicity got its minimum at 200 MPa. When the pressure was higher than 300 MPa, the hydrophobic groups were

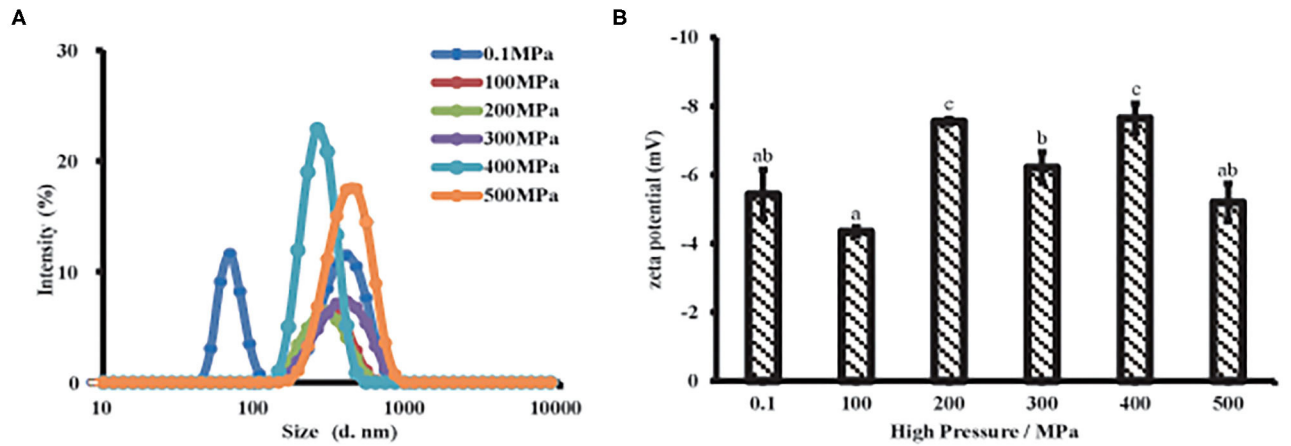

FIGURE 3 | Particle properties of MP solution from the scallop mantle under the UHP treatment. Particle size **(A)** and zeta potential **(B)**.

exposed to the outer of the protein from the interior, which was beneficial for the binding of ANS.

Effect of UHP Treatment on Dispersion Behavior of MP From Scallop Mantle

Particle Size and Zeta Potential Distribution

Particle size was a key factor that characterized the proteins aggregation and affected proteins solubility. As shown in **Figure 3A** and **Supplementary Table S1**, the untreated samples exhibited a bimodal and broader particle distribution, while MP samples had a unimodal and narrow distribution after UHP treatment. The particle size of MP presented a significantly decrease under the UHP treatment and achieved the minimum at 200 MPa. Initial protein polymer was broken into small particles by the violent agitation during UHP process. It had a close relation to the denaturation of protein molecules and the rupture of non-covalent bonds caused by the separation of muscle proteins, depolymerization of actin and myosin. However, the particle size increased when the pressure was over 200 MPa, indicating that protein polymers were formed again resulting from intermolecular desulfurization bridges and hydrophobic interactions as previous studies reported (6). The results showed that MP would undergo interruption and depolymerization during UHP treatment.

Zeta potential was related to the dotted residues located or near the surface of the suspended particle, which was closely linked to proteins dispersibility and aggregation (29). All samples were exhibited a negative charge (**Figure 3B**) due to the negatively charged amino acid residues like glutamic acid at neutral PH (18). After the UHP treatment, the absolute zeta potential increased, meaning more dotted side chains were exposed to the surface of the dispersed particles, which was beneficial to improve the solubility and *in vitro* digestibility of MP. With respect to the untreated sample, a high absolute zeta potential was presented in treated ones except 100 MPa, which means particle aggregation was easily formed and hard to separate because the electrostatic repulsion between the protein particles was weak (30). The samples possessed a high absolute zeta potential after UHP treatment at 200 and 400 MPa, respectively. The results were consistent with the particle size. Small protein particles had more charge sites exposed on the suspended particles than big ones because of the bigger surface area. As is known that the high absolute zeta potential on protein particles could strengthen the electrostatic repulsion between particles, which might give rise to an increase in solubility and a decrease in protein aggregation (31). Therefore, the higher absolute zeta potential, the protein particles had (∼8 mV) after the UHP treatment, the stronger electrostatic repulsion existed among the protein particles, and the higher the MP solubility. The UHP treatment of 200 MPa endowed MP, the minimum particle size and the maximum absolute zeta potential as described in **Figures 3A,B**, which might promote the dissolution of MP solutions (29).

Microstructure

The microstructure plays an important role in the functional properties of proteins. AFM was a common technical means to characterize the MP microstructures (32). As displayed in **Figure 4**, the untreated protein particles gathered with a mainly rough and non-homogeneous morphology, and the height of around 327 nm. MP treated below or equal to 200 MPa had a dense and homogeneous network with many filaments and irregular cavities, especially at 200 MPa. With the UPH treatment over 200 MPa, MP exhibited a large and heterogeneous structure due to the MP denaturation excessively and exposure of interior hydrophobic and sulfhydryl groups. It also was related to the relative speed of protein unfolding and aggregation. When the speed of protein aggregation was faster than that of unfolding, the dense and uniform structure would be formed, and vice versa (6).

Solubility and Turbidity

Solubility mainly reflects the denaturation and polymerization of protein while turbidity reflects the degree of protein aggregation. The MP solubility of the scallop mantle significantly increased

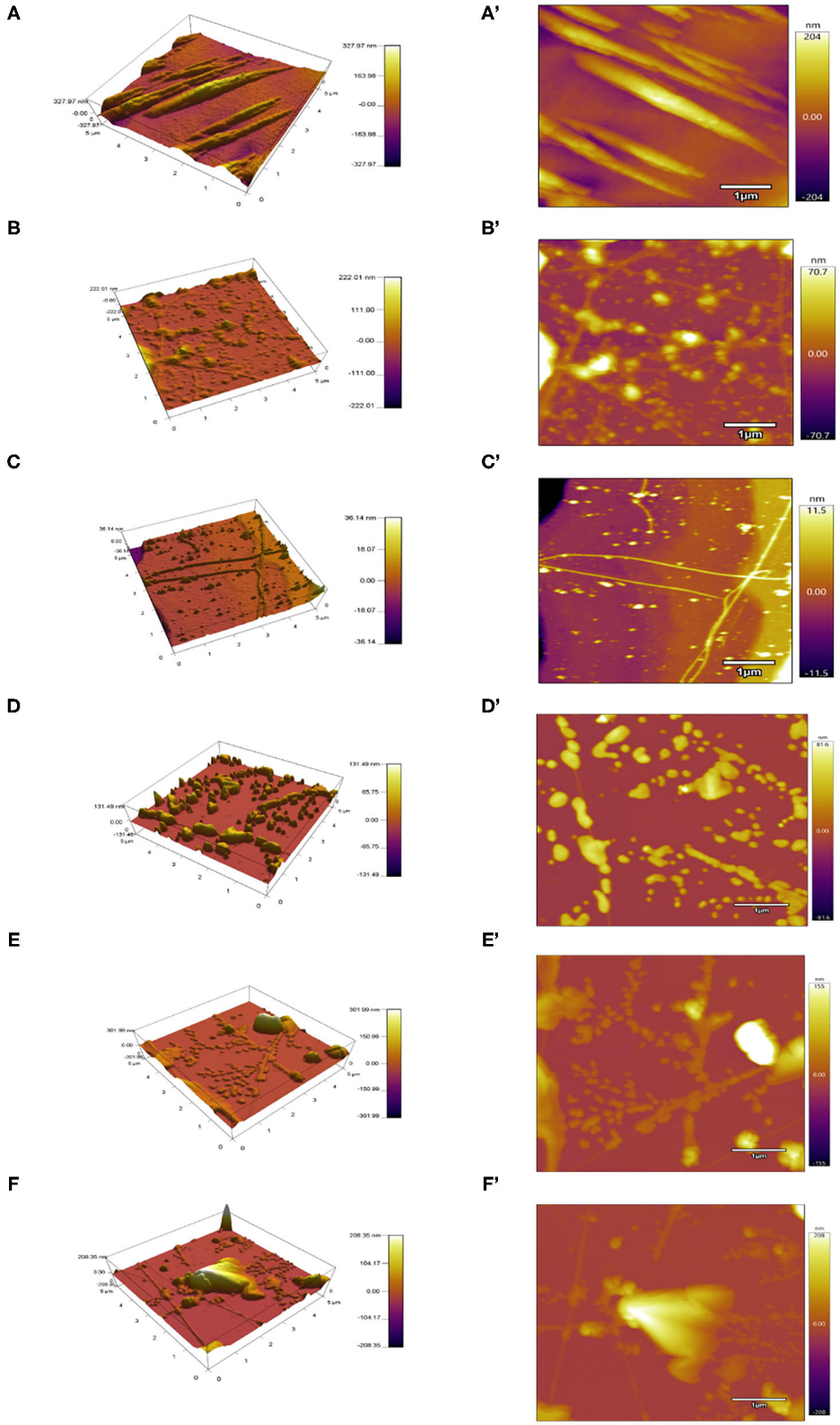

FIGURE 4 | Atomic force microscopy (AFM) images of different UHP treated MP solutions from the scallop mantle. 3D view **(A–F)** and top view **(A'–F')**.

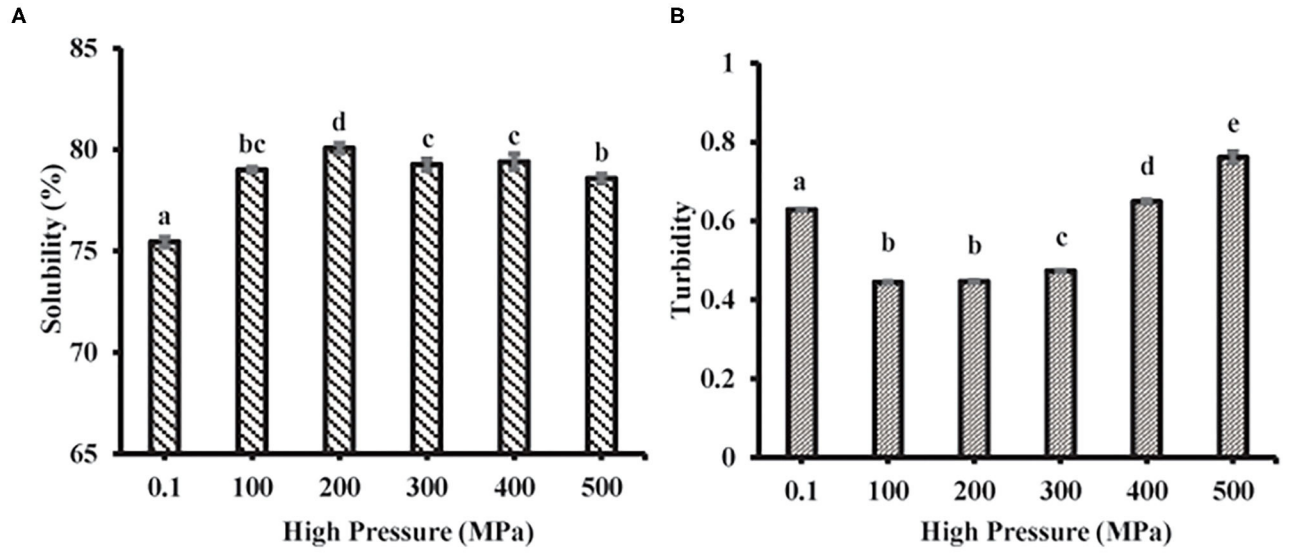

FIGURE 5 | Solubility **(A)** and turbidity **(B)** of MP from the scallop mantle under the UHP treatment.

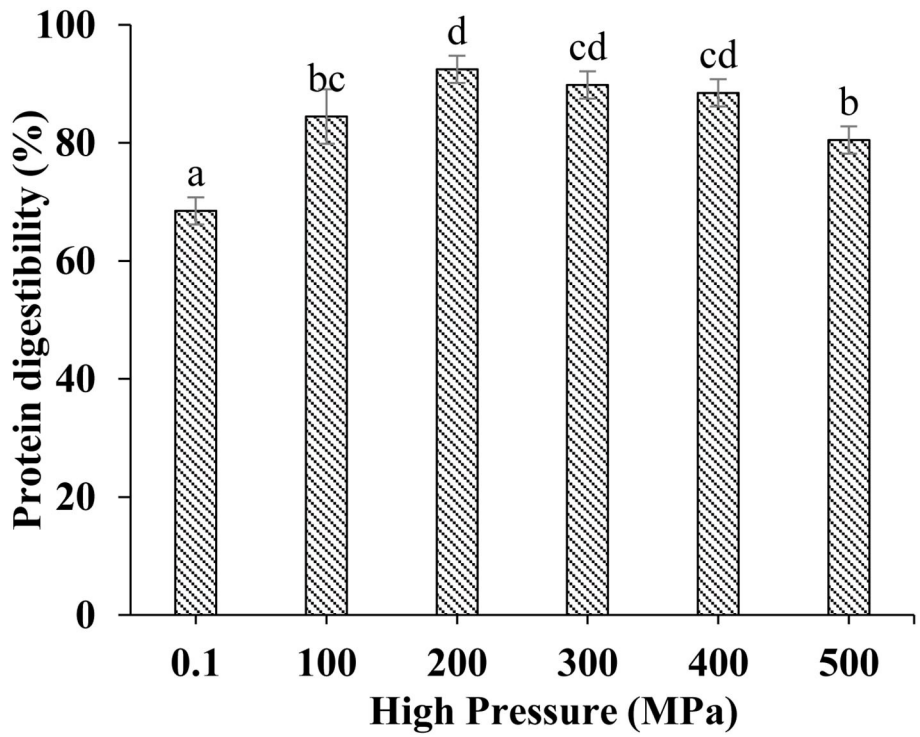

FIGURE 6 | *In vitro* digestibility of MP from the scallop mantle treated by the UHP treatment.

after UHP treatment and reached the highest level at 200 MPa (**Figure 5A**). It might be induced by the depolymerization of actin and actomyosin under UHP treatment. It was in accordance with the previous report that the increase of protein solubility resulted from the increase of shear treatment, which could disrupt newly formed polymers and prompt the interaction of unfolded protein and water molecules (33). The solubility reduction of MP from scallop mantle might be attributed to the fact that high-pressure treatment (≥300 MPa) promoted the formation of insoluble protein aggregates through non-disulfide

and disulfide bonds relying on the exposure of the interior hydrophobic resides and sulfhydryl groups (34). The results were consistent with a previous study that the solubility of MP from beef muscle increased at 200 MPa but deceased when the pressure was over 200 MPa (34). Moreover, it could be speculated from the data of particle size and solubility that the MP solubility was inversely proportional to its particle size because small particle size was beneficial to the protein–water interaction (35).

The turbidity changes of MP samples after different UHP treatments were shown in **Figure 5B**. UHP-treatment decreased the turbidity of MP solution when the pressure was below 400 MPa. The turbidity results were also in agreement with the tendency of particle size (**Figure 3A**) due to high shear energy waves. The turbidity decrease ($\leq$300 MPa) demonstrated that the decrease of protein aggregation. When the pressure was over 300 MPa, the turbidity increased with the increase of pressure caused by the myosin aggregation after the unfolding of the α-helix. The results were in accordance with the previous results on the particle size of MP solution, which indicated that the decrease of protein aggregation was the main reason for the increase of protein solubility (35).

Effect of UHP Treatment on *in vitro* Digestion of MP From Scallop Mantle

Protein digestibility was an important indicator to evaluate the nutritional value of food protein, especially for poor digestion people. The *in vitro* digestibility changes of different treated MP samples were shown in **Figure 6**. UHP could enhance the MP of scallop mantle *in vitro* digestibility. And 200 MPa was the best pressure. The *in vitro* digestibility of MP increased from 68.47 ± 2.31% to 92.47 ± 2.30% at 200 MPa. The digestibility was associated with the spatial structure of proteins under different UHP treatment (36). The extents of protein digestion in the gastrointestinal tract depends on the contents of Phe, Tyr, Trp, Lys, and Arg, the target cleavage sites of pepsin or trypsin, which was affected by the exposure of amino acids in protein side chain through protein unfolding and aggregation during UHP treatment. Ultrahigh pressure would break the chemical bonds and forces like hydrogen bonds, disulfide bonds, hydrophobicity, and Van der Waals forces as forementioned (37). The results were consistent with particle size, surface hydrophobicity, and solubility (38).

CONCLUSIONS

The present study demonstrated that the UHP treatment had apparent impacts on the physicochemical properties and digestibility of MP. The UHP treatment was an effective method to exposing interior hydrophobic and sulfhydryl contents. The digestibility *in vitro* of MP was negatively correlated to its surface hydrophobicity, particle size, and turbidity but positively correlated to its solubility. The 200 MPa was the optimum pressure to improve solubility and *in vitro* digestibility of MP from scallop mantle. Since the effect of UHP treatment on physicochemical properties and digestibility of MP were revealed, studies are underway to investigate the digestible scallop products. It would lay a scientific theoretical foundation for the development of digestible scallop products and comprehensive utilization of scallop mantle MPs.

DATA AVAILABILITY STATEMENT

The original contributions presented in the study are included in the article/**Supplementary Material**, further inquiries can be directed to the corresponding author.

AUTHOR CONTRIBUTIONS

XL: conceptualization, data curation, formal analysis, methodology, and writing–original draft. KM: methodology, conceptualization, and software. YS: supervision, funding acquisition, and writing–review and editing. GT: conceptualization, supervision, and writing–review and editing. QD: methodology and data curation. WD: methodology and writing–original draft. All authors contributed to the article and approved the submitted version.

FUNDING

This study was supported financially by the National Key R&D Program of China (2019YFD0902003).

SUPPLEMENTARY MATERIAL

The Supplementary Material for this article can be found online at: https://www.frontiersin.org/articles/10.3389/fnut.2022.873578/full#supplementary-material

REFERENCES

1. Tan K, Liu H, Zhang H, Li S, Zheng H. Carotenoids content and lipid nutritional quality variation in tissues of male and female polymorphic (golden and brown) noble scallops Chlamys nobilis. *Aquacultur.* (2021) 536:736483. doi: 10.1016/j.aquaculture.2021.736483
2. Dai H, Sun Y, Xia W, Ma L, Li L, Wang Q, et al. Effect of phospholipids on the physicochemical properties of myofibrillar proteins solution mediated by NaCl concentration. *Lwt-food science and technology.* (2021) 141:110895. doi: 10.1016/j.lwt.2021.110895
3. Han JR, Yan JN, Sun SG, Tang Y, Shang WH, et al. Characteristic antioxidant activity and comprehensive flavor compound profile of scallop (Chlamys farreri) mantle hydrolysates-ribose Maillard reaction products. *Food Chem.* (2018) 261:337–47. doi: 10.1016/j.foodchem.2018.04.044
4. Ding QY, Tian GF, Wang XH, Deng WY, Mao KM, Sang YX. Effect of ultrasonic treatment on the structure and functional properties of mantle proteins from scallops (Patinopecten yessoensis). *Ultrasonics Sonochemistry.* (2021) 79:105770. doi: 10.1016/j.ultsonch.2021.105770
5. Hall AE, Moraru CI. Comparative effects of high pressure processing and heat treatment on in vitro digestibility of pea protein and starch. *NPJ Science of Food.* (2022) 6:2. doi: 10.1038/s41538-021-00116-0
6. Zhang Z, Regenstein JM, Zhou P, Yang Y. Effects of high intensity ultrasound modification on physicochemical property and water in myofibrillar protein gel. *Ultrason Sonochem.* (2017) 34:960–7. doi: 10.1016/j.ultsonch.2016.08.008

7. Peng ZY, Zhu MM, Zhang J, Zhao SM, He HJ, Kang ZL, et al. Physicochemical and structural changes in myofibrillar proteins from porcine longissimus dorsi subjected to microwave combined with air convection thawing treatment. *Food Chem.* (2021) 343:128412. doi: 10.1016/j.foodchem.2020.128412
8. Wang R, Jiang S, Li Y, Xu Y, Zhang T, Zhang F, et al. Effects of high pressure modification on conformation and digestibility properties of oyster protein. *Molecules.* (2019) 24:3273. doi: 10.3390/molecules24183273
9. Kaur L, Astruc T, Venien A, Loison O, Cui J, Irastorza M, et al. High pressure processing of meat: effects on ultrastructure and protein digestibility. *Food Function.* (2016) 7:2389–97. doi: 10.1039/C5FO01496D
10. Zhang L, Li Q, Hong H, Luo Y. Prevention of protein oxidation and enhancement of gel properties of silver carp (Hypophthalmichthys molitrix) surimi by addition of protein hydrolysates derived from surimi processing by-products. *Food Chem.* (2020) 316:126343. doi: 10.1016/j.foodchem.2020.126343
11. Gornall AG, Bardawill CJ, David MM. Determination of serum proteins by means of the biuret reaction. *J Biol Chem.* (1949) 177:751–66. doi: 10.1016/S0021-9258(18)57021-6
12. Laemmli UK. Cleavage of structural proteins during the assembly of the head of bacteriophage T4. *Nature (Load).* (1970) 227:680–5. doi: 10.1038/227680a0
13. Wu C, Yan X, Wang T, Ma W, Xu X, Du M, et al. self-sorted gel network formed by heating a mixture of soy and cod proteins. *Food Function.* (2019) 10:5140–51. doi: 10.1039/C9FO00560A
14. Jia N, Wang L, Shao J, Liu D, Kong B. Changes in the structural and gel properties of pork myofibrillar protein induced by catechin modification. *Meat Sci.* (2017) 127:45–50. doi: 10.1016/j.meatsci.2017.01.004
15. Jiang L, Wang J, Li Y, Wang Z, Liang J, Wang R, et al. Effects of ultrasound on the structure and physical properties of black bean protein isolates. *Food Research International.* (2014) 62:595–601. doi: 10.1016/j.foodres.2014.04.022
16. Zhang Z, Yang Y, Zhou P, Zhang X, Wang J. Effects of high pressure modification on conformation and gelation properties of myofibrillar protein. *Food Chem.* (2017) 217:678–86. doi: 10.1016/j.foodchem.2016.09.040
17. Guo XY, Peng ZQ, Zhang YW, Liu B, Cui YQ. The solubility and conformational characteristics of porcine myosin as affected by the presence of l-lysine and l-histidine. *Food Chem.* (2015) 170:212–7. doi: 10.1016/j.foodchem.2014.08.045
18. Guo Z, Huang Z, Guo Y, Li B, Yu W, Zhou L, et al. Effects of high-pressure homogenization on structural and emulsifying properties of thermally soluble aggregated kidney bean (Phaseolus vulgaris L) proteins. *Food Hydrocolloids.* (2021) 119:106835. doi: 10.1016/j.foodhyd.2021.106835
19. Liu Q, Kong B, Xiong YL, Xia X. Antioxidant activity and functional properties of porcine plasma protein hydrolysate as influenced by the degree of hydrolysis. *Food Chem.* (2010) 118:403–10. doi: 10.1016/j.foodchem.2009.05.013
20. Liu YF, Oey I, Bremer P, Carne A, Silcock P. Effects of pH, temperature and pulsed electric fields on the turbidity and protein aggregation of ovomucin-depleted egg white. *Food Res Int.* (2017) 91:161-170. doi: 10.1016/j.foodres.2016.12.005
21. Khulal U, Ghnimi S, Stevanovic N, Rajkovic A, Cirkovic Velickovic T. Aggregability and digestibility study of fruit juice fortified camel milk powder proteins. *LWT-Food Sci Technol.* (2021) 152:112250. doi: 10.1016/j.lwt.2021.112250
22. Gonzalez A, Nobre C, Simoes LS, Cruz M, Loredo A, Rodriguez-Jasso RM, et al. Evaluation of functional and nutritional potential of a protein concentrate from Pleurotus ostreatus mushroom. *Food Chem.* (2021) 346:128884. doi: 10.1016/j.foodchem.2020.128884
23. Li YP, Zhang XH, Lu F, Kang ZL, et al. Effect of sodium bicarbonate and sodium chloride on aggregation and conformation of pork myofibrillar protein. *Food Chem.* (2021) 350:129233. doi: 10.1016/j.foodchem.2021.129233
24. Cao Y, Xiong YL, et al. Chlorogenic acid-mediated gel formation of oxidatively stressed myofibrillar protein. *Food Chem.* (2015) 180:235–43. doi: 10.1016/j.foodchem.2015.02.036
25. Li S, Zhang R, Lei D, Huang Y, Cheng S, Zhu Z, et al. Impact of ultrasound, microwaves and high-pressure processing on food components and their interactions. *Trends Food Sci Technol.* (2021) 109:1–15. doi: 10.1016/j.tifs.2021.01.017
26. Cando D, Herranz B, Javier Borderias A, Moreno HM, et al. Effect of high pressure on reduced sodium chloride surimi gels. *Food Hydrocoll.* (2015) 51:176–87. doi: 10.1016/j.foodhyd.2015.05.016
27. Long S, Huang M, Jing W, Qi X, Hammad H, Ma M, et al. A study of storage impact on ovalbumin structure of chicken egg. *J Food Eng.* (2017) 219:1–7. doi: 10.1016/j.jfoodeng.2017.08.028
28. Yang HH, Zhong C, Sun LC, Li YK, Chen H, Wu GP. Effects of partial substitution of NaCl on myofibrillar protein properties from pearl mussel Hyriopsis cumingii muscle: structural characteristics and aggregation behaviors. *Food Chemi.* (2021) 356:129734. doi: 10.1016/j.foodchem.2021.129734
29. Chen X, Zou Y, Han M, Pan L, Xing T, Xu X, et al. Solubilisation of myosin in a solution of low ionic strength L-histidine: significance of the imidazole ring. *Food Chem.* (2016) 196:42–9. doi: 10.1016/j.foodchem.2015.09.039
30. Li X, Yun L, Hua Y, Qiu A, Cui S. Effect of concentration, ionic strength and freeze-drying on the heat-induced aggregation of soy proteins. *Food Chem.* (2007) 104:1410–7. doi: 10.1016/j.foodchem.2007.02.003
31. Hu S, Wu J, Zhu B, Du M, Wu C, Yu C, et al. Low oil emulsion gel stabilized by defatted Antarctic krill (Euphausia superba) protein using high-intensity ultrasound. *Ultrason Sonochem.* (2021) 70:105294. doi: 10.1016/j.ultsonch.2020.105294
32. Ren Z, Chen Z, Zhang Y, Zhao T, Ye X, Gao X, et al. Functional properties and structural profiles of water-insoluble proteins from three types of tea residues. *LWT-Food Sci Technol.* (2019) 110:324–31. doi: 10.1016/j.lwt.2019.04.101
33. Rouwhorst J, Baalen CV, Velikov K, Habibi M, Peter Schall EL. Protein microparticles visualize the contact network and rigidity onset in the gelation of model proteins. *NPJ Sci Food.* (2021) 5:32. doi: 10.1038/s41538-021-00111-5
34. Marcos B, Mullen AM. High pressure induced changes in beef muscle proteome: Correlation with quality parameters. *Meat Sci.* (2014) 97:11–20. doi: 10.1016/j.meatsci.2013.12.008
35. Jun S, Yaoyao M, Hui J, Obadi M, Zhongwei C, Bin X. Effects of single- and dual-frequency ultrasound on the functionality of egg white protein. *J Food Eng.* (2020) 277:109902. doi: 10.1016/j.jfoodeng.2020.109902
36. Carbonaro M, Maselli P, Nucara A. Structural aspects of legume proteins and nutraceutical properties. *Food Res Int.* (2015) 76:19–30. doi: 10.1016/j.foodres.2014.11.007
37. Zhang X, Chen X, Gong Y, Li Z, Guo Y, Yu D, et al. Emulsion gels stabilized by soybean protein isolate and pectin: Effects of high intensity ultrasound on the gel properties, stability and beta-carotene digestive characteristics. *Ultrasonics Sonochemistry*. (2021) 79:105756. doi: 10.1016/j.ultsonch.2021.105756
38. Zhang F, Jiang S, Feng X, Wang R, Zeng M, Zhao Y. Effect of heat treatment on physicochemical state and in vitro digestion of salt-soluble protein from Pacific oyster (Crassostrea gigas). *LWT-Food Sci Technol.* (2020) 134:110126. doi: 10.1016/j.lwt.2020.110126

Conflict of Interest: The authors declare that the research was conducted in the absence of any commercial or financial relationships that could be construed as a potential conflict of interest.

Publisher's Note: All claims expressed in this article are solely those of the authors and do not necessarily represent those of their affiliated organizations, or those of the publisher, the editors and the reviewers. Any product that may be evaluated in this article, or claim that may be made by its manufacturer, is not guaranteed or endorsed by the publisher.

frontiers | Frontiers in Nutrition

ORIGINAL RESEARCH
published: 14 April 2022
doi: 10.3389/fnut.2022.877132

Assessment of Variations in Round Green Tea Volatile Metabolites During Manufacturing and Effect of Second-Drying Temperature *via* Nontargeted Metabolomic Analysis

Huajie Wang[1,2†], *Yaya Yu*[1†], *Wen Ouyang*[1,3], *Yongwen Jiang*[1], *Jinjin Wang*[1], *Jinjie Hua*[1*] *and Haibo Yuan*[1*]

[1] *Key Laboratory of Tea Biology and Resources Utilization, Ministry of Agriculture, Tea Research Institute, Chinese Academy of Agricultural Sciences, Hangzhou, China,* [2] *Department of Tea Science, College of Agriculture and Biotechnology, Zhejiang University, Hangzhou, China,* [3] *State Key Laboratory of Tea Plant Biology and Utilization, College of Tea and Food Science and Technology, Anhui Agricultural University, Hefei, China*

OPEN ACCESS

Edited by:
Jinkai Zheng,
Institute of Food Science and Technology (CAAS), China

Reviewed by:
Tao Feng,
Shanghai Institute of Technology, China
Ya-Fang Shang,
Hefei University of Technology, China

***Correspondence:**
Jinjie Hua
huajinjie@tricaas.com
Haibo Yuan
192168092@tricaas.com

† These authors have contributed equally to this work

Specialty section:
This article was submitted to Food Chemistry, a section of the journal Frontiers in Nutrition

Received: *16 February 2022*
Accepted: *21 March 2022*
Published: *14 April 2022*

Citation:
Wang H, Yu Y, Ouyang W, Jiang Y, Wang J, Hua J and Yuan H (2022) Assessment of Variations in Round Green Tea Volatile Metabolites During Manufacturing and Effect of Second-Drying Temperature via Nontargeted Metabolomic Analysis. Front. Nutr. 9:877132. doi: 10.3389/fnut.2022.877132

Round green tea (RGT) is widely distributed and presents a high yield in China. The quality of RGT can be determined by its aroma; however, the transformation and formation of volatile metabolites during RGT processing remain unclear. In this study, 173 volatile compounds (nine categories) were identified totally from RGT *via* gas chromatography-mass spectrometry with infrared-assisted headspace-solid phase microextraction. These substances exhibited different changing trends during various procedures, with the most intense transformation occurring during fixation, followed by pan-frying and second drying; moreover, 51 substances were screened, mainly containing fatty acid-derived volatiles (i.e., (E)-2-hexen-1-ol, Hexanal, pentanal, hexanal) and glycoside-derived volatiles (i.e., linalool, geraniol, benzyl alcohol, benzaldehyde), and their evolution during processing was clarified. Furthermore, the effect of the second-drying temperature on volatile compound metabolism was clarified, and 90°C was the best temperature for RGT aroma. This research lays a foundation for in-depth quality control and the aroma formation mechanism of RGT.

Keywords: round green tea, volatile metabolites, second-drying temperature, fatty acid-derived volatiles, glycoside-derived volatiles, nontargeted metabolomic analysis

INTRODUCTION

Green tea has gained immense interest among consumers worldwide due to its green leaves and soup color, high fragrance, brisk and mellow taste, and various physiological activities such as anticancer, antioxidant, antiradiation, and antibacterial properties (1–4). Green tea can be classified into flat-shape, curled-shape, round (bead)-shape, needle (bud)-shape, and strip-shape, based on its appearance type (5). Round green tea (RGT), such as Yongxi Huoqing green tea in Anhui province, Fenghua curled tea and Pingshui Rizhu tea in Zhejiang Province, and Emerald tea in Guizhou Province, are widely consumed in China owing to their unique quality characteristics including tight, heavy, and sturdy round shape, green glossy color, high fragrance, and brisk and mellow taste (6, 7). Moreover, RGT accounts for a large proportion of green tea exported from China and is consumed by people worldwide.

Aroma is a key factor in evaluating the quality of green tea and affects its market value. The volatile compounds in green tea mainly include alcohols, aldehydes, ketones, esters, aromatic hydrocarbons, and terpenes (8). In tea, the volatile compounds arise from two sources—fresh tea leaves and substances formed during processing. These substances can be classified into four categories from different precursors: amino acid-derived volatiles, wherein amino acids undergo a Strecker reaction under the action of heat, and Maillard reaction with sugars to produce aldehydes, ketones, furans, pyrazines, and high-boiling volatile compounds (9, 10); glycoside-derived volatiles and glycoside-derived Non-volatiles, which release bound volatile compounds such as linalool and geraniol under the action of glycosidase or heat (11); lipid-derived volatiles, wherein lipids are first degraded to produce linolenic acid and other fatty acids, followed by production of lower-pointing alcohols and aldehydes (12); and carotenoid-derived volatiles, wherein carotenoids are precursors of volatile compounds such as ionone, 2,6,10,10-tetramethyl-1-oxaspiro[4.5]dec-6-en-8-one, and β-tanshinone (13).

The combination of processing technologies directly affects the formation pathways of volatile compounds and the type and quality of the green tea aroma (14). Moreover, tea leaves with distinct shapes made using different processing techniques have different cell breakage rates and material leaching rates, resulting in various aroma types, for example, flat and striped teas often exhibit floral and chestnut aromas, and needle-shaped teas often reveal delicate aromas (15, 16). Previous studies have reported the aroma of flat striped, needle-shaped, curly-shaped green teas (7, 17, 18); however, little research has been conducted on the aroma of RGT. The processing technology of RGT includes spreading, fixation, rolling, pan-frying, roll-roasting, and second-hot air drying. Among these, spreading promotes the loss of low-boiling compounds, such as (z)-3-hexen-1-ol and (E)-2-hexenal (19). Fixation may increase the formation of high boiling point substances, such as 3-methyl-butanal, linalool, and trans-β-ionone, under high temperature (8). Pan frying, the key process for shape formation and internal quality of RGT, is generally performed twice or thrice, with an initial increase in temperature and time, followed by a gradual decrease. Repeated pan frying helps to form round, tight, and heavy shape, and can trigger the biochemical reaction in the leaves under prolonged heat, which is conducive to the transformation and retention of quality components and lays the foundation for the formation of excellent quality. Roll-roasting and second-hot air drying promotes further emission of grass-flavored substances, formation of high-boiling substances, and the Maillard reaction of amino acids and soluble sugars to form heterocyclic substances such as furans and pyrazines at high temperatures (20).

The current research on RGT only focuses on the effect of processing technology on the sensory evaluation results and the total amount of physical and chemical components (21, 22). Non-targeted metabolomics is a novel analytical tool that allows the simultaneous determination of numerous substance components and comprehensive analysis of metabolites changes. It has been widely used in the analysis of Non-volatile and volatile metabolites of tea in recent years (23–25). However, few studies have reported the formation of aroma quality of RGT and volatile metabolite variations during manufacturing; moreover, the effect of RGT processing technology on the metabolism of volatile compounds remains to be elucidated. Therefore, this study uses the "Jiu Keng" fresh tea leaves as the raw material to process RGT and to obtain samples of the whole process (spreading, fixation, rolling, pan-frying, roll-roasting, and second drying). In addition, three second-drying temperatures (70°C, 90°C, and 110°C) were set to make RGT. Volatile compounds of these tea samples were detected using infrared-assisted-solid-phase microextraction (IRAE-HS-HPME) and gas chromatography-mass spectrometry (GC-MS) platforms. Multiple statistical analysis methods were used to elucidate the dynamic evolution of volatile compounds and the key metabolic pathways of volatiles biosynthesis during the processing of RGT, and the influence of different second-drying temperatures on volatile metabolites conversion. This study can provide a theoretical reference and objective basis for the mechanism underlying the formation of the aroma of high-quality RGT.

MATERIALS AND METHODS

Experimental Materials

Fresh tea leaves (FTL) of JiuKeng (*Camellia sinensis L.*) were collected from the Zhejiang Kaihua tea production area (29°10′ N, 118°10′ E; at an elevation of 700 m a.s.l.) in April 2020. The moisture content of the FTL was ∼78%. Each shoot comprised two leaves and one bud.

All the chromatography-grade volatile standards were purchased from Shanghai Yuanye Biological Technology Company (Shanghai, China). The purity of these chemical standards was ≥98%.

Green Tea Processing

(1) FTL (25 kg) were spread 2–3 cm thickness on each wooden net plates (1 m × 1 m) for 12 h at the temperature 19–22°C with a relative air humidity of 60% environment until the moisture reached 70.0%.

(2) Fixation was performed using a roller fixation machine (80-cm type, electromagnetic roller fixation machine, Ningbo Yaojiangyuan Machinery Co., Ltd., Ningbo, China), the temperature of rolling was 300°C, the speed of rolling was 22 rpm, the fixation time was 120 s, and 120 kg of tea leaves were treated per hour. The fixated tea leaves (FTS) spreading and resurgence was conducted at 0.5 h on the wooden net plates.

Abbreviations: FTL, Fresh tea leaves; STL, Spread tea leaves; FTS, Fixated tea leaves; FLS, Spread Fixated tea leaves; RTS, Rolled tea leaves; PF1, Pan-fried 1 leaves; PF2, Pan-fried 2 leaves; PF3, Pan-fried 3 leaves; DTL, Depilated tea leaves; RPL, Rotary pot first-dried leaves; BHL, Box hot air second-dried leaves; BHL70, The temperature of box hot air second-dried is 70°C; BHL90, The temperature of box hot air second-dried is 90°C; BHL110, The temperature of box hot air second-dried is 110°C; RGT, Round green tea; IRAE-HS-SPME, Infrared-assisted headspace-solid phase microextraction; GC-MS, Gas chromatography-mass spectrometry; MEV, Multiple experiment viewer; PLS-DA, Partial least-squares discriminant analysis; VIP, Variable importance projection.

(3) The cooled fixated tea leaves (FLS) were subjected to rolling for 30 min in a rolling machine (6CR-50 type, Zhejiang Shangyang Machinery Co., Ltd., Quzhou, China) using the following sequences: no-pressure rolling (5 min), light-pressure rolling (10 min), intermediate-pressure rolling (10 min), and no-pressure rolling (5 min).
(4) The rolled leaves (RTL) were pan-fired thrice in a double-pan roasting machine (6CCGQ-50 type, Zhejiang Shangyang Machinery Co., Ltd., Quzhou, China). First, RTL was treated for 20 min under a pan temperature of 210°C with a fried speed of 38 r/min until the leaves achieved a moisture content of 27.5%, as the pan-fried 1 leaves (PF1); thereafter, PF1 was treated for 40 min at a pan temperature of 180°C with a fried speed of 32 rpm until the leaves reached a moisture content of 15.0%, as the pan-fried 2 leaves (PF2); and PF2 was treated for 25 min at a pan temperature of 200°C with a fried speed of 32 rpm until the leaves had a moisture content of 10.0% (pan-fried 3 leaves (PF3).
(5) The pan-fried three leaves (PF3) were depilated for 15 min in a depilating machine (100-type, Zhejiang Shangyang Machinery Co., Ltd., Quzhou, China).
(6) The depilated leaves (DTL) were dried at 100°C for 15 min in a six-edge roasting machine (6CCP-60 type, Zhejiang Shangyang Machinery Co., Ltd., Quzhou, China) until 7.50% of leaf water content was achieved; thereafter, the leaves were spread out for a further 30 min, as the rotary pot first-dried leaves (RPL).
(7) Eventually, the samples were independently dried at 70°C, 90°C, and 110°C for 30 min until complete dryness was achieved in a box hot air-drying machine (Zhejiang Shangyang Machinery Co., Ltd., Quzhou, China); these dried at 70°C, 90°C, 110°C in box hot-air as the second-dried leaves (BHL70, BHL90, BHL110).

The overall production process of RGT is illustrated in **Figure 1**.

Analysis of the Volatile Compounds Present in the RGT Samples

Sample Pretreatment

The green tea samples (0.5 g) were accurately weighed (0.001 g), and 20 mg/L ethyl caprate (10 μL) were added to a 20 mL headspace vial along with boiled distilled water (1 mL). The headspace vial cap was immediately tightened, and the protective cap was impaled using a DVB/CAR/PDMS fiber (2cm) head with a manual handle (SPME, Supelco, Commonwealth of Pennsylvania, USA). Thereafter, the vial was heated over a 100 W infrared (IR) device (Qiyi Lighting Company, Zhejiang, China) for 15 min, and the fiber head was inserted into the GC-MS inlet and desorbed at 250°C for 5 min. Each sample was subjected thrice to IR-assisted headspace-solid-phase microextraction (8).

GC-MS Analysis

The gas chromatograph (7890B−7000C, Agilent Technologies, Palo Alto, CA, USA) equipped with a HP-5 ms ultra-inert capillary column (30 m × 0.25 mm × 0.25 μm) was used in the splitless injection mode with a high-purity helium (99.999%) flow at 1.0 mL/min for GC-MS analysis. The GC injector temperature was maintained at 250°C, and the temperature program of following column was employed: initial temperature, 50°C (held for 5 min), increased to 150°C at a rate of 4°C/min (held for 2 min), and increased to 270°C at a rate of 10°C/min (held for 6 min) (26, 27).

Qualitative and Quantitative Analyses

For qualitative analysis, the volatile metabolites with a similarity of >80% to the NIST11 standard library (22) were screened using the Agilent Mass Hunter unknown analysis program. Kovàts retention indices for each compound were obtained by calculating the linear formula of n-alkanes (C7-C40) and by comparing with theoretical retention indices referred to the literature value with the same or equivalent chromatographic column on the NIST Chemistry WebBook (http://webbook.nist.gov/chemistry/), based on the difference of RI within 30 (8). Moreover, some key aroma substances, such as 1-hexanol, (E)-4-heptenal, octanal, 1-decanol, linalool, naphthalene, decanal, geraniol, indole, α-ionone, cedrol, trans-β-ionone, hexadecenoic acid ethyl ester, and linoleic acid ethyl ester were identified further with authentic standards. For quantitative analysis, the mass concentrations of the volatile metabolites were calculated regarding the internal standard method using equation:

$$\mathbf{Ci} = (\mathbf{Cis} \times \mathbf{Ai})/\mathbf{Ais} \quad (1)$$

C_i represents the concentration of any volatile metabolites (μg/L), C_{is} is the concentration of the internal standard (μg/L) (ethyl caprate, 20 mg/L), A_i is the chromatographic peak area of any metabolites, and A_{is} represents the chromatographic peak area of the internal standard (27).

OAV

The OAV is the ratio of the concentration of volatile compounds in a sample to the odor threshold (28), calculated according to equation:

$$\mathbf{OAV} = \mathbf{c}/\mathbf{OT} \quad (2)$$

c is the concentration of the metabolites in the green tea sample (μg/L), and OT represents the odor threshold of the corresponding components in water (μg/L).

Statistical Analysis

The tests were repeated in triplicate, and the results of each test were expressed as the average of three replicates. The analyze the principal components affecting the volatile metabolites according to the different green tea processing using SIMCA P13 software (Umetrics, Umea, Sweden). MEV 9.0 software (https://mev-tm4-org.caas.cn) was used to generate heatmaps of key differential metabolites. SAS software (version 9.4; SAS Institute Inc., Cary, USA) was used to analyze the significant differences in the concentration of volatile compounds according to different treatments.

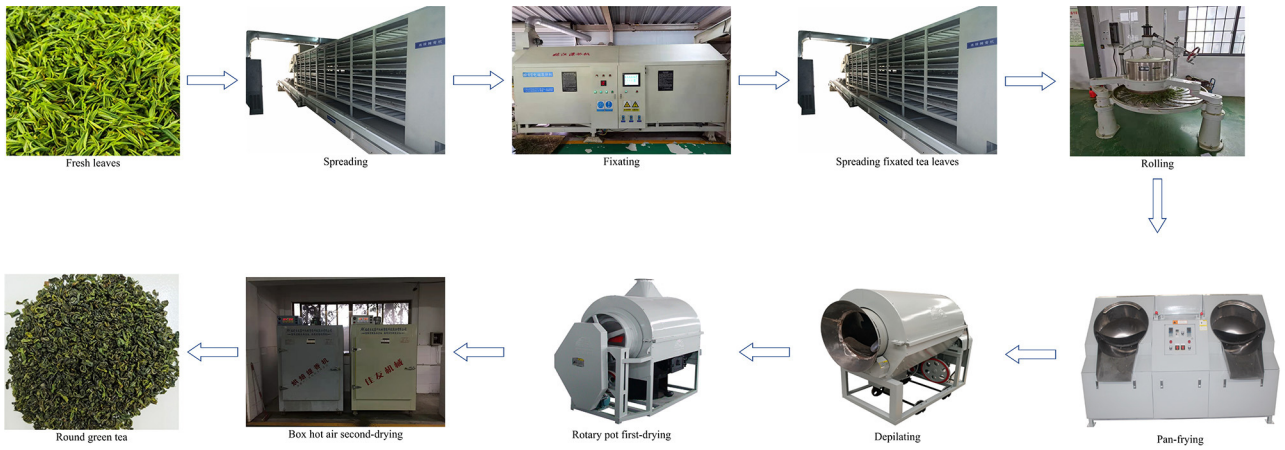

FIGURE 1 | Flow chart of round green tea processing.

RESULTS

Analysis of Volatile Compounds During the Processing of Green Tea

Overview of the Profile of Volatile Compounds in RGT

In total, 173 volatile compounds were identified (**Supplementary Table S1**) in this study, including 32 alcohols, 14 aldehydes, 17 ketones, 31 esters, 16 terpenes, 15 aromatic hydrocarbons, 28 alkanes, 3 furans, and 17 other types.

Moreover, a Non-supervised metrology PCA tool was used to conduct a comprehensive analysis of these 173 volatile compounds, as depicted in the score plot (**Figure 2A**). All tea samples revealed marked separation and clustering. FTL and STL are on the left side of the score plot, whereas the samples of FTS and subsequent samples are on the right. The trajectory plot (**Figure 2B**) clearly depicts stepwise alterations and distinct differences in volatile compounds from fresh leaves to finished leaves. Furthermore, a great change was observed in volatile compounds after fixation, and a further shift occurred in the pan-fried and box hot air drying; however, minor variations were observed during rolling, depilation, and rotary pot first-drying.

Dynamic Changes of Volatile Categories During RGT Processing

Nine categories of volatile compounds underwent remarkable changes during RGT processing. Changes in the content of different categories of volatile compounds are illustrated in **Figure 2C**; the contents of alcohols and aldehydes slightly increased in STL and markedly decreased in FTS; that of aldehydes significantly increased in RTL and PF2 and then decreased ($p < 0.05$); and the ketones markedly decreased in STL, FTS, and BHL, and increased in FLS and RPL. The ester content decreased throughout the process, and the sharpest decline was observed after fixation; terpenes increased in STL, significantly decreased in FTS, and slightly fluctuated in FLS ($p < 0.05$); and aromatic hydrocarbons revealed an alternate decreasing and increasing trend in FTS. The content of furans initially increased before the third pan-fried process and then decreased in DTL and BHL. The contents of alkanes and others (such as benzoic acid, hydrazide, benzyl nitrile, and 2-hexyl-5-pentylpyrrolidine) showed downward trends, particularly in fixation. The total volatile compound content revealed following trend: FTL > STL > RTL > FLS > FTS > PF2 > PF3 > PF1 > RPL > DTL > BHL (**Supplementary Table S1**). From the proportion of categories (**Figure 2D**), alcohols accounted for the highest proportion in the whole process (30.9–37.5%); moreover, the proportion of aldehydes increased significantly in RTL, PF2, and BHL ($p < 0.05$), whereas that of esters decreased in the process ($p < 0.05$). The proportion of ketones increased significantly in the FTS and decreased in the BHL ($p < 0.05$). The terpenes increased in the STL and then decreased. It is speculated that the activity of glycoside hydrolase increased during spreading, thereby promoting the release of terpene volatile compounds. Furans and aromatic hydrocarbons occupied a small proportion in the whole process (0.9–4.8%).

Differential Compound Screening and Evolution Analysis During RGT Processing

Analysis of the volatile compounds indicate that volatile compounds undergo drastic changes during processing. To clearly distinguish the important compounds in the process and to determine the law of their evolution, 51 substances were screened *via* variable projection importance (VIP) in the PLS-DA analysis (VIP > 1) and one-way analysis of variance ($p < 0.05$), as depicted in the loading diagram of PLS-DA (**Figure 3A**). Moreover, 51 substances mainly include alcohols, aldehydes, esters, ketones, aromatics hydrocarbons, terpenes, and furans, such as (4E)-4-hexen-1-ol, acetate, hexanal, heptanal, octanal, benzene acetaldehyde, 3-methyl-butanal, 2-methyl-butanal, benzene acetaldehyde, 2,5-dimethyl-benzaldehyde, 2-heptanone, α-cadinol, 3,7-dimethyl-1,5,7-octatrien-3-ol, 1-penten-3-ol, 1-pentanol, (E)-2-hexen-1-ol, acetate, styrene, (Z)-hexanoic acid, 3-hexenyl ester, α-ionone, and isophorone (**Figure 3B**).

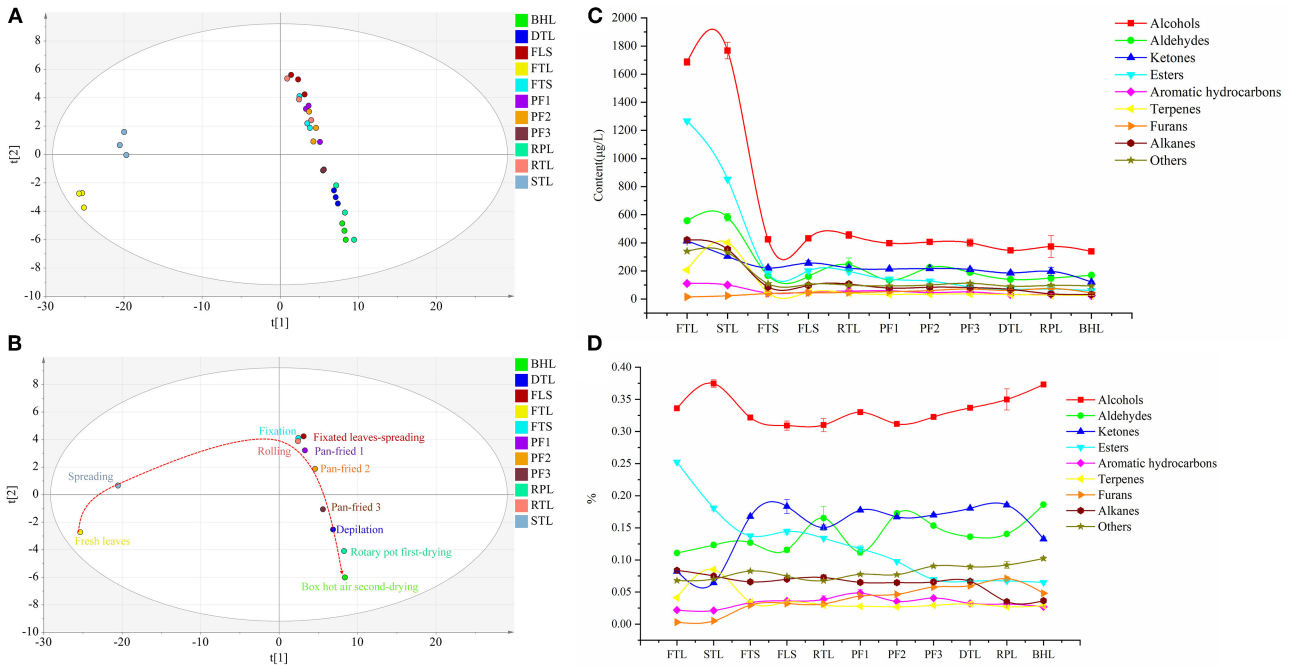

FIGURE 2 | (A) Principal Component Analysis (PCA) score scatter plot composed of all volatile compounds in the round green tea process. **(B)** The dynamic metabolic trajectory plot of volatile compounds, drawn by scatting of the Principal Component Analysis (PCA) scores t[1] vs. t[2]. **(C)** Variation trend chart of different types of volatile compounds content in different processes of round green tea. **(D)** Variation of the proportion of different types of volatile compounds in different process of round green tea.

Evolution of Key Different Compounds and Their Related Compounds During Processing

From the 51 compounds obtained in section Differential Compound Screening and Evolution Analysis During RGT Processing, the metabolic transformation rules of 34 key volatile compounds with definite aroma characteristics (9, 13) were revealed. Combined with the transformation and metabolism-related substances, this study clarified the evolutionary law of total 48 volatile compounds in the process of RGT, which contained 21 fatty acid-derived volatile substances, 18 glycoside-derived volatile substances, 7 amino acid-derived volatile substances, and 3 carotenoid-derived volatiles (**Supplementary Figure S1**).

Fatty Acid-Derived Volatiles

Lipids are important precursors for the formation of volatile compounds in green tea. The degradation products of unsaturated fatty acids or saturated fatty acids, such as α-linolenic acid and linoleic acid, can form C6-aldehydes under the action of heat or lipoxidase (LOX), and then further undergo redox reaction, isomerization, and may form esters, as well as chemical reactions to generate corresponding ketones, and alcohols (8). **Figure 4A** illustrates such compound changes during processing of RGT: under the action of lipoxidase, the hexanal, pentanal and heptanal derived from linoleic acid showed an upward trend, whereas (E)-2-hexen-1-ol, acetate decreased sharply. Hexanal, 1-hexanol, 1-pentanol, 1-heptanol and (E)-3-hexen-1-ol derived from linoleic acid and α-linolenic acid decreased significantly after fixating, whereas (E)-2-hexen-1-ol, acetate showed increased trend. During the spreading process, under the action of hydrolases, oxidases, and isomerases, hydrolysis of esters is increased, and the degradation of lipids results in the formation of corresponding alcohols and aldehydes, under the heat of fixation, the oxidation and esterification were promoted, these results are consistent with the existing findings (19, 29). High boiling point compounds, such as pentanal, heptanal, hexanal, and 2-heptanone, 6-methyl-5-hepten-2-one, and 1-penten-3-ol (**Supplementary Figure S1**) increased significantly during pan-fried process ($p < 0.05$), likely because the process of rolling promoted the fragmentation of tea tissue cells, resulting in a large amount of unsaturated fatty acids overflowing. Thus, these unsaturated fatty acids underwent strong thermal oxidation reactions under long-term high temperature treatment of pan-fried to form alcohols, aldehydes with high boiling points. Furthermore, heat fixation and pan frying increased the volatilization of low-boiling alcohols and induce the formation of corresponding aldehydes, ketones esters by oxidation, isomerization, esterification reactions.

Glycoside-Derived Volatiles

Glycoside-derived volatiles generally exhibit floral, sweet, and fruity aromas and form an important component of green tea aroma (11). During the process, monoterpene alcohols (linalool, and geraniol) or aromatic alcohols (benzyl alcohol

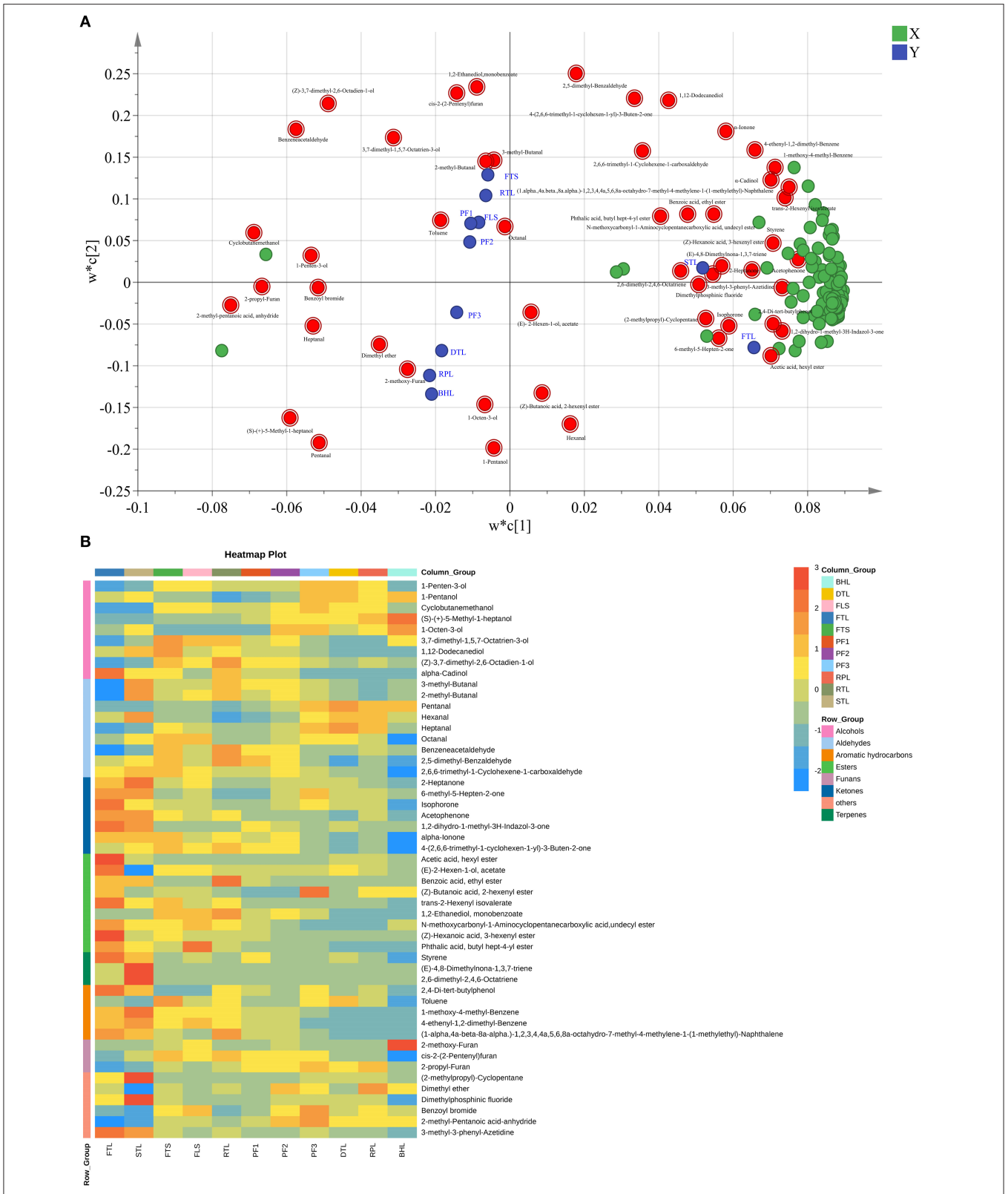

FIGURE 3 | (A) Loading diagram of Partial Least Squares Discrimination Analysis (PLS-DA) model. **(B)** Heat map of 51 difference volatile compounds.

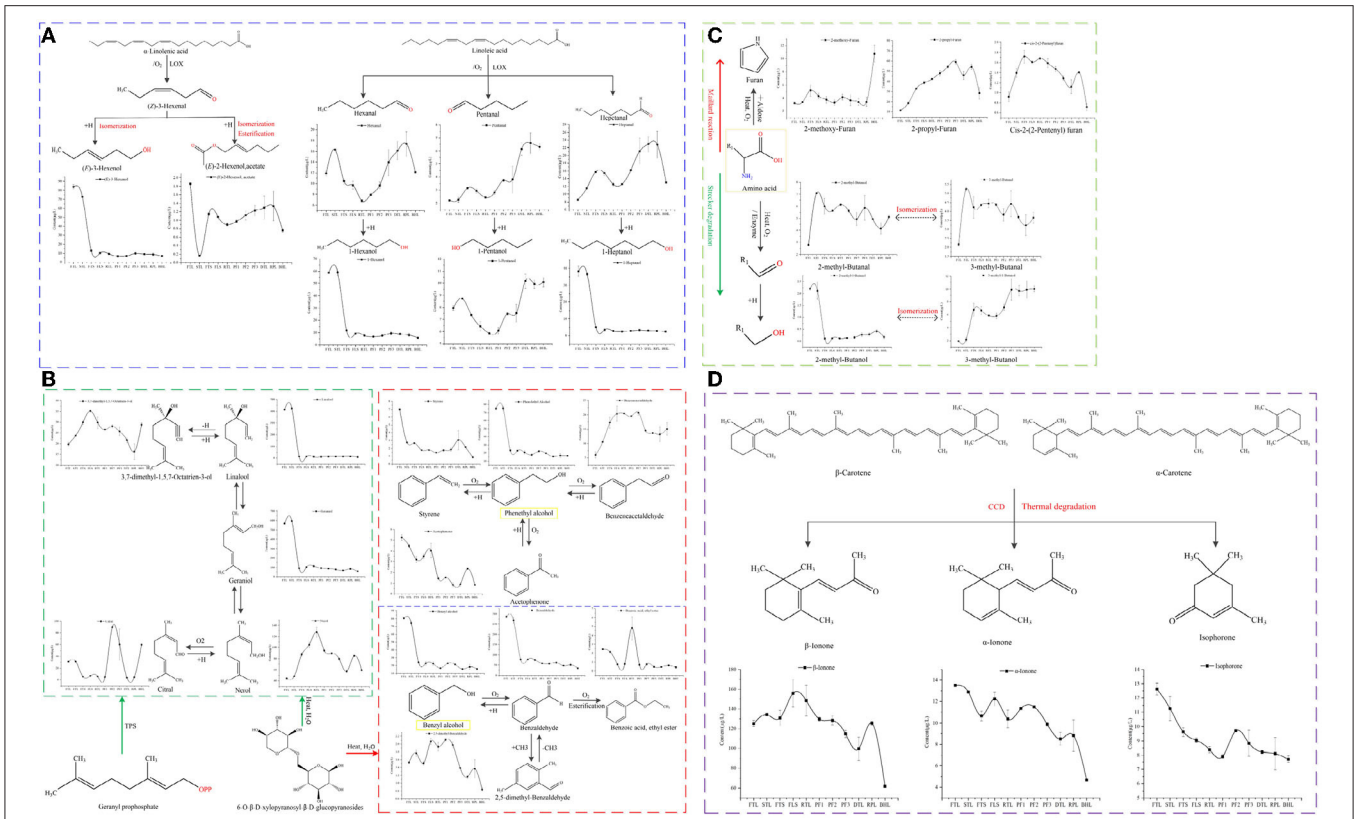

FIGURE 4 | Evolution of compounds from different sources: **(A)** Fatty derived volatiles, **(B)** Glycoside-derived volatiles, **(C)** Amino acid-derived volatiles, and **(D)** Carotenoid-derived volatiles.

and phenylethanol) can be liberated by glycosidic enzymes or heat reaction. In this study, the levels monoterpene alcohols, such as linalool, geraniol markedly decreased after fixation (**Figure 4B**), whereas the dehydrogenation compound (3,7-dimethyl-1,5,7-octatrien-3-ol), isomerisation compound (nerol) considered important components of the floral and fruity aroma of green tea (28), remarkably increased. The levels of methyl salicylate, alfa-copaene, cubenene, α-cadinol, etc., (**Supplementary Figure S1**) markedly decreased in FTS, whereas those of citral, as the oxide of nerol, which is the isomer of geraniol and linalool, were significantly increased in PF2 and BHL, particularly in PF2 ($p < 0.05$). This indicates that the isomerization of linalool, geraniol and the oxidation reaction of nerol may generate citral under long-term high-temperature treatment of PF2 (11). The level of aromatic compounds, such as benzyl alcohol, benzaldehyde, styrene, phenylethyl alcohol markedly decreased after fixation, while corresponding oxides (benzene acetaldehyde) was increased. Benzoic acid, ethyl ester was increased significantly after rolling process, which may relate to the increase of cell fragmentation rate under the action of external force and high leaching rate. The high temperature treatment of RPL promoted the oxidation and methylation reaction to form acetophenone, 2,5-dimethyl-benzaldehyde. Many glycoside-derived volatiles disappeared during the fixation process, which is consistent with the results of previous studies (11). It is speculated that in a high-temperature environment, some volatiles are lost and recombine with glycosides to form nonvolatile compounds; furthermore, they undergo oxidation, isomerization, and other reactions (8).

Amino Acid-Derived Volatiles

Amino acid-derived volatiles are generally derived from the Strecker reaction of amino acids and the Maillard reaction of amino acids with sugars (9). Acid-derived volatiles were identified in this study (**Figure 4C**). Among these, 2-methyl-butanal and 3-methyl-butanal increased significantly after spreading ($p < 0.05$), which is related to the reaction of leucine and isoleucine with glutamine under the action of transaminase and decarboxylase. After fixation, the levels of 3-methyl-butanal, 2-methyl-butanal, and 2-methyl-butanol were significantly reduced ($p < 0.05$), whereas those of 3-methyl-butanol significantly increased ($p < 0.05$). Moreover, at high temperatures, oxidation reaction was triggered, and strong reduction reaction and isomerization reaction also occurred (10); however, their contents in PF3 and BHL have rebounded, which is related to the high temperature and long-term treatment at this stage to promote the Strecker reaction of amino acids and oxidation and isomerization. 2-methoxy-furan, cis-2-(2-pentenyl) furan, and 2-propyl-furan are the Maillard reaction products; the levels of 2-methoxy-furan increased in FTS, PF2,

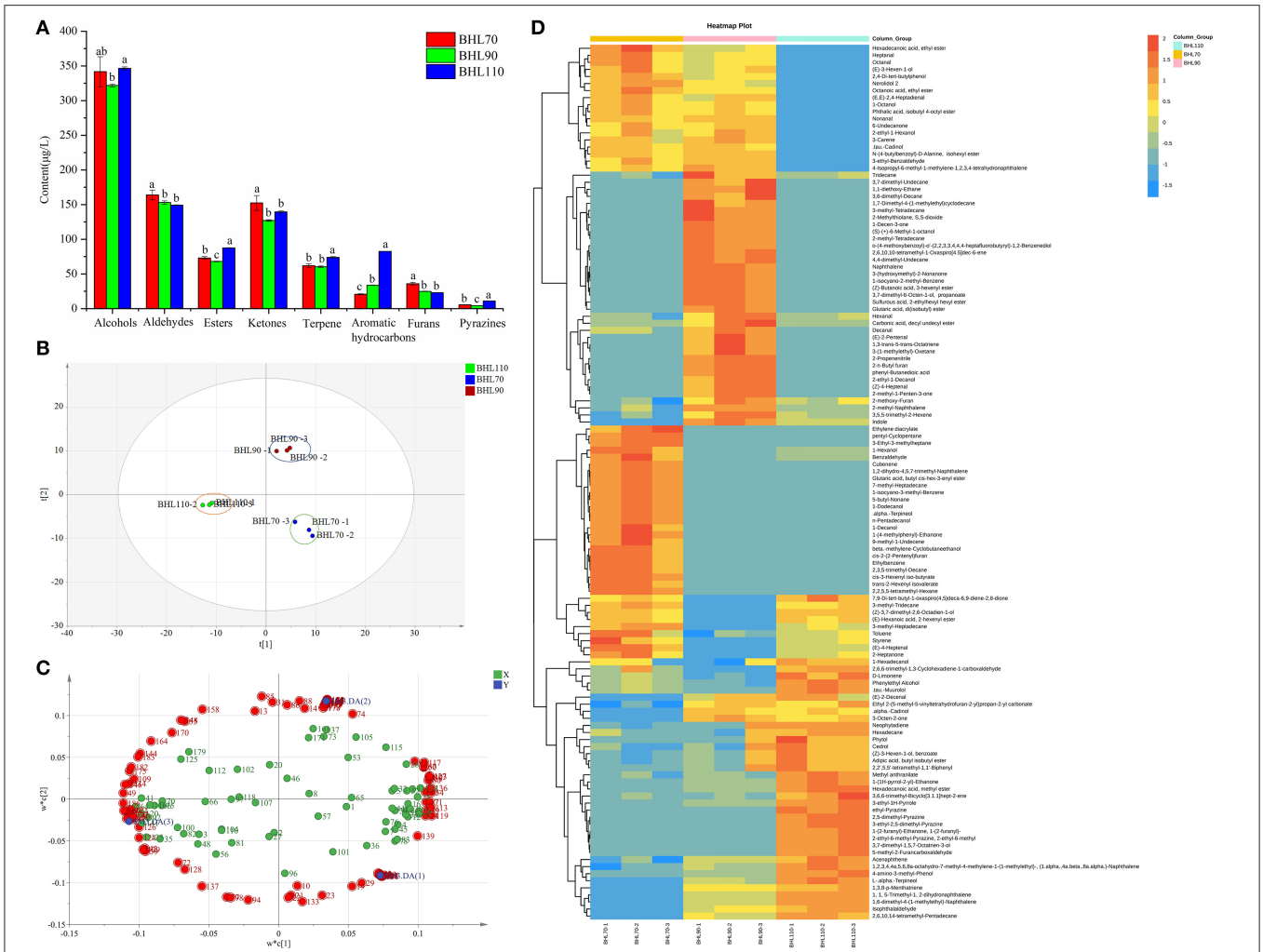

FIGURE 5 | (A) Histogram of different types of volatile compounds of round green tea by different second-drying temperature. **(B)** Partial Least Squares Discrimination Analysis (PLS-DA) score. **(C)** Loading diagram for volatile compounds of round green tea by different second-drying temperature. **(D)** Heat map of 117 difference volatile compounds. Different letters indicate the significance of the difference of the same type substance at different temperatures through LSD test ($p < 0.05$).

BHL, particularly in BHL, which is consistent with the results of the existing research (9), and 2-propyl-furan exhibited an upward trend in most processes but decreased in DTL and BHL. Moreover, cis-2-(2-pentenyl) furan increased in STL, FTS, and RPL, whereas it decreased in BHL significantly ($p < 0.05$), which contradicts the existing research that high temperature and long-term drying is conducive to the Maillard reaction (30), and may be related to the further transformation of these two substances at high temperatures.

Carotenoid-Derived Volatiles

Carotenoids can generate ionone, 2,6,10,10-tetramethyl-1-oxaspiro [4.5] dec-6-en-8-one, and other floral and fruity substances under enzymatic oxidation and heat, and are important precursors of the formation of green tea aroma (9). The evolution of β-ionone, α-ionone and isophorone is depicted in **Figure 4D**; β-ionone, α-ionone increased during FLS and RPL, and the decrease was most obvious at BHL (29). Isophorone is another carotenoid-derived volatile (31), which exhibited decreased trend before PF2, but increased mostly in PF2 and further decreased. The rebound in PF1 and PF2 is related to the increase in cell disruption and the overflow of its precursor substances, which further promotes its synthesis under the action of high temperature (32).

Effect of Box Hot Air Second-Drying Temperature on Volatile Compounds

In section Analysis of Volatile Compounds During the Processing of Green Tea discussion, it was found that the hot air drying process is crucial in the formation of aroma during RGT processing. Therefore, this study will further discuss the influence of different second-drying temperatures on the volatile compounds of RGT.

Volatile Profile of Green Tea Under Different Box Hot Air Second-Drying Temperature

In total, 247 volatile compounds were obtained in different second-drying temperature samples (**Supplementary Table S2**). The comparison of different temperature samples revealed that alcohols and furans were significantly higher in BHL70 ($p < 0.05$), whereas alkanes, terpenes, aromatic hydrocarbons, and pyrazines were higher in BHL110 than in other samples, and the contents of various compounds (such as alkanes, terpenes, aromatic hydrocarbons, alcohols, and furans) were moderate in BHL90 (**Figure 5A**). Substances with green aroma, such as (E)-3-hexen-1-ol, 1-hexanol, 1-decanol, hexanal, (E)-2-hexenal, and (E)-4-heptenal were higher in BHL70; naphthalene, 2-methoxy-furan, (E)-2-pentenal, 3-octen-2-one, and 2,6,10,10-tetramethyl-1-oxaspiro [4.5] dec-6-ene were higher in BHL90; whereas 3-ethyl-1H-pyrrole, 2-ethyl-6-methyl-pyrazine, 3-ethyl-2,5-dimethyl-pyrazine, and roast aroma were higher in BHL110 than BHL90 and BHL70 (**Supplementary Table S2**).

PLS-DA

To further clarify the effect of the second-drying temperature on volatile compounds and obtain key differential compounds, PLS-DA analysis (33) was conducted in this study based on 247 volatile compounds. The score map is illustrated in **Figure 5B**, and three groups of samples were distinguished. While detecting t [1], BHL70 and BHL90 were on the right side of the figure, and BHL110 was on the left side of the figure. The model parameters were $R^2X = 0.941$, $R^2Y = 0.998$, and $Q^2 = 0.988$, indicating that the model is stable and reliable and has strong predictive ability.

To obtain the key volatile compounds that distinguish samples at different second-drying temperatures, variable importance of projection (VIP) and difference significance analysis were used to screen differential substances. In total, 117 substances (load diagram, **Figure 5C**), such as benzaldehyde, octanal, D-Limonene, naphthalene, hexanal, 3-ethyl-1H-Pyrrole, (E)-3-Hexen-1-ol, 2,5-dimethyl-pyrazine, and trans-β-ionone, were obtained. **Supplementary Figure S2** illustrates the changes in 117 substances under different second-drying temperatures. The heatmap (**Figure 5D**) showed the changes of 117 differential compounds under different second-drying treatments clearly. Octanal, (E, E)-2,4-heptadienal, 1-Octanol, nonanal, and (E)-4-heptenal, with a grassy aroma, were higher in BHL70; 2-methoxy-furan, (E)-2-pentenal, 3-octen-2-one, and 2,6,10,10-tetramethyl-1-oxaspiro [4.5] dec-6-ene were higher in BHL90; and 3-ethyl-1H-pyrrole, 2-ethyl-6-methyl-pyrazine, and 3-ethyl-2,5-dimethyl-pyrazine were higher in BHL110. This result follows the previous studies reporting that significantly lower temperatures lead to greater retention of grass-flavored substances and insufficient formation of high-boiling aromatic substances ($p < 0.05$), whereas higher temperature can significantly promote the Maillard reaction of amino acids and sugars to produce too many pyrazines, which imparts a baking flavor to the tea (34).

OAV

OAV analysis is frequently applied to evaluate the contribution of volatile compounds in aroma (27, 35). Odor thresholds and characteristics of the 41 patients (**Supplementary Table S3**) consuming the 117 substances were obtained based on previous studies (8, 36–39). Of these, 21 substances (**Table 1**), with important contributions to aroma, were screened out according to the principle of OAV > 1. In particular, the OAV of trans-β-ionone is >9,000, and 1-octanol is >450, both of which are important components of aroma composition (8, 38). From the perspective of different second-drying temperature treatments, the OAVs of 1-hexanol, (E)-4-heptenal, octanal, 1-octanol, nerolidol 2, benzaldehyde with green, and flower aroma were higher in BHL70 than in the other treatments, whereas naphthalene, 2,6,10,10-tetramethyl-1-oxaspiro [4.5] dec-6-ene and decanal significantly contributed to BHL90 ($p < 0.05$). These compounds, such as 3,7-dimethyl-1,5,7-octatrien-3-ol, 2,5-dimethyl-pyrazine, ethyl-pyrazine, 2-ethyl-6-methyl-pyrazine, and 3-ethyl-2,5-dimethyl-pyrazine with roasted aroma are only present in BHL110; however, due to the high threshold of these substances, their OAV <1, but the relatively low OAV values of other substances highlight the baking flavor.

DISCUSSION

Processing technology and second-drying temperature are key factors in the formation of RGT aroma (8, 39). In this study, the concentration of all the identified volatile compounds have undergone substantial changes during tea processing, particularly during the fixation process, followed by pan-frying and second-drying, which is consistent with previous reports (7, 8). Under the high-temperature fixation treatment, many low-boiling point alcohols, aldehydes, and esters are lost and transformed, and violent degradation, isomerization, redox, and other reactions occur, consequently forming high-boiling point compounds. During the pan-fried process, the tea leaves and pot wall are repeatedly rubbed. Therefore, the cell fragmentation rate increases, and the volatile compounds and their precursors are further released from the cells. Moreover, high temperature increases thermochemical reactions and promotes the formation of furans, aldehydes, and aromatic hydrocarbons with high-boiling point. During the box hot air second-drying, few low-boiling volatile compounds were further lost. This could be related to the large consumption of precursor compounds in fixation and pan-frying process. The levels of fatty acid-derived volatiles and glycoside-derived volatiles have undergone considerable changes during RGT processing, especially during the fixation process. Under high temperature condition during the fixation process, the temperature of tea leaves changes from 20 ∼ 25°C to 70 ∼ 80°C, the moisture content of tea leaves changes from 70 to 30% ∼ 40%, the state of enzymes changes from active to inactive, and a series of enzymatic chemical reactions and thermochemical reactions take place in the tea leaves in 2 ∼ 5 min. High temperature can promote the degradation of lipids to generate free fatty acids, which generate alcohols and aldehydes volatiles under the effect of heat-induced oxidation. The increase in glycoside-derived volatiles in fixation process may be due to the simultaneous enzymatic hydrolysis and thermochemical degradation of glycosides. This result is

TABLE 1 | Aroma characteristics and OAV values of 21 different volatile compounds (OAV > 1) in different second-drying temperature samples.

Name	OT μg/L)[A]	Aroma characteristics[B]	BHL70	BHL90	BHL110
1-Hexanol	0.7	Green, cut grass	10.14 ± 1.89a	2.37 ± 0.259b	4.13 ± 0.40b
2-Heptanone	1	pieplant, musty	2.15 ± 0.61a	0.00 ± 0.00c	1.34 ± 0.15b
(E)-4-Heptenal	0.02	Green	67.08 ± 15.33a	0.00 ± 0.00c	28.55 ± 2.95b
Heptanal	3	Heavy, planty green odor	5.94 ± 1.25a	3.98 ± 0.62b	0.71 ± 0.05c
Benzaldehyde	3	almond-like smell	2.27 ± 0.29a	1.04 ± 0.09b	1.24 ± 0.03b
Octanal	0.7	Green, fatty, citruse	5.88 ± 1.49a	3.96 ± 0.54b	0.00 ± 0.00c
1-Octanol	0.022	Green, citrus, fatty, coconut-like	533.65 ± 89.58a	450.99 ± 37.79b	0.00 ± 0.00c
Nonanal	1	candle-like, sweet orange-like, fatty and floral	29.97 ± 4.34a	29.62 ± 1.38a	0.00 ± 0.00b
Decanal	0.1	Aldehyde-like, candle-like, fatty and citrus-like aroma	18.96 ± 2.78b	27.89 ± 2.26a	16.44 ± 0.34b
1-Decanol	0.023	Orange, floral	25.13 ± 7.39a	0.00 ± 0.00b	0.00 ± 0.00b
Nerolidol 2	0.25	Floral, green, citrus, woody, waxy	11.08 ± 0.74a	6.98 ± 0.67b	0.00 ± 0.00c
tau-Cadinol	0.44	Tar, camphor, and greasy	5.42 ± 0.56a	5.49 ± 0.44a	0.00 ± 0.00b
Naphthalene	0.44	Pungent, dry, tarry odor	0.00 ± 0.00b	4.57 ± 0.09a	0.00 ± 0.00b
2,6,10,10-tetramethyl-1-Oxaspiro [4.5] dec-6-ene	0.2	Fruity, woody, slightly camphor-like	0.00 ± 0.00b	6.25 ± 0.11a	0.00 ± 0.00b
3,7-dimethyl-1,5,7-Octatrien-3-ol	110	Moldy	0.00 ± 0.00b	0.00 ± 0.00b	0.63 ± 0.03a
2,5-dimethyl-Pyrazine	1,750	Roasted	0.00 ± 0.00b	0.00 ± 0.00b	0.001 ± 0.00a
ethyl-Pyrazine	4,000	Nutty coffee, cocoa-like	0.00 ± 0.00b	0.00 ± 0.00b	0.00 ± 0.00a
5-methyl-2-Furancarboxaldehyde	500	Caramel, bready, coffee-like	0.00 ± 0.00b	0.00 ± 0.00b	0.01 ± 0.00a
2-ethyl-6-methyl-Pyrazine	40	Roasted	0.00 ± 0.00b	0.00 ± 0.00b	0.11 ± 0.00a
3-ethyl-2,5-dimethyl-Pyrazine	8.6	Roasted potato, cocoa-like, nutty	0.00 ± 0.00b	0.00 ± 0.00b	0.41 ± 0.01a
trans-beta-Ionone	0.007	Violet-like, floral, and raspberry-like	9,676.94 ± 1,134.50a	9,260.63 ± 769.57a	10,176.88 ± 592.00a

Different letters (a, b, c) represent the significance of the difference between the same substance at different second drying temperatures through LSD test ($p < 0.05$).
OTs: Odor thresholds in water. The values were calculated according to reported references.
[A]*(8, 24, 25, 27, 31–34).*
[B]*http://www.thegoodscentscompany.com/search3.php?qOdor=20126-765&submit.x=9&submit.y=9.*

consistent with the previous reports that lipids and glycosides undergo drastic changes during fixation (11, 29, 40).

The second-drying temperature also had a great effect on the levels of volatile compounds. When the temperature was too low (70°C), the dry-heat reaction was insufficient and several green grass-flavor alcohols and aldehydes were retained (11). Therefore, the tea sample exhibited a faint scent. However, when the temperature was too high (110°C), the dry-heat reactions (Maillard reaction, Caramelization reaction, etc.) were too intense and several baking-flavor volatiles were generated (34). At the appropriate temperature (90°C), the content of each compound was moderate and the proportion of various types of volatile compounds was coordinated. In brief, the temperature at which biochemical reactions occur at a moderate rate to avoid overfired flavor is the best temperature to produce high-quality RGT.

CONCLUSIONS

In this study, the evolution of volatile compounds during the processing of RGT was investigated using IR-HS-SPME technology combined with GC-MS, and the effects of different second-drying temperatures on the formation of volatile compounds were clarified. Fixation is considered the most drastic process of volatile metabolite conversion, followed by pan-fried and box hot air second-drying. Moreover, 51 key volatile substances were screened out, and fatty acid-derived volatiles and glycoside-derived volatiles changed most dramatically during processing. Substances with excellent aroma flavor, such as nonanal, decanal, tau-cadinol, naphthalene, and 2,6,10,10-tetramethyl-1-oxaspiro [4.5] dec-6-ene were significantly higher under BHL90 treatment ($p < 0.05$) and 90°C was the most suitable temperature for the second-drying processing of RGT. This study provides a theoretical basis and technical guidance for the processing of high-quality RGT and lays a foundation for in-depth exploration of the aroma formation mechanism during green tea processing. As only the precursors of part volatile metabolites are known, the number of classified volatile compounds discussed in this study is limited. In future research, we need to assess the volatile precursor substances, analyze the relationship between Non-volatile compounds and volatile compounds, and explore the mechanism of RGT aroma formation.

DATA AVAILABILITY STATEMENT

The original contributions presented in the study are included in the article/**Supplementary Material**, further inquiries can be directed to the corresponding authors.

AUTHOR CONTRIBUTIONS

HW: conceptualization, investigation, formal analysis, software, writing–original draft, and editing. YY: investigation, resources, and writing–review and editing. WOY and JW: investigation. YJ: data curation software. JH: project administration, writing–review, and editing. HY: funding acquisition and supervision. All authors contributed to the article and approved the submitted version.

FUNDING

This work was supported by the Science and Technology Innovation Project of the Chinese Academy of Agricultural Sciences (CAAS-ASTIP-TRICAAS), the open fund of State Key Laboratory of Tea Plant Biology and Utilization (SKLTOF20210110), and the National Science Foundation of China (31972465).

SUPPLEMENTARY MATERIAL

The Supplementary Material for this article can be found online at: https://www.frontiersin.org/articles/10.3389/fnut.2022.877132/full#supplementary-material

REFERENCES

1. Aoshima H, Ayabe S. Prevention of the deterioration of polyphenol-rich beverages. *Food Chem.* (2007) 100:350–5. doi: 10.1016/j.foodchem.2005.09.052
2. Yan HM, Zhong YZ, Duan YH, Chen QH, Li FN. Antioxidant mechanism of tea polyphenols and its impact on health benefits. *Anim Nutr.* (2020) 6:115–23. doi: 10.1016/j.aninu.2020.01.001
3. Bag A, Mondal A, Majumder A, Banik A. Tea and its phytochemicals: hidden health benefits & modulation of signaling cascade by phytochemicals. *Food Chem.* (2021) 371:131098. doi: 10.1016/j.foodchem.2021.131098
4. Shang A, Li JH, Zhou DD, Gan RY, Li HB. Molecular mechanisms underlying health benefits of tea compounds. *Free Radic Biol Med.* (2021) 172:181–200. doi: 10.1016/j.freeradbiomed.2021.06.006
5. Bai XB, Li B, Deng HX. Research progress of green tea shaping equipment in China. *Chin Tea Process.* (2021) 2021:5–11. doi: 10.15905/j.cnki.33-1157/ts.2021.02.001
6. Yu FL, Guo L, Zhu Y, Dai WD, Zhang Y, Du QZ, et al. Variation of aroma components of particle type green tea during the manufacturing process. *Food Sci Technol Res.* (2015) 40:45–50+56. doi: 10.13684/j.cnki.spkj.2015.10.010
7. Hu X, Wei YM, Fang SM, Wang YJ, Xu SS, et al. Study on continuous shaping technology of granular green tea. *Chin Tea Process.* (2020) 2020:27–34. doi: 10.15905/j.cnki.33-1157/ts.2020.03.006
8. Wang HJ, Hua JJ, Jiang YW, Yang YQ, Wang JJ, Yuan HB. Influence of fixation methods on the chestnut-like aroma of green tea and dynamics of key aroma substances. *Food Res Int.* (2020) 136:109479. doi: 10.1016/j.foodres.2020.109479
9. Ho CT, Zheng X, Li SM. Tea aroma formation. *Food Sci Hum Well.* (2015) 4:9–27. doi: 10.1016/j.fshw.2015.04.001
10. Wan XC. Biochemistry of tea. Third Edition. China Agricultural Publishing House, Beijing (2003). p. 160–80.
11. Li PL, Zhu Y, Lu ML, Yang C, Xie DC, Tan JF, et al. Variation patterns in the content of glycosides during green tea manufacturing by a modification-specific metabolomics approach: Enzymatic reaction promoting an increase in the glycosidically bound volatiles at the pan firing stage. *Food Chem.* (2019) 279:80–7. doi: 10.1016/j.foodchem.2018.11.148
12. Li J, Hua JJ, Yuan HB, Deng YL, Zhou QH, Yang YQ, et al. Investigation on green tea lipids and their metabolic variations during manufacturing by nontargeted lipidomics. *Food Chem.* (2021) 339:128114. doi: 10.1016/j.foodchem.2020.128114

13. Chen QC, Zhu Y, Liu YF, Liu Y, Dong CW, Lin Z, et al. Black tea aroma formation during the fermentation period. *Food Chem.* (2022) 374:131640. doi: 10.1016/j.foodchem.2021.131640
14. Dong C, He C, Zhu JY, Qu FF, Ran MQ, Ai ZY, et al. Effect of shaping methods on the quality of E-Cha No.10 green tea products. *J Yunnan Agric Univ*. (2020) 35:139–48. doi: 10.12101/j.issn.1004-390X(n).201805002
15. Zhou TS, Mi XL, Wang YC, Yu YB, Li SL, Qi YG. Effect of different processing techniques on the quality of "Shaancha 1" green tea. *Food science.* (2017) 38:148–54. doi: 10.7506/spkx1002-6630-201703025
16. Chen L, Ji KW. Research progress on the relationship between tea shape and quality (continued). *TEA IN FUJIAN*. (2000) 2000:2–4. doi: 10.3969/j.issn.1005-2291.2000.02.001
17. Fan QY, Lan XP, Li WC, Wang JP, Tang XL. Effects of different processing techniques on the quality of green tea by Jingbai 2#. *Chin Tea Process*. (2017) 2017:54–6+71. doi: 10.15905/j.cnki.33-1157/ts.2017.z2.011
18. Flaig M, Qi S, Wei GD, Yang XG, Schieberle P. Characterization of the key odorants in a high-grade chinese green tea beverage (Camellia sinensis; Jingshan cha) by means of the sensomics approach and elucidation of odorant changes in tea leaves caused by the tea manufacturing process. *J Agric Food Chem.* (2020) 68:5168–79. doi: 10.1021/acs.jafc.0c01300
19. Yu XL. Effects of different withering methods on components metabolism related to color, aroma and taste quality in green tea. *Hua Agric Univ*. (2020) 133–65. doi: 10.27158/d.cnki.ghznu.2020.000041
20. Zhu YM, Dong JJ, Jin J, Liu JH, Zheng XQ, Lu JL, et al. Roasting process shaping the chemical profile of roasted green tea and the association with aroma features. *Food Chem.* (2021) 353:129428. doi: 10.1016/j.foodchem.2021.129428
21. Guo YL, Lai LL. Process optimization of rolled and curled green tea made of big leaves species. *Chin J Tropic Crops*. (2011) 32:2152–6. doi: 10.3969/j.issn.1000-2561.2011.11.030
22. Guo L, Yu FL, Zhao F, Zhang Y, Zhu Y, Dai WD, et al. Correlation of physical properties of granular green tea with its appearance quality. *Food Sci*. (2020) 41:25–30. doi: 10.7506/spkx1002-6630-20190930-367
23. Xue JJ, Liu PP, Guo GY, Wang WW, Zhang JY, Wang W, et al. Profiling of dynamic changes in non-volatile metabolites of shaken black tea during the manufacturing process using targeted and non-targeted metabolomics analysis. *LWT*. (2022) 156:113010. doi: 10.1016/j.lwt.2021.113010
24. Chen S, Liu HH, Zhao XM, Li XL, Shan WN, Wang XX, et al. Non-targeted metabolomics analysis reveals dynamic changes of volatile and non-volatile metabolites during oolong tea manufacture. *Food Res Intern.* (2020) 128:108778. doi: 10.1016/j.foodres.2019.108778
25. Zhou JT, Yu XL, He C, Qiu AD, Li YC, Shu QN, et al. Withering degree affects flavor and biological activity of black tea: a non-targeted metabolomics approach. *LWT*. (2020) 130:109535. doi: 10.1016/j.lwt.2020.109535
26. Yang YQ, Zhang MM, Hua JJ, Deng YL, Jiang YW, Li J, et al. Quantitation of pyrazines in roasted green tea by infrared-assisted extraction coupled to headspace solid-phase microextraction in combination with GC-qqq-MS/MS. *Food Res Intern.* (2020) 134:109167. doi: 10.1016/j.foodres.2020.109167
27. Zhang MM, Yang YQ, Yuan HB, Hua JJ, Deng YL, Jiang YW, et al. Contribution of addition theanine/sucrose on the formation of chestnut-like aroma of green tea. *LWT*. (2020) 129:109512. doi: 10.1016/j.lwt.2020.109512
28. Zhu JC, Niu YW, Xiao ZB. Characterization of the key aroma compounds in Laoshan green teas by application of odour activity value (OAV), gas chromatography-mass spectrometry-olfactometry (GC-MS-O) and comprehensive two-dimensional gas chromatography mass spectrometry (GC×GC-qMS). *Food Chem.* (2021) 339:128136. doi: 10.1016/j.foodchem.2020.128136
29. Wang HJ, Hua JJ, Yu QY, Li J, Wang JJ, Deng YL, et al. Widely targeted metabolomic analysis reveals dynamic changes in non-volatile and volatile metabolites during green tea processing. *Food Chem.* (2021) 363:130131. doi: 10.1016/j.foodchem.2021.130131
30. Yang ZY, Baldermann S, Watanabe N. Recent studies of the volatile compounds in tea. *Food Res Intern.* (2013) 53:585–99. doi: 10.1016/j.foodres.2013.02.011
31. Ravichandran R. Carotenoid composition, distribution and degradation to flavour volatiles during black tea manufacture and the effect of carotenoid supplementation on tea quality and aroma. *Food Chem.* (2002) 78:23–8. doi: 10.1016/S0308-8146(01)00303-X
32. Guo L, Zhao F, Chen JZ, Wang SQ, Yu FL, Zhang Y, et al. Analysis of aroma characteristic components of granular green tea. *Tea Comm.* (2021) 48:287–92. doi: 10.3969/j.issn.1009-525X.2021.02.014
33. Zhong JY, Chen N, Huang SC, Fan XW, Zhang Y, Ren DB, et al. Chemical profiling and discrimination of green tea and Pu-erh raw tea based on UPLC–Q–Orbitrap–MS/MS and chemometrics. *Food Chem.* (2020) 326:126760. doi: 10.1016/j.foodchem.2020.126760
34. Yang YQ, Chen JY, Jiang YW, Qian MC, Deng YL, Xie JL, et al. Aroma dynamic characteristics during the drying process of green tea by gas phase electronic nose and gas chromatography-ion mobility spectrometry. *LWT*. (2022) 154:112691. doi: 10.1016/j.lwt.2021.112691
35. Guo XY, Ho CT, Schwab W, Wan XC. Aroma profiles of green tea made with fresh tea leaves plucked in summer. *Food Chem.* (2021) 363:130328. doi: 10.1016/j.foodchem.2021.130328
36. Wang MQ, Ma WJ, Shi J, Zhu Y, Lin Z, Lv HP. Characterization of the key aroma compounds in Longjing tea using stir bar sorptive extraction (SBSE) combined with gas chromatography-mass spectrometry (GC–MS), gas chromatography-olfactometry (GC–O), odor activity value (OAV), and aroma recombination. *Food Res Intern.* (2020) 130:108908. doi: 10.1016/j.foodres.2019.108908
37. Guo XY, Ho CT, Wan XC, Zhu H, Liu QO, Wen Z. Changes of volatile compounds and odor profiles in Wuyi rock tea during processing. *Food Chem.* (2021) 341:128230. doi: 10.1016/j.foodchem.2020.128230
38. Zhu Y, Lv HP, Shao CY, Kang SY, Zhang Y, Guo L, et al. Identification of key odorants responsible for chestnut-like aroma quality of green teas. *Food Res Intern.* (2018) 108:74–82. doi: 10.1016/j.foodres.2018.03.026
39. Liao XL, Yan JN, Wang B, Meng Q, Zhang LY, Tong HR. Identification of key odorants responsible for cooked corn-like aroma of green teas made by tea cultivar 'Zhonghuang 1'. *Food Res Intern.* (2020) 136:109355. doi: 10.1016/j.foodres.2020.109355
40. Cui JL, Katsuno T, Totsuka K, Ohnishi T, Takemoto H, Mase N, et al. Characteristic fluctuations in glycosidically bound volatiles during tea processing and identification of their unstable derivatives. *J Agric Food Chem.* (2016) 64:1151–7. doi: 10.1021/acs.jafc.5b05072

Conflict of Interest: The authors declare that the research was conducted in the absence of any commercial or financial relationships that could be construed as a potential conflict of interest.

Publisher's Note: All claims expressed in this article are solely those of the authors and do not necessarily represent those of their affiliated organizations, or those of the publisher, the editors and the reviewers. Any product that may be evaluated in this article, or claim that may be made by its manufacturer, is not guaranteed or endorsed by the publisher.

frontiers | Frontiers in Nutrition

ORIGINAL RESEARCH
published: 27 April 2022
doi: 10.3389/fnut.2022.884829

Enzymatic Synthesis of Diacylglycerol-Enriched Oil by Two-Step Vacuum-Mediated Conversion of Fatty Acid Ethyl Ester and Fatty Acid From Soy Sauce By-Product Oil as Lipid-Lowering Functional Oil

*Konglong Feng[1], Huaiyi Fang[2], Guo Liu[1], Weijie Dai[3], Mingyue Song[1], Jiangyan Fu[4], Linfeng Wen[1], Qixin Kan[1], Yunjiao Chen[1], Yuanyou Li[5], Qingrong Huang[6] and Yong Cao[1]**

[1] Guangdong Provincial Key Laboratory of Nutraceuticals and Functional Foods, College of Food Science, South China Agricultural University, Guangzhou, China, [2] College of Marine Sciences, Beibu Gulf University, Qinzhou, China, [3] Guangdong Huiertai Biotechnology Co., Ltd., Guangzhou, China, [4] Guangdong Meiweixian Flavoring Foods Co., Ltd., Zhongshan, China, [5] Guangdong Laboratory for Lingnan Modern Agriculture, College of Marine Sciences, South China Agricultural University, Guangzhou, China, [6] Department of Food Science, Rutgers University, New Brunswick, NJ, United States

OPEN ACCESS

Edited by:
Jinkai Zheng, Institute of Food Science and Technology (CAAS), China

Reviewed by:
Zhenjun Zhu, Jinan University, China
Kaavya Rathnakumar, University of Wisconsin-Madison, United States

***Correspondence:**
Yong Cao
caoyong2181@scau.edu.cn

Specialty section:
This article was submitted to Food Chemistry, a section of the journal Frontiers in Nutrition

Received: *27 February 2022*
Accepted: *24 March 2022*
Published: *27 April 2022*

Citation:
Feng K, Fang H, Liu G, Dai W, Song M, Fu J, Wen L, Kan Q, Chen Y, Li Y, Huang Q and Cao Y (2022) Enzymatic Synthesis of Diacylglycerol-Enriched Oil by Two-Step Vacuum-Mediated Conversion of Fatty Acid Ethyl Ester and Fatty Acid From Soy Sauce By-Product Oil as Lipid-Lowering Functional Oil. Front. Nutr. 9:884829. doi: 10.3389/fnut.2022.884829

Soy sauce by-product oil (SSBO), a by-product of the soy sauce production process, is the lack of utilization due to an abundance of free fatty acid (FFA) and fatty acid ethyl ester (EE). The utilization of low-cost SSBO to produce value-added diacylglycerol (DAG)-enriched oil and its applications are promising for the sustainability of the oil industry. The objective of this study was to utilize SSBO containing a high content of EE and FFA as raw material to synthesize DAG-enriched oil and to evaluate its nutritional properties in fish. Based on different behaviors between the glycerolysis of EE and the esterification of FFA in one-pot enzymatic catalysis, a two-step vacuum-mediated conversion was developed for the maximum conversions of EE and FFA to DAG. After optimization, the maximum DAG yield (66.76%) and EE and FFA conversions (96 and 93%, respectively) were obtained under the following optimized conditions: lipase loading 3%, temperature 38°C, substrate molar ratio (glycerol/FFA and EE) 21:40, a vacuum combination of 566 mmHg within the initial 10 h and 47 mmHg from the 10th to 14th hour. Further nutritional study in fish suggested that the consumption of DAG-enriched oil was safe and served as a functional oil to lower lipid levels in serum and liver, decrease lipid accumulation and increase protein content in body and muscle tissues, and change fatty acid composition in muscle tissues. Overall, these findings were vital for the effective utilization of SSBO resources and the development of future applications for DAG-enriched oil as lipid-lowering functional oil in food.

Keywords: diacylglycerol, soy sauce by-product oil, enzymatic synthesis, a two-step vacuum-mediated conversion, lipid-lowering, functional oil

INTRODUCTION

High-fat intake results in an increased risk of obesity, hyperlipidemia, cardiovascular disease, and other metabolic syndromes, which is always a great concern nowadays. A novel healthy structured lipid has attracted much research interest due to its unique health benefits, such as calorie reduction, anti-obesity, and lipid-lowering properties (1). Moreover, a variety of novel structured healthy lipids are developed in recent years, in which diacylglycerol (DAG), is one of the more suitable alternatives to the conventional high-calorie triacylglycerol (TAG) oil, is a research hotspot (2). DAG consists of 1,3-DAG and 1,2-DAG forms, whose structure is constituted by a glycerol backbone esterified with two fatty acids. Previous studies have reported that the consumption of DAG can prevent weight gain and fat deposition, lowers postprandial hyperlipidemia and serum TAG levels, and improves glucose metabolism (3–9). These health benefits are ascribed to the metabolic differences of DAG oil in the compositions and positional distributions of fatty acids (10). DAG, especially 1,3-DAG, are hydrolyzed to 1(3)-MAG after digestion, which is not efficiently hydrolyzed again and reassembled as TAG. Hence, the consumption of DAG oil could not be stored up as fat in adipose tissue and the body. Nowadays, on the basics of its safety for human consumption and its many acclaimed health benefits, DAG oil is commercially available in Japan and United States (11). Nevertheless, DAG oil has not yet been a great success in the market due to non-uniform scientific reports and the lack of economic competitiveness and technical sophistication in the production of DAG (12).

Diacylglycerol (DAG) is a minor natural component in various edible oils with a maximum level of up to 10% (13). Thus, considering the increasing demand for DAG enriched oil, many approaches have been investigated to synthesize DAG. Enzymatic synthesis of DAG was widely employed for its environmentally friendly processes, higher yield, and mild conditions (14). DAG can be produced through esterification, glycerolysis, partial hydrolysis, and so on. Among these approaches, an enzymatic esterification is a common approach for the production of DAG-enrich oil, in which fatty acids (FFA) are esterified with glycerol using lipase (15, 16). Glycerolysis is the most economical and industrial promising method for the production of DAG (17). The high content of DAG (about 60-65%) was synthesized by enzymatic glycerolysis using commercial lipases (18), and the docosahexaenoic acid-rich DAG-rich oil was also produced by lipase-catalyzed glycerolysis of microbial oil in a solvent-free system (19). Additionally, Awadallak et al. provided a new approach to producing a high content of DAG (55.6%) from linseed oil by combining enzymatic glycerolysis and esterification (20). To date, various raw materials, including triglycerides of edible oils, high-acid oil, fatty acid, and fatty acid ethyl ester (EE), have been used as a substrate for DAG production (4, 20–23). However, none of the studies have reported on the synthesis of DAG from the refined soy sauce by-product oil (SSBO) containing a high content of EE and FFA (49.96 and 30.21%, respectively). SSBO is a by-product of the soy sauce production process, and its utilization was restricted due to an abundance of free fatty acid (FFA) and dark color (24). In the previous study, an effective approach was proposed to reduce FFA content in high-acid soy sauce residue oil through low-cost and reusable biocatalysis (ANL-MARE) catalyzed esterification, which could convert high content of FFA (61.26%) to DAG-enriched soy sauce residue oil (25). Although ANL-MARE had the higher capability in the conversion of FFA to DAG, it was not effectively glycerolysis of EE in the optimum conditions for enzymatic deacidification. Besides, SSBO contains a higher content of EE in this study than that in our previous study. Thus, the optimum conditions for enzymatic deacidification were not suitable for the glycerolysis of EE. FFA and EE might be good raw materials as acyl group donors, especially for the synthesis of high content 1,3-DAG by using a 1,3 specific lipase. The higher DAG yield might be able to obtain when EE was able to effectively transform into DAG by transesterification with glycerol, along with enzymatic deacidification of SSBO. Moreover, SSBO has an advantage in large annual production and low cost. Hence, the present study proposed to use SSBO for the synthesis of valuable DAG-enriched oil by combined conversion of EE and FFA from SSBO with glycerol. Although many studies on DAG production *via* enzymatic esterification and glycerolysis have been performed, a combination of glycerolysis of EE and esterification of FFA in one-pot enzymatic catalysis is rarely studied (**Scheme 1**). DAG oil has unique nutritional properties concerning lower body fat metabolism (26). However, to our knowledge, little work investigates the nutritional properties of DAG-enriched oil from SSBO. It is expected that DAG-enriched oil will be used as functional oil.

In this study, DAG-enriched oil was synthesized using a low-cost SSBO containing a high content of EE and FFA as raw material and a non-commercial immobilized *Aspergillus niger* lipase (ANL-MARE) as a catalyst. Based on the different behaviors between the transesterification of EE and the esterification of FFA in one-pot enzymatic catalysis, a two-step vacuum-mediated conversion was developed for the conversions of EE and FFA to DAG. Subsequently, reaction conditions were optimized through a single factor experiment and response surface methodology (RSM). The nutritional properties of DAG-enriched oil from SSBO were evaluated in fish.

MATERIALS AND METHODS

Materials

Food-grade glycerol and SSBO were obtained from Guangdong Huiertai Biotechnology Co., Ltd. (Guangzhou, China). SSBO was preliminary refined by desalted, degummed, dewaxed, dehydrated, and bleached, respectively. The non-commercial immobilized Aspergillus niger lipase (ANL-MARE) was prepared by Guangdong Provincial Key Laboratory of Nutraceuticals and Functional Foods (25). Edible Soybean oil was purchased from a local market. Total triglyceride (TG) and total cholesterol (TC) were supplied by Nanjing Jiancheng Bio-Engineering Institute Co., Ltd. (Nanjing, China). Chromatographic-grade n-hexane, isopropyl alcohol, and formic acid were bought from Aladdin Reagent Co. Ltd. (Shanghai, China).

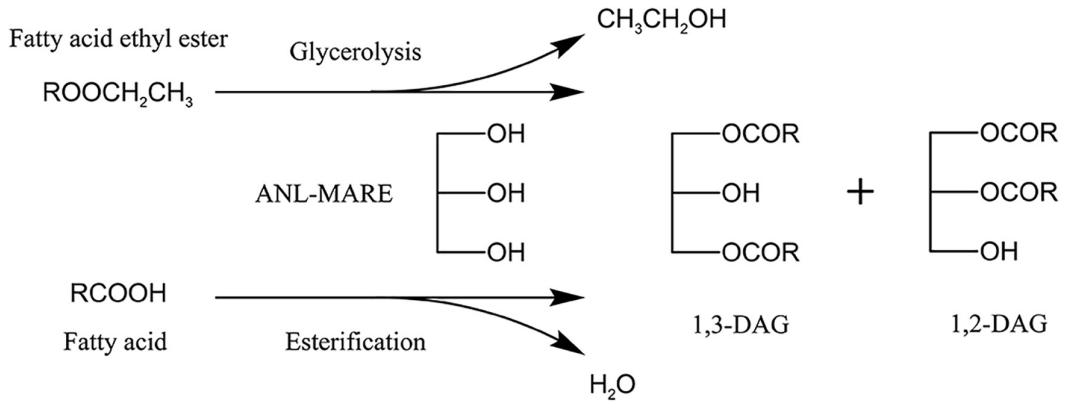

SCHEME 1 | ANL-MARE catalyzed the synthesis of DAG-enriched oil by a two-step vacuum-mediated conversion of EE and FFA.

Effects of Vacuum on the One-Pot Conversion of Fatty Acid Ethyl Ester and Fatty Acid From Soy Sauce By-Product Oil

A vacuum-driven air bubbling operation was carried out in a vacuum rotary evaporator (27). Approximately 50 g of the refined SSBO, with high EE and FFA, and 3% ANL-MARE dosage were incubated for 10 min in a 250-ml round-bottom flask. Subsequently, the reaction was started by adding glycerol (molar ratio of glycerol to FFA and EE, 1:2) at 55°C under different vacuum levels with air gas bubbling. During the reaction, a 200 μl aliquot was collected from the reaction mixture at a variety of time points and analyzed by high-performance liquid chromatography (HPLC) as described below.

A Two-Step Vacuum-Mediated Conversion of Ethyl Ester and Free Fatty Acid From Soy Sauce By-Product Oil to Diacylglycerol -Enriched Oil

According to the results in different vacuum levels, a two-step vacuum process was proposed for maximizing esterification of FFA and glycerolysis of EE. In the first step, the reaction was carried out within the initial 8 h under a low vacuum level (647 mmHg). After most of the EE was transformed, a high vacuum level (47 mmHg) was applied to transform the residual FFA in the reaction mixture from the 8th to the 10th hour.

Optimization of Reaction Conditions for the Synthesis of Diacylglycerol

Firstly, substrate molar ratio (glycerol/FFA and EE), temperature, ANL-MARE loading, and reaction time were further optimized by a single factor experiment. The effect of a variables on the yield of DAG content, EE, and FFA conversion were analyzed.

Subsequently, response surface methodology (RSM) was used to obtain the optimal reaction conditions. Based on the results of the single factor experiment, the substrate mole ratio, temperature, substrate molar ratio (glycerol/FFA and EE), and the first step vacuum level were selected as the optimizing factors. A three-factor-three-level Box Behnken design (BBD) was used to generate factor combinations using Design Expert 8.0.6 software (Stat-Ease Inc., Minneapolis, MN, United States) (**Table 1**).

Analysis of Acylglycerol Composition by High-Performance Liquid Chromatography

The acylglycerol composition of raw SSBO and reaction products were determined by a normal phase HPLC (LC-15, Shimadzu, Japan) equipped with a refractive index detector. The samples were dissolved into the mobile phase (21:1:0.004, v/v/v, n-hexane/isopropyl alcohol/formic acid), and then, eluted *via* the gradient elution of the mobile phase. The chromatographic conditions were set as follows: column temperature, 30°C; flow rate, 1 mL/min; sample injection volume, 10 μl. The content of each lipid class was calculated by peak-areas percentages. The DAG content was calculated based on the sum peak area of 1,3-DAG and 1,2-DAG concerning the total peak areas. The conversions of EE or FFA were calculated as the glycerolysis of EE amount or the esterified FFA amount to the initial EE or FFA amount.

Clinical Study, Sample Collection, and Experimental Design

Nile tilapia were supplied by Guangdong Tilapia Breeding Farm, Guangdong, China. Fish were adaptively fed for 2 weeks in the aquaculture facility of the South China Agricultural University. After acclimation, the fish were randomly divided into the DAG-enriched oil (DGO) and soybean oil (SBO) groups (150 individuals each, 6 circular tanks). The detailed components of the two experimental diets are shown in **Supplementary Table 1**. During the feeding experiment, the fish were fed the diets twice a day. At the end of 8 weeks trial, all fish from each tank were weighed and measured individually before being anesthetized with clove oil. Twelve fishes per group (4 fish/tank) were used for physiological and biochemical analyses. Plasma samples were obtained from blood by centrifugation for further serum

TABLE 1 | Response surface methodology (RSM) design and corresponding results of diacylglycerol (DAG) yield and the conversion of EE and FFA.

Run	Temperature (°C)	GLY:EE&FFA	Vacuum (mmHg)	Final composition (%)					Conversion (%)	
				DAG	TAG	MAG	EE	FFA	EE	FFA
1	45 (0)	4:7 (1)	347 (−1)	59.80	15.59	16.01	4.78	3.81	90.43	87.39
2	35 (-1)	1:2 (0)	347 (−1)	63.00	17.40	10.34	6.14	3.13	87.72	89.66
3	45 (0)	1:2 (0)	497 (0)	62.91	25.13	7.40	1.80	2.76	96.39	90.86
4	45 (0)	4:7 (1)	647 (1)	63.26	17.39	14.37	2.27	2.72	95.46	91.01
5	35 (-1)	1:2 (0)	647 (1)	65.61	18.52	8.73	2.87	4.26	94.25	85.90
6	55 (1)	3:7 (−1)	497 (0)	50.95	39.58	3.44	3.77	2.26	92.46	92.51
7	35 (-1)	3:7 (−1)	497 (0)	61.81	19.94	4.87	5.68	7.70	88.64	74.51
8	55 (1)	1:2 (0)	647 (1)	59.74	28.79	7.36	1.94	2.18	96.12	92.80
9	55 (1)	1:2 (0)	347 (−1)	44.99	14.20	12.32	24.24	4.25	51.49	85.92
10	45 (0)	1:2 (0)	497 (0)	63.94	24.48	7.53	2.26	1.79	95.48	94.07
11	45 (0)	1:2 (0)	497 (0)	62.63	24.30	8.12	2.58	2.36	94.84	92.18
12	45 (0)	3:7 (−1)	347 (−1)	56.52	30.23	3.21	6.40	3.64	87.19	87.96
13	45 (0)	1:2 (0)	497 (0)	63.07	23.95	8.06	2.98	1.95	94.03	93.54
14	45 (0)	3:7 (−1)	647 (1)	56.74	31.68	3.35	3.81	4.42	92.37	85.37
15	55 (1)	4:7 (1)	497 (0)	47.74	13.36	18.26	14.02	6.62	71.94	78.10
16	35 (-1)	4:7 (1)	497 (0)	63.81	16.76	14.14	2.62	2.67	94.75	91.15
17	45 (0)	1:2 (0)	497 (0)	62.92	23.29	8.02	2.90	2.87	94.19	90.51

GLY: glycerol, FFA: free fatty acid, EE: fatty acid ethyl esters, MAG: monoglyceride, DAG: diacylglycerol, TAG: triacylglycerol.

biochemical analysis. Once the blood sampling was finished, the liver and adipose tissue were individually collected and weighed after sacrifice. The muscle was dissected without skin. A part of muscle tissue was used for texture analysis and another part was frozen for further analysis. All samples were rapidly frozen in liquid nitrogen and then stored at –80°C.

Biochemical Estimation of Serum and Liver

The serum TC, TG, high-density lipoprotein cholesterol (HDL-C), low-density lipoprotein cholesterol (LDL-C), alanine transaminase (ALT), and aspartate transaminase (AST) levels were determined using an automatic biochemical analyzer (Beckman Coulter chemistry analyzer AU5800 series, Tokyo, Japan), according to manufacturer's instruction. The hepatic TG and TC levels were measured using commercially available kits (Nanjing Jiancheng Bioengineering Institute, Nanjing, China).

Analysis of Fatty Acids Composition in Muscle by Gas Chromatography-Mass Spectrometry

The determination of fatty acid composition in muscle was performed according to a previously described method with some modifications (28). The muscle samples were dried by vacuum freeze-drying, and then, the total lipids of the liver were extracted from the dried muscle samples according to Folch's procedure (29). Fatty acid methyl esters were prepared by referring to the method of Liu et al. (30) and then determined using GC-MS (Agilent 6890-5973N, Agilent Technologies, United States) equipped with a DB-WAX capillary column (60 m, 0.25 μm i.d., film thickness, Agilent Technologies, United States). The results were presented as the percentage of each fatty acid concerning the total fatty acids.

Analysis of the Proximate Composition of Whole Fish and Muscle Tissues

Six fish or 6 muscle samples were randomly selected from each group for measuring the proximate composition of whole fish and muscle tissues. The determination of proximate composition, including the contents of moisture, ash, crude lipid, and crude protein, was performed according to a previously described method (31).

Characterization of Muscle Texture Properties and Edible Quality

Six fresh muscle samples per group were used for measurement of muscle texture properties and edible quality after the muscle was dissected without skin. The muscle texture properties were assayed according to the method of Wang et al. (32). The edible quality was assayed according to the method of Lv et al. (31).

Statistical Analysis

Data were expressed as means ± SD. The data in the enzymatic synthesis of DAG were analyzed by using a one-way analysis of variance (ANOVA) with SPSS 21.0 software (IBM Corporation, Armonk, New York), and different letters were indicated significant differences according to Duncan s multiple range test ($P < 0.05$). Additionally, differences between the SBO and DGO groups were determined with Student's *t*-test. $P < 0.05$ was considered statistical significance.

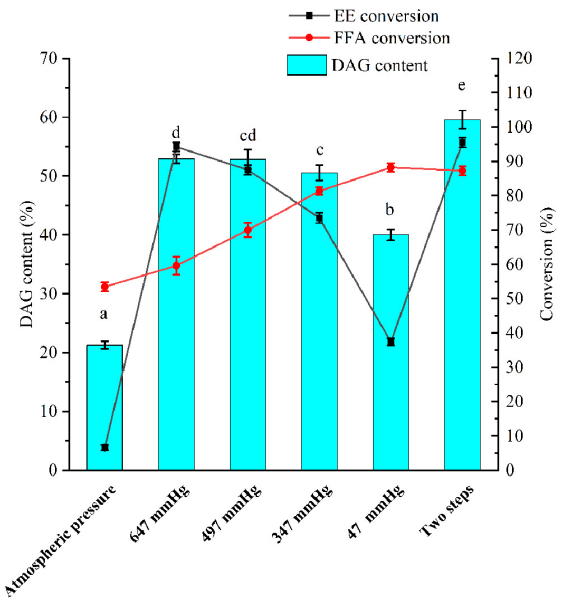

FIGURE 1 | A two-step vacuum-mediated conversion of fatty acid ethyl ester and fatty acid from soy sauce by-product oil (SSBO) to diacylglycerol (DAG)-enriched oil. Reaction condition: SSBO with high ethyl esther (EE) and free fatty acid (FFA): 50 g, ANL-MARE load: 3%, substrate molar ratio (glycerol/EE and FFA): 1:2, temperature: 55°C, different vacuum with air bubbling or two-step vacuum process, 150 rpm and reaction time: 8 h or 10 h. FFA: free fatty acid, EE: fatty acid ethyl esters, DAG: diacylglycerol. The different letters indicate significant differences at $P < 0.05$.

RESULTS

A Two-Step Vacuum-Mediated Conversion of Ethyl Ester and Free Fatty Acid From Soy Sauce By-Product Oil to Diacylglycerol-Enriched Oil

A vacuum was employed to remove produced water and ethanol in a vacuum-driven air bubbling operation, thereby increasing the conversion of FFA and EE, as well as the yield of DAG. The EE and FFA from SSBO were served as acyl group donors in this reaction (**Scheme 1**), while the lipase showed different behaviors between the glycerolysis of EE and the esterification of FFA with glycerol (**Figures 1**, **2**). Under atmospheric pressure, the conversion of FFA achieved about 50% during the first 2 h of the reaction, while only a little EE was transformed (**Figure 2A**). Also, no significant changes in the conversion of FFA and EE were observed after 2 h. As the vacuum levels increased from 647 to 47 mmHg, the conversion of FFA gradually enhanced the maximum (88.24%). The conversion of EE significantly increased as the vacuum levels increased from atmospheric pressure to 647 mmHg, up to the maximum value (94.24%), but decreased significantly as the vacuum levels increased above 647 mmHg. Meanwhile, the yield of DAG showed a similar tendency, achieving a maximum (52.93%) at 647 mmHg (**Figure 1**). From these results, it is clear that a high vacuum level favored the esterification of FFA, whereas a low vacuum level was conducive to the glycerolysis of EE. Vacuum levels higher than 647 mmHg were not suitable for glycerolysis of EE but accelerated the esterification of FFA, which might be attributed to transesterification activity drop with lower water content and the shifted equilibrium to esterification in lower water content. The water content or water activity of the system was likely associated with a vacuum. These results also implied that the water activity requirements for optimum efficacy were higher for glycerolysis of EE than that for esterification of FFA. Although the glycerolysis of EE and the esterification of FFA happened at the same time, EE and FFA did not convert maximally under a vacuum level. Thus, to maximize the synthesis of DAG, a two-step vacuum process was proposed for maximizing the esterification of FFA and glycerolysis of EE (**Figure 2F**). In the first step, the reaction was carried out within the initial 8 h under a low vacuum level (647 mmHg), in which the transesterification activity of EE was superior to the esterification activity of FFA. After most of the EE was transformed, a high vacuum level (47 mmHg) was applied to transform the residual FFA in the reaction mixture. In this approach, the conversions of EE and FFA were 95.46 and 87.28%, respectively. And this approach exhibited a conversion to DAG as high as 59.57%, which was notably higher than the single vacuum process. Therefore, a two-step vacuum process was used for the subsequent experimentation.

Optimization of Reaction Conditions for the Synthesis of Diacylglycerol Using Single Factor Experiment and Response Surface Methodology

Effects of Substrate Molar Ratio (Glycerol/Free Fatty Acid and Ethyl Ester)

To maximize the synthesis of DAG, reaction conditions, including substrate molar ratio, temperature, ANL-MARE loading, and reaction time, were further optimized. As a substrate in the reaction, glycerol not only shows poor miscibility in the reaction system that decreases the reaction rate but also exhibits a formidable water binder that decreases water activity in the reaction system (21, 33). Hence, the optimization of the substrate molar ratio of the glycerol to FFA and EE was crucial to the product composition and the performance of immobilized lipase. The molar ratio of glycerol to FFA and EE exhibited an apparent effect on the product composition (**Supplementary Figure 1A**). The DAG yield markedly increased with the increase of molar ratio from 3:7 to 1:2, but remarkably declined and then remained unchanged when the molar ratio was increased greater than 1:2 (**Figure 3A**). The conversion of EE and FFA showed a similar tendency. Although increasing glycerol amount could enhance DAG yield to some extent, excess presence of glycerol not only decreased reaction rate, but also had a negative effect on the stability of immobilized lipase (34). Therefore, a 1:2 molar ratio was the most appropriate substrate molar ratio for further optimization.

Effects of Temperature

Temperatures ranging from 35 to 65°C were optimized (**Figure 3B**). Reaction temperature had a significant effect

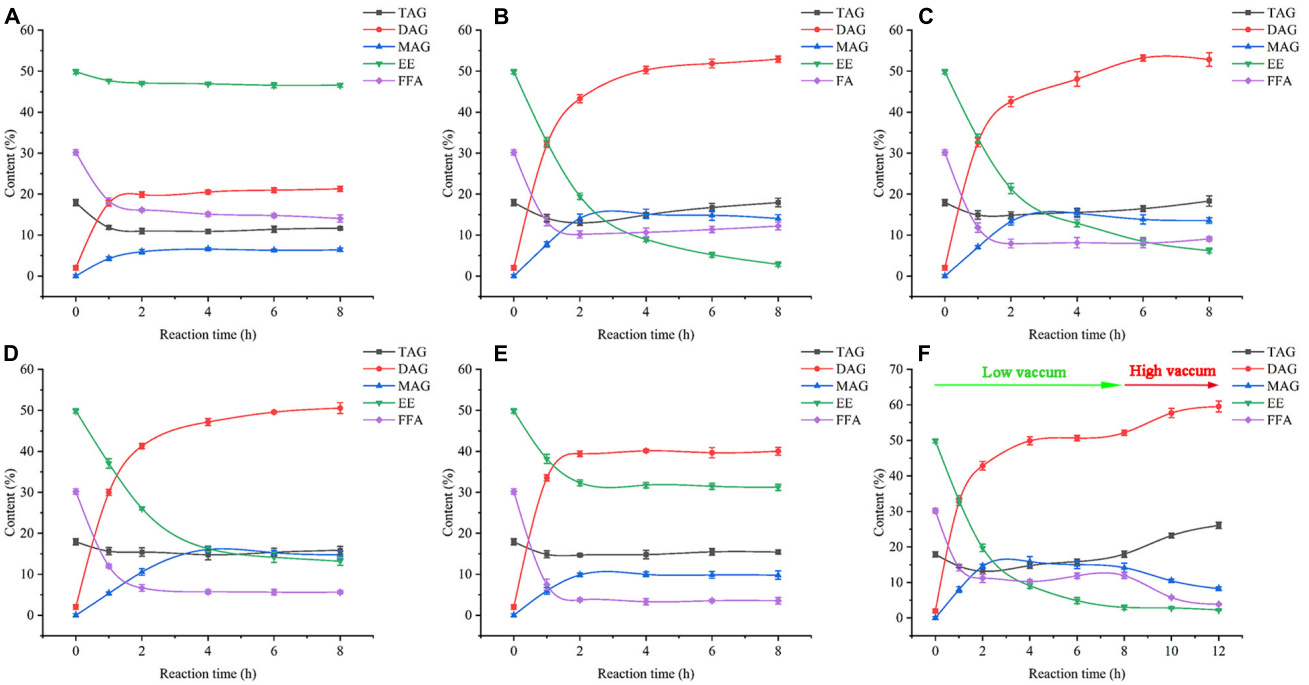

FIGURE 2 | Time course of lipid composition analysis under the condition of various vacuum **(A)** Atmospheric pressure, **(B)** 647 mmHg, **(C)** 497 mmHg, **(D)** 347 mmHg, **(E)** 47 mmHg, and **(F)** Two-step vacuum process). FFA: free fatty acid, EE: fatty acid ethyl esters, MAG: monoglyceride, DAG: diacylglycerol, TAG: triacylglycerol.

on the product composition (**Supplementary Figure 1B**). The highest DAG content was achieved as 64.11% at 40°C. As the temperature further increased from 45 to 55°C, the DAG yield decreased slowly, but the content sharply declined at 65°C. Conversely, the content of TAG showed a continuously increasing tendency with temperature increasing from 35 to 55°C (**Supplementary Figure 1B**). The findings were directly in line with previous findings, in which higher temperatures promote acyl migration and are conducive to synthesizing TAG (35). Although the highest DAG content was obtained at 40°C, the conversions of EE and FFA were lower at 40°C than those at 45°C. Thus, to obtain the highest conversion to DAG and the higher conversions of EE and FFA, a temperature of 45°C was chosen for further experimentation.

Effects of ANL-MARE Loading

As shown in **Figure 3C**, the DAG yield significantly increased with the increasing lipase loading from 1.5% to 3% and remained unchanged after further increased lipase loading over 3%. The highest DAG content was obtained as 63.37% at ANL-MARE loading of 3%. As the lipase loading increased, the contents of FFA and EE continuously declined, while the TAG content continuously increased (**Supplementary Figure 1C**). This could be ascribed to the catalytic efficiency being significantly enhanced with more addition of lipase. Therefore, considering the economy, the ANL-MARE loading of 3% was selected in this study.

Effects of Reaction Time

In this study, three-time processes were optimized (**Figure 3D**). The DAG content elevated rapidly within the initial 2 h and raised slowly after 8 h. A significant increase in the conversion of EE was observed within the time under a low vacuum, whereas the increment was insignificant after the high vacuum was applied (**Supplementary Figure 2A**). The maximum conversion of EE was observed at the time process, in which a high vacuum in the second step was applied after 10 h. The conversion of FFA increased rapidly within the initial 2 h, achieving about 68% (**Supplementary Figure 2B**). Then, it somewhat decreased due to the accumulation of produced water under low vacuum, but significantly increased until high vacuum was applied. Therefore, to maximize the conversions of EE and FFA, the reaction was used low vacuum (647 mmHg) within the initial 10 h, and then, high vacuum from the 10th to 14th hour in this study. Under this time process, 64% DAG was obtained and the conversion of EE and FFA were achieved at 96.42 and 95.34%, respectively.

Analysis of Response Surface Methodology for the Optimum Conditions

To further investigate the relationship and the interaction between any two parameters on DAG yield, a three-level three-factor BBD was employed (**Table 1**). As shown in **Table 2**, the model was significant at $P < 0.001$, and the multiple correlation coefficient of R^2 and the adjusted R^2 were 0.9311 and 0.8426, respectively. These results from ANOVA suggested that the models were suitable for predicting the DAG yield within the

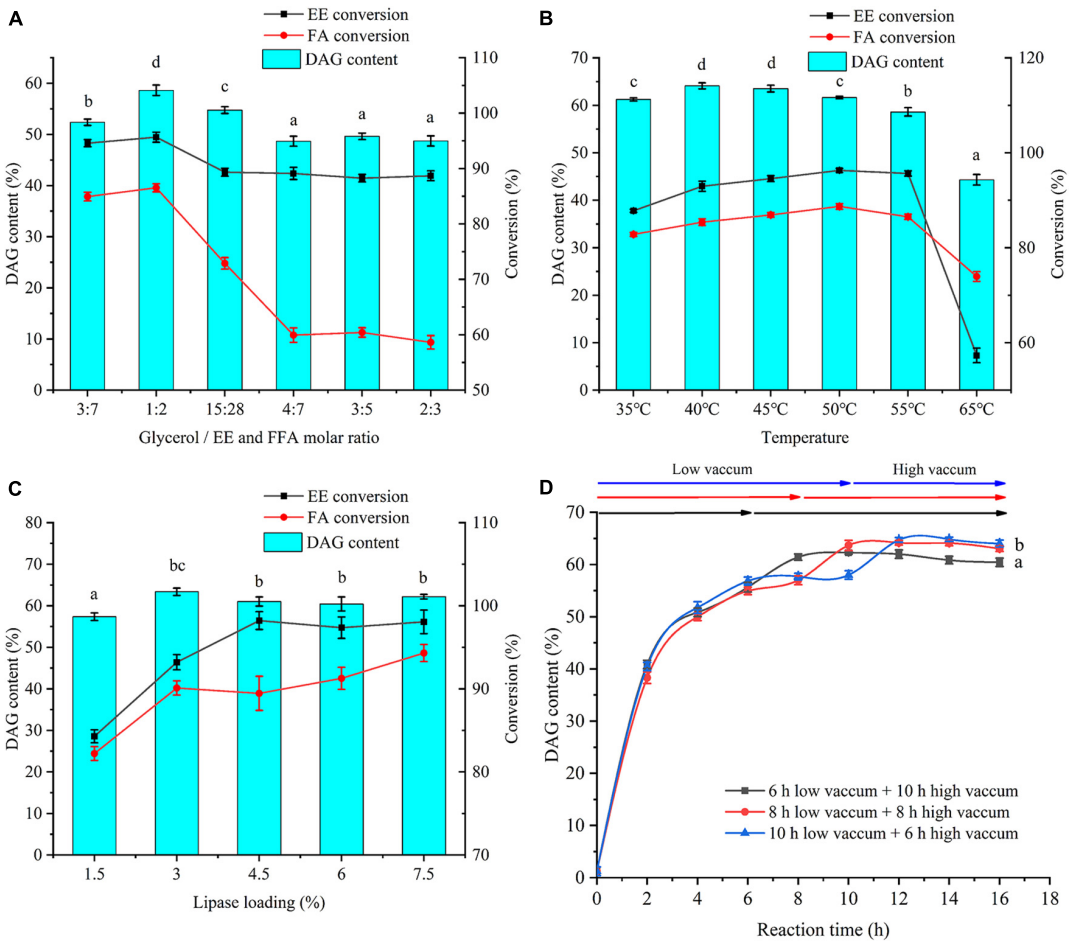

FIGURE 3 | Effects of substrate molar ratio (glycerol/FFA and EE) **(A)**, temperature **(B)**, ANL-MARE loading **(C)**, and reaction time **(D)** on DAG content, EE, and FFA conversion. The different letters indicate significant differences at $P < 0.05$.

range of variables determined. According to the significance of each coefficient in **Table 2**, the independent factors, temperature, and the initial vacuum, the quadratic terms of temperature and substrate molar ratio, and the interactions between temperature and initial vacuum had significant influences on the DAG yield. The results implied that variables of temperature and initial vacuum were acted a critical role in the DAG yield and showed a negative linear relation to the DAG yield. An increment of temperature and vacuum resulted in a reduction of DAG yield. The relationships between independent variables and DAG yield in 3D response surfaces were shown in **Figure 4**. Based on the analysis of RSM, the optimal conditions for maximum DAG yield (66.13%) were a temperature of 37.96°C, a substrate molar ration of 211:400, and the first step vacuum level of 566 mmHg. Under the predicted optimal conditions, we slightly modified conditions for experimental feasibility and convenience. The modified conditions were as follows: a temperature of 38°C, a substrate molar ration of 21:40, the first step vacuum level of 566 mmHg within the initial 10 h, and the second step vacuum level of 47 mmHg from 10th to 14th hour. Under the modified optimal conditions, a yield of 66.39% of DAG was obtained experimentally, which showed a good agreement with the predicted values and further proved the validity of models.

Scale-Up Trial and Physicochemical and Compositional Characterization of Diacylglycerol-Enriched Oil

To further prepare DAG-enriched oil for nutritional studies, a 20-time substrate (1 kg high-acid oil) scale-up trial was performed under the above-optimized process conditions. After 14 h enzymatic reaction, DAG content in the crude product was approximately 66%, suggesting that the reaction was scalable.

Physicochemical properties and composition of the preliminary refined SSBO with high EE and FFA and DAG-enriched oil were determined (**Table 3**). After catalytic reaction, DAG-enriched oil contained a higher content of DAG, achieving 66.76% (62.62% of 1,3-DAG and 4.14% of 1,2-DAG), followed by 19.31% TAG, 10.04% monoglyceride (MAG), 1.88% EE, and 2% FFA. In addition, DAG-enriched oil also showed a low acid value (3.79 mg KOH/g) and peroxide value (3.28 mmol/kg), which reached the food additive standard of mono and diglycerides.

TABLE 2 | Regression coefficients and analysis of variance for response surface model fitting.

Source	Sum of squares	*df*	Mean square	*F*-value	*P*-value	Significant [1]
Model	550.56	9.00	61.17	10.52	0.0026	significant
A-Temperature	322.61	1.00	322.61	55.46	0.0001	**
B-Substrate molar ratio	9.22	1.00	9.22	1.58	0.2485	
C-Vacuum	55.30	1.00	55.30	9.51	0.0177	*
AB	6.78	1.00	6.78	1.16	0.3162	
AC	36.80	1.00	36.80	6.33	0.0401	*
BC	2.64	1.00	2.64	0.45	0.5223	
A^2	63.37	1.00	63.37	10.89	0.0131	*
B^2	41.35	1.00	41.35	7.11	0.0322	*
C^2	3.24	1.00	3.24	0.56	0.4795	
Residual	40.72	7.00	5.82			
Lack of Fit	39.73	3.00	13.24	53.36	0.0011	significant
Pure Error	0.99	4.00	0.25			
Cor Total	591.28	16.00				
R^2	0.9311					
Adj R^2	0.8426					

[1] *significant difference was indicated by * $P < 0.05$ and ** $P < 0.01$, respectively.*

The fatty acid composition of DAG-enriched oil was mainly composed of 48.07% linoleic acid, 23.71% oleic acid, 12.80% palmitic acid, 8.99% linolenic acid, and 5.02% stearic acid, which was similar to soybean oil. Meanwhile, the energy value of DAG-enriched oil (39.16 kJ/g) was also similar to that of soybean oil (39.53 kJ/g). Although the fatty acid composition and energy value of DAG-enriched oil resembled those of soybean oil, DAG-enriched oil contained a higher content of DAG than soybean oil (0.92%). Consumption of oils with higher content of DAG, particularly 1,3-DAG, has positive physiological effects in anti-obesity and the reduction of postprandial TAG levels (26). In this study, DAG-enriched oil had a high content of DAG (66.76%), especially a high content of 1,3-DAG, after enzymatic reaction, which might show a higher nutritive value than that of TAG oil. Hence, further studies need to investigate the nutritional properties and applications of this DAG-enriched oil.

Nutritional Studies of Diacylglycerol-Enrich Oil in Fish

Effect of Dietary Diacylglycerol-Enriched Oil on Growth Performance of Fish

To investigate the nutritional effect of dietary DAG-enriched oil, we used fish (Nile tilapia) as a model organism. Soybean oil, a common edible oil, was chosen as reference TAG oil, for whose fatty acid composition was similar to that of DAG-enriched oil. In this study, the fish were fed a diet containing 4.3 wt% fat in the form of DAG-enriched oil or soybean oil for 8 weeks. As shown in **Table 4**, there were no significant differences in growth performance, including final body weight, weight gain, specific growth rate, feed intake, survival rate and condition factor, between the SBO and

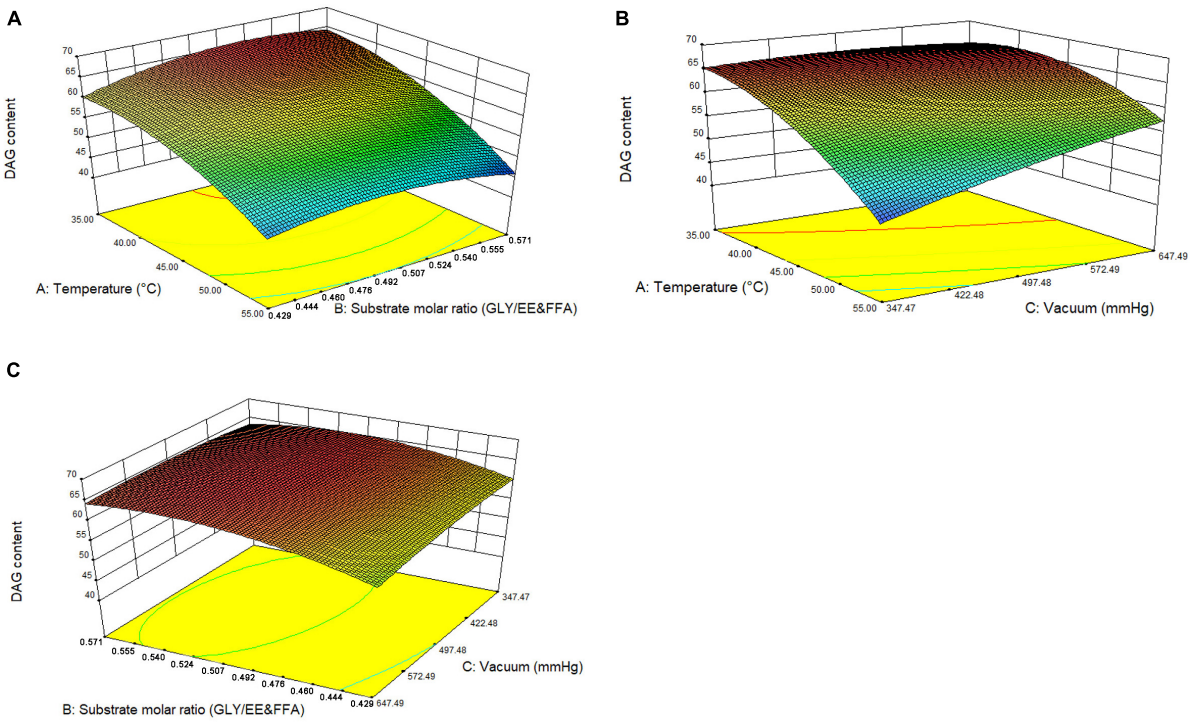

FIGURE 4 | 3D response surface graphs for the pairwise interactive effects on the conversion of EE and FFA to DAG yield. **(A)** temperature *vs.* substrate molar ratio, **(B)** temperature *vs.* vacuum, **(C)** substrate molar ratio *vs.* vacuum.

TABLE 3 | Physicochemical and compositional characterization of DAG-enriched oil.

	Soybean oil (SBO)	Refined SSBO	DAG-enriched oil (DGO)
Acid value (mg/g)	0.64 ± 0.03	57.73 ± 0.39	3.79 ± 0.24
Peroxide value (mmol/kg)	3.88 ± 0.47	3.05 ± 0.28	3.28 ± 0.23
Energy value (kJ/g)	39.53 ± 0.11	-	39.16 ± 0.09
Lipid content (%)			
TAG	98.64 ± 0.27	18.33 ± 0.69	19.31 ± 0.76
DAG	0.92 ± 0.13	1.49 ± 0.46	66.76 ± 1.37 (62.62% 1,3-DAG, 4.14% 1,2-DAG)
MAG	0.00 ± 0.00	0.00 ± 0.00	10.04 ± 0.42
FFA	0.44 ± 0.09	30.21 ± 0.89	2.00 ± 0.38
EE	0.00 ± 0.00	49.96 ± 0.62	1.88 ± 0.25
Fatty acid composition			
C14:0	0.11 ± 0.00	0.11 ± 0.01	0.08 ± 0.02
C16:0	12.78 ± 0.07	13.59 ± 0.26	12.80 ± 0.10
C16:1	0.15 ± 0.00	0.16 ± 0.04	0.08 ± 0.00
C18:0	5.35 ± 0.09	5.63 ± 0.38	5.02 ± 0.02
C18:1	26.65 ± 0.16	24.07 ± 0.77	23.71 ± 0.04
C18:2	46.57 ± 0.31	45.97 ± 1.74	48.07 ± 0.80
C18:3	6.99 ± 0.15	9.15 ± 0.33	8.99 ± 0.02
C20:0	0.50 ± 0.01	0.46 ± 0.02	0.41 ± 0.00
C20:1	0.31 ± 0.07	0.28 ± 0.02	0.31 ± 0.00
C22:0	0.59 ± 0.03	0.59 ± 0.03	0.52 ± 0.02

GLY: glycerol, FFA: free fatty acid, EE: fatty acid ethyl esters, MAG: monoglyceride, DAG: diacylglycerol, TAG: triacylglycerol, SBO: soybean oil, SSBO: soy sauce by-product oil, DGO: DAG-enriched oil.

TABLE 4 | Effects of DAG-enriched oil on growth performance, feed coefficient, and organ indices in fish.

	SBO group	DGO group
Initial body weight (g)	16.91 ± 0.23	16.93 ± 0.27
Final body weight (g)	124.28 ± 6.06	121.15 ± 8.33
Weight gain rate (%)	594.73 ± 26.92	565.51 ± 35.11
Specific growth rate (%)	3.46 ± 0.07	3.38 ± 0.09
Feed coefficient	1.12 ± 0.08	1.23 ± 0.07
Feed intake (g)	2816.33 ± 56.42	2925.70 ± 73.06
Survival rate (%)	94.67 ± 6.11	93.33 ± 8.33
Condition factor (g/cm^3)	3.41 ± 0.13	3.47 ± 0.10
Viscerosomatic index (%)	9.09 ± 0.92	8.50 ± 0.65*
Hepatosomatic index (%)	1.53 ± 0.33	1.56 ± 0.12
Intraperitoneal fat ratio (%)	0.64 ± 0.03	0.60 ± 0.04

** indicates significant differences between the SBO and DGO groups at $P < 0.05$.*

DGO groups ($P > 0.05$). Moreover, no significant changes in hepatosomatic index and intraperitoneal fat ratio were observed between the SBO and DGO groups ($P > 0.05$). Notably, viscerosomatic index significantly decreased in the DGO group compared with the SBO group ($P < 0.05$). Overall, dietary DAG-enriched oil did not affect the growth performance of fish. The results also implied that the DAG-enriched oil was proven to be safe.

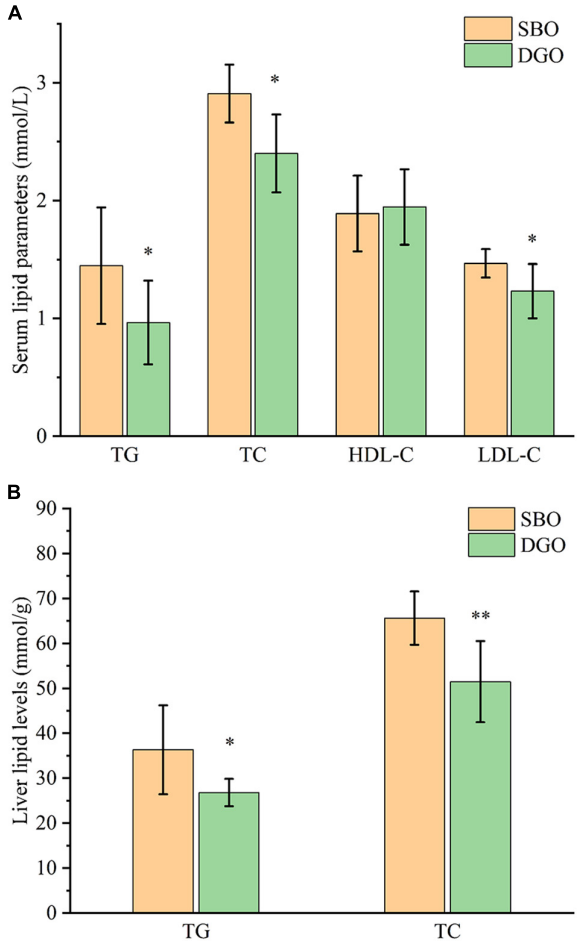

FIGURE 5 | Effects of DAG-enriched oil on serum **(A)** and liver **(B)** lipid levels in fish. * and ** indicate significant differences between the SBO and DGO groups at $P < 0.05$ and $P < 0.01$, respectively. TG: total triglyceride, TC: total cholesterol, HDL-C: high-density lipoprotein cholesterol, LDL-C: low-density lipoprotein cholesterol, SBO: soybean oil, DGO: DAG-enriched oil.

Effect of Dietary Diacylglycerol-Enriched Oil on Lipid Levels in Serum and Liver

Compared with fish fed an SBO diet, fish fed a DAG-enriched oil diet had significantly lower serum levels of TG, TC, and LDL-C by 33%, 17%, and 16%, respectively ($P < 0.05$), but did not affect serum HDL-C, ALT, and AST levels (**Figure 5A** and **Supplementary Figure 5**). Furthermore, dietary DAG-enriched oil remarkably decreased hepatic TG and TC levels by 26% and 21%, respectively ($P < 0.05$) (**Figure 5B**). The results indicated that dietary DAG-enriched oil could lower lipid levels in serum and liver.

Effect of Dietary Diacylglycerol-Enriched Oil on Proximate Composition of Whole Fish and Muscle Tissues

Compared with the SBO group, crude lipid content in the whole body was significantly lowered in the DGO group, and crude protein content in whole body was slightly increased but not significantly different (**Figure 6A**). Moreover, dietary

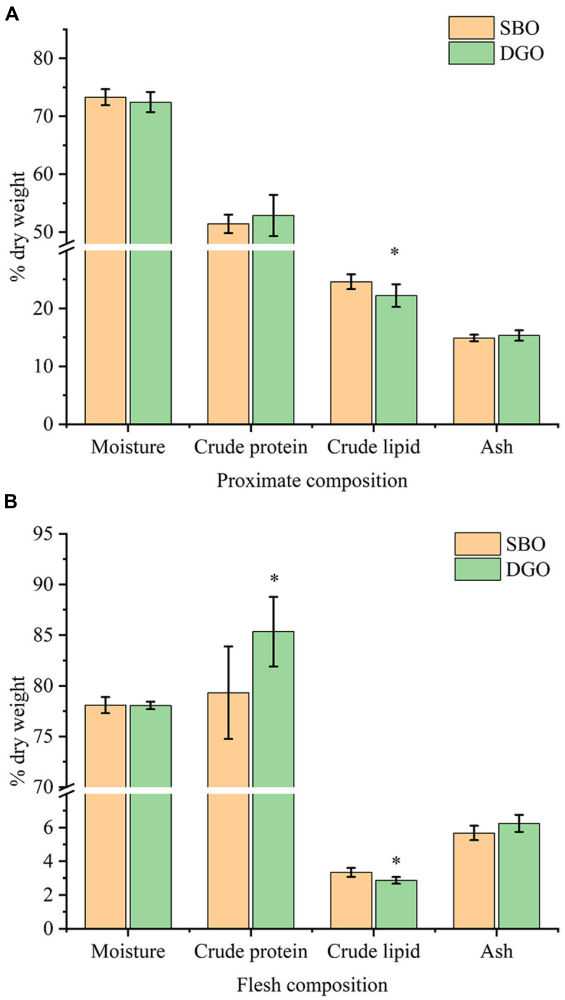

FIGURE 6 | Effects of DAG-enriched oil (DGO) on the nutrient composition of whole-body **(A)** and muscle tissues **(B)** in fish. * indicates significant differences between the SBO and DGO groups at $P < 0.05$.

DAG-enriched oil reduced significantly crude lipid content in muscle and increased crude protein content (**Figure 6B**). The contents of moisture and ash in the whole body and muscle were barely different between the SBO and DGO groups as shown in **Figure 6**. Therefore, dietary DAG-enriched oil could decrease lipid accumulation, and increased protein content in the whole fish and muscle tissues.

Effect of Dietary Diacylglycerol-Enriched Oil on Textural Properties and Edible Quality of Muscle Tissues

The textural properties and edible quality of fish muscle are shown in **Table 5**. All textural properties of muscle were similar in fish from SBO and DGO groups ($P > 0.05$). Dietary DAG-enriched oil had no changes on cooking percentage but had significantly a lower water loss rate than that of consumption of SBO, suggesting that dietary DAG-enriched oil could improve edible quality of muscle tissues.

TABLE 5 | Effects of DAG-enriched oil on textural properties and edible quality in fish.

Muscle quality	SBO group	DGO group
Textural properties		
Hardness (gf)	339.65 ± 54.15	336.93 ± 51.94
Viscosity (mJ)	−2.75 ± 0.76	−2.75 ± 1.12
Springiness (mm)	0.26 ± 0.04	0.26 ± 0.04
Chewiness (mJ)	26.96 ± 7.38	27.36 ± 8.78
Gumminess (mJ)	99.97 ± 15.24	99.95 ± 18.17
Cohesiveness	0.29 ± 0.03	0.30 ± 0.04
Resilience	0.35 ± 0.01	0.35 ± 0.03
Edible quality		
Cooking percentage (%)	78.37 ± 1.61	79.98 ± 4.62
Water loss rate (%)	5.52 ± 1.04	3.92 ± 1.11*

**indicates significant differences between the SBO and DGO groups at $P < 0.05$.*

Effect of Dietary Diacylglycerol-Enriched Oil on Fatty Acid Composition of Muscle Tissues

Overall, dietary DAG-enriched oil showed no changes on the content of total saturated fatty acids (SFA), monounsaturated fatty acids (MUFA) and polyunsaturated fatty acids (PUFA) (**Table 6**). Notably, for a specific FA, C18:3n3, C20:2n6, and C20:3n3 contents in muscle were significantly increased in fish fed a DAG-enriched oil diet compared to consumption of SBO, while C18:2n6 content was significantly lowered ($P < 0.05$). In addition, a lower content of n-6 PUFA and a higher ratio of n-3/n-6 PUFA were observed in a fish-fed DAG-enriched oil diet compared to consumption of SBO. The content of n-3 PUFA in the DGO group tended to be higher than that in the SBO group but the difference was not significant ($P > 0.05$). The results indicated that dietary DAG-enriched oil could change fatty acid composition in muscle tissues.

DISCUSSION

This study proposed a two-step vacuum-mediated conversion of EE and FFA from SSBO to DAG-enriched oil by catalyzed ANL-MARE. Enzymatic production of DAG from different materials has been reported in recent studies (14, 36, 37). Li et al. obtained 44.8% medium-chain, and medium- and long-chain fatty acid DAG *via* esterification of high purity monoacylglycerols (MAG) and caprylic acid catalyzed by Novozyme 435 (35). FFA could esterified with glycerol or MAG to produce a higher DAG yield *via* esterification reaction compared to the other reactions (27, 38). Nevertheless, high purity of free fatty acids is an expensive feedstock for production of DAG, which is not suitable for the actual application. Additionally, high-acid oil exists in natural sources, such as high-acid rice bran oil with 30 to 40% FFA. Several studies have reported that high-acid rice bran oil was used for production of DAG (about 27.98%-38.99% yield) by catalysis of Lipozyme RM IM, and the process not only was effective to reduce FFA, but also was utilized to produce high-value oils (23, 39). DAG also could be prepared by lipase-catalyzed glycerolysis of TAG oil, in which could obtain about 20 to 60% DAG content (26, 40). Moreover, few studies utilized fatty acid ethyl esters as an acyl donor for production of DAG by enzymatic glycerolysis

with glycerol (21, 41). Our findings demonstrated that DAG-enriched oil was produced by combined glycerolysis of EE and esterification of FFA with glycerol, using a low-cost refined SSBO containing a high content of EE and FFA as raw material. A high content of DAG (around 66%) was obtained in this study, especially a higher content of 1,3-DAG (62.62%), which was higher than that of esterification of high-acid oil and glycerolysis of TAG oil in the previous studies (19, 37, 39). These results were attributable to the higher conversion of EE and FFA to DAG through a two-step vacuum-mediated catalysis by 1,3-specific lipase ANL-MARE. Previous studies have reported that a single FFA or EE are transformed into DAG through a single reaction process (21, 37), and FFA, as an acyl donor, has shown a higher reaction rates and conversions than EE (42). However, few studies performed one-pot conversion of the mixture substrate of EE and FFA to DAG by an enzymatic method. The reactions were comprised of glycerolysis and esterification, because EE and FFA could serve as acyl group donors. Our results suggested that the lipases showed different behaviors between glycerolysis of EE and esterification of FFA with glycerol. A high vacuum level favored the esterification of FFA, whereas a low vacuum level was conducive to the glycerolysis of EE. In line with previous studies, most glycerolysis is carried out under micro-aqueous environment, but esterification reaction requires a lower water content (14). Therefore, a two-step vacuum process was proposed for maximizing the conversions of EE and FFA to DAG. In the first step, the reaction was carried out within an earlier stage under a low vacuum level, in which the glycerolysis activity of EE was superior to the esterification activity of FFA. After most of EE were transformed, a high vacuum level was applied to transform the residual FFA in the reaction mixture. After optimized reaction conditions, the DAG yield achieved 66% and the conversion rates of EE and FFA were up to 96% and 93%, respectively. Hence, this study has succeeded in the production of DAG-enriched oil through a two-step vacuum-mediated conversion of EE and FFA from refined SSBO by the catalysis of ANL-MARE. Moreover, to sustainably utilize SSBO for the production of DAG-enriched oil is not only high-value use of SSBO, but also lends great economic potentiality.

Extensive human and animal studies have reported that dietary DAG oil, especially 1,3-DAG, could reduce postprandial TG levels, lower serum lipids, suppress fat accumulation and body weight gain (3–7). The nutritional study of DAG-enriched oil from SSBO was also evaluated in fish. Although DAG-enriched oil had a similar energy value and fatty acid composition to TAG oil (soybean oil), our results suggested that dietary DAG-enriched oil significantly lowered serum levels of TG, TC and LDL-C, hepatic TG and TC levels, and lipid accumulation in body and muscle tissues when compared with TAG oil. Our results were broadly in line with previous research (6, 43). Meanwhile, a recent study has also reported similar results after supplementation of DAG oil rich in 50% commercial 1,3-diolein in Nile tilapia (44). Furthermore, the health benefits of DAG oil rich in 1,3-DAG might be ascribed to the structural differences between DAG and TAG, thereby showing different routes from common TAG oil in absorption and metabolism (10). In the present study, 1,3-DAG was a major constituent of the dietary DAG-enriched oil (up to 62.62% in oil). Based on these findings, it is reasonable for us to postulate that characteristics of 1,3-DAG absorption and metabolism were responsible for the health benefits of dietary DAG-enriched oil in this study. However, future study would be gained insight into the investigation of its molecular mechanism. Meanwhile, dietary DAG-enriched oil could increase protein content in the muscle tissues of fish in the present study. The benefit of DAG in the enhancement of protein absorption and deposition might be attributed to the feature of DAG emulsification. Previous studies have demonstrated that emulsifier positively affected on nutrient digestibility in animals (45). DAG might be able to promote the incorporation of nutrients into micelles and increase the absorption and bioavailability of nutrients. Hence, DAG-enriched oil would be a prospective application in edible oil and lipid-based delivery systems for the enhancement of the absorption and bioavailability of nutrients or nutraceuticals. Finally, dietary DAG-enriched oil also resulted in a lower percentage of n-6 PUFA, a high percentage of C18:3n3, C20:3n3, and total n-3 PUFA, as well as a higher ratio of n-3/n-6 PUFA in this study. These findings were similar to research showing that postprandial palmitic acid, stearic acid, and linoleic acid levels were lower after the consumption of medium-chain DAG (9). Additionally, the hydrolysis, absorption, and utilization efficiency of fatty acids are associated with the

TABLE 6 | Effects of DAG-enriched oil on muscle fatty acid composition of fish.

Fatty acids	SBO group	DGO group
C14:0	1.83 ± 0.52	2.69 ± 0.79
C16:0	22.17 ± 2.47	18.83 ± 2.52*
C18:0	11.13 ± 0.51	11.45 ± 1.62
C20:0	0.33 ± 0.37	0.39 ± 0.09
ΣSFA[1]	35.46 ± 2.00	33.36 ± 2.29
C16:1	1.92 ± 1.02	3.26 ± 1.67
C18:1n9	23.08 ± 4.63	23.76 ± 1.81
C20:1	0.89 ± 0.77	1.69 ± 0.52
C22:1n9	0.47 ± 0.41	0.41 ± 0.22
ΣMUFA[2]	26.36 ± 4.91	29.13 ± 0.88
C18:2n6	23.44 ± 1.41	20.60 ± 2.19*
C18:3n6	1.00 ± 0.08	1.12 ± 0.22
C18:3n3	1.61 ± 0.80	3.32 ± 0.54**
C20:2n6	1.41 ± 0.72	2.27 ± 0.52*
C20:3n3	1.99 ± 0.25	2.72 ± 0.50*
C20:4n6	3.60 ± 1.07	2.70 ± 0.27
C20:4n3	1.20 ± 0.65	1.47 ± 0.25
C20:5n3	2.54 ± 1.20	1.86 ± 0.23
C22:6n3	1.40 ± 0.38	1.46 ± 0.16
ΣPUFA[3]	38.18 ± 3.47	37.51 ± 1.66
Σn-3 PUFA[4]	8.74 ± 2.18	10.83 ± 1.37
Σn-6 PUFA[5]	29.45 ± 1.82	26.68 ± 1.95*
n-3/n-6 PUFA	0.30 ± 0.07	0.41 ± 0.07*

** and ** indicate significant differences between the SBO and DGO groups at $P < 0.05$ and $P < 0.01$, respectively.*

[1] ΣSFA: saturated fatty acids (C14:0, C16:0, C18:0, C20:0).

[2] ΣMUFA: monounsaturated fatty acids (C16:1, C18:1n9, C20:1, C22:1n9).

[3] ΣPUFA: polyunsaturated fatty acids (C18:2n6, C18:3n3, C18:3n6, C20:2n6, C20:3n3, C20:4n6, C20:4n3, C20:5n3, C22:6n3).

[4] Σn-3 PUFA: polyunsaturated fatty acids (C18:3n3, C20:3n3, C20:4n3, C20:5n3, C22:6n3).

[5] Σn-6 PUFA: polyunsaturated fatty acids (C18:2n6, C18:3n6, C20:2n6, C20:4n6).

location of fatty acids on the glycerol backbone (30). Therefore, we concluded that dietary DAG-enriched oil could improve fatty acid composition in muscle tissues. Together, DAG-enriched oil exhibited beneficial effects on lowering lipids in the serum, liver, muscle tissues, and body of fish and enhanced the absorption and deposition of protein.

CONCLUSION

The DAG-enriched oil was successfully prepared by a combined glycerolysis and esterification using SSBO containing a high content of EE and FFA as raw material and ANL-MARE as a catalyst. To maximally transform EE and FFA into high DAG content, a two-step vacuum-mediated conversion was proposed in one-pot enzymatic catalysis. Furthermore, the nutritional properties of DAG-enriched oil in fish were improved compared with TAG oil, in which dietary DAG-enriched oil reduced lipid levels in serum and liver, decreased lipid accumulation, and increased protein content in body and muscle tissues. Thus, this study provided a promising way in the production of DAG-enriched oil from SSBO and expanded its application in nutrition, which was of great significance for the development of DAG and the sustainability of oil industry. Further study is needed to prepare higher purity of DAG and to understand its mechanism of action to lower lipid and increase the bioavailability of nutrients.

DATA AVAILABILITY STATEMENT

The raw data supporting the conclusions of this article will be made available by the authors, without undue reservation.

ETHICS STATEMENT

The animal study was reviewed and approved by Institutional Animal Care and Use Committee of the South China Agricultural University.

AUTHOR CONTRIBUTIONS

KF, WD, YL, and YC designed the experiment. KF, HF, GL, and QK conducted enzymatic synthesis of DAG-enriched oil and the animal experiments. KF, HF, MS, and YJC did experimental analysis and analyzed the data. KF, JF, LW, QH, and YC wrote and revised the manuscript. All authors contributed to the article and approved the submitted version.

FUNDING

This work was financially supported by Study on the Formation Mechanism of Flavor Metabolites and Intelligent Manufacturing in Cantonese Soy Sauce (CXTD2020006), Program for Guangdong Introducing Innovative and En-trepreneurial Teams (2019ZT08N291), and Guangdong Provincial Key Laboratory of Nutraceuticals and Functional Foods (2018B030322010).

SUPPLEMENTARY MATERIAL

The Supplementary Material for this article can be found online at: https://www.frontiersin.org/articles/10.3389/fnut.2022.884829/full#supplementary-material

REFERENCES

1. Guo Y, Cai Z, Xie Y, Ma A, Zhang H, Rao P, et al. Synthesis, physicochemical properties, and health aspects of structured lipids: a review. *Compr Rev Food Sci Food Saf.* (2020) 19:759–800. doi: 10.1111/1541-4337.12537
2. Lai O. Diacylglycerol oils: nutritional aspects and applications in foods. In: Talbot G, editor. *Reducing Saturated Fats in Foods*. Amsterdam: Elsevier (2011).
3. Prabhavathi Devi BLA, Gangadhar KN, Prasad RBN, Sugasini D, Rao YPC, Lokesh BR. Nutritionally enriched 1,3-diacylglycerol-rich oil: low calorie fat with hypolipidemic effects in rats. *Food Chem.* (2018) 248:210–6. doi: 10.1016/j.foodchem.2017.12.066
4. Wang B, Zhang M, Ge W, He K, Cheng F. Microencapsulated duck oil diacylglycerol: preparation and application as anti-obesity agent. *LWT Food Sci Technol.* (2019) 101:645–52. doi: 10.1016/j.lwt.2018.11.061
5. Lu H, Guo T, Fan Y, Deng Z, Luo T, Li H. Effects of diacylglycerol and triacylglycerol from peanut oil and coconut oil on lipid metabolism in mice. *J Food Sci.* (2020) 85:1907–14. doi: 10.1111/1750-3841.15159
6. Anikisetty M, Gopala Krishna AG, Panneerselvam V, Kamatham AN. Diacylglycerol (DAG) rich rice bran and sunflower oils modulate lipid profile and cardiovascular risk factors in Wistar rats. *J Funct Foods.* (2018) 40:117–27. doi: 10.1016/j.jff.2017.10.049
7. Yuan Q, Ramprasath VR, Harding SV, Rideout TC, Chan YM, Jones PJ. Diacylglycerol oil reduces body fat but does not alter energy or lipid metabolism in overweight, hypertriglyceridemic women. *J Nutr.* (2010) 140:1122–6. doi: 10.3945/jn.110.121665
8. Maki KC, Mustad V, Dicklin MR, Geohas J. Postprandial metabolism with 1,3-diacylglycerol oil versus equivalent intakes of long-chain and medium-chain triacylglycerol oils. *Nutrients.* (2009) 25:627–33. doi: 10.1016/j.nut.2008.11.028
9. Lee A, Yoo HJ, Kim M, Kim M, Choi J-H, Lee C, et al. Effects of equivalent medium-chain diacylglycerol or long-chain triacylglycerol oil intake *via* muffins on postprandial triglycerides and plasma fatty acids levels. *J Funct Foods.* (2019) 53:299–305. doi: 10.1016/j.jff.2018.12.021
10. Kondo H, Hase T, Murase T, Tokimitsu I. Digestion and assimilation features of dietary DAG in the rat small intestine. *Lipids.* (2003) 38:25–30. doi: 10.1007/s11745-003-1027-7
11. Morita O, Soni MG. Safety assessment of diacylglycerol oil as an edible oil: a review of the published literature. *Food Chem Toxicol.* (2009) 47:9–21. doi: 10.1016/j.fct.2008.09.044
12. Rudkowska I, Roynette CE, Demonty I, Vanstone CA, Jew S, Jones PJH. Diacylglycerol: efficacy and mechanism of action of an anti-obesity agent. *Obes Res.* (2005) 13:1864–76. doi: 10.1038/oby.2005.229
13. Flickinger BD, Matsuo N. Nutritional characteristics of DAG oil. *Lipids.* (2003) 38:129–32. doi: 10.1007/s11745-003-1042-8
14. Phuah E-T, Tang T-K, Lee Y-Y, Choong TS-Y, Tan C-P, Lai O-M. Review on the current state of diacylglycerol production using enzymatic approach. *Food Bioprocess Technol.* (2015) 8:1169–86. doi: 10.1007/s11947-015-1505-0
15. Guo Z, Sun Y. Solvent-free production of 1,3-diglyceride of CLA: strategy consideration and protocol design. *Food Chem.* (2007) 99:1076–84. doi: 10.1016/j.foodchem.2005.11.011

16. Lo S-K, Cheong L-Z, Arifin N, Tan C-P, Long K, Yusoff MSA, et al. Diacylglycerol and triacylglycerol as responses in a dual response surface-optimized process for diacylglycerol production by lipase-catalyzed esterification in a pilot packed-bed enzyme reactor. *J Agric Food Chem.* (2007) 55:5595–603. doi: 10.1021/jf0706676
17. Sun S, Lv Y, Wang G. Enhanced surfactant production using glycerol-based deep eutectic solvent as a novel reaction medium for enzymatic glycerolysis of soybean oil. *Ind Crops Prod.* (2020) 151:112470. doi: 10.1016/j.indcrop.2020.112470
18. Kristensen JB, Xu X, Mu H. Diacylglycerol synthesis by enzymatic glycerolysis: screening of commercially available lipases. *J Am Oil Chem Soc.* (2005) 82:329–34. doi: 10.1007/s11746-005-1074-5
19. Zou X, Nadege K, Ninette I, Wen Y, Wu S, Jiang X, et al. Preparation of docosahexaenoic acid-rich diacylglycerol-rich oil by lipase-catalyzed glycerolysis of microbial oil from *Schizochytrium* sp. in a solvent-free system. *J Am Oil Chem Soc.* (2019) 97:263–70. doi: 10.1002/aocs.12311
20. Awadallak JA, da Silva EA, da Silva C. Production of linseed diacylglycerol-rich oil by combined glycerolysis and esterification. *Ind Crops Prod.* (2020) 145:111937. doi: 10.1016/j.indcrop.2019.111937
21. Vazquez L, Gonzalez N, Reglero G, Torres C. Solvent-free lipase-catalyzed synthesis of diacylgycerols as low-calorie food ingredients. *Front Bioeng Biotechnol.* (2016) 4:6. doi: 10.3389/fbioe.2016.00006
22. Li D, Qin X, Wang J, Yang B, Wang W, Huang W, et al. Hydrolysis of soybean oil to produce diacylglycerol by a lipase from *Rhizopus oryzae*. *J Mol Catal B Enzym.* (2015) 115:43–50. doi: 10.1016/j.molcatb.2015.01.009
23. Lu Y, Zou X, Han W, Jiang Y, Jin Q, Li L, et al. Preparation of diacylglycerol-enriched rice bran oil by lipase-catalyzed deacidification in packed-bed reactors by continuous dehydration. *J Oleo Sci.* (2016) 65:151–9. doi: 10.5650/jos.ess15238
24. Zhao L, Zhang Y, He L, Dai W, Lai Y, Yao X, et al. Soy sauce residue oil extracted by a novel continuous phase transition extraction under low temperature and its refining process. *J Agric Food Chem.* (2014) 62:3230–5. doi: 10.1021/jf405459v
25. Feng K, Huang Z, Peng B, Dai W, Li Y, Zhu X, et al. Immobilization of *Aspergillus niger* lipase onto a novel macroporous acrylic resin: stable and recyclable biocatalysis for deacidification of high-acid soy sauce residue oil. *Bioresour Technol.* (2020) 298:122553. doi: 10.1016/j.biortech.2019.122553
26. Lee WJ, Zhang Z, Lai OM, Tan CP, Wang Y. Diacylglycerol in food industry: synthesis methods, functionalities, health benefits, potential risks and drawbacks. *Trends Food Sci Technol.* (2020) 97:114–25. doi: 10.1016/j.tifs.2019.12.032
27. Zhong N, Gui Z, Xu L, Huang J, Hu K, Gao Y, et al. Solvent-free enzymatic synthesis of 1, 3-diacylglycerols by direct esterification of glycerol with saturated fatty acids. *Lipids Health Dis.* (2013) 12:65. doi: 10.1186/1476-511X-12-65
28. Jia R, Cao L-P, Du J-L, He Q, Gu Z-Y, Jeney G, et al. Effects of high-fat diet on steatosis, endoplasmic reticulum stress and autophagy in liver of tilapia (*Oreochromis niloticus*). *Front Mar Sci.* (2020) 7:363. doi: 10.3389/fmars.2020.00363
29. Jfolch J, Lees M, Sloane Stanley GH. A simple method for the isolation and purification of total lipids from animal tissues. *J Biol Chem.* (1957) 226:497–509. doi: 10.1007/s11745-002-1004-1
30. Liu Y, Jiao JG, Gao S, Ning LJ, McHele Limbu S, Qiao F, et al. Dietary oils modify lipid molecules and nutritional value of fillet in nile tilapia: a deep lipidomics analysis. *Food Chem.* (2019) 277:515–23. doi: 10.1016/j.foodchem.2018.11.020
31. Lv HB, Ma YY, Hu CT, Lin QY, Yue JJ, Chen LQ, et al. The individual and combined effects of hypoxia and high-fat diet feeding on nutrient composition and flesh quality in nile tilapia (*Oreochromis niloticus*). *Food Chem.* (2021) 343:128479. doi: 10.1016/j.foodchem.2020.128479
32. Wang J, Jiang H, Alhamoud Y, Chen Y, Zhuang J, Liu T, et al. Integrated metabolomic and gene expression analyses to study the effects of glycerol monolaurate on flesh quality in large yellow croaker (*Larimichthys crocea*). *Food Chem.* (2021) 367:130749. doi: 10.1016/j.foodchem.2021.130749 doi:
33. Ferreira-Dias S, Da Fonseca M. Glycerolysis of olive oil: batch operational stability of *Candida rugosa* lipase immobilized in hydrophilic polyurethane foams. *Bioprocess Eng.* (1995) 13:311–5. doi: 10.1007/bf00369563
34. Wang X, Wang X, Wang W, Jin Q, Wang X. Synthesis of docosapentaenoic acid-enriched diacylglycerols by enzymatic glycerolysis of *Schizochytrium* sp. oil. *Bioresour Technol.* (2018) 262:278–83. doi: 10.1016/j.biortech.2018.04.061
35. Li G, Chen J, Ma X, Zhang Z, Liu N, Wang Y. Enzymatic preparation and facile purification of medium-chain, and medium- and long-chain fatty acid diacylglycerols. *LWT Food Sci Technol.* (2018) 92:227–33. doi: 10.1016/j.lwt.2018.02.032
36. Liu X, Shi W, Xu L, Yang B, Liao S, Lan D, et al. Two-step enzymatic synthesis of alpha-linolenic acid-enriched diacylglycerols with high purities from silkworm pupae oil. *Bioprocess Biosyst Eng.* (2021) 44:627–34. doi: 10.1007/s00449-020-02471-w
37. Wang S, Lee WJ, Wang Y, Tan CP, Lai OM, Wang Y. Effect of purification methods on the physicochemical and thermodynamic properties and crystallization kinetics of medium-chain, medium-long-chain, and long-chain diacylglycerols. *J Agric Food Chem.* (2020) 68:8391–403. doi: 10.1021/acs.jafc.0c01346
38. Wang X, Xiao J, Zou W, Han Z, Jin Q, Wang X. Improved enzymatic synthesis route for highly purified diacid 1,3-diacylglycerols. Process Biochem. (2015) 50:388–94. doi: 10.1016/j.procbio.2014.12.020
39. Song Z, Liu Y, Jin Q, Li L, Wang X, Huang J, et al. Lipase-catalyzed preparation of diacylglycerol-enriched oil from high-acid rice bran oil in solvent-free system. *Appl Biochem Biotechnol.* (2012) 168:364–74. doi: 10.1007/s12010-012-9780-y
40. Zhao X, Sun Q, Qin Z, Liu Q, Kong B. Ultrasonic pretreatment promotes diacylglycerol production from lard by lipase-catalysed glycerolysis and its physicochemical properties. *Ultrason Sonochem.* (2018) 48:11–8. doi: 10.1016/j.ultsonch.2018.05.005
41. Rosu R, Iwasaki Y, Shimidzu N, Doisaki N, Yamane T. Enzymatic synthesis of glycerides from DHA-enriched PUFA ethyl ester by glycerolysis under vacuum. *J Mol Catal B Enzym.* (1998) 4:191–8. doi: 10.1016/s1381-1177(97)00035-0
42. Liu N, Li D, Wang W, Hollmann F, Xu L, Ma Y, et al. Production and immobilization of lipase PCL and its application in synthesis of α-linolenic acid-rich diacylglycerol. *J Food Biochem.* (2018) 42:e12574. doi: 10.1111/jfbc.12574
43. Han L, Sun R, Wang Y, Luo J, Peng X. Soybean diacylglycerol regulates lipid metabolism in D-galactose-induced aging rats by altering gut microbiota and gene expression of colonic epithelial cells. *Food Funct.* (2022) 13:1437–46. doi: 10.1039/d1fo04140a
44. Zhang H, Luo Y, Lu D-L, Jiao J-G, Li L-Y, Qin J-G, et al. Diacylglycerol oil reduces fat accumulation and increases protein content by inducing lipid catabolism and protein metabolism in nile tilapia (*Oreochromis niloticus*). *Aquaculture.* (2019) 510:90–9. doi: 10.1016/j.aquaculture.2019.05.035
45. Upadhaya SD, Lee JS, Jung KJ, Kim IH. Influence of emulsifier blends having different hydrophilic-lipophilic balance value on growth performance, nutrient digestibility, serum lipid profiles, and meat quality of broilers. *Poult Sci.* (2018) 97:255–61. doi: 10.3382/ps/pex303

Conflict of Interest: WD is employed by Guangdong Huiertai Biotechnolgy Co. Ltd. JF is employed by Guangdong Meiweixian Flavoring Foods Co. Ltd.

The remaining authors declare that the research was conducted in the absence of any commercial or financial relationships that could be construed as a potential conflict of interest.

Publisher's Note: All claims expressed in this article are solely those of the authors and do not necessarily represent those of their affiliated organizations, or those of the publisher, the editors and the reviewers. Any product that may be evaluated in this article, or claim that may be made by its manufacturer, is not guaranteed or endorsed by the publisher.

frontiers | Frontiers in Nutrition

ORIGINAL RESEARCH
published: 02 May 2022
doi: 10.3389/fnut.2022.884086

Volatile Flavor Compounds of *Pugionium cornutum* (L.) Gaertn. Before and After Different Dehydration Treatments

Haoyu Li[1,2], *Qian Wu*[1], *Qiannan Liu*[1], *Lihua Jin*[1], *Bang Chen*[1], *Cong Li*[1]*, *Jianbo Xiao*[3] *and Yehua Shen*[1]*

[1] *Key Laboratory of Synthetic and Natural Functional Molecule of the Ministry of Education, College of Chemistry and Materials Science, National Demonstration Center for Experimental Chemistry Education, Northwest University, Xi'an, China,* [2] *Shaanxi Key Laboratory of Chemical Reaction Engineering, College of Chemistry and Chemical Engineering, Yan'an University, Yan'an, China,* [3] *Department of Analytical Chemistry and Food Science, Faculty of Food Science and Technology, University of Vigo-Ourense, Ourense, Spain*

OPEN ACCESS

Edited by:
Jinkai Zheng,
Institute of Food Science and Technology (CAAS), China

Reviewed by:
Jie Zheng,
Jinan University, China
José S. Câmara,
Universidade da Madeira, Portugal

***Correspondence:**
Cong Li
licong@nwu.edu.cn
Yehua Shen
yhshen@nuw.edu.cn

Specialty section:
This article was submitted to Food Chemistry, a section of the journal Frontiers in Nutrition

Received: *25 February 2022*
Accepted: *01 April 2022*
Published: *02 May 2022*

Citation:
Li H, Wu Q, Liu Q, Jin L, Chen B, Li C, Xiao J and Shen Y (2022) Volatile Flavor Compounds of Pugionium cornutum (L.) Gaertn. Before and After Different Dehydration Treatments. Front. Nutr. 9:884086. doi: 10.3389/fnut.2022.884086

Pugionium cornutum (L.) Gaertn (also *Pugionium*) is a special Mongolian vegetable, belonging to the *Cruciferous* family, growing in arid and semi-arid areas of northern China, with a unique flavor and potential health benefits. This article aims to describe the profile of volatile flavor compounds in fresh and different dehydrated samples, establish the fingerprint, and identify the characteristic compounds. The fresh *Pugionium* sample and 3 kinds of dehydrated samples were analyzed. Headspace/gas chromatography-ion migration spectrometry (HS/GC-IMS) and solid-phase microextraction/gas chromatography-mass spectrometry (SPME/GC-MS) were used for identification and relative quantification. HS/GC-IMS identified 78 compounds, whereas SPME/GC-MS identified 53 compounds. Principal component analysis (PCA), clustering analysis, and partial least squares discriminant analysis (PLS-DA) were used as appropriate to investigate variations in volatile compounds among *Pugionium* samples and identify distinctive compounds. The first two principal components described 76.5% and 69.5% of the variance of the data from HS/GC-IMS and SPME/GC-MS, respectively. By clustering analysis, 4 kinds of *Pugionium* samples could be classified into four independent groups. The similarity between fresh *Pugionium* and natural dehydration *Pugionium* was higher than the other two dehydrated samples, indicating that natural dehydration can better preserve the flavor of *Pugionium*. Most aldehydes and alcohols increased following different dehydration procedures, whereas esters decreased, and the dehydrated *Pugionium* samples have more harmonious and less pungent aroma than the fresh *Pugionium*. PLS-DA model analysis revealed that the marker compounds (VIP scores > 1) discriminating the flavor of the four samples for HS/GC-IMS and SPME/GC-MS were 24 and 15 compounds, respectively, such as 2-phenylethyl isothiocyanate, 1-butene-4-isothiocyanate and other isothiocyanates, 2-propanone, nonanal,

gamma-butyrolactone, 2,3-butanediol, 3-methyl-2-butenenitrile, and pentanal. Analysis of volatile compounds might be useful for monitoring the quality of *Pugionium* and guiding the cooking methods and processing technologies. More study is required to discover if the various volatile flavor compounds have biological or physiological impacts on nutrition.

Keywords: *Pugionium cornutum* (L.) Gaertn., volatile flavor compounds, different dehydration treatments, HS/GC-IMS, SPME/GC-MS, isothiocyanates (ITCs)

INTRODUCTION

Pugionium cornutum (L.) Gaertn. (abbreviated *Pugionium*) is a *Cruciferous* plant that grows well in arid and semi-arid northern China. *Pugionium* has been proven effective as windbreakers in anti-desertification, conserving local sand, soil, and water, and of great ecological significance for desertification control due to its excellent drought-tolerant and deep-root system.

Pugionium is not only a well-known pioneer sand-fixing plant (1), but it has also been a popular vegetable among the locals for a long time. *Pugionium* is rich in proteins, dietary fiber, vitamins C and B_2, and mineral elements, especially the content of Ca, which is significantly higher than other common vegetables such as cabbage, spinach, and celery (2). Because of its nutritious quality and distinct pungent flavor, locals have developed a variety of cooking methods to make *Pugionium* delicious, including a cold dish in sauce, pickling, and stir-frying, also for friends from other places. *Pugionium* also contains high levels of functional components, such as phenolics, flavonoids, polysaccharides, and alkaloids, which exhibit multiple health-promoting properties. More importantly, according to the records of *Medicinal Plants in Desert Areas of China*, the dehydrated plants can also be used as medicine, with the function of pain relief, detoxification, and digestion promotion. Recognized for its special taste and health-beneficial properties, *Pugionium* has been consumed for decades as an ordinary vegetable and Chinese traditional medicine.

Generally speaking, flavor volatile components, which help stimulate people's sense of smell and taste, impact greatly the flavor and even the overall evaluation of food (3, 4). There are two common means of analyzing volatile components in food, namely, sensory analysis and instrumental analysis: the levels of sensory analysis vary with different research groups or individuals, for their uneven professional competence, and the analysis results are often subjective and arbitrary, much less the fact that the sensory analysis cannot detect the change of volatile components at the molecular level. On the contrary, the instrumental analysis, objective and fact-based, can well explain the change in the chemical composition of food flavor and the relationship between it and sensory experience, to better help understand the formation or change mechanism of certain volatile components (5), for example, gas chromatography-mass spectrometry (GC-MS) (6), gas chromatography-olfactometry (GC-O) (7, 8), and gas chromatography-ion migration spectrometry (GC-IMS) (3, 9, 10).

However, the picking season of *Pugionium* is only from July to September every year. With the water content of fresh *Pugionium* as high as about 90%, its respiration rate is much quicker than normal. Fresh *Pugionium* is prone to rot, which leads to the loss of its commercial value. As the northern desert region of China is economically underdeveloped, the most common and reliable way to achieve the long-term preservation goal of *Pugionium* is dehydration, which can maximize the value while maintaining the cost. However, dehydration causes *Pugionium*'s shape and odor to change significantly, especially the pungent odor will be greatly reduced.

Studying the volatile flavor components of *Pugionium* is very meaningful for its application in food and medicine. However, there has been less research on the identification of *Pugionium* flavor volatile compounds. This study chose three kinds of *Pugionium* samples with different dehydration treatments (i.e., freeze dehydration, hot air dehydration, and natural dehydration) to comprehensively characterize the differences in flavor volatile compositions and establish the fingerprint of *Pugionium*. HS/GC-IMS and SPME/GC-MS combined multivariate statistical analysis were used with mild, simple, and fast sample pretreatment. This research will help to further investigate the mechanism of *Pugionium* taste synthesis and give a theoretical foundation for selecting dehydration methods, as well as a reliable reference for category identification and food quality control during *Pugionium cornutum* (L.) Gaertn. industrial production in the field.

MATERIALS AND METHODS

Sample Preparation

Pugionium cornutum (L.) Gaertn. were purchased from a local vegetable market (Yulin, Shaanxi, China) in August 2020. *Pugionium cornutum* (L.) Gaertn. samples were treated using four methods given as follows: (a) fresh *Pugionium* (FP), (b) dehydrated by draft drying cabinet (60°C) to constant weight (HDP), (c) obtained after freeze dehydration (cryo-temperature−60°C, vacuum below 50 Pa) (FDP), and (d) dehydrated under natural ventilation and sunlight at average outdoor temperature (30 ± 2)°C to constant weight (NDP).

HS/GC-IMS Analysis

The gas-phase ion mobility spectrum FlavourSpec® (the Department of Shandong Hai Neng Science Instrument Co., Ltd., China) was used for a test run.

Headspace

Samples were weighed and placed into a headspace sample vial (20 ml), and then, samples were incubated at 500 rpm at 60°C for

15 min. After incubation, 500 μl of headspace was automatically injected into the injector (60°C, spitless mode) by means of a heated syringe at 65°C.

GC-IMS

The samples were driven into a chromatographic column MXT-5 (15 m × 0.53 mm × 1 μm, 60°C) by N_2 (purity ≥ 99.999 %, as carrier gas) at a programmed flow as follows: 0–2 min, 2 ml/min; 2–30 min, 100 ml/min. The drift tube was maintained at 45°C under N_2 as a drift gas at 150 ml/min.

Statistical data analysis was performed by Laboratory Analytical Viewer to view the spectrum, the reporter plug-in was directly used to compare the spectral differences, and the gallery plot plug-in can provide a more direct presentation of the differences of volatile flavor compounds among different samples. Using n-ketone C4∼C9 as an external standard reference, the retention index (RI) of each volatile compound was calculated. The identification of volatile compounds was performed by comparing the RI [built-in National Institute of Standards and Technology (NIST) 2018 database] and drift time (GC-IMS Library). In addition, the content of each volatile compound was calculated by the normalization method based on the peak intensity. The analysis was performed three times for each sample.

SPME/GC-MS Analysis

The volatile components of the samples were extracted using SPME and analyzed using GC-MS, an Agilent 7890B instrument (Agilent Technologies, Inc., Santa Clara, CA) equipped with LECO Pegsus BT mass selective detector. The capillary column used is the DB-wax column (30 m × 0.25 mm × 0.25 μm).

SPME

Samples (1 g) were weighed and transferred to a 20 ml vial, and 2 μl of 2-octanol (100 μg/ml) and 1,2-dichlorobenzene (100 μg/ml) was added as internal standard, followed by equilibrating and vibrating at 50°C for 15 min. Then, an SPME fiber coated with 50/30 μm DVB/CAR/PDMS was exposed to the headspace of the glass vial for 30 min with continuous oscillation (250 rpm). Once the volatiles were collected, the fiber was retracted and transferred immediately to the injector port of the GC instrument; the fiber was desorbed at 260°C for 5 min in splitless mode.

GC-MS

He was used as carrier gas at a flow rate of 1 ml/min. The heating program was set as follows: the initial temperature was 40°C which was held for 5 min; the temperature was increased to 220°C at the rate of 5°C/min, then to 250 at 20°C/min, and retained for 2.5 min. The temperature of the injection port, ion source, and quadrupole was 260, 230, and 150°C, respectively. The electron ionization energy of the mass selective detector was 70 eV. The MS was operated in the full scan mode, and the chromatogram was recorded by monitoring the total ion currents in the m/z range of 20–400. The full running time was 50 min.

Based on mass spectra and the use of the Openchrom software, the volatile compounds were identified, the result of which was used to compare with those in the NIST 2020 database (using the match factor threshold of 80%).

Data Analysis

The PCA and PLS-DA were processed by the software SIMCA (Version 14.1, Sweden). Advanced Heatmap Plots were performed using the OmicStudio tools at https://www.omicstudio.cn. All the results were the means of three tests conducted exactly in the same fashion, and the data were expressed as means ± standard deviation.

RESULTS AND DISCUSSION

HS/GC-IMS Analysis

In order to facilitate observation and highlight the differences in volatile flavor compounds in fresh and different dehydrated *Pugionium* samples, the top view plots (**Figure 1A**) were used (with the FP map as the reference, the spectrum of the other samples was deducted from the reference), while red color indicated that the concentration of the substance was higher than the reference, and blue color indicated that the concentration of the substance was lower than the reference. Likewise, the darker the color, the greater the difference (4, 11).

Figure 1B is a two-dimensional map synthesized by GC and IMS, which makes a more intuitive analysis of different components in the fresh and three different dehydrated *Pugionium* samples with higher qualitative accuracy (12). The lower part of the spectrum (in red frame) was relatively dense with material points, and the 50–450 s part of the spectrum was amplified for easy observation. The diversity of concentrations in some single compounds proved likely to produce multiple signals or spots (dimers or trimers) (13).

According to data, a total of 110 different characteristic signal peaks were detected, as a result of which 78 compounds were identified (**Supplementary Table 1**), including 16 esters, 25 aldehydes, 12 alcohols, 1 phenol, 8 ketones, 4 sulfur compounds, 2 acids, 1 furan, 2 nitriles, 4 terpenes, and 3 others. The relative contents of esters in FP were the highest, accounting for 56.35 % of the total volatile flavor compounds, but the content drops significantly after dehydration to only about 25%. On the contrary, the contents of aldehydes after dehydration increased significantly from 7.37% of fresh to 25–30% of dehydrated samples, and the highest in HDP was 30.77%, while alcohols increased from 9.19 to 16.80% (FDP), 16.38% (HDP), and 24.46% (NDP), respectively. Esters, aldehydes, and alcohols are the principal flavor components of fresh *Pugionium*, whereas the main components were transformed into aldehydes, esters, and alcohols after different drying treatments, indicating that the dehydration process may expedite the dissolution of esters and the creation of aldehydes and alcohols.

Among the volatile substances, esters, aldehydes, and alcohols all have distinctive flavors. The precursor of many esters is amino acids and fatty acids, and it is important for the flavor and quality of flavor. Gamma-nonalactone is an aroma substance that can bring a pleasant taste, smelling like cream or coconut, but 1-butene-4-isothiocyanate and other isothiocyanates can produce an unpleasant pungent and sulfur flavor. Alcohols will be

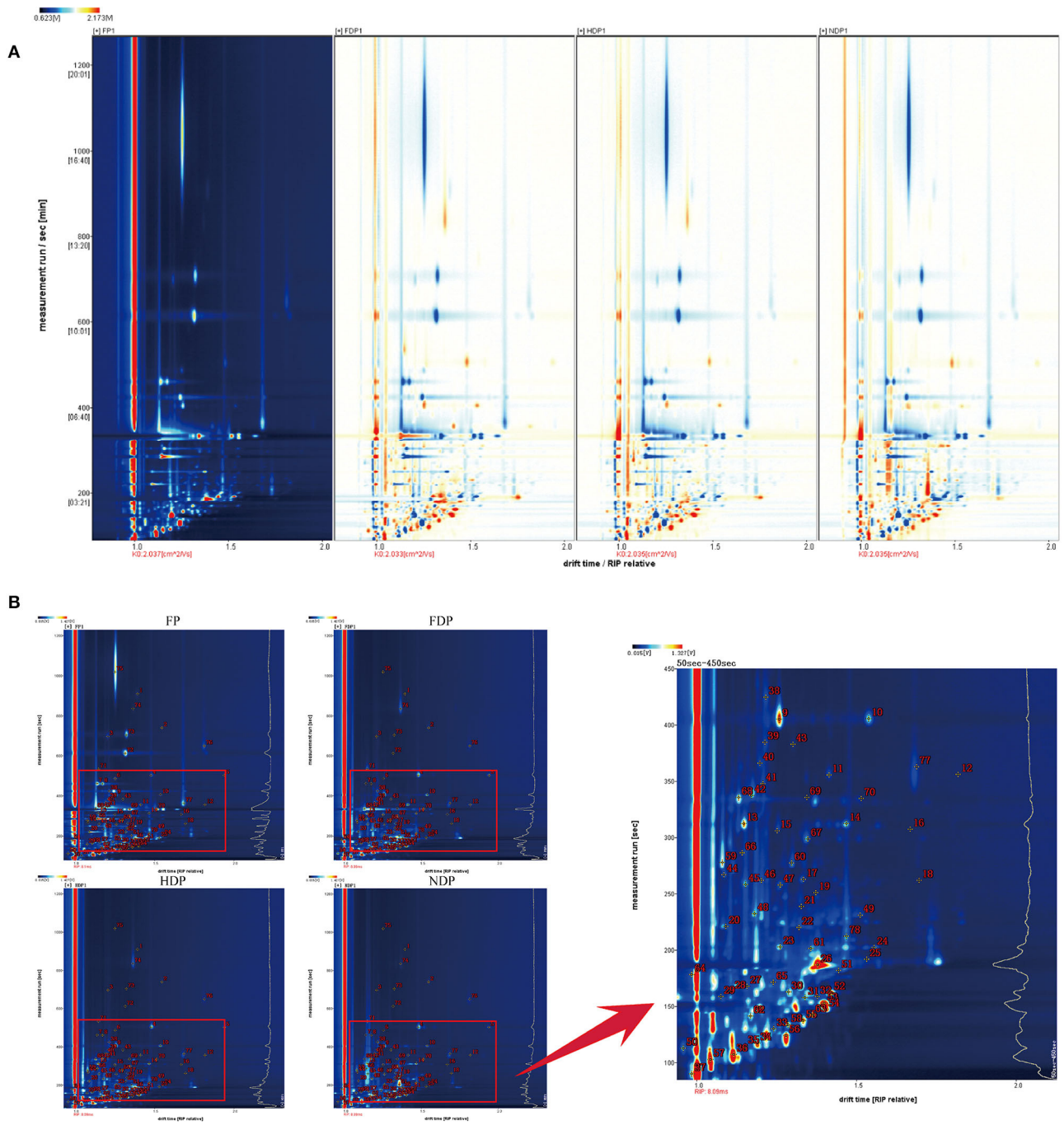

FIGURE 1 | The top view plots **(A)** and qualitative analysis spectra **(B)** of fresh and different dehydrated *Pugionium* samples.

oxidized by fats to generate special aromas, and 1-hexanol is a key volatile flavor compound that can impart a strong and pleasant aroma, accompanied by the fragrance of fruits and vegetables (14). While aldehydes are derived from amino acid metabolism or fatty acid oxidation (15), aldehydes have special flavors for almond, fruit, and grass, such as nonanal, benzaldehyde, and pentanal. It can be seen that each volatile substance has its unique flavor, which together leads to the difference in flavor and quality between fresh and three dehydrated *Pugionium* samples.

At present, HS/GC-IMS analysis is more advantageous at obtaining the overall fingerprint information. The fingerprinting technique is employed to further compare the volatile flavor compounds in each group of fresh and different dehydrated *Pugionium*. The redder/brighter the color of an individual cell,

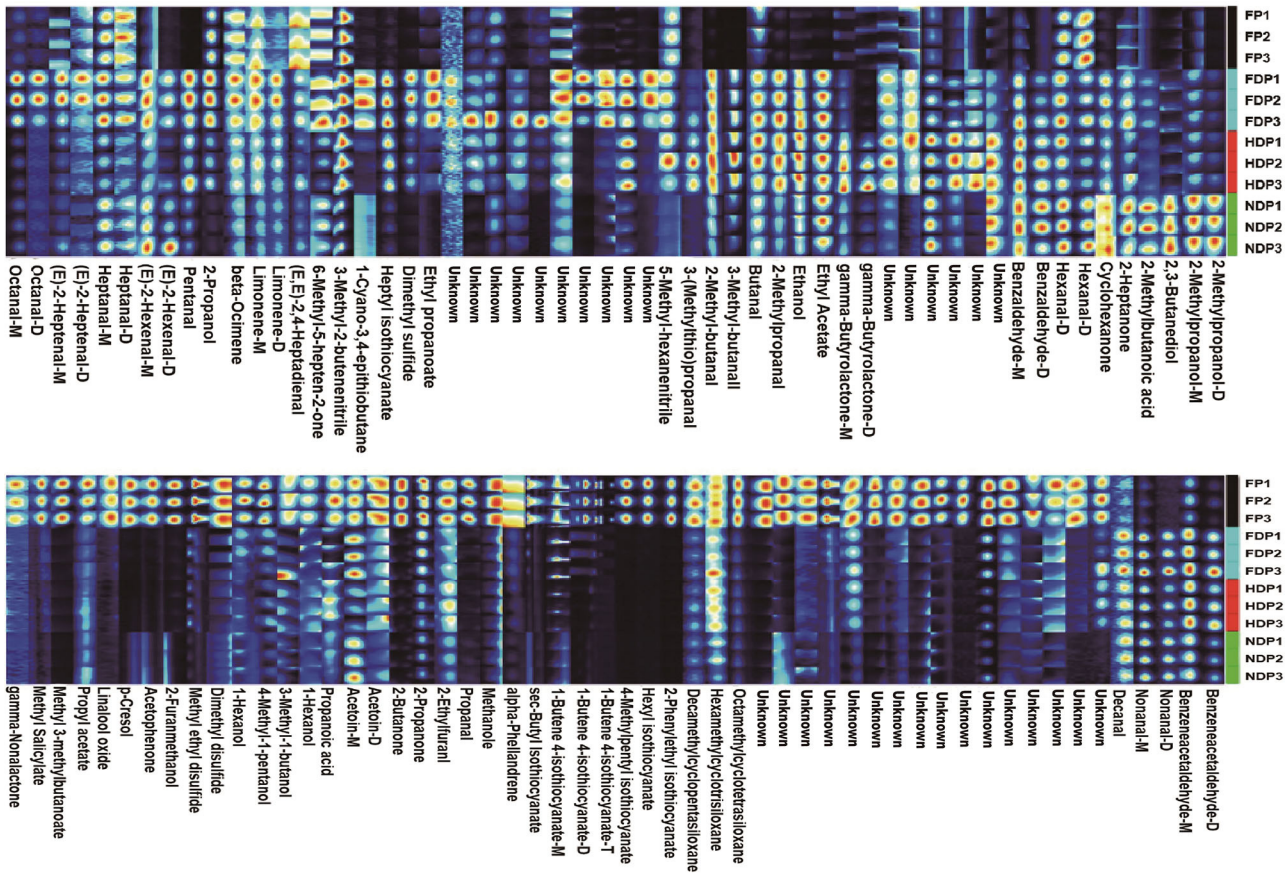

FIGURE 2 | Fingerprint of volatile flavor compounds of fresh and different dehydrated *Pugionium* samples.

the higher the content level, so it can compare the intensity of the spots to determine how the volatile flavor compounds changed (increase, decrease, disappear, or fluctuate) (16, 17), which can provide a more direct and revealing comparison, as well as the dynamic changes before and after dehydration of each substance.

In **Figure 2**, high levels of methyl 3-methylbutanonate, 1-butene-4-isothiocyanate, 4-methylpentyl-isothiocyanate, and other isothiocyanates, 2-butanone, propanal, acetophenone, dimethyl disulfide, and p-cresol were abundant in fresh *Pugionium*, underwent a drastic decrease in content levels from high to low after different dehydration treatments; for example, methyl 3-methylbutanoate and 2-butanone had the lowest contents in NDP, the lowest levels of 4-methylpentyl isothiocyanate and acetophenone were found in FDP, while propanal, dimethyl disulfide, and p-cresol appeared in HDP. Also, the pungent odors were perceivably reduced to a great extent, likely because they were subject to loss or dissipation when exposed to light, heat, or vacuum treatment. Besides, the substances, namely, benzeneacetaldehyde, nonanal, 2-propanol, pentanal, 6-methyl-5-heptene-2-one, heptyl-isothiocyanate, and 3-methyl-2-butenenitrile, were not found or were extremely low in FP, but they increased remarkably in FDP, so as benzaldehyde, 2-methyl-butanal, 3-methyl-butanal, 2-methylpropanal, ethanol, ethyl acetate, and gamma-butyrolactone were the highest in HDP. In addition, cyclohexanone, 2-methylbutanoic acid, 2,3-butanediol, and 2-methylpropanol were the highest content levels in NDP.

This finding demonstrates that different dehydration treatments have an obvious influence on the flavor substances of *Pugionium*. Under varying dehydration conditions, the signals of some compounds that are sensitive to temperature/pressure/enzyme and are easily decomposed/degradable tend to disappear or decrease, such as 1-butene-4-isothiocyanate, dimethyl disulfide, and benzeneacetaldehyde, while the intensity of some other signals increases, for example, 2-methyl-butanal, 2,3-butanediol, which may be caused by chemical reactions (Lipid degradation, Maillard reaction, and the metabolism of some macromolecules, e.g., amino acids and glucosinolates) (18). As a result, the products of these chemical reactions mostly contributed to the varied fragrance composition of the four *Pugionium* samples.

SPME/GC-MS Analysis

Due to the current limitation of the GC-IMS database in chemical identification, SPME/GC-MS was more advantageous for the identification of individual compounds (9). According to the

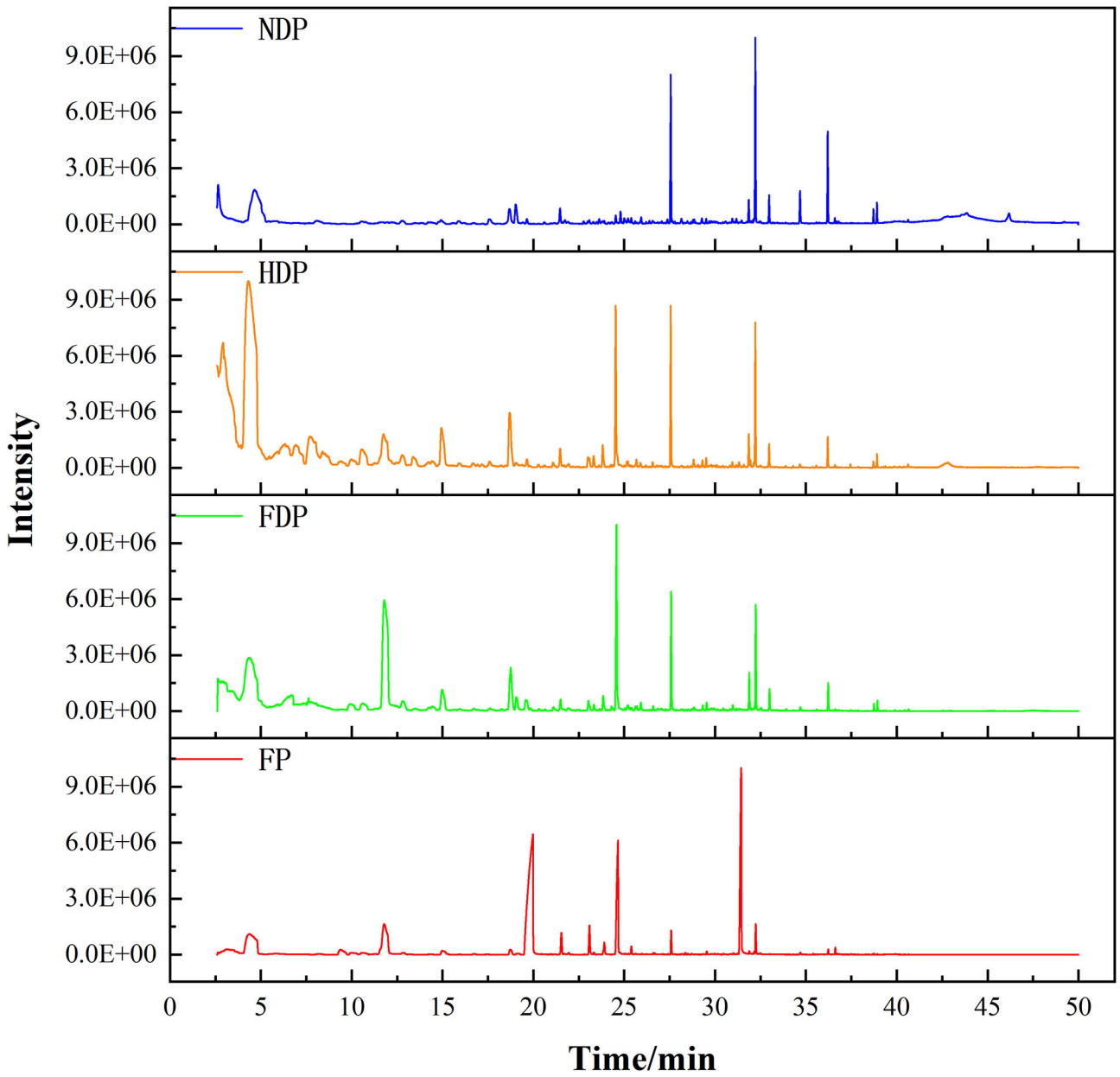

FIGURE 3 | The total ion chromatogram of fresh and different dehydrated *Pugionium* samples.

HS/GC-IMS total ion chromatogram of different samples of *Pugionium* (**Figure 3**), the peak time of volatiles has a small difference, but significant differences in the peak intensity, showing that dehydration causes the formation/transformation of distinct volatile compounds. In this study, by searching the NIST mass spectrometry database and selecting compounds with a similarity >80, 53 different volatile compounds were identified by SPME/GC-MS, mainly esters, aldehydes, alcohols, ketones, and so on. **Supplementary Table 2** shows the relative contents of volatile components of *Pugionium* treated with fresh and different dehydration methods using the peak area normalization method to calculate for relative quantitative analysis of each compound.

The results of SPME/GC-MS revealed that esters (37.16 ± 0.88 %), nitriles (23.83 ± 1.09 %), and sulfur compounds (22.55 ± 1.42 %) were the main volatile compounds in FP. After dehydration, the relative contents of esters had dropped to 16–20%, the sulfur compounds had decreased from 22.55 ± 1.42% in FP to FDP (9.78 ± 0.23%), HDP (5.75 ± 0.16%), and NDP (8.36 ± 0.17%), while aldehydes, ketones, and alcohols all increased significantly, aldehydes (2.35% in FP) rose to 19.95% in HDP, ketones (2.32% in FP) rose to

11.32% in FDP, and alcohols (4.35% in FP) rose to 25.18% in NDP.

Esters were found in FP (3), FDP (11), HDP (3), and NDP (19), including 7 kinds of isothiocyanates [such as sec-butyl isothiocyanate, 1-butene-4-isothiocyanate (M/D/T)], which emit a strong pungent odor (20), ethyl acetate, methyl nonanoate, 5,6,7,7a-tetrahydro-4,4,7a-trimethyl-2(4H)-benzofuranone, 2,2,4-trimethyl-1,3-pentanediol diisobutyrate, and hexanoic acid, 3,5,5-trimethyl-, nonyl ester. The nitriles (3-methyl-2-butenenitrile, 5-methyl-hexanenitrile, and benzenepropanenitrile) are degradation products of various glucosinolates, which are one of the causes for the pungent and spicy smell of fresh *Pugionium* and also the major flavor substance. Sulfur compounds (e.g., 1-cyano-3,4-epithiobutane and dimethyl disulfide) often have a lower olfactory threshold and are more prone to unpleasant odors. Alcohols, including 1-hexanol, ethanol, phenylethyl alcohol, 1-pentanol, 2-heptanol, and 2,3-butanediol, were the widely detected compounds. During the volatilization process, alcohols usually play the role of "dragging" other components to volatilize and "assisting" the flavor, mainly manifested as soft stimulation, slightly sweet and strong feeling, which can set off the ester aroma and make the aroma richer. Aldehydes, such as nonanal, benzeneacetaldehyde, benzaldehyde, and others, tend to have fresh notes of grass, citrus, fat, and some of the herbs.

That is, the key volatile compounds associated with the fresh *Pugionium* are esters, nitriles, and sulfur compounds, which provide a pungent smell; however, alcohols, aldehydes, and ketones are more related to the final dehydration products, which could explain why they had less pungent smells, they had more prominent herbaceous sweet flavors, and they are more acceptable than the fresh *Pugionium* by aromas.

Multivariate Statistical Analysis

For an in-depth comparison of the differences between the fresh and dehydrated *Pugionium* samples treated with different dehydration states, we chose PCA and clustering analysis for multivariate statistical analysis of the results obtained from HS/GC-IMS and SPME/GS-MS, respectively.

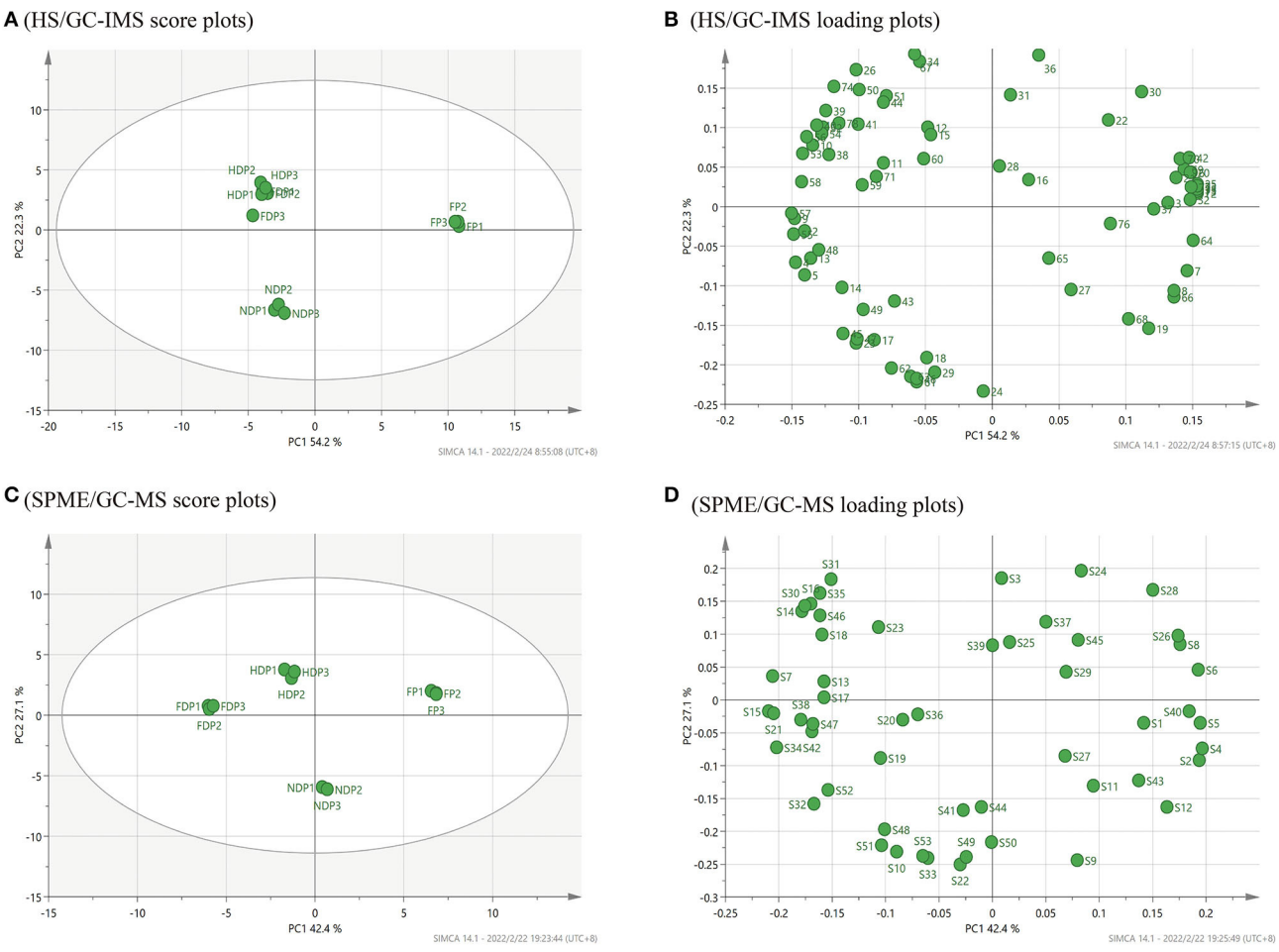

FIGURE 4 | PCA analysis of volatile flavor compounds of fresh and different dehydrated *Pugionium* samples by HS/GC-IMS and SPME/GC-MS, respectively. **(A,C)** are PCA score plots; **(B,D)** are PCA loading plots.

Principal Component Analysis

According to HS/GC-IMS, in **Figure 4A**, the cumulative variance contribution rate of the first PCA and the second principal component was 76.5 % (PC1 54.2 %, PC2 22.3 %), indicating that the core components were effectively retained during data processing through linear transformation and dimensionality reduction (21), the PCA model has a better effect. By either PC1 or PC2, the FP was clustered in the right middle side of the map central, the HDP and FDP were closer and clustered in the second quadrant, and the NDP was clustered in the third quadrant, all of which were far from the FP. These suggested that in terms of volatile flavor composition, the HDP was more similar to the FDP, the NDP had as many differences in flavor from the FP as it did from the FDP or HDP, and the three samples of dehydration both were of greater differences from the FP. Moreover, the PCA loading plots of **Figure 4B** revealed that 1-butanol, 2-butanone, dimethyl disulfide, methyl ethyl disulfide, 1-butene-4-isothiocyanate-D, linalool oxide, and alpha-phellandrene were mainly related to the FP. Heptanal-D, acetoin-M, 2-methylbutanoic acid, and 6-methyl-5-hepten-2-one were

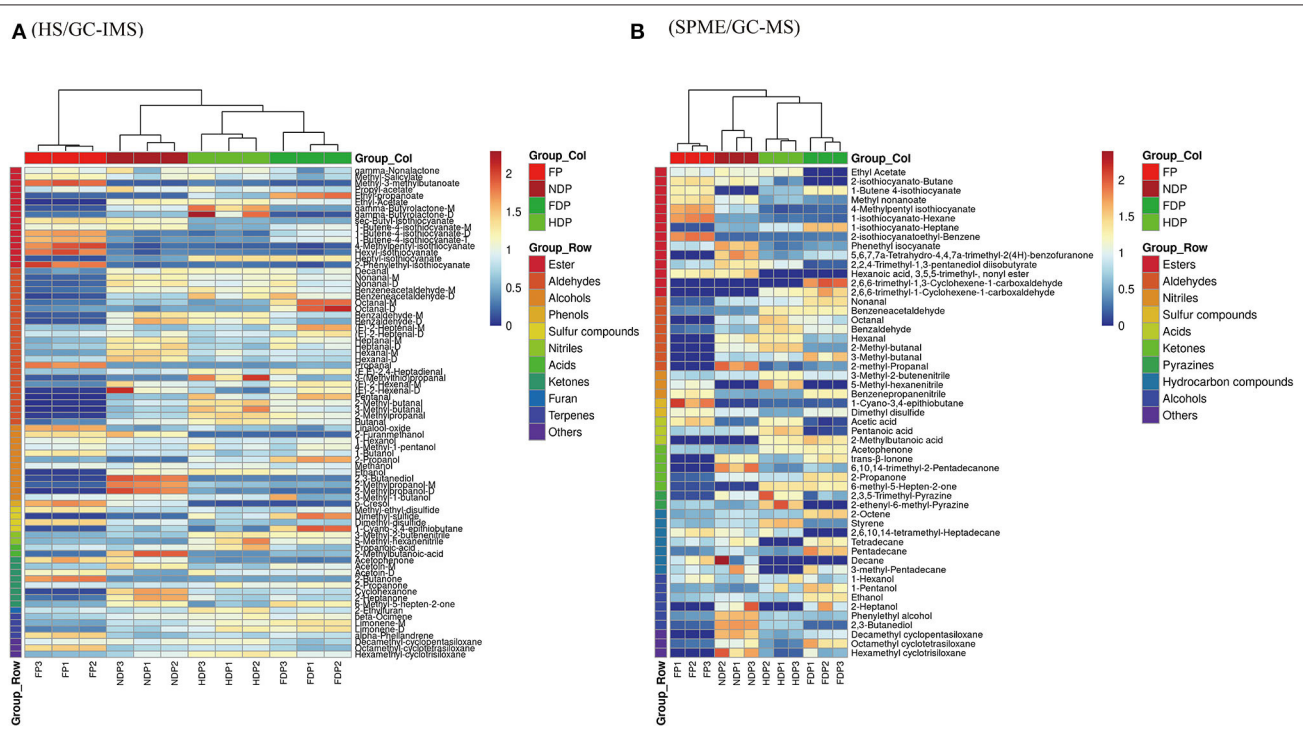

FIGURE 5 | Clustering analysis assesses the variance of volatile flavor compounds of fresh and different dehydrated *Pugionium* samples according to HS/GC-IMS **(A)** and SPME/GC-MS **(B)**.

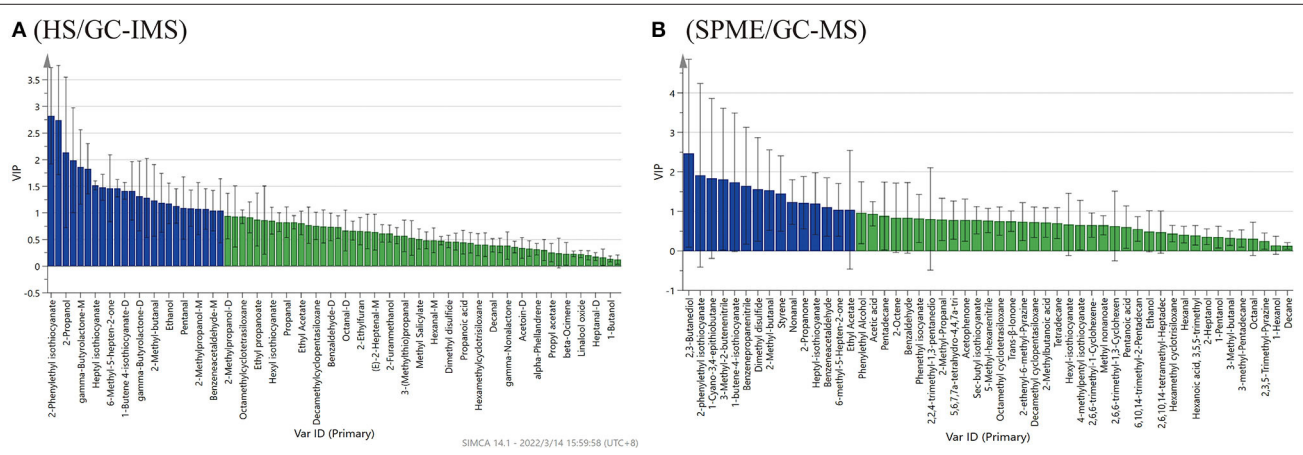

FIGURE 6 | PLS-DA analysis of VIP score plots of the volatile flavor compounds by HS/GC-IMS **(A)** and SPME/GC-MS **(B)**.

mainly related to NDP. Octanal (M and D), (E)-2-heptenal-M, gamma-butyrolactone-M, and 1-cyano-3,4-epithiobutane were mainly related to the HDP and the FDP.

Figure 4C shows the PCA score plots of volatile compounds identified by SPME/GC-MS. The combined variance contribution rate of the first principal component (PC1 42.4 %) and the second principal component (PC2 27.1 %) was 69.5%. In the distribution plot, with FP in the first quadrant, NDP in the fourth quadrant, and HDP and FDP in the second quadrant, the four samples were easily distinguished, suggesting significant differences between fresh and dehydrated *Pugionium* samples. **Figure 4D** shows that the PCA loading plots of hexyl-isothiocyanate, 2-phenylethyl isothiocyanate, 1-cyano-3,4-epithiobutane, and

TABLE 1 | The relative contents of ITCs (VIP > 1) in different *Pugionium* samples by both HS/GC-IMS and SPME/GC-MS.

No.	Name	CAS	VIP scores	The relative content %			
				FP	FDP	HDP	NDP
HS/GC-IMS							
75	2-phenylethyl-isothiocyanate	2257-09-2	2.82	24.30 ± 2.03	2.62 ± 0.72	3.69 ± 0.31	2.96 ± 0.92
68	1-butene-4-isothiocyanate-M	3386-97-8	1.99	6.64 ± 0.19	5.88 ± 0.41	3.26 ± 0.25	7.23 ± 0.17
74	Heptyl-isothiocyanate	4426-83-9	1.52	0.51 ± 0.05	4.54 ± 0.18	4.71 ± 0.24	1.52 ± 0.15
66	Sec-butyl-isothiocyanate	4426-79-3	1.48	6.10 ± 0.22	2.26 ± 0.08	2.39 ± 0.06	5.18 ± 0.34
70	1-butene-4-isothiocyanate-T	3386-97-8	1.46	5.22 ± 0.11	3.17 ± 0.19	1.42 ± 0.05	1.30 ± 0.30
69	1-butene-4-isothiocyanate-D	3386-97-8	1.41	5.00 ± 0.11	2.60 ± 0.34	0.90 ± 0.23	1.02 ± 0.11
72	4-methylpentyl-isothiocyanate	17608-07-0	1.09	3.63 ± 0.29	0.31 ± 0.10	0.40 ± 0.06	5.18 ± 0.13
SPME/GC-MS							
S8	2-phenylethyl-isothiocyanate	2257-09-2	1.92	15.61 ± 0.38	2.68 ± 0.10	2.26 ± 0.09	1.98 ± 0.06
S3	1-butene-4-isothiocyanate	3386-97-8	1.74	9.94 ± 0.22	9.73 ± 0.10	4.88 ± 0.04	0.38 ± 0.08
S7	Heptyl-isothiocyanate	4426-83-9	1.20	0.40 ± 0.03	4.54 ± 0.02	2.57 ± 0.03	1.62 ± 0.05

Ps: The No. 68/69/70 and S3 refer to the same volatile compounds, so do No. 75 and S8, No. 74 and S7.

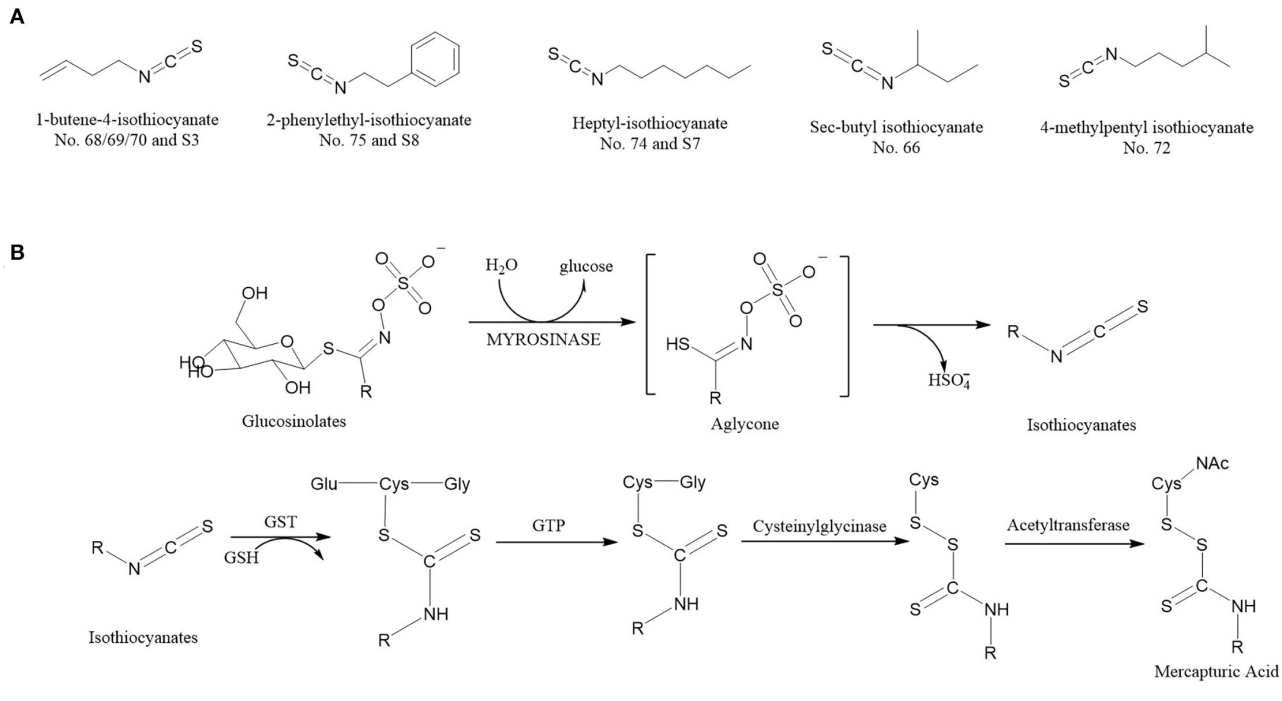

FIGURE 7 | The ITCs (VIP score > 1) structural formula **(A)** (The No. 68/69/70 and S3 refer to the same volatile compounds, so do No. 75 and S8, No. 74 and S7. Nos. 68, 69, 70, 74, and 75 come from **Supplementary Table 1**; S3, S7, and S8 from **Supplementary Table 2**). Reaction scheme **(B)** for the conversion of glucosinolates to isothiocyanates by myrosinases and isothiocyanates to mercapturic acids. GST, Glutathione S-transferase; GTP, G-glutamyl transpeptidase; GSH, glutathione.

2,6,10,14-tetramethyl-heptadecane were mainly associated with the FP. 3-methyl-pentadecane, phenylethyl alcohol, and 2,3-butanediol were mainly related to NDP. 1-isothiocyanato-heptane, 2,6,6-trimethyl-1,3-cyclohexene-1-carboxaldehyde, and octanal were mainly related to the FDP, and the 3-methyl-2-butenenitrile and styrene were mainly associated with HDP.

Comparing the two PCA score plots (**Figures 4A,C**), it can be noticed that HS/GC-IMS can only divide 4 *Pugionium* samples into 3 regions, and the distinction between HDP and FDP is not obvious. However, SPME/GC-MS can distribute FP/FDP/HDP/NDP in various locations, which means that SPME/GC-MS can better distinguish four *Pugionium* samples, and even achieve paired separation.

Clustering Analysis

The sensitivity of volatile compounds varies depending on the detection methods used, which may lead to some compounds being ignored. The clustering analysis was performed on the relationship between the fresh and three dehydrated *Pugionium* samples based on flavor volatile compounds by HS/GC-IMS and SPME/GC-MS results; the change in volatile compounds across different samples was compared, and the association between fresh and dehydration samples was also determined. The closer the branches of the two samples are, the closer the changing trend of the expression levels of volatile flavor substances in the two samples is.

The HS/GC-IMS heatmap (**Figure 5A**) changed considerably before and after dehydration, with changes such as sec-butyl-isothiocyanate, nonanal-M, 3-methyl-2-butenenitrile, 2-propoanone, and others congruent with the fingerprint's prior results. After clustering calculation, HDP showed the least similarity to FP, and NDP had the most consistency in the volatile contents of the dehydrated samples and fresh *Pugionium*, indicating that natural dehydration may maintain the volatile components effectively.

Clustering analysis was also performed on the SPME/GC-MS findings (**Figure 5B**). The relative contents of those volatile compounds that were present in low concentrations in FP changed significantly (e.g., 2-methyl-propanal and styrene) after treatment with different dehydration methods, with 2-methyl-propanal being the highest in NDP and styrene being the highest in HDP, indicating that different dehydration methods had a significant impact on the changes in volatile compound contents. FDP and FP have the least similarity, whereas NDP and FP have the most, which is consistent with the HS/GC-IMS finding.

Overall, the results obtained by clustering heatmaps are consistent with the previous PCA results and can be supplemented. That is, clustering analysis was able to classify four different *Pugionium* samples based on changes in the relative content of volatile components and showed a degree of similarity with fresh *Pugionium*, indicating that natural dehydration can better preserve the volatile components of fresh *Pugionium*.

Marker Volatile Flavor Compounds

The PLS-DA model analysis was performed to identify the contribution of the volatile chemical variables to differentiate, in discrimination analysis, variables with variable importance in the projection (VIP) values larger than 1, which generally suggests significance. The larger the VIP values, the more significant the factors in varying the samples are (22).

Based on the results of HS/GC-IMS, with the goodness-of-fit parameter R2X = 0.979, the model explanatory ability R2Y = 0.996, and the predictive ability Q2 = 0.972. **Figure 6A** showed 24 compounds with VIP scores >1 by HS/GC-IMS, including 2-phenylethyl isothiocyanate, 1-butene-4-isothiocyanate (M, D and T), heptyl-isothiocyanate, octanal-M, benzeneacetaldehyde, sec-butyl-isothiocyanate, ethanol, 2,3-butanediol, and 6-methyl-5-hepten-2-one. By the PLS-DA of SPME/GC-MS, the R2X was 0.989, the R2Y was 0.999, and the Q2 was 0.997. **Figure 6B** showed 15 compounds (VIP scores > 1), including ethyl acetate, 1-butene-4-isothiocyanate, heptyl-isothiocyanate, 2-phenylethyl-isothiocyanate, nonanal, benzeneacetaldehyde, 2-methyl-butanal, 3-methyl-2-butenenitrile, benzenepropanenitrile, 1-cyano-3,4-epithiobutane, dimethyl disulfide, 2-propanone, 6-methyl-5-hepten-2-one, styrene, and 2,3-butanediol. These compounds could be used as characteristics to discriminate flavor compositions of the four *Pugionium* samples. Among the compounds mentioned above, 10 volatile compounds were co-owned to both by HS/GC-IMS and SPME/GC-MS, including 3 esters (i.e., sec-butyl isothiocyanate, 1-butene-4-isothiocyanate, and 2-phenylethyl isothiocyanate), 3 aldehydes (i.e., nonanal, benzeneacetaldehyde, and 2-methyl-butanal), 2 ketones (i.e., 2-propanone and 6-methyl-5-hepten-2-one), 1 alcohol (i.e., 2,3-butanediol), and 1 nitrile (i.e., 3-methyl-2-butenenitrile).

Among these characteristic compounds, isothiocyanate (ITC) is a kind of substance with definite biological function. ITCs have excellent antioxidant capabilities, anti-inflammatory capabilities (23), and anti-cancer performance (24), so it has attracted widespread attention. **Table 1**, **Figure 7A** showed the ITCs having VIP scores > 1 and their relative contents in different *Pugionium* samples before and after dehydration processing.

According to relevant literature, different types of ITCs can inhibit the development of cancers to varying degrees, such as skin cancer, stomach cancer, bowel cancer, esophagus cancer, and breast cancer (19, 25). ITCs have been discovered to aid enzymes in inhibiting the formation of carcinogens, containing cancer cells till they die down and preventing aberrant cell proliferation in the pre-cancer stage (26, 27). Meanwhile, some ITCs have been shown to prevent the growth of a wide range of bacteria, including antibiotic-resistant strains (28), and are effective at eradicating *Helicobacter pylori*.

At present, nearly 100 types of ITCs have been found in natural plants, among which allyl isothiocyanate, benzyl isothiocyanate, phenyl isothiocyanate, phenyl ethyl isothiocyanate, and sulforaphane (29) types can be obtained in daily diet. The predominant types of ITCs in different plants are different, for example, ITCs are found abundant in *Cruciferous* vegetables (20), *Broccoli* and *Broccoli bud* mainly contain sulforaphane

(30), *Celery* mainly contains phenyl isothiocyanate, *Chinese cabbage* mainly contains 3-butenyl, 4-pentenyl isothiocyanates (31, 32).

The ITCs have a highly electrophilic central carbon atom in the N = C = S structure, which generates reactive oxygen species upon hydrolysis and subsequently causes oxidative DNA damage (33). Under different processing conditions, each glucosinolate can be decomposed into different ITCs with the participation of enzymes (34–36), and these ITCs are responsible for almost all biological activities of the compounds. **Figure 7B** shows the reaction scheme that ITCs are produced *via* glucosinolate hydrolysis initiated by the myrosinase family of enzymes. The process begins with myrosinase-catalyzed hydrolysis of the thioglucoside linkage, formatting H_2O, glucose, and an unstable aglycone, which continues to react to form ITCs (37). Once generated, ITCs are absorbed and metabolized by sequential enzymatic reactions and conjugated to glutathione by glutathione S-transferase, then metabolized sequentially by g-glutamyl transpeptidase, cysteinyl glycinase, and acetyltransferase ultimately to mercapturic acids (20, 38).

CONCLUSION

In this study, two approaches of HS/GC-IMS and SPME/GC-MS were performed to analyze the volatile flavor compounds of fresh and dehydrated *Pugionium cornutum* (L.) Gaertn under different dehydration treatments (FDP/HDP/NDP). In total, 78 volatile compounds by HS/GC-IMS were identified, and 53 volatile compounds by SPME/GC-MS were identified. The dehydration methods exert a significant influence on the relative content of volatile flavor compounds: following dehydration, the majority of esters decreased, while aldehydes and alcohols increased, which may explain why the pungent smell of the dehydrated products is noticeably reduced, and the dehydrated *Pugionium* samples smell soft and slightly sweet.

In addition, PCA and clustering analysis from both HS/GC-IMS and SPME/GC-MS also demonstrated that fresh and three dehydrated *Pugionium* samples could be clearly divided, and the similarity between NDP and FP was higher than the other two dehydrated samples, indicating that natural dehydration can better preserve the volatile components of *Pugionium*. Based on PLS-DA analysis of the volatile compounds in these samples by HS/GC-IMS and SPME/GC-MS, 24 and 15 substances were implicated to have a potential contribution to the aroma of *Pugionium*, respectively. In addition, 5 kinds of isothiocyanates were selected as characteristic volatile components, which have excellent antioxidant, anti-inflammatory, and anti-cancer capabilities.

Analysis of volatile compounds may be useful for monitoring the quality of fresh and dehydrated *Pugionium* and guiding the cooking methods and processing technologies, and more study is required to discover if the various volatile flavor compounds have biological or physiological effects, thereby providing theoretical support for the development of the edible and medical value.

DATA AVAILABILITY STATEMENT

The original contributions presented in the study are included in the article/**Supplementary Materials**, further inquiries can be directed to the corresponding authors.

AUTHOR CONTRIBUTIONS

HL: investigation, formal analysis, and writing—original draft. QW: investigation and visualization. QL: drawing and software. LJ: data curation and writing—review and editing. BC: methodology and software. CL: writing—review and editing and funding acquisition. JX: editing and supervision. YS: supervision and validation. All authors read and approved the manuscript.

FUNDING

This work was supported by funding from the Key Research and Development Program of Shaanxi Province (2019TSLNY03-02) and the Yulin Science and Technology Planning Project (2018-2-21).

ACKNOWLEDGMENTS

Many thank to the *Amygdalus pedunculata* Pall Engineering Technology Research Center of the State Forestry and Grassland Administration, the Key Laboratory of Yulin Desert Plant Resources, the Northwest University, and the Yan'an University for providing experimental conditions. We also thank Andrew for suggestions on English writing.

SUPPLEMENTARY MATERIAL

The Supplementary Material for this article can be found online at: https://www.frontiersin.org/articles/10.3389/fnut.2022.884086/full#supplementary-material

REFERENCES

1. Wang Q, Abbott RJ, Yu Q-S, Lin K, Liu J-Q. Pleistocene climate change and the origin of two desert plant species, *Pugionium cornutum* and *Pugioniumdolabratum* (*Brassicaceae*), in northwest China. *New Phytol.* (2013) 199:277–87. doi: 10.1111/nph.12241
2. Li H-Y, Li C, Zhang C-X, Chen B, Hui L, Shen Y-H. Compositional and gastrointestinal prokinetic studies of *Pugionium (L.). Food Chem.* (2015) 186:285–91. doi: 10.1016/j.foodchem.2015.03.146
3. Wang S, Chen H, Sun B. Recent progress in food flavor analysis using gas chromatography–ion mobility spectrometry (GC–IMS). *Food Chem.* (2020) 315:126158. doi: 10.1016/j.foodchem.2019.126158
4. He W, Ren F, Wang Y-Q, Gao X, Wang X-X, Dai X, et al. Application of GC-IMS in Detection of Food Flavor Substances. *IOP Conf Ser Earth Environ Sci.* (2020) 545:012030. doi: 10.1088/1755-1315/545/1/012030
5. Haley LV, Romeskie JM, GC-IMS. A technology for many applications. *Proc SPIE Int Soc Opt Eng.* (1998) 3575:375–83.
6. Zeng X-F, Liu J-L, Dong H, Bai W-D, Yu L-M, Li X-M. Variations of volatile flavor compounds in cordyceps militaris chicken soup after enzymolysis pretreatment by SPME combined with GC-MS, GC×GC-TOF MS and GC-IMS. *Int J Food Sci Tech.* (2020) 55:509–16. doi: 10.1111/ijfs.14294

7. Zhu J-C, Wang L-Y, Xiao Z-B, Niu Y-W. Characterization of the key aroma compounds in mulberry fruits by application of gas chromatography-olfactometry (GC-O), odor activity value (OAV), gas chromatography-mass spectrometry (GC-MS) and flame photometric detection (FPD). *Food Chem.* (2018) 245:775–85. doi: 10.1016/j.foodchem.2017.11.112
8. Jia X, Wang L-F, Zheng C, Yang Y-N, Wang X-Y, Hui J, et al. Key Odorant differences in fragrant *Brassica napus* and *Brassica juncea* oils revealed by gas chromatography–olfactometry, odor activity values, and aroma recombination. *J Agric Food Chem.* (2020) 68:14950–60. doi: 10.1021/acs.jafc.0c05944
9. Chen Y, Li P, Liao L-Y, Qin Y-Y, Jiang L-W, Liu Y. Characteristic fingerprints and volatile flavor compound variations in liuyang douchi during fermentation via HS-GC-IMS and HS-SPME-GC-MS. *Food Chem.* (2021) 361:130055. doi: 10.1016/j.foodchem.2021.130055
10. Yang Y, Wang B, Fu Y, Shi Y-G, Chen F-L, Guan H-N, et al. HS-GC-IMS with PCA to analyze volatile flavor compounds across different production stages of fermented soybean whey tofu. *Food Chem.* (2020) 346:128880. doi: 10.1016/j.foodchem.2020.128880
11. Guo Y, Chen D, Dong Y-F, Ju H-P, Wu C, Lin S-Y. Characteristic volatiles fingerprints and changes of volatile compounds in fresh and dried Tricholoma matsutake Singer by HS-GC-IMS and HS-SPME-GC-MS. *J Chromatogr B.* (2018) 1099:46–55. doi: 10.1016/j.jchromb.2018.09.011
12. Taylor C, Lough F, Stanforth SP, Schwalbe EC, Fowlis IA, Dean JR. Analysis of Listeria using exogenous volatile organic compound metabolites and their detection by static headspace-multi-capillary column-gas chromatography-ion mobility spectrometry (SHS-MCC-GC-IMS). *Anal Bioanal Chem.* (2017) 409:4247–56. doi: 10.1007/s00216-017-0375-x
13. Li M-Q, Yang R-W, Zhang H, Wang S-L, Chen D, Lin S-Y. Development of a flavor fingerprint by HS-GC-IMS with PCA for volatile compounds of tricholoma matsutake singer. *Food Chem.* (2019) 290:32–9. doi: 10.1016/j.foodchem.2019.03.124
14. Chung HY. Volatile components in fermented soybean (glycine max) curds. *J Agric Food Chem.* (1999) 47:2690–6. doi: 10.1021/jf981166a
15. Otero L, Horrillo MC, García M, Sayago I, Aleixandre M, Ma JF, et al. Detection of Iberian ham aroma by a semiconductor multisensorial system. *Meat Sci.* (2003) 65:1175–85. doi: 10.1016/S0309-1740(02)00347-9
16. Liu D-Y, Bai L, Feng X, Chen Y-P, Zhang D-N, Yao W-S, et al. Characterization of Jinhua ham aroma profiles in specific to aging time by gas chromatography-ion mobility spectrometry (GC-IMS). *Meat Sci.* (2020) 168:108178. doi: 10.1016/j.meatsci.2020.108178
17. Song J-X, Shao Y, Yan Y-M, Li X-H, Peng J, Guo L. Characterization of volatile profiles of three colored quinoas based on GC-IMS and PCA. *LWT-Food Sci Technol.* (2021) 146:111292. doi: 10.1016/j.lwt.2021.111292
18. Newton AE, Fairbanks AJ, Golding M, Andrewes P, Gerrard JA. The role of the Maillard reaction in the formation of flavour compounds in dairy products - not only a deleterious reaction but also a rich source of flavour compounds. *Food Funct.* (2012) 3:1231–41. doi: 10.1039/c2fo30089c
19. Hecht SS. Chemoprevention by isothiocyanates. *J Cell Biochem.* (1995) 59:195–209. doi: 10.1002/jcb.240590825
20. Cedrowski J, Dabrowa K, Przybylski P, Krogul-Sobczak A, Litwinienko G. Antioxidant activity of two edible isothiocyanates: sulforaphane and erucin is due to their thermal decomposition to sulfenic acids and methylsulfinyl radicals. *Food Chem.* (2021) 353:129213. doi: 10.1016/j.foodchem.2021.129213
21. Rodriguez-Campos J, Escalona-Buendía HB, Orozco-Avila I, Lugo-Cervantes E. Jaramillo-Flores ME. Dynamics of volatile and non-volatile compounds in cocoa (Theobroma cacao L) during fermentation and drying processes using principal components analysis. *Food Res Int.* (2011) 44:250–8. doi: 10.1016/j.foodres.2010.10.028
22. Juan L, Xu Y-X, Du W-B, Jin L-X, Ren P-F, Ren F, et al. Comparative analysis of aroma compounds in Chinese traditional dry-rendered fat by HS/GC-IMS, SPME/GC-MS, and SPME/GC-O. *J Food Compos Anal.* (2022) 107:104378. doi: 10.1016/j.jfca.2021.104378
23. Lohning A, Kidachi Y, Kamiie K, Sasaki K, Ryoyama K, Yamaguchi H. 6-(methylsulfinyl) hexyl isothiocyanate (6-MITC) from Wasabia japonica alleviates inflammatory bowel disease (IBD) by potential inhibition of glycogen synthase kinase 3 beta (GSK-3β). *Eur J Med Chem.* (2021) 216:113250. doi: 10.1016/j.ejmech.2021.113250
24. Dinh TN, Parat MO, Ong YS, Khaw KY. Anticancer activities of dietary benzyl isothiocyanate: A comprehensive review. *Pharmacol Res.* (2021) 169:105666. doi: 10.1016/j.phrs.2021.105666
25. Fahey JW, Zalcmann AT, Talalay P. The chemical diversity and distribution of glucosinolates and isothiocyanates among plants. *Phytochemistry.* (2001) 56:5–51. doi: 10.1016/S0031-9422(00)00316-2
26. Li T, Zhang YS. Dietary isothiocyanates inhibit the growth of human bladder carcinoma cells. *J Nutr.* (2004) 134:2004–10. doi: 10.1093/jn/134.8.2004
27. Lenzi M, Fimognari C, Hrelia P. Sulforaphane as a promising molecule for fighting cancer. *Adv Nutr Cancer.* (2014) 159:207–23. doi: 10.1007/978-3-642-38007-5_12
28. Fahey JW, Haristoy X, Dolan PM, Kensler TW, Scholtus I, Stephenson KK, et al. Sulforaphane inhibits extracellular, intracellular, and antibiotic-resistant strains of Helicobacter pylori and prevents benzo[a]pyrene-induced stomach tumors. *Proc Natl Acad Sci USA.* (2002) 99:7610–5. doi: 10.1073/pnas.112203099
29. Gianni ED, Fimognari C. Anticancer mechanism of sulfur-containing compounds. *Enzymes.* (2015) 37:167–92. doi: 10.1016/bs.enz.2015.05.003
30. Hafezian SM, Azizi SN, Biparva P, Bekhradnia A. High-efficiency purification of sulforaphane from the broccoli extract by nanostructured SBA-15 silica using solid-phase extraction method. *J Chromatogr B.* (2019) 1108:1–10. doi: 10.1016/j.jchromb.2019.01.007
31. Daxenbichler ME, Vanetten CH, Williams PH. Glucosinolates and derived products in cruciferous vegetables. analysis of 14 varieties of Chinese cabbage. *J Agric Food Chem.* (1979) 27:34–7. doi: 10.1021/jf60221a023
32. Zhao D-Y, Tang J, Ding X-L. Correlation between flavour compounds and sensory properties of potherb mustard (brassica Juncea, coss) pickle. *Food Sci Technol Int.* (2007) 40:439–47. doi: 10.1016/j.lwt.2005.12.002
33. Murata M, Yamashita N, Inoue S, Kawanishi S. Mechanism of oxidative DNA damage induced by carcinogenic allyl isothiocyanate. *Free Radical Biol Med.* (2000) 28:797–805. doi: 10.1016/S0891-5849(00)00168-4
34. Wolf MA, Claudio PP. Benzyl isothiocyanate inhibits HNSCC cell migration and invasion, and sensitizes HNSCC cells to cisplatin. *Nutr Cancer.* (2014) 66:285–94. doi: 10.1080/01635581.2014.868912
35. Das BN, Kim Y-W, Keum Y-S. Mechanisms of Nrf2/Keap1-dependent phase ii cytoprotective and detoxifying gene expression and potential cellular targets of chemopreventive isothiocyanates. *Oxidative Med Cell Longev.* (2013) 2013:839409. doi: 10.1155/2013/839409
36. Vanduchova A, Anzenbacher P, Anzenbacherova E. Isothiocyanate from broccoli, sulforaphane, and its properties. *J Med Food.* (2019) 22:121–6. doi: 10.1089/jmf.2018.0024
37. Liou CS, Sirk SJ, Diaz CAC, Klein AP, Fischer CR, Higginbottom SK, et al. A metabolic pathway for activation of dietary glucosinolates by a human gut symbiont. *Cell.* (2020) 180:717–28. doi: 10.1016/j.cell.2020.01.023
38. Wu X, Zhou Q-H, Xu K. Are isothiocyanates potential anti-cancer drugs? *Acta Pharmacol Sin.* (2009) 30:501–12. doi: 10.1038/aps.2009.50

Conflict of Interest: The authors declare that the research was conducted in the absence of any commercial or financial relationships that could be construed as a potential conflict of interest.

Publisher's Note: All claims expressed in this article are solely those of the authors and do not necessarily represent those of their affiliated organizations, or those of the publisher, the editors and the reviewers. Any product that may be evaluated in this article, or claim that may be made by its manufacturer, is not guaranteed or endorsed by the publisher.

frontiers | Frontiers in Nutrition

ORIGINAL RESEARCH
published: 16 May 2022
doi: 10.3389/fnut.2022.881865

Effects of the Baking Process on the Chemical Composition, Sensory Quality, and Bioactivity of *Tieguanyin* Oolong Tea

Ying Gao[1], Qing-Qing Cao[1], Yu-Hong Chen[1], Daniel Granato[2], Jie-Qiong Wang[1], Jun-Feng Yin[1], Xue-Bo Zhang[3], Fang Wang[1], Jian-Xin Chen[1] and Yong-Quan Xu[1]**

[1] Tea Research Institute, Chinese Academy of Agricultural Sciences, National Engineering Research Center for Tea Processing, Key Laboratory of Tea Biology and Resources Utilization, Hangzhou, China, [2] Department of Biological Sciences, Faculty of Science and Engineering, University of Limerick, Limerick, Ireland, [3] National Tea Quality Supervision and Inspection Center, Fujian, China

OPEN ACCESS

Edited by:
Jinkai Zheng,
Institute of Food Science and Technology (CAAS), China

Reviewed by:
Sean F. O'Keefe,
Virginia Tech, United States
Lijun Sun,
Northwest A&F University, China

***Correspondence:**
Yong-Quan Xu
yqx33@126.com
Jun-Feng Yin
yinjf@tricaas.com

Specialty section:
This article was submitted to Food Chemistry, a section of the journal Frontiers in Nutrition

Received: *23 February 2022*
Accepted: *06 April 2022*
Published: *16 May 2022*

Citation:
Gao Y, Cao Q-Q, Chen Y-H, Granato D, Wang J-Q, Yin J-F, Zhang X-B, Wang F, Chen J-X and Xu Y-Q (2022) Effects of the Baking Process on the Chemical Composition, Sensory Quality, and Bioactivity of Tieguanyin Oolong Tea. Front. Nutr. 9:881865. doi: 10.3389/fnut.2022.881865

Tieguanyin oolong tea (TOT), a semi-oxidized tea originating from Anxi county in China, is categorized into jade TOT, medium-baked TOT, and deep-baked TOT, based on different baking processes. To study the effects of baking, chemical analysis, sensory evaluation, and bioactivity assessments of the three TOTs were conducted. The results indicated that the baking process promoted the formation of colored macromolecules (e.g., theabrownins), which affected the color of tea infusion. Free amino acids underwent the Maillard reaction and generated specific Maillard reaction products, such as 5-hydroxymethylfurfural and furfural, which modified the taste and aroma. Floral and fresh volatiles were remarkably reduced, while multiple new volatiles were produced, forming a typically baked aroma. The antioxidant activity and antibacterial activity were reduced after baking, which might be associated with the decrease of monomeric catechins. These results provide a scientific basis for understanding the changes caused by the baking process.

Keywords: oolong tea, baking process, free radical scavenging activity, anti-advanced glycation end products, antibacterial, sensory properties, catechins

INTRODUCTION

Tieguanyin tea (TOT) is a semi-oxidized oolong tea from Anxi county, Fujian province, China. It is popular in south China and among Chinese expatriates in Southeast Asia. Jade TOT, medium-baked TOT, and deep-baked TOT are three significant types of TOTs. The jade TOT is produced by harvesting fresh tea leaves, withering, bruising, partial oxidation, fixing, shaping, and drying (1). The medium-baked TOT is produced by baking the jade TOT, and the deep-baked TOT is produced by baking the medium-baked TOT once more. The first baking is usually set at about 105°C for 3–8 h, and the second baking is set at about 115°C for 2–6 h. The three TOTs have distinguishing flavor

characteristics and different target customers. The jade TOT is green, smells floral, tastes brisk and is preferred by females and youngsters (2). The deep-baked TOT is the favorite for the locals in Anxi county and is the most traditional and expensive TOT. Compared with the jade version, the deep-baked TOT color is darker, the aroma and the taste are more complex. The deep-baked TOT looks brownish, has a typical roast aroma, tastes mellow and thick with a strong sweet aftertaste. The sensory property of the medium-baked TOT falls in between the above two TOTs. Many customers feel that the flavor of medium-baked TOT is mediocre, not as distinctive as the other two TOTs. Therefore, medium-baked TOT is the least popular one among the three TOTs.

The flavor is caused by a specific combination of taste and aroma compounds. As a semi-oxidized tea, TOT not only contains flavor components originally from fresh tea leaves, but also flavor components generated during processes, especially the partial oxidation process. Plenty of them is oxidized intermediates, which may further convert to other substances under heat treatment or long-term storage (3), leading to the flavor alteration of TOT. Catechins are one of the flavor components which are remarkably changed during oolong tea processing. Catechins, featuring secondary metabolites in tea, are vital contributors to tea infusions' bitter and astringent taste. However, they are chemically active, and part of them may undergo oxidation and polymerization to form new flavor molecules like theaflavins (TFs) and theasinensins during oolong tea processing (4). These intermediates can continue to form complex molecules under certain conditions (5). As catechins and their derivatives possess different sensory properties, the changes in these chemicals affect the sensory profile of the tea. Wang et al. found that by baking green tea, the composition and content of catechins were altered, resulting in a less astringent taste (6).

It is worth noting that many flavor compounds in tea are also bioactive compounds, suggesting that the alteration of bioactivity may occur along with the flavor alteration of tea. For example, catechins, mentioned above as major taste components, are the main bioactive components for the antioxidant and antibacterial activity of unfermented and semi-fermented tea (7). Lv et al. demonstrated that the content and composition of catechins in green teas made with different enzyme-inactivating processing technologies were varied, and the chemical composition was correlated to the sensory property and the antioxidant activity of green teas (8). Wang et al. proved that the baking process modified the sensory quality of Wuyi rock tea, as well as decreased the total phenolic content and free radical scavenging activity (9).

The baking process to produce medium-baked and deep-baked TOTs is conducted in a heated environment where the temperature exceeds over 100°C. Under this condition, not only catechins, but also other vulnerable components tend to transform into more stable products. To find out how baking dramatically converts the flavor and whether baking modifies the bioactivity, the differences among jade TOT, medium-baked TOT, and deep-baked TOT on the chemical composition, sensory quality, free radical scavenging activity, anti-advanced glycation end products (AGEs) activity, and antibacterial potential were investigated.

MATERIALS AND METHODS

Tea Samples

The jade TOT (BT0), medium-baked TOT (BT1), and deep-baked TOT (BT2) samples were provided by Chanxinyuan (Fujian) Tea Industry Co., Ltd. (Fujian, China). BT0 was baked at 107°C for 210 min after 12-day storage to produce BT1 and then baked at 115°C for 150 min after 22-day storage to produce BT2.

Preparation of Infusions

Each tea sample was ground and filtered through a 60 Tyler mesh sieve. The tea powder was brewed with distilled water (3:500 w/v) at 100°C for 40 min, cooled to room temperature, and centrifuged at 8,000 *g* for 10 min to obtain the supernatant for the analysis of non-volatile chemical composition. Part of the supernatant was vacuum dried to prepare the tea extracts to assess antibacterial activity. The detailed parameters of vacuum drying were frozen at −30°C for 3 h and freeze-dried for 36 h (0–33 h increasing to 25°C and kept at 25°C for 3 h). The vacuum level was less than 50 Pa.

Sensory Evaluation and Instrumental Color

Based on the national standard GB/T 23776-2018 (10), the color, aroma, and taste of the three tea samples were evaluated by a professional sensory evaluation team consisting of seven qualified panelists, with ages ranging from 25 to 50 years old, three males and four females. The intensities of aroma and taste attributes were scored. Score 0–2 mean "extremely weak," 2–4 mean "weak," 4–6 mean "neutral," 6–8 mean "strong," and 8–10 mean "extremely strong." Each evaluation was replicated three times on different days with a randomized order of samples for each test to assure reproducibility in the sensory analysis.

The color analysis of tea infusions was measured by a spectrophotometer (Konica Minolta, CM-3500d) by recording the CIE $L^*a^*b^*$ color space parameters.

To determine which part of the tea infusion contributed to the differential colors among samples, Vivaspin 20 ultrafiltration units (Product Nos. 28932358, 28932360, and 28932362, Cytiva, Marlborough, MA, United States) were used. Each tea infusion was filtered through membranes with a 3/10/50 kDa molecular weight cut-off, accordingly, *via* centrifuging at 4,000 *g* for 40 min at 37°C.

Determination of Non-volatile Chemical Composition

The total phenolic content, free amino acids, soluble proteins, soluble sugars, soluble polysaccharides, flavones, TFs, thearubigins (TRs), and theabrownins (TBs) were measured according to previously published methods (11). In brief, the contents of total polyphenols and free amino

acids were determined based on the national standard GB/T 8313-2008 and GB/T 8314-2013, respectively (11). The content of soluble proteins was determined using a commercial protein assay kit (Bradford Protein Assay Kit, Product No. P0006, Beyotime Biotechnology, Haimen, China). The content of flavones was determined according to the following procedures. A 0.5 mL sample solution was added to 10 mL 1% aluminum trichloride, mixed, stayed at room temperature for 10 min, and read the absorbance at 420 nm. The contents of TFs, TRs, and TBs were determined by Robert's method (12). The contents of eight catechins, gallic acid, and caffeine were determined using an HPLC method (13).

The content of soluble sugars was determined using the anthrone-sulfuric acid method. One milliliter sample solution was added to 4 mL anthrone-sulfuric acid (2 mg/mL), mixed, water-bathed at 100°C for 10 min, cooled to room temperature, and read the absorbance at 620 nm. The determination of soluble polysaccharides was the same as that of soluble sugars but with different pretreatment. The sample solution was added to 95% ethanol (1:5 v/v), stored at 4°C overnight, centrifuged at 8,500 *g* for 10 min to get the polysaccharide precipitation, and re-dissolve it with distilled water to prepare the solution for the anthrone-sulfuric acid assay. The contents of free amino acid components were determined using an amino acid analyzer (Hitachi 835-50, Tokyo, Japan) with a former established method (14).

The untargeted analysis was carried out using a previously established UPLC-QE-Orbitrap-MS method (11). The separation was performed on an ACQUITY UPLC HSS T3 column (1.8 μm, 2.1 mm × 100 mm, Waters, Milford, MA, United States) using a Dionex Ultimate 3000 RS system (Thermo Fisher). A 0.1% formic acid in water and acetonitrile was used as mobile phases A and B. The gradient changes of mobile phases were 0–1 min, 5% B; 1–2 min, 5–10% B; 2–6 min, 10–35% B; 6–8.5 min, 35–100% B; 8.5–9.5 min, 100% B; 9.5–10 min, 100–5% B; and 10–12 min, 5% B. The total flow rate was 0.3 mL/min. The column temperature was 40°C. The MS analysis was conducted using the QE-Orbitrap mass spectrometer (Thermo Scientific, United States) with electrospray ionization (ESI), operating in the positive and negative ionization full scan modes. Auxiliary gas and sheath gas flow rates were 10 and 45 (arbitrary units), respectively. The auxiliary gas heater temperature was 300°C. The capillary temperature was 320°C. The spray voltage was 3.1 kV and the S-lens RF level was 50 V. The normalized collision energy (NCE) was 30 eV. The resolution of the full scan and ddMS2 were 70,000 and 35,000, respectively. The full MS scan ranges were set from *m/z* 66.7 to 1,000. Data were acquired and processed using ThermoXcalibur 3.0 software (Thermo Scientific, United States). Tentative identification of non-volatiles was based on comparing retention time, *m/z* values, and MS/MS fragments with standards or data from databases (e.g., Massbank and MzCloud) when standards were unavailable. Relative quantitation was calculated by comparing the relative intensities of the parent ions among samples and presented in a heat map after converting to *Z*-scores of the rows.

Determination of Volatile Chemical Composition

The volatile chemical composition was investigated by the headspace solid-phase micro-extraction/gas chromatography-mass spectrometry (HS-SPME-GC-MS) (15). Before the extraction, the fiber of the SPME needle [50/30 μm divinylbenzene/carboxen/polydimethylsiloxane, StableFlex (2 cm), Product No. 57348-U, Supelco, Bellefonte, PA, United States] was kept at 250°C for 10 min to remove the remaining volatiles. A 0.5 g tea powder was added to a 50 mL glass vial and mixed with 5 mL boiling water and 30 μL ethyl caprate (internal standard). The glass vial was sealed immediately, gently vortexed, and incubated at 60°C. An SPME needle was inserted into the glass vial through the cap to absorb volatiles for 1 h. Then, the SPME needle was inserted into the injection port of GC to desorb volatiles at 250°C for 5 min.

Volatile organic compounds were determined by an Agilent 6890 gas chromatograph coupled with an Agilent HP 5973 mass selective detector (Agilent, Wilmington, DE, United States). The separation was performed on a DB-5MS capillary column (30 m × 250 μm × 0.25 μm) with the following GC conditions, which were the GC inlet temperature of 250°C, the split ratio of 15:1, the carrier gas (high purity helium) flow of 1.0 mL/min, the linear flow velocity of carrier gas of 40 cm/s. The column temperature was set as follows: 0–2 min, 40°C; 2–24.5 min, 40–85°C; 24.5–26.5 min, 85°C; 26.5–64.5 min, 85–180°C; 64.5–66.5 min, 180°C; 66.5–71.5 min, 180–230°C; and 71.5–73.5 min, 230°C.

The MS conditions were the temperature of the ion source of 230°C, the voltage of 70 eV, and the scan ranging from *m/z* 40 to 400. Tentative identification of volatiles was made by comparing the MS fragmentation patterns with data from the National Institute for Standards and Technology database (NIST 08, match percentage >80%). The relative abundance of each volatile was calculated by comparing the peak area of each compound to the total peak area.

Determination of *in vitro* Antioxidant Activity

The 2,2-diphenyl-1-picrylhydrazyl (DPPH) radical scavenging activity was assessed using the protocol described by Xu et al. (16). The 2,2′-azinobis-(3-ethylbenzothiazoline-6-sulfonic acid) (ABTS) scavenging activity was determined according to the protocol described by Re et al. (17). The hydroxyl radical scavenging activity was assessed using a commercial kit (Hydroxyl Free Radical Assay Kit, Product No. A018-1-1, Nanjing Jiancheng Bioengineering Institute, Nanjing, China), according to the manufacturer's instructions. All analyses were conducted in triplicates.

Determination of Anti-advanced Glycation End Products Activity

The effects of TOTs on the formation of AGEs were investigated in bovine serum albumin (BSA) + glucose, BSA + methylglyoxal, and BSA + glyoxal systems, respectively, based on a previously published method with some modifications (18). In the

BSA + glucose system, 200 μL of 15 mmol/L glucose, 200 μL of 30 mg/mL BSA, and 200 μL of tea infusion were mixed and incubated at 100°C for 1 h. The relative fluorescence was measured using a multi-functional microplate reader (excitation/emission = 370/440 nm) (Thermo Scientific Varioskan Flash, Waltham, MA, United States). In the BSA + methylglyoxal system, glucose was replaced by 200 μL of 1.5 mmol/L methylglyoxal. In the BSA + glyoxal system, glucose was replaced by 200 μL of 1.5 mmol/L glyoxal.

Determination of Antibacterial Activity

The minimum inhibitory concentrations (MICs) against *Salmonella typhi* [CMCC (B) 50071], *Shigella flexneri* [CMCC (B) 51572], β-hemolytic *Streptococcus* [CMCC (B) 32210], *Staphylococcus aureus* [CMCC (B) 26003], and *Escherichia coli* [CMCC (B) 44102] were determined using the micro-dilution method (19).

Each strain was plated on an agar plate and incubated at 37°C for 24 h. A single colony was used to inoculate 10 mL of sterile broth and incubated at 37°C for 24 h. Then the suspension was diluted to 2×10^5 CFU/mL. To investigate the effects of the three tea samples on the growth of each strain, BT0, BT1, and BT2 extracts were dissolved in sterile broth to prepare a 2 mg/mL solution and serially diluted to reach the final concentrations of 0.5, 1, and 2 mg/mL, respectively. A 100 μL bacterial suspension was mixed with 100 μL tea extract solution and then added to a 96-well plate. The positive control was 100 μL bacterial suspension mixed with 100 μL sterile broth. The 96-well plate was incubated overnight at 37°C and then observed. MICs are defined as the lowest concentration of an antimicrobial agent that would inhibit the visible growth of a microorganism after overnight incubation.

Statistical Analysis

The data are presented as the mean ± standard error of the mean (SEM). All experiments were carried out in triplicate and repeated in three independent sets of experiments. The results were analyzed with SPSS version 18.0 for Windows (SPSS, Chicago, IL, United States), using a one-way analysis of variance and a *post hoc* test (two-sided Dunnett's test) to evaluate differences among groups. P-values < 0.05 were considered to be statistically significant.

RESULTS AND DISCUSSION

Effects of Baking on the Non-volatiles and the Color of Infusion

The color of the infusion is an aspect to assess the sensory quality of tea. Sensory evaluation (**Figure 1A**) indicated that the baking process significantly darkened the color of tea infusion, turning it from honey yellow, golden yellow, to orange. Instrumental analysis of color (**Figure 1B**) showed that the a^* value turned from −2.31 to −0.96, the b^* value increased from 15.4 to 23.0, and the L^* value decreased from 95.6 to 92.6 after twice baking. It indicated that the baking process brought more red and yellow tones but less luminosity to TOT infusion, which was in accordance with the results of the visual observation. Separating the tea infusion using centrifugal filters with 3, 10, and 50 kDa molecular weight cut-off (MWCO), accordingly, it was found that the color differences among the three tea infusions were mainly attributed to constituents that could not pass through the 10 kDa MWCO filter (**Figure 1C**). The orange/golden yellow pigments in BT2 had higher molecular weights than in BT1, suggesting that the baking process promoted the formation of colored macromolecules.

Previous studies revealed that flavonol glycosides and tea pigments (e.g., TFs, TRs, and TBs) contributed to the color of tea infusion (20). As flavonol glycosides are small molecules, it is speculated that TRs and TBs may cause the differences on the color of TOT infusions. TRs and TBs are heterogeneous water-soluble polymers of catechins. TRs, whose average molecular weight range from ∼700 to 40,000 Da, usually present red color. TBs, characterized by their high molecular weight and complex structure, usually present brown color and are negatively related to the brightness of tea infusions. BT2 contained higher TRs and TBs than BT0 and BT1, and BT1 contained higher TBs than BT0 (**Table 1**). Deducing from the fact that the content of TRs in BT1 was insignificantly different from that in BT0, but the redness was enhanced in the BT1 infusion (**Figure 1B**), there might be something else attributing to the redness of TOT infusions besides TRs. The content of TBs was increased while the brightness of tea infusion was decreased as the baking degree increased, demonstrating that TBs reduced the brightness of TOT infusions. The cause of the increase of TRs and TBs might be the accelerated oxidization and polymerization of catechins induced by the heat and aerobic environment during the baking process (21). A 7.4 and 17.4% loss of total monomeric catechins were detected in BT1 and BT2 (**Table 2**), respectively, supporting the hypothesis.

Effects of Baking on the Non-volatiles and Taste

Taste is the most crucial aspect of oolong tea's sensory quality, based on GB/T 23776-2018. Sensory evaluation indicated that the baking process remarkably increased the thickness, sweet aftertaste, and bitterness, while reducing TOT infusion's umami taste (**Figure 1D**).

Soluble polysaccharides were candidate contributors to the thickness of tea infusions. A 20% increase in the content of soluble polysaccharides was detected in BT2 (**Table 1**). It was reported that some polysaccharides increased the kokumi sensation (22), a taste impression combined of thickness, mouthfulness, and continuity, as they influenced the viscosity of fluids (23). Tea that tasted smooth and thick, such as ripe Pu'er tea and aged white tea, usually had abundant soluble polysaccharides. Heat treatment could promote the degradation of insoluble polysaccharides, thereby increasing the content of soluble polysaccharides in tea infusions. It was possible that the increase of soluble polysaccharides after baking also contributed to the thick taste. TRs might have an impact on the thickness

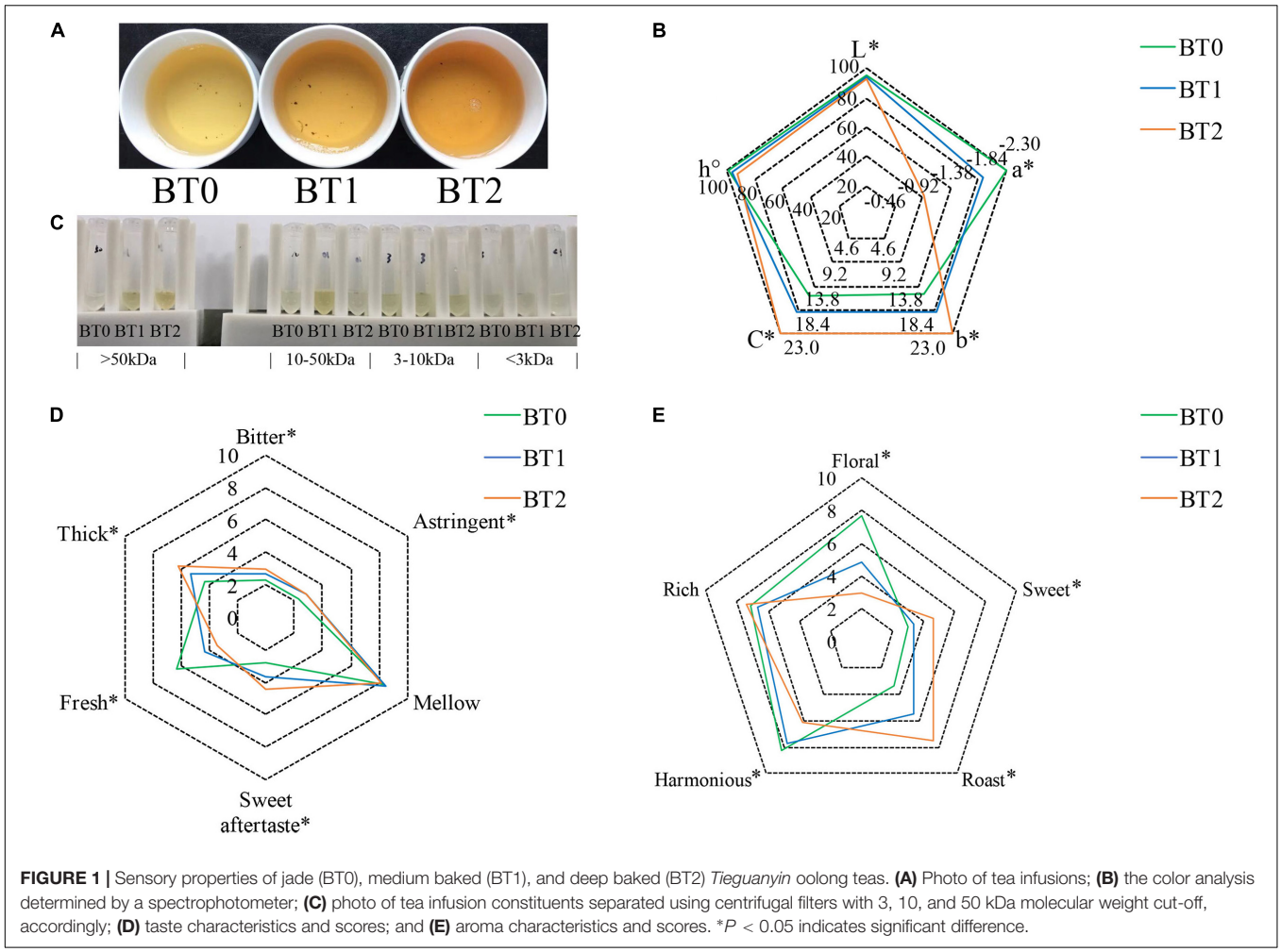

FIGURE 1 | Sensory properties of jade (BT0), medium baked (BT1), and deep baked (BT2) *Tieguanyin* oolong teas. **(A)** Photo of tea infusions; **(B)** the color analysis determined by a spectrophotometer; **(C)** photo of tea infusion constituents separated using centrifugal filters with 3, 10, and 50 kDa molecular weight cut-off, accordingly; **(D)** taste characteristics and scores; and **(E)** aroma characteristics and scores. *$P < 0.05$ indicates significant difference.

TABLE 1 | The chemical compositions of jade (BT0), medium-baked (BT1), and deep-baked (BT2) *Tieguanyin* oolong teas.

Contents (mg/g)	BT0	BT1	BT2
Polyphenols	94.76 ± 4.52^{a}	94.60 ± 6.14^{a}	85.33 ± 0.84^{b}
Free amino acids	28.69 ± 0.88^{a}	20.49 ± 0.15^{b}	12.70 ± 0.00^{c}
Soluble proteins	28.99 ± 0.67^{a}	28.36 ± 0.69^{ab}	27.50 ± 0.66^{b}
Soluble sugars	77.28 ± 0.77^{a}	76.19 ± 0.77^{a}	72.94 ± 1.92^{b}
Soluble polysaccharides	15.95 ± 0.77^{b}	16.46 ± 2.97^{ab}	19.10 ± 1.08^{a}
Flavones	8.53 ± 0.30^{ab}	8.16 ± 0.23^{b}	9.12 ± 0.68^{a}
TFs	0.47 ± 0.11^{ab}	0.37 ± 0.01^{b}	0.41 ± 0.00^{a}
TRs	12.36 ± 0.33^{b}	12.40 ± 0.30^{b}	13.01 ± 0.23^{a}
TBs	10.07 ± 0.40^{c}	11.04 ± 0.23^{b}	12.31 ± 0.03^{a}

The same letter within each row indicates no significant difference ($P > 0.05$).

TABLE 2 | The contents of monomeric catechins, gallic acid, and caffeine in jade (BT0), medium-baked (BT1), and deep-baked (BT2) *Tieguanyin* oolong teas.

Contents (mg/g)	BT0	BT1	BT2
Gallic acid (GA)	1.03 ± 0.01^{c}	1.22 ± 0.02^{b}	1.36 ± 0.01^{a}
Gallocatechin (GC)	12.33 ± 0.49^{a}	8.25 ± 0.24^{b}	7.58 ± 0.03^{c}
Epigallocatechin (EGC)	22.06 ± 1.20^{a}	21.82 ± 0.21^{a}	18.65 ± 0.10^{b}
Catechin (C)	1.59 ± 0.01^{a}	1.38 ± 0.01^{b}	1.17 ± 0.01^{c}
Caffeine	16.73 ± 0.16^{b}	17.05 ± 0.06^{a}	16.54 ± 0.12^{b}
Epigallocatechin gallate (EGCG)	38.01 ± 1.66^{a}	37.45 ± 0.35^{a}	34.69 ± 0.71^{b}
Epicatechin (EC)	7.10 ± 0.10^{a}	6.90 ± 0.04^{b}	5.64 ± 0.01^{c}
Gallocatechin gallate (GCG)	8.75 ± 0.82^{a}	7.29 ± 0.24^{b}	6.47 ± 0.28^{c}
Epicatechin gallate (ECG)	7.64 ± 0.09^{a}	7.25 ± 0.21^{b}	6.18 ± 0.13^{c}
Catechin gallate (CG)	0.62 ± 0.00^{a}	0.49 ± 0.03^{b}	0.35 ± 0.01^{c}
Total monomeric catechins	98.09 ± 4.35^{a}	90.83 ± 0.90^{b}	80.74 ± 0.72^{c}

The same letter within each row indicates no significant difference ($P > 0.05$).

of TOT infusions as well, because TRs were previously found to contribute to the mouth feel (thickness) (24).

Gallic acid, a degradation product of catechins, was associated with the sweet aftertaste of TOT infusions. Gallic acid was previously reported to improve the sweet aftertaste of tannase-treated autumn green tea (25). In this study, a 18 and 32% increase of gallic acid were detected in BT1 and BT2, respectively (**Table 2**), which was consistent with the gradual enhancement of sweet aftertaste after baking. Along with the increase of gallic acid, was the decrease of catechins. Among the eight catechins analyzed by HPLC, six were decreased after the first baking process, and eight were reduced after the second baking. Several

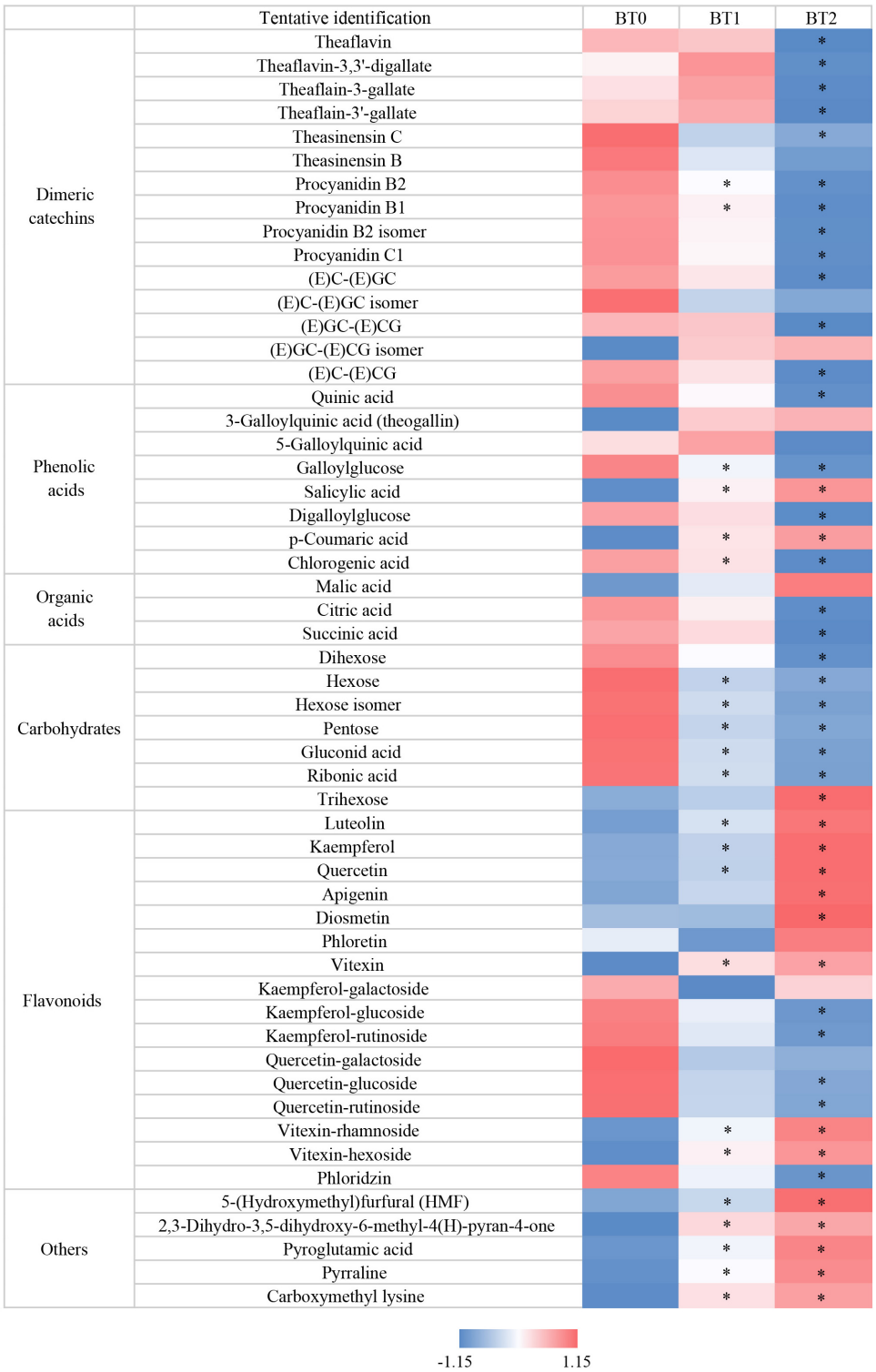

FIGURE 2 | Heatmap of *Z*-score normalized relative abundances of non-volatiles identified by UPLC-QE-Orbitrap-MS. *$P < 0.05$ indicates significant difference.

dimeric catechins (e.g., theasinensins and procyanidins) were reduced after baking (**Figure 2**). In details, about 30% of TFs, 10% of theasinensins, and 30% of procyanidins were lost after twice baking. In a previous study, high-temperature processing (roasting) during tea production decreased monomeric catechins and increased gallic acid (26). Our results supported that the

degradation of catechins were universal during the baking process of tea. Catechins and their derivatives are essential to the taste of oolong tea by enhancing bitterness and astringency (14). Monomeric catechins usually taste astringent and bitter, while dimeric catechins taste more astringent and less bitter than monomeric catechins (11). The bitterness and astringency were not reduced though catechins were decreased after baking (**Figure 1D**). On the contrary, both sensory attributes were enhanced, implying that other bitter and astringent compounds might be generated during the baking process.

It was assumed that the Maillard reaction was responsible to the bitterness of baked TOT infusions. The Maillard reaction is a chemical reaction between reducing sugars and amino acids upon the baking process, which produces a series of flavor compounds and modifies the sensory properties (e.g., bitterness) of baked foods (27, 28). Previous research demonstrated that the Maillard reaction impacted the quality of green tea and oolong tea (10, 29). In this study, 55% of total free amino acids was consumed after twice baking (**Table 1**). The contents of dihexose, hexoses, and pentose significantly decreased in baking. At the same time, the levels of 5-hydroxymethylfurfural (5-HMF) and 2,3-dihydro-3,5-dihydroxy-6-methyl-4(H)-pyran-4-one (DDMP), two typical intermediates of Maillard reaction with a bitter taste (30), in BT2 was 7.7-fold and 2.6-fold of that in BT0. These data proved the presence of the Maillard reaction during the baking process of TOT and its role in the chemical and taste changes of baked TOTs.

It was aware that the occurrence of the Maillard reaction was accompanied by the consumption of free amino acids. A total of 17 free amino acids were detected, including 14 proteinogenic amino acids and 3 non-protein amino acids (i.e., theanine, β-aminoisobutyric acid, and γ-aminobutyric acid) (**Table 3**). Theanine and glutamic acid, major umami compounds in tea (31), were the two most abundant free amino acids. Together, the two accounted for about 60% of total free amino acids in TOT infusions. However, merely 24.3% of theanine and 32.7% of glutamic acid remained after baking twice, which led to the reduced umami taste of baked TOT infusions (**Figure 1D**). Our previous study suggested that the free amino acid content was positively correlated to the taste quality of TOTs (1). The baking-induced decrease of free amino acids might hamper the taste of TOTs, but benefit the formation of typical roast aroma *via* the Maillard reaction.

Effects of Baking on the Volatiles and Aroma

Aroma is the second important aspect of oolong tea's sensory quality, based on GB/T 23776-2018. Sensory evaluation indicated that the baking process transformed the aroma from floral to sweet and roast (**Figure 1E**).

The changes of volatiles after baking were the basis of the changes in the aroma. **Table 4** indicated that the baking process significantly increased the number of volatiles. A total of 74, 85, and 102 volatiles were identified in BT0, BT1, and BT2, respectively. Among them, 61 volatiles were detected in all three samples. BT2 contained more unique volatiles than the other two. It indicated that the baking process promoted the formation of new volatiles, many of which belonged to heterocycles.

Floral volatiles were the main volatiles detected in BT0. Although the number of floral volatiles did not vary considerably among the three teas, their relative abundances did. The relative abundances of floral volatiles accounted for 46.6% of total volatiles in BT0. (E)-Nerolidol, indole, and benzeneacetaldehyde were the top three abundant floral volatiles in BT0, making up 37.4% of total volatiles. The baking process decreased the contents of floral volatiles. The loss of floral volatiles occurred during the first and second baking stages, but was more severe during the second stage. The relative abundance of floral volatiles dropped to 19.7% in BT2. Previous study indicated that high temperature hampered the floral volatiles in TOT, i.e., β-ionone, jasmine, and nerolidol (32). Our results were partially in accordance with it. The differences might be caused by the differences in the raw material and the conditions of heat treatment. In addition, multiple green volatiles [e.g., cis-3-hexenyl isovalerate, heptanal, hexyl hexanoate, (Z)-3-hexen-1-yl hexanoate, hexanal, and 2-pentyl-furan], citrus volatiles (e.g., octanal and D-limonene), and herbal volatiles (e.g., α-farnesene and myrtenyl acetate) were reduced or disappeared after baking. The sum of the relative abundances of green/citrus/herbal volatiles decreased from 16.4 to 8.7%, leading to a less refreshing aroma in BT2.

Meanwhile, the types and relative abundances of sweet, caramel, and roast volatiles were significantly increased. Six, 12, and 14 sweet, caramel, and roast volatiles were identified in BT0, BT1, and BT2, accounting for 1.6, 5.3, and 11.0% of total volatiles, respectively. The relative abundances of toluene, phenethyl hexanoate, furfural, and 1-ethyl pyrrole gradually increased with baking. The relative abundances of these volatiles in BT2 were at least twice as much as that in BT0, respectively. Notably, the relative abundance of furfural, a volatile with a sweet and baked bready aroma and a typical intermediate of the Maillard reaction, was 11-fold higher in BT2 than that in BT0. Methyl 3-hexanoate, 2-acetyl furan, and 1-methyl-pyrrole, which existed in BT1 and BT2 but not in BT0, were enriched in BT2. Methyl acetate, farnesol, methyl 2-furoate, and 1-furfuryl pyrrole were merely detected in BT2. Earlier study revealed that 1-ethyl pyrrole was positively correlated with the grade of deep-baked TOT, while methyl acetate was initially decreased but then increased with the declining grade of deep-baked TOT (33). In this study, the two volatiles were accumulated in BT2, implying that the baking process was important for the formation of the aroma property of deep-baked TOT. It was noticed that many volatiles generated or accumulated during baking were pyrroles, furans, and their derivatives, which were Maillard reaction products, indicating that the baking process mainly reshaped the aroma *via* the Maillard reaction.

In addition to volatiles with known aroma characteristics, 27 volatiles detected in BT2 but not in BT0 were with unknown aroma characteristics. The contents of these compounds

TABLE 3 | The contents of free amino acid components in jade (BT0), medium-baked (BT1), and deep-baked (BT2) *Tieguanyin* oolong teas.

Content (μg/g)	BT0	BT1	BT2
Aspartate	$1,047.4 \pm 54.8^{a}$	893.8 ± 255.3^{a}	576.8 ± 61.0^{b}
Threonine	576.1 ± 34.5^{a}	456.5 ± 64.6^{b}	232.2 ± 17.2^{c}
Serine	$1,447.7 \pm 29.7^{a}$	$1,107.9 \pm 121.7^{b}$	508.8 ± 55.5^{c}
Asparagine	436.5 ± 32.2^{a}	385.9 ± 167.5^{a}	21.0 ± 3.2^{b}
Glutamic acid	$3,266.5 \pm 211.5^{a}$	$2,044.9 \pm 226.0^{b}$	$1,066.7 \pm 33.7^{c}$
Theanine	$18,030.3 \pm 2,679.5^{a}$	$11,112.8 \pm 1,612.5^{b}$	$4,382.8 \pm 214.4^{c}$
Glycine	94.7 ± 4.5^{a}	80.5 ± 4.7^{b}	51.9 ± 1.2^{c}
Alanine	$1,258.8 \pm 45.8^{a}$	$1,064.3 \pm 85.3^{b}$	564.4 ± 7.9^{c}
Valine	628.1 ± 35.0^{a}	487.6 ± 60.6^{b}	270.9 ± 6.2^{c}
Cystine	96.5 ± 6.1^{a}	67.2 ± 7.4^{b}	21.5 ± 1.5^{c}
Isoleucine	113.6 ± 14.1^{a}	84.0 ± 22.3^{b}	36.4 ± 3.8^{c}
Leucine	146.2 ± 17.2^{a}	107.8 ± 22.9^{a}	52.3 ± 0.3^{b}
Tyrosine	305.0 ± 4.6^{a}	243.6 ± 39.2^{b}	124.7 ± 17.3^{c}
Phenylalanine	158.5 ± 17.3^{a}	142.7 ± 11.5^{a}	112.3 ± 6.0^{b}
β-Aminoisobutyric acid	257.0 ± 68.9^{a}	191.7 ± 32.2^{a}	77.7 ± 6.2^{b}
γ-Aminobutyric acid	178.8 ± 10.5^{a}	112.4 ± 20.4^{a}	49.3 ± 3.6^{b}
Lysine	223.0 ± 19.4^{a}	198.3 ± 19.9^{a}	90.7 ± 15.7^{b}

The same letter within each row indicates no significant difference ($P > 0.05$).

accounted for 14.4% of total volatiles. Most of them were complex structures, containing at least one cyclic ring. Little information on the aroma properties of these compounds could be found. It is necessary to use gas chromatography-olfactometry to investigate the aroma properties of these compounds and assess whether they contribute to the aroma of tea in further studies.

Effects of Baking on the Chemical Composition and Bioactivity

Chemical analysis revealed that the baking process dramatically altered the compositions and contents of catechins and their derivatives, flavones, free amino acids, and soluble sugars, many of which were bioactive compounds (**Tables 1**, **2**, **3** and **Figure 2**). Hence, it was wondered whether the baking process also altered the bioactivity of TOTs. Antioxidant property is a featuring bioactivity of oolong tea. Free radicals are highly oxidizing and may damage macromolecules in the living system *via* inducing oxidative stress. Scavenging free radicals is an important strategy for antioxidants to exert their functions. Thus, free radical scavenging assays are often applied to evaluate the antioxidant activity. Recently, anti-AGEs formation assays are gaining attention as another way to evaluate antioxidant activity. Reactive oxygen species and free radicals participate in the formation of AGEs, and AGEs can induce oxidative stress *via* binding to their cell surface receptor (34). Many antioxidants possess inhibitory effects on the formation of AGEs (35). In this study, the above two assays were conducted to assess the antioxidant activity of three TOTs (**Figures 3A–F**). Antibacterial property is another featuring bioactivity of oolong tea. The MICs against five bacteria were used to determine the antibacterial activity (**Figure 3G**).

The effects of baking on the free radical scavenging activity are disadvantageous. The ABTS, DPPH, and hydroxyl radical scavenging activities of BT2 were significantly reduced compared with BT0 (**Figures 3A–C**). Earlier researches suggested that the ethyl acetate fraction of TOT, which had higher contents of phenolics, flavonoids, procyanidins, sugars, and catechin monomers, exhibited stronger antioxidant capacity than the n-butanol fraction and water fraction of TOT (36). Su et al. demonstrated that monomeric catechins played critical roles in anti-oxidation (37). It was reported that the trans-catechins possessed higher free radical scavenging activity than the corresponding cis-epicatechins, and the gallated catechins possessed higher antioxidant activity than the corresponding non-gallated catechins (38). Lee et al. tested the ABTS and DPPH scavenging activities of seven monomeric catechins. Compared with non-gallated catechins, gallated catechins did exhibit stronger ABTS and DPPH scavenging activities (39). Su et al. demonstrated that two major catechins, i.e., epigallocatechin gallate (EGCG) and epigallocatechin (EGC), contributed significantly to oolong tea's DPPH and superoxide radical scavenging activities. Guo et al. investigated the hydroxyl radical scavenging activity of four epi-form catechins. The results indicated that their ability to scavenge hydroxyl radicals decreased in the order of epicatechin gallate (ECG) > epicatechin (EC) > EGCG > EGC (40). In our research, the changing trends of catechins contents, particularly the changing trends of epi-form catechins contents, were consistent with the changing trends of free radical scavenging activity during baking. It suggested that the decrease of catechins was an important cause of the baking-mediated decreased free radical scavenging activity of TOT.

The effects of baking on inhibiting the formation of AGEs are inconsistent in different reaction systems. Dietary AGEs are formed in foods during the thermal process, and they are a main source of AGEs in the body (41). The formation of AGEs begins between a carbonyl group of reducing sugar (e.g.,

TABLE 4 | Volatile compounds in jade (BT0), medium-baked (BT1), and deep-baked (BT2) *Tieguanyin* oolong teas determined by GC-MS.

Retention time	CAS number	Molecular formula	Molecular weight	Name	Relative abundance%			Aroma properties
					BT0	BT1	BT2	
1.642	75-18-3	C_2H_6S	62	Dimethyl sulfide	0.342 ± 0.056^{a}	0.292 ± 0.051^{a}	<LOQ ^{b}	Sulfury
1.732	79-20-9	$C_3H_6O_2$	74	Methyl acetate	<LOQ ^{b}	<LOQ ^{b}	0.526 ± 0.170^{a}	Sweet fruity
1.741	1191-16-8	$C_7H_{12}O_2$	128	Prenyl acetate	<LOQ ^{b}	0.440 ± 0.006^{a}	<LOQ ^{b}	Sweet banana, fruity
1.800	78-84-2	C_4H_8O	72	Isobutyraldehyde	<LOQ ^{b}	0.069 ± 0.008^{a}	0.073 ± 0.009^{a}	Malty, aldehydic
2.023	111-30-8	$C_5H_8O_2$	100	Glutaraldehyde	0.060 ± 0.009^{b}	0.089 ± 0.010^{a}	0.105 ± 0.007^{a}	Pungent
2.077	534-22-5	C_5H_6O	82	2-Methylfuran	0.080 ± 0.012^{b}	0.083 ± 0.010^{b}	0.147 ± 0.027^{a}	Ethereal, acetone, chocolate
2.329	NIST#: 194652	$C_7H_{10}O_2$	126	3-Methyl-4-propenyl-oxetan-2-one	0.052 ± 0.004^{a}	0.050 ± 0.007^{a}	0.054 ± 0.003^{a}	/
2.376	926-54-5	C_6H_{10}	82	Trans-2-methyl-1,3-pentadiene	0.089 ± 0.006^{a}	0.068 ± 0.002^{b}	<LOQ ^{c}	/
2.445	96-38-8	C_6H_8	80	5-Methyl-1,3-cyclopentadiene	<LOQ ^{b}	<LOQ ^{b}	0.032 ± 0.005^{a}	/
2.479	590-86-3	$C_5H_{10}O$	86	3-Methylbutanal	0.074 ± 0.021^{a}	0.044 ± 0.005^{b}	0.055 ± 0.007^{ab}	Fruity, pungent, nutty, cocoa
2.582	96-17-3	$C_5H_{10}O$	86	2-Methylbutanal	0.179 ± 0.031^{a}	0.135 ± 0.018^{a}	0.225 ± 0.025^{a}	Musty, cocoa, coffee, nutty
2.816	96-41-3	$C_5H_{10}O$	86	Cyclopentanol	<LOQ ^{b}	<LOQ ^{b}	0.075 ± 0.024^{a}	Musty, aromatic
2.888	1629-58-9	C_5H_8O	84	1-Penten-3-one	0.238 ± 0.027^{a}	0.252 ± 0.047^{a}	0.167 ± 0.025^{b}	Pungent, peppery, garlic
3.073	589-91-3	$C_7H_{14}O$	114	4-Methylcyclohexanol	0.576 ± 0.075^{a}	0.487 ± 0.021^{a}	0.375 ± 0.027^{b}	Aromatic
3.182	50521-50-1	$C_6H_{10}O_2$	114	1,4-Butanediol, 2,3-bis(methylene)-	<LOQ ^{b}	<LOQ ^{b}	0.041 ± 0.002^{a}	/
3.415	30316-00-8	$C_7H_{11}N$	109	2-Methyl-5-hexenenitrile	0.038 ± 0.007^{ab}	0.059 ± 0.013^{a}	0.035 ± 0.007^{b}	/
3.480	1943-79-9	$C_8H_9NO_2$	151	Methylcarbamic acid phenyl ester	<LOQ ^{b}	<LOQ ^{b}	0.071 ± 0.011^{a}	/
3.633	625-28-5	C_5H_9N	83	Isovaleronitrile	0.035 ± 0.008^{c}	0.060 ± 0.007^{b}	0.130 ± 0.009^{a}	/
3.761	96-54-8	C_5H_7N	81	1-Methyl-pyrrole	<LOQ ^{c}	0.026 ± 0.001^{b}	0.046 ± 0.004^{a}	Smoky, woody
3.883	497-03-0	C_5H_8O	84	(E)-2-Methyl-2-butenal	<LOQ ^{b}	0.054 ± 0.010^{a}	0.060 ± 0.009^{a}	Strong green
4.022	21856-89-3	$C_6H_{12}O_2$	116	6-Hydroxyhexan-2-one	<LOQ ^{b}	<LOQ ^{b}	0.077 ± 0.013^{a}	/
4.075	55230-25-6	$C_6H_{10}O$	98	2-Methyl-5,6-dihydro-2H-pyran	<LOQ ^{c}	0.069 ± 0.006^{b}	0.108 ± 0.015^{a}	/
4.168	89182-08-1	C_5H_8O	84	Cyclobut-1-enylmethanol	0.368 ± 0.057^{a}	0.359 ± 0.012^{a}	0.413 ± 0.053^{a}	/
4.420	108-88-3	C_7H_8	92	Toluene	0.154 ± 0.030^{c}	0.278 ± 0.035^{b}	0.695 ± 0.119^{a}	Sweet
4.837	4054-38-0	C_7H_{10}	94	1,3-Cycloheptadiene	0.073 ± 0.003^{a}	0.063 ± 0.002^{b}	0.060 ± 0.012^{ab}	/
5.302	141-79-7	$C_6H_{10}O$	98	Mesityl oxide	<LOQ ^{b}	0.132 ± 0.029^{a}	<LOQ ^{b}	Honeylike
5.381	66-25-1	$C_6H_{12}O$	100	Hexanal	2.563 ± 0.419^{a}	2.111 ± 0.326^{a}	1.502 ± 0.204^{b}	Fresh green
5.689	617-92-5	C_6H_9N	95	1-Ethyl pyrrole	0.573 ± 0.103^{b}	1.529 ± 0.197^{a}	1.707 ± 0.188^{a}	Burnt
6.433	98-01-1	$C_5H_4O_2$	96	Furfural	0.434 ± 0.068^{c}	2.102 ± 0.280^{b}	5.295 ± 0.368^{a}	Sweet, woody, baked bread
7.330	6728-26-3	$C_6H_{10}O$	98	(E)-2-Hexenal	0.402 ± 0.059^{a}	0.400 ± 0.061^{a}	0.253 ± 0.010^{b}	Green banana, fatty
7.962	106-42-3	C_8H_{10}	106	p-Xylene	0.084 ± 0.018^{c}	0.191 ± 0.006^{b}	1.162 ± 0.120^{a}	Aromatic
8.970	110-43-0	$C_7H_{14}O$	114	2-Heptanone	0.271 ± 0.027^{b}	0.332 ± 0.052^{ab}	0.379 ± 0.054^{a}	Fruity
9.467	6728-31-0	$C_7H_{12}O$	112	(Z)-4-Heptenal	0.181 ± 0.032^{a}	0.191 ± 0.034^{a}	0.173 ± 0.015^{a}	Green, creamy
9.607	111-71-7	$C_7H_{14}O$	114	Heptanal	0.404 ± 0.019^{a}	0.282 ± 0.035^{b}	0.255 ± 0.031^{b}	Green, fatty
9.706	2199-41-9	$C_7H_{11}N$	109	2,3,5-Trimethyl-1H-pyrrole	<LOQ ^{c}	0.201 ± 0.046^{b}	0.286 ± 0.023^{a}	/

(Countinued)

TABLE 4 | (Countinued)

Retention time	CAS number	Molecular formula	Molecular weight	Name	Relative abundance%			Aroma properties
					BT0	BT1	BT2	
9.895	1192-62-7	$C_6H_6O_2$	110	2-Acetyl furan	<LOQ ^{c}	0.124 ± 0.016^{b}	0.262 ± 0.013^{a}	Caramel, sweet
10.086	1558-17-4	$C_6H_8N_2$	108	4,6-dimethyl-pyrimidine	<LOQ ^{c}	0.199 ± 0.032^{b}	0.301 ± 0.025^{a}	/
10.309	56342-53-1	$C_6H_8N_2$	108	1-Methyl-3-vinyl-1H-pyrazole	<LOQ ^{b}	0.140 ± 0.018^{a}	0.179 ± 0.024^{a}	/
10.511	930-87-0	$C_7H_{11}N$	109	1,2,5-Trimethylpyrrole	<LOQ ^{c}	0.132 ± 0.023^{b}	0.165 ± 0.002^{a}	/
10.834	106-70-7	$C_7H_{14}O_2$	130	Methyl hexanoate	0.111 ± 0.016^{a}	0.111 ± 0.006^{a}	0.126 ± 0.008^{a}	Fruity
11.197	2396-78-3	$C_7H_{12}O_2$	128	Methyl 3-hexenoate	<LOQ ^{c}	0.074 ± 0.013^{b}	0.165 ± 0.006^{a}	Earthy, sweet, slightly fruity
11.860	589-33-3	$C_8H_{13}N$	123	1-Butylpyrrole	<LOQ ^{b}	<LOQ ^{b}	0.034 ± 0.010^{a}	/
12.746	100-52-7	C_7H_6O	106	Benzaldehyde	2.992 ± 0.322^{b}	3.651 ± 0.060^{a}	3.844 ± 0.165^{a}	Bitter almond, cherry
13.614	611-13-2	$C_6H_6O_3$	126	Methyl 2-furoate	<LOQ ^{b}	<LOQ ^{b}	0.272 ± 0.038^{a}	Caramel
14.389	110-93-0	$C_8H_{14}O$	126	6-Methyl-5-hepten-2-one	2.451 ± 0.453^{a}	2.131 ± 0.369^{a}	2.006 ± 0.054^{a}	Green, lemongrass, citrus
14.692	3777-69-3	$C_9H_{14}O$	138	2-Pentyl-furan	0.747 ± 0.310^{a}	0.627 ± 0.061^{a}	<LOQ ^{b}	Green, beany
14.697	80255-20-5	$C_9H_{13}NO_2$	167	1-(2-Nitro-2-propenyl)-cyclohexene	<LOQ ^{b}	<LOQ ^{b}	0.937 ± 0.064^{a}	/
15.071	4313-03-5	$C_7H_{10}O$	110	(E,E)-2,4-Heptadienal	6.334 ± 0.175^{c}	9.387 ± 0.823^{b}	11.103 ± 0.022^{a}	Fatty, green
15.573	124-13-0	$C_8H_{16}O$	128	Octanal	0.494 ± 0.081^{a}	0.446 ± 0.045^{a}	<LOQ ^{b}	Citrus
15.581	513-23-5	$C_{10}H_{18}O$	154	Isothujol	<LOQ ^{b}	<LOQ ^{b}	0.573 ± 0.090^{a}	/
16.770	527-84-4	$C_{10}H_{14}$	134	o-Cymene	0.666 ± 0.068^{ab}	0.543 ± 0.087^{b}	0.768 ± 0.071^{a}	Citrus
17.072	5989-27-5	$C_{10}H_{16}$	136	D-Limonene	3.924 ± 0.331^{a}	3.333 ± 0.396^{ab}	2.907 ± 0.500^{b}	Lemon, citrus
17.386	2408-37-9	$C_9H_{16}O$	140	2,2,6-Trimethyl-cyclohexanone	0.169 ± 0.020^{ab}	0.141 ± 0.023^{b}	0.185 ± 0.008^{a}	Pungent, citrus
17.759	3338-55-4	$C_{10}H_{16}$	136	(Z)-β-Ocimene	<LOQ ^{b}	<LOQ ^{b}	0.290 ± 0.019^{a}	Warm floral, sweet
17.963	122-78-1	C_8H_8O	120	Benzeneacetaldehyde	5.576 ± 0.401^{a}	3.804 ± 0.345^{b}	1.700 ± 0.068^{c}	Hyacinth, sweet floral
18.216	1877-77-6	C_7H_9NO	123	3-Amino-benzenemethanol	<LOQ ^{c}	2.851 ± 0.056^{b}	4.065 ± 0.121^{a}	/
18.248	264628-15-1	C_9H_{12}	120	5-Methylenecycloocta-1,3-diene	1.549 ± 0.034^{a}	<LOQ ^{b}	*<LOQ*^{b}	/
18.418	5794-03-6	$C_{10}H_{16}$	136	(+)-Camphene	<LOQ ^{b}	0.788 ± 0.124^{a}	0.796 ± 0.029^{a}	Camphor, fresh herbal
18.423	7785-70-8	$C_{10}H_{16}$	136	D-(+)-α-Pinene	1.095 ± 0.043^{a}	<LOQ ^{b}	<LOQ ^{b}	Harsh, terpene, aromatic
18.914	14296-81-2	C_9H_{12}	120	Cyclohexane, 1,2,4-tris(methylene)-	0.400 ± 0.031^{a}	0.462 ± 0.183^{a}	0.392 ± 0.032^{a}	/
19.162	2548-87-0	$C_8H_{14}O$	126	(E)-2-Octenal	0.480 ± 0.061^{b}	0.644 ± 0.100^{b}	0.740 ± 0.017^{a}	Fatty, fresh cucumber
19.363	41898-89-9	C_9H_{12}	120	2,4-Dimethyl-2,3-heptadien-5-yne	<LOQ ^{c}	0.299 ± 0.044^{b}	0.450 ± 0.051^{a}	/
19.932	30086-02-3	$C_8H_{12}O$	124	(E,E)-3,5-Octadien-2-one	1.783 ± 0.108^{c}	2.188 ± 0.078^{b}	2.418 ± 0.136^{a}	Fruity, green, grassy
20.280	NIST#: 129149	$C_8H_{12}N_2$	136	Imidazole, 4-methyl-5-[2-methyl-2-propenyl]-	<LOQ ^{b}	<LOQ ^{b}	0.385 ± 0.032^{a}	/
20.878	514-95-4	$C_{10}H_{16}$	136	1,5,5-Trimethyl-6-methylene-cyclohexene	<LOQ ^{b}	<LOQ ^{b}	0.389 ± 0.030^{a}	/
20.879	NIST#: 274055	$C_{14}H_{20}O_3$	236	Acetic acid, 2-(7-methylenebicyclo[3.3.1]oct-2-enyloxy)ethyl ester	0.240 ± 0.046^{a}	0.297 ± 0.053^{a}	<LOQ ^{b}	/

(Countinued)

TABLE 4 | (Countinued)

Retention time	CAS number	Molecular formula	Molecular weight	Name	Relative abundance%			Aroma properties
					BT0	BT1	BT2	
21.049	5989-33-3	$C_{10}H_{18}O_2$	170	(Z)-Linalool oxide (furanoid)	0.141 ± 0.028^{c}	0.205 ± 0.036^{b}	0.272 ± 0.014^{a}	Earthy, floral sweet, woody
21.180	1195-32-0	$C_{10}H_{12}$	132	1-Methyl-4-(1-methylethenyl)-benzene	<LOQ ^{b}	<LOQ ^{b}	0.220 ± 0.030^{a}	Phenolic, spicy, guaiacol
21.623	56846-98-1	$C_{19}H_{30}O_2$	290	13,16-Octadecadiynoic acid, methyl ester	<LOQ ^{b}	<LOQ ^{b}	0.414 ± 0.048^{a}	/
21.631	28638-29-1	$C_9H_{18}O$	142	2,3,4-Trimethyl-5-hexen-3-ol	0.247 ± 0.033^{b}	0.379 ± 0.055^{a}	<LOQ ^{c}	/
22.079	78-70-6	$C_{10}H_{18}O$	154	Linalool	1.535 ± 0.216^{a}	1.130 ± 0.141^{b}	0.762 ± 0.037^{c}	Floral, sweet, citrus
22.267	29957-43-5	$C_{10}H_{16}O$	152	Dehydrolinalool	3.362 ± 0.294^{b}	5.533 ± 0.532^{a}	2.762 ± 0.171^{c}	/
22.420	124-19-6	$C_9H_{18}O$	142	Non-anal	0.728 ± 0.004^{a}	0.623 ± 0.116^{ab}	0.526 ± 0.041^{b}	Rose, orange, waxy
22.604	50868-73-0	$C_8H_{11}NO$	137	2-Methoxy-6-methylaniline	<LOQ ^{c}	0.740 ± 0.098^{b}	1.182 ± 0.181^{a}	/
23.028	19945-61-0	$C_{11}H_{18}$	150	(E)-4, 8-Dimethyl-1,3,7-non-atriene	1.735 ± 0.097^{a}	1.132 ± 0.188^{b}	0.796 ± 0.044^{c}	/
24.016	1079-01-2	$C_{12}H_{18}O_2$	194	Myrtenyl acetate	0.241 ± 0.011^{a}	<LOQ ^{b}	<LOQ ^{b}	Herbal, fresh
24.417	140-29-4	C_8H_7N	117	Phenyl acetonitrile	4.060 ± 0.188^{c}	5.946 ± 0.449^{b}	7.726 ± 0.456^{a}	Aromatic
24.867	3682-17-5	$C_9H_9NO_3$	179	α-(Hydroxyimino)-benzenepropanoic acid	0.726 ± 0.115^{b}	0.592 ± 0.012^{b}	1.217 ± 0.109^{a}	/
25.993	73476-31-0	$C_8H_{11}NO_2$	153	Methyl 1,5-dimethyl-2-pyrrolecarboxylate	<LOQ ^{b}	<LOQ ^{b}	0.218 ± 0.011^{a}	/
26.377	91253-94-0	$C_{11}H_{18}O$	166	2-Naphthol, 1,2,3,4,4a,5,6,7-octahydro-4a-methyl-	<LOQ ^{b}	<LOQ ^{b}	0.253 ± 0.003^{a}	/
27.364	22767-95-9	$C_{12}H_{16}O_2$	192	Benzenepropanoic acid 1-methylethyl ester	<LOQ ^{b}	<LOQ ^{b}	0.350 ± 0.044^{a}	/
27.492	1438-94-4	C_9H_9NO	147	1-Furfuryl pyrrole	<LOQ ^{b}	<LOQ ^{b}	1.072 ± 0.089^{a}	Plastic, waxy, coffee
28.439	119-36-8	$C_8H_8O_3$	152	Methyl salicylate	1.322 ± 0.074^{b}	1.395 ± 0.292^{b}	2.418 ± 0.136^{a}	Wintergreen mint
28.990	99172-18-6	$C_{10}H_{14}O$	150	2-Ethylidene-6-methyl-3,5-heptadienal	0.408 ± 0.085^{a}	0.367 ± 0.052^{a}	0.413 ± 0.045^{a}	/
30.424	432-25-7	$C_{10}H_{16}O$	152	β-Cyclocitral	0.670 ± 0.038^{a}	0.583 ± 0.044^{b}	0.625 ± 0.021^{ab}	Tropical, saffron, herbal
31.709	35154-45-1	$C_{11}H_{20}O_2$	184	cis-3-Hexenyl isovalerate	0.399 ± 0.052^{a}	0.199 ± 0.029^{b}	0.228 ± 0.018^{b}	Fresh green apple
31.905	4677-90-1	$C_{14}H_{20}O$	204	Mayurone	<LOQ ^{b}	<LOQ ^{b}	0.066 ± 0.009^{a}	/
32.111	10032-15-2	$C_{11}H_{22}O_2$	186	Butanoic acid, 2-methyl-, hexyl ester	0.187 ± 0.016^{a}	0.077 ± 0.024^{b}	0.114 ± 0.018^{b}	Green, spicy
32.931	472-66-2	$C_{11}H_{18}O$	166	β-Homocyclocitral	0.077 ± 0.009^{a}	<LOQ ^{b}	<LOQ ^{b}	Cooling woody, camphor
33.134	6290-37-5	$C_{14}H_{20}O_2$	220	Phenethyl hexanoate	0.199 ± 0.019^{c}	0.279 ± 0.049^{b}	0.416 ± 0.009^{a}	Sweet, honey, floral
34.462	NIST#: 196695	$C_{13}H_{20}O$	192	1H-2-Indenone,2,4,5,6,7,7a-hexahydro-3-(1-methylethyl)-7a-methyl	<LOQ ^{b}	<LOQ ^{b}	0.406 ± 0.041^{a}	/
35.280	120-72-9	C_8H_7N	117	Indole	14.935 ± 1.281^{a}	11.255 ± 0.990^{b}	6.260 ± 1.066^{c}	Floral
35.739	6125-24-2	$C_8H_9NO_2$	151	2-Nitroethyl-benzene	3.588 ± 0.199^{a}	3.483 ± 0.130^{a}	<LOQ ^{b}	Floral, spicy
35.761	700-88-9	$C_{11}H_{14}$	146	Cyclopentylbenzene	<LOQ ^{b}	<LOQ ^{b}	2.508 ± 0.104^{a}	/

(Countinued)

TABLE 4 | (Countinued)

Retention time	CAS number	Molecular formula	Molecular weight	Name	Relative abundance%			Aroma properties
					BT0	BT1	BT2	
36.624	35845-67-1	$C_{13}H_{18}O$	190	3,6-Nonadien-5-one, 2,2,8,8-tetramethyl-	<LOQ ^{b}	<LOQ ^{b}	0.510 ± 0.030^{a}	/
38.889	30364-38-6	$C_{13}H_{16}$	172	Dehydro-ar-ionene	0.092 ± 0.003^{c}	0.176 ± 0.024^{b}	0.567 ± 0.041^{a}	Licorice
39.037	475-03-6	$C_{13}H_{18}$	174	α-Ionene	0.066 ± 0.001^{b}	0.067 ± 0.004^{b}	0.129 ± 0.007^{a}	Grassy
40.805	63435-25-6	$C_{13}H_{18}$	174	Benzene, 2-(2-butenyl)-1,3,5-trimethyl-	<LOQ ^{b}	<LOQ ^{b}	0.096 ± 0.003^{a}	/
40.963	31501-11-8	$C_{12}H_{22}O_2$	198	(Z)-3-Hexen-1-yl hexanoate	1.970 ± 0.077^{a}	1.461 ± 0.185^{b}	1.215 ± 0.056^{b}	Fruity, green
41.308	6378-65-0	$C_{12}H_{24}O_2$	200	Hexyl hexanoate	0.837 ± 0.035^{a}	0.681 ± 0.046^{b}	0.447 ± 0.032^{c}	Fresh cut grass
41.470	488-10-8	$C_{11}H_{16}O$	164	Jasmone	0.805 ± 0.047^{a}	0.917 ± 0.093^{a}	0.543 ± 0.088^{b}	Floral, jasmine, woody, herbal
42.615	87-44-5	$C_{15}H_{24}$	204	Caryophyllene	0.100 ± 0.007^{a}	0.091 ± 0.014^{a}	<LOQ ^{b}	Woody, spicy, clove
42.968	6901-97-9	$C_{13}H_{20}O$	192	α-Ionone	0.167 ± 0.019^{b}	0.195 ± 0.013^{ab}	0.214 ± 0.016^{a}	Floral
43.225	NIST#: 187519	$C_{13}H_{18}O$	190	4-(2,4,4-Trimethyl-cyclohexa-1,5-dienyl)-but-3-en-2-one	0.113 ± 0.010^{b}	0.306 ± 0.038^{a}	0.339 ± 0.009^{a}	/
43.968	103-52-6	$C_{12}H_{16}O_2$	192	β-Phenylethyl butyrate	0.352 ± 0.038^{a}	0.362 ± 0.047^{a}	0.338 ± 0.047^{a}	Sweet floral
44.550	3879-26-3	$C_{13}H_{22}O$	194	Neryl acetone	0.276 ± 0.031^{a}	0.242 ± 0.042^{a}	0.302 ± 0.029^{a}	Fatty, metallic
44.808	18794-84-8	$C_{15}H_{24}$	204	(E)-β-Famesene	0.774 ± 0.138^{a}	0.674 ± 0.082^{a}	0.781 ± 0.132^{a}	Woody
45.148	4602-84-0	$C_{15}H_{26}O$	222	Farnesol	<LOQ ^{b}	<LOQ ^{b}	0.135 ± 0.020^{a}	Mild fresh sweet
45.938	14901-07-6	$C_{13}H_{20}O$	192	β-Ionone	0.719 ± 0.072^{a}	0.818 ± 0.099^{a}	0.519 ± 0.020^{b}	Floral, woody
46.093	81968-62-9	$C_{15}H_{24}O$	220	(1R,7S,E)-7-Isopropyl-4,10-dimethylenecyclodec-5-enol	0.731 ± 0.111^{a}	<LOQ ^{b}	0.667 ± 0.025^{a}	/
46.310	7460-74-4	$C_{13}H_{18}O_2$	206	2-Phenylethyl valerate	0.540 ± 0.062^{a}	0.427 ± 0.077^{ab}	0.392 ± 0.036^{b}	Fruity, rose
46.784	13474-59-4	$C_{15}H_{24}$	204	trans-α-Bergamotene	0.553 ± 0.003^{a}	0.402 ± 0.144^{ab}	0.316 ± 0.032^{b}	Woody, warm, tea
47.000	6892-80-4	$C_{15}H_{26}O$	222	Widdrol	<LOQ ^{b}	<LOQ ^{b}	0.300 ± 0.060^{a}	/
47.173	25524-95-2	$C_{10}H_{16}O_2$	168	(Z)-7-Decen-5-olide	0.664 ± 0.082^{a}	<LOQ ^{b}	*<LOQ*^{b}	Creamy, jasmine
47.443	502-61-4	$C_{15}H_{24}$	204	α-Farnesene	3.635 ± 0.287^{a}	2.630 ± 0.222^{b}	2.112 ± 0.097^{c}	Herbal, citrus
50.173	40716-66-3	$C_{15}H_{26}O$	222	(E)-Nerolidol	16.85 ± 1.533^{a}	13.879 ± 1.656^{a}	7.859 ± 0.679^{b}	Floral

The same letter within each row indicates no significant difference ($P > 0.05$). LOQ is short for the limit of quantification.

glucose) and a free amino group, which generates an unstable Schiff base. It spontaneously cyclizes and undergoes the Amadori rearrangement, producing intermediates with highly reactive carbonyl groups, such as glyoxal and methylglyoxal (42). These products further react with free amino groups to form stable AGEs. Many AGEs are highly oxidant and pro-inflammatory, usually regarded as harmful to health (43). In this study, the baking process weakened the activity of TOTs in blocking the formation of AGEs in the BSA + glucose reaction system and the BSA + methylglyoxal reaction system, while hardly affecting that in the BSA + glyoxal reaction system (**Figures 3D–3F**). Earlier research indicated that catechins, including catechin (C), EC, ECG, EGC, and EGCG, could inhibit the formation of AGEs *via* scavenging reactive oxygen species (44). Sang et al. found that EGCG efficiently trapped reactive dicarbonyl compounds (methylglyoxal and glyoxal) to prevent the formation of AGEs (45). Besides catechins, several flavonols and flavones also had anti-AGEs activity. Quercetin, kaempferol, apigenin, and luteolin were proved to inhibit the formation of AGEs by trapping reactive dicarbonyls (46). A further study revealed that the hydroxyl groups at the 3′-, 4′-, 5-, and 7-positions affected the inhibitory activity (47). Although the contents of catechins decreased, the contents of several flavonols and flavones were increased after baking (**Figure 2**). It might explain why the anti-AGEs activity was hardly reduced in the BSA + glyoxal reaction system.

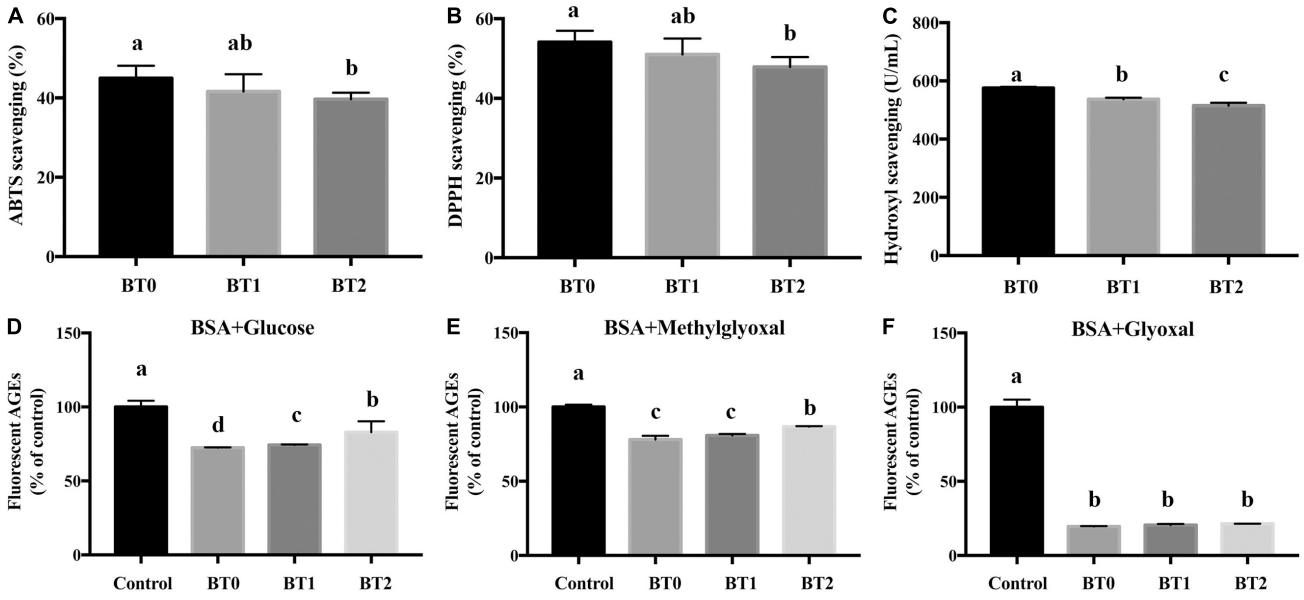

G

	Concentration (mg/mL)	0	0.25	0.5	1	2
Salmonella typhi	BT0	+	+	+	+	-
	BT1	+	+	+	+	-
	BT2	+	+	+	+	+
Shigella flexneri	BT0	+	+	+	+	+
	BT1	+	+	+	+	+
	BT2	+	+	+	+	+
β-hemolytic Streptococcus	BT0	+	+	+	-	-
	BT1	+	+	+	+	-
	BT2	+	+	+	+	-
Staphylococcus aureus	BT0	+	+	+	-	-
	BT1	+	+	+	-	-
	BT2	+	+	+	+	-
Escherichia coli	BT0	+	+	+	+	+
	BT1	+	+	+	+	+
	BT2	+	+	+	+	+

FIGURE 3 | Bioactivities of jade (BT0), medium baked (BT1), and deep baked (BT2) *Tieguanyin* oolong teas. **(A)** ABTS scavenging activity; **(B)** DPPH scavenging activity; **(C)** hydroxyl scavenging activity; relative fluorescent AGEs formation in the bovine serum albumin (BSA) + glucose system **(D)**, BSA + methylglyoxal system **(E)**, and BSA + glyoxal system **(F)**; **(G)** minimum inhibitory concentrations of the three tea extracts against five bacteria. "+" means visible growth of the bacteria, while "–" means no visible bacterial growth. The same letter within each column indicates no significant difference ($P > 0.05$).

The effects of baking on antibacterial activity are disadvantageous (**Figure 3G**). The MIC is the lowest concentration of a substance which prevents the visible growth of a bacterium or bacteria. A substance with low MICs is considered an effective antimicrobial agent. Compared with BT2, the MICs of BT0 and BT1 against *S. typhi* and *S. aureus* were lower, respectively. The MIC of BT0 against β-hemoly*tic Streptococcus* was lower than the MIC of BT1. The results indicated that the baking process attenuated the inhibition of TOTs against certain bacteria. Chou et al. proved that oolong tea had inhibitory effects on several micro-organisms (48). Monomeric polyphenols, which had a high affinity to proteins, were regarded as active antibacterial compounds (49). Some volatiles also displayed antibacterial activity, and there were synergistic interactions among specific volatiles. α-Pinene was capable of suppressing *S. aureus* (50). Indole, the second most abundant volatile in BT0, inhibited *Streptococcus mutans*. The combination of β-caryophyllene or δ-cadinene enhanced the inhibitory effects of indole against bacteria (51). The contents of monomeric catechins and the volatiles mentioned above (e.g., indole, α-pinene, and caryophyllene) were decreased after baking. The change was in accordance with the reduced antibacterial activity of BT1 and BT2. It implied that the loss of monomeric catechins and some volatiles during the baking process might be responsible for the baking-mediated decreased antibacterial activity of TOT.

CONCLUSION

This study assessed and compared the chemical composition, sensory quality, and bioactivity of three TOTs with different baking degrees. According to the results, the baking process dramatically modified the chemical composition of TOTs, particularly in catechins, amino acids, and volatiles. The baking-induced changes of chemical components led to the darkened color of tea infusion, roast aroma, and enhanced sweet aftertaste. Since many flavor components are also bioactive components, the changes of chemical components also affected bioactivity. Adverse impacts of the baking process on the free radical scavenging activity and antibacterial activity were observed, probably due to the decrease of monomeric catechins. The results obtained herein fill the gap on the effects of the baking process of oolong tea and indicate that the baking process might be a double-edged sword, which enriches the flavor while attenuating the bioactivity. Future studies can focus on exploring the superior bioactivity of baked TOTs and developing processing technologies of TOTs that retain the typical sensory quality of baked TOTs but with less loss of bioactive components.

DATA AVAILABILITY STATEMENT

The raw data supporting the conclusions of this article will be made available by the authors, without undue reservation.

AUTHOR CONTRIBUTIONS

YG, J-FY, and Y-QX conceived and designed the experiments. YG, Q-QC, FW, J-XC, X-BZ, and Y-QX performed the experiments. YG, Q-QC, Y-HC, and J-QW analyzed the data. YG and DG wrote the manuscript. All authors have read and agreed to the final version of the manuscript.

FUNDING

This research was supported by the National Natural Science Foundation of China (31872709), the Central Level, Scientific Research Project (Y2021CG06), the China Agriculture Research System of MOF and MARA (CARS-19), and the Innovation Project for the Chinese Academy of Agricultural Sciences.

REFERENCES

1. Xu YQ, Liu PP, Shi J, Gao Y, Wang QS, Yin JF. Quality development and main chemical components of Tieguanyin oolong teas processed from different parts of fresh shoots. *Food Chem.* (2018) 249:176–83. doi: 10.1016/j.foodchem.2018.01.019
2. Feng TQ. Comparison of Jade oolong tea and deep baked oolong tea. *China Tea.* (2005) 5:18–9.
3. Wen W. *The Research on Quality Chemistry and Anti-Inflammatory of Anxi Tieguanyin Tea*. Changsha: Hunan Agricultural University (2018).
4. Zhang J, Cui H, Xue J, Wang W, Wang W, Le T, et al. Adsorption equilibrium and thermodynamics of tea theasinensins on HP20-A high-efficiency macroporous adsorption resin. *Foods.* (2021) 10:2971. doi: 10.3390/foods10122971
5. Hua J, Wang H, Yuan H, Yin P, Wang J, Guo G, et al. New insights into the effect of fermentation temperature and duration on catechins conversion and formation of tea pigments and theasinensins in black tea. *J Sci Food Agric.* (2021) 102:2750–60. doi: 10.1002/jsfa.11616
6. Wang JQ, Fu YQ, Chen JX, Wang F, Feng ZH, Yin JF, et al. Effects of baking treatment on the sensory quality and physicochemical properties of green tea with different processing methods. *Food Chem.* (2022) 380:132217. doi: 10.1016/j.foodchem.2022.132217
7. Narukawa M, Noga C, Ueno Y, Sato T, Misaka T, Watanabe T. Evaluation of the bitterness of green tea catechins by a cell-based assay with the human bitter taste receptor hTAS2R39. *Biochem Biophys Res Commun.* (2011) 405:620–5. doi: 10.1016/j.bbrc.2011.01.079
8. Lv HP, Liang MZ, Zhang Y, WAng LB, Lin Z. Major chemical components and antioxidant activity in tea infusion of tea products obtained from the special tea germplasm 'Zijuan' using different processing technologies. *Food Sci*. (2016) 37:122–7.
9. Wang L, Guan XQ, Yu NH, Lin ZQ, Zhang YL. Effect of different baking degree on antioxidant activity and quality of Wuyi rock tea. *Food Sci Technol.* (2020) 45:68–74.
10. Zhu YM, Dong JJ, Jin J, Liu JH, Zheng XQ, Lu JL, et al. Roasting process shaping the chemical profile of roasted green tea and the association with aroma features. *Food Chem.* (2021) 353:129428. doi: 10.1016/j.foodchem.2021.129428
11. Gao Y, Wang JQ, Fu YQ, Yin JF, Shi J, Xu YQ. Chemical composition, sensory properties and bioactivities of *Castanopsis* lamontii buds and mature leaves. *Food Chem*. (2020) 316:126370. doi: 10.1016/j.foodchem.2020.126370
12. Roberts EAH, Smith RF. Spectrophotometric measurements of theaflavins and thearubigins in black tea liquors in assessments of quality in teas. *Analyst.* (1961) 86:94–8. doi: 10.1039/an9618600094
13. Xu YQ, Hu XF, Tang P, Jiang YW, Yuan HB, Du QZ, et al. The major factors influencing the formation of sediments in reconstituted green tea infusion. *Food Chem.* (2015) 172:831–5. doi: 10.1016/j.foodchem.2014.09.143
14. Liu PP, Yin JF, Chen GS, Wang F, Xu YQ. Flavor characteristics and chemical compositions of oolong tea processed using different semi-fermentation times. *J Food Sci Technol.* (2018) 55:1185–95. doi: 10.1007/s13197-018-3034-0
15. Xu YQ, Chen JX, Du QZ, Yin JF. Improving the quality of fermented black tea juice with oolong tea infusion. *J Food Sci Technol.* (2017) 54:3908–16. doi: 10.1007/s13197-017-2849-4
16. Xu YQ, Gao Y, Granato D. Effects of epigallocatechin gallate, epigallocatechin and epicatechin gallate on the chemical and cell-based antioxidant activity, sensory properties, and cytotoxicity of a catechin-free model beverage. *Food Chem.* (2021) 339:128060. doi: 10.1016/j.foodchem.2020.128060
17. Re R, Pellegrini N, Proteggente A, Pannala A, Yang M, Rice-Evans C. Antioxidant activity applying an improved ABTS radical cation decolorization assay. *Free Radic Biol Med.* (1999) 26:1231–7. doi: 10.1016/s0891-5849(98)00315-3
18. Li XM, Deng RH, Kong YH, Xia QQ, Lv LS. Inhibitory effect of rutin on the formation of advanced glycation end products (AGEs) from bovine serum albumin. *Food Sci.* (2014) 35:85–9.
19. Eloff JN. A sensitive and quick microplate method to determine the minimal inhibitory concentration of plant extracts for bacteria. *Planta Med.* (1998) 64:711–3. doi: 10.1055/s-2006-957563
20. Zhang L. *Effects of Baking Technics on the Quality of Wuyi Rock-Essence Tea*. Chongqing: Southwest Universiy (2018).
21. Lin YP, Liu SB, Huang YB, Zhan SQ, Zhang JM, Chen RB. Effect of baking degrees on the quality of Wuyi Rock Tea "Dahongpao". *Food Res Dev.* (2020) 41:49–54.
22. Lin ST, Hao GX, Long M, Lai F, Li QQ, Xiong YM, et al. Oyster (Ostrea plicatula Gmelin) polysaccharides intervention ameliorates cyclophosphamide-Induced genotoxicity and hepatotoxicity in mice via the Nrf2-ARE pathway. *Biomed Pharmacother.* (2017) 95:1067–71. doi: 10.1016/j.biopha.2017.08.058

23. Passos CP, Costa RM, Ferreira SS, Lopes GR, Cruz MT, Coimbra MA. Role of coffee caffeine and chlorogenic acids adsorption to polysaccharides with impact on brew immunomodulation effects. *Foods.* (2021) 10:378. doi: 10.3390/foods10020378
24. Zhu K, Ouyang J, Huang J, Liu Z. Research progress of black tea thearubigins: a review. *Crit Rev Food Sci Nutr.* (2021) 61:1556–66. doi: 10.1080/10408398.2020.1762161
25. Cao QQ, Zou C, Zhang YH, Du QZ, Yin JF, Shi J, et al. Improving the taste of autumn green tea with tannase. *Food Chem.* (2019) 277:432–7. doi: 10.1016/j.foodchem.2018.10.146
26. Jiang H, Zhang MT, Wang DX, Yu F, Zhang N, Song CK, et al. Analytical strategy coupled to chemometrics to differentiate *Camellia* sinensis tea types based on phenolic composition, alkaloids, and amino acids. *J Food Sci.* (2020) 85:3253–63. doi: 10.1111/1750-3841.15390
27. Lindenmeier M, Faist V, Hofmann T. Structural and functional characterization of pronyl-lysine, a novel protein modification in bread crust melanoidins showing in vitro antioxidative and phase I/II enzyme modulating activity. *J Agr Food Chem.* (2002) 50:6997–7006. doi: 10.1021/jf020618n
28. Jiang D, Peterson DG. Identification of bitter compounds in whole wheat bread. *Food Chem.* (2013) 141:1345–53. doi: 10.1016/j.foodchem.2013.03.021
29. Xiang LW, Chen WT. Effects of Maillard reaction on the quality of oolong tea. *Chem Eng Equipment.* (2012) 7:13–7.
30. Li H. *Study on the Formation Pathway and Regulation Mechanism of Main Bitter Compounds in Maillard Reaction*. Guangzhou: South China University of Technology (2019).
31. Guo X, Ho CT, Schwab W, Wan X. Effect of the roasting degree on flavor quality of large-leaf yellow tea. *Food Chem.* (2021) 347:129016. doi: 10.1016/j.foodchem.2021.129016
32. Cao QQ, Fu YQ, Wang JQ, Zhang L, Wang F, Yin JF, et al. Sensory and chemical characteristics of Tieguanyin oolong tea after roasting. *Food Chem X.* (2021) 12:100178. doi: 10.1016/j.fochx.2021.100178
33. Wang W, Jin S, Guo Y. Exploration of a method of distinguishing different nongxiang tieguanyin tea grades based on aroma determined by GC-MS combined with chemometrics. *Molecules.* (2019) 24:1707. doi: 10.3390/molecules24091707
34. Dzib-Guerra WD, Escalante-Erosa F, Garcia-Sosa K, Derbre S, Blanchard P, Richomme P, et al. Anti-advanced glycation end-product and free radical scavenging activity of plants from the Yucatecan Flora. *Pharmacognosy Res.* (2016) 8:276–80. doi: 10.4103/0974-8490.188883
35. Starowicz M, Zielinski H. Inhibition of advanced glycation end-product formation by high antioxidant-leveled spices commonly used in European Cuisine. *Antioxidants (Basel).* (2019) 8:100. doi: 10.3390/antiox8040100
36. Wang Y, Kong D, Gao Y, Ying L, Huang Q, Xu P. Chemical characterization and bioactivity of phenolics from Tieguanyin oolong tea. *J Food Biochem.* (2019) 43:e12894. doi: 10.1111/jfbc.12894
37. Su XG, Duan J, Jiang YM, Duan XW, Chen F. Polyphenolic profile and antioxidant activities of oolong tea infusion under various steeping conditions. *Int J Mol Sci.* (2007) 8:1196–205. doi: 10.3390/i8121196
38. Guo Q, Zhao B, Shen S, Hou J, Hu J, Xin W. ESR study on the structure-antioxidant activity relationship of tea catechins and their epimers. *Biochim Biophys Acta.* (1999) 1427:13–23. doi: 10.1016/s0304-4165(98)00168-8
39. Lee LS, Kim SH, Kim YB, Kim YC. Quantitative analysis of major constituents in green tea with different plucking periods and their antioxidant activity. *Molecules.* (2014) 19:9173–86. doi: 10.3390/molecules19079173
40. Guo Q, Zhao B, Li M, Shen S, Xin W. Studies on protective mechanisms of four components of green tea polyphenols against lipid peroxidation in synaptosomes. *Biochim Biophys Acta.* (1996) 1304:210–22. doi: 10.1016/s0005-2760(96)00122-1
41. Nowotny K, Schroter D, Schreiner M, Grune T. Dietary advanced glycation end products and their relevance for human health. *Ageing Res Rev.* (2018) 47:55–66. doi: 10.1016/j.arr.2018.06.005
42. Popova EA, Mironova RS, Odjakova MK. Non-enzymatic glycosylation and deglycating enzymes. *Biotechnol Biotechnol Equipment.* (2010) 24:1928–35. doi: 10.2478/v10133-010-0066-7
43. Uribarri J, Woodruff S, Goodman S, Cai W, Chen X, Pyzik R, et al. Advanced glycation end products in foods and a practical guide to their reduction in the diet. *J Am Diet Assoc.* (2010) 110:911–6. doi: 10.1016/j.jada.2010.03.018
44. Wu CH, Yen GC. Inhibitory effect of naturally occurring flavonoids on the formation of advanced glycation endproducts. *J Agric Food Chem.* (2005) 53:3167–73. doi: 10.1021/jf048550u
45. Sang S, Shao X, Bai N, Lo CY, Yang CS, Ho CT. Tea polyphenol (-)-epigallocatechin-3-gallate: a new trapping agent of reactive dicarbonyl species. *Chem Res Toxicol.* (2007) 20:1862–70. doi: 10.1021/tx700190s
46. Ronsisvalle S, Panarello F, Longhitano G, Siciliano EA, Montenegro L, Panico A. Natural flavones and flavonols: relationships among antioxidant activity, glycation, and metalloproteinase inhibition. *Cosmetics.* (2020) 7:71. doi: 10.3390/cosmetics7030071
47. Matsuda H, Wang T, Managi H, Yoshikawa M. Structural requirements of flavonoids for inhibition of protein glycation and radical scavenging activities. *Bioorg Med Chem.* (2003) 11:5317–23. doi: 10.1016/j.bmc.2003.09.045
48. Chou CC, Lin LL, Chung KT. Antimicrobial activity of tea as affected by the degree of fermentation and manufacturing season. *Int J Food Microbiol.* (1999) 48:125–30. doi: 10.1016/s0168-1605(99)00034-3
49. Sasaki H, Matsumoto M, Tanaka T, Maeda M, Nakai M, Hamada S, et al. Antibacterial activity of polyphenol components in oolong tea extract against *Streptococcus* mutans. *Caries Res.* (2004) 38:2–8. doi: 10.1159/000073913
50. Raman A, Weir U, Bloomfield SF. Antimicrobial effects of tea-tree oil and its major components on *Staphylococcus* aureus, Staph. epidermidis and Propionibacterium acnes. *Lett Appl Microbiol.* (1995) 21:242–5. doi: 10.1111/j.1472-765x.1995.tb01051.x
51. Muroi H, Kubo I. Combination effects of antibacterial compounds in green tea flavor against *Streptococcus* mutans. *J Agr Food Chem.* (1993) 41:1102–5. doi: 10.1021/jf00031a017

Conflict of Interest: The authors declare that the research was conducted in the absence of any commercial or financial relationships that could be construed as a potential conflict of interest.

frontiers | Frontiers in Nutrition

ORIGINAL RESEARCH
published: 19 May 2022
doi: 10.3389/fnut.2022.884400

Widely Targeted Metabolomics Analysis of the Changes to Key Non-volatile Taste Components in *Stropharia rugosoannulata* Under Different Drying Methods

*Yi Liu[1,2,3], Fangbo Meng[1], Pengyu Tang[1], Daomei Huang[1], Qixing Li[1] and Mao Lin[1,3]**

[1] Institute of Agricultural Products Processing, Guizhou Academy of Agricultural Sciences, Guiyang, China, [2] Guizhou Vocational College of Foodstuff Engineering, Guiyang, China, [3] Guizhou Characteristic Food Technology Co., Ltd, Guiyang, China

OPEN ACCESS

Edited by:
Jinkai Zheng, Institute of Food Science and Technology (CAAS), China

Reviewed by:
Jinping Gu, Zhejiang University of Technology, China
Tao Feng, Shanghai Institute of Technology, China

***Correspondence:**
Mao Lin
linmao520132@163.com

Specialty section:
This article was submitted to Food Chemistry, a section of the journal Frontiers in Nutrition

Received: *26 February 2022*
Accepted: *11 April 2022*
Published: *19 May 2022*

Citation:
Liu Y, Meng F, Tang P, Huang D, Li Q and Lin M (2022) Widely Targeted Metabolomics Analysis of the Changes to Key Non-volatile Taste Components in Stropharia rugosoannulata Under Different Drying Methods. Front. Nutr. 9:884400. doi: 10.3389/fnut.2022.884400

Stropharia rugosoannulata is an extremely perishable edible fungi product, and drying can delay its deterioration, however, drying will affect its flavor, especially the non-volatile taste substances dominated by amino acids, nucleotides, organic acids and carbohydrates. Currently, which drying method is the most suitable for the drying of *S. rugosoannulata* remains unknown, we need to fully consider the economic efficiency of the method and the impact on flavor. But we have limited comprehensive knowledge of the changed non-volatile taste metabolites as caused by drying processes. Here, an LC-MS/MS-based widely targeted metabolome analysis was conducted to investigate the transformation mechanism of *S. rugosoannulata* non-volatile taste components after undergoing hot air drying (HAD), vacuum freeze drying (VFD), and microwave vacuum drying (MVD). A total of 826 metabolites were identified, 89 of which—48 amino acids, 25 nucleotides, 8 organic acids, and 8 carbohydrates—were related to non-volatile taste. The drying method used and the parts of *S. rugosoannulata* (stipe and pileus) influenced the differences found in these metabolites. The possible mechanisms responsible for such chemical alterations by different drying methods were also investigated by a Kyoto Encyclopedia of Genes and Genomes (KEGG) pathway analysis. Amino acid metabolism (alanine, aspartate, and glutamate metabolism; glycine, serine, and threonine metabolism; arginine and proline metabolism; valine, leucine, and isoleucine biosynthesis) was the main metabolic pathway involved. Pathway enrichment analysis also identified differences in non-volatile taste components among three drying methods that may be closely related to the applied drying temperature. Altogether, the results indicated that as an economical and convenient drying method, HAD is conducive to improving the flavor of *S. rugosoannulata* and thus it harbors promising potential for practical applications.

Keywords: drying methods, formation mechanism, non-volatile taste components, stropharia rugosoannulata, widely targeted metabolomics

INTRODUCTION

Stropharia rugosoannulata is a precious edible mushroom that has been widely cultivated in many countries, but especially in Southwest China (1). Several studies reported that *S. rugosoannulata* harbors various proteins, polysaccharides, phenols, mineral elements (2) in addition to several bioactive compounds whose benefits include antioxidant (3), antitumor (4), anti-diabetic (5), anti-viral (6) properties, and so forth. In addition, there are some non-volatile flavor components, such as free amino acids, organic acids, nucleotides, which can produce an umami taste that is among the most prominent characteristics of mushrooms (7). In recent years, because of its texture, rich nutrition, and unique flavor, it has quickly become one of the world's best-selling mushrooms (2).

However, fresh *S. rugosoannulata* are prone to rapid spoilage and deterioration due to microbial and physical factors, causing incalculable damage to its economic value (8). Among the various techniques used to extend its shelf-life, dehydration is the most effective preservation method for this prized mushroom (9). The three main dehydration methods are hot air drying (HAD), vacuum freeze drying (VFD), and microwave vacuum drying (MVD), which are now the most popular dehydration techniques applied to mushrooms (10). However, drying can effect the taste components, appearance, and nutrients of the mushrooms (11). We should therefore fully consider both practical and economic aspects when choosing a suitable drying method for *S. rugosoannulata.*

Because of its easy operation and low cost, HAD is the most frequently applied mode of preservation worldwide (12). As pointed out by many researchers, exposure to higher temperatures can induce the Maillard reaction and thereby affect flavor compounds (13). For example, HAD technology can enhance the umami taste of mushrooms by increasing the content of organic acids (14) and amino acids (15, 16). However, a heat treatment that lasts too long can seriously damage other characteristic flavor substances and concentration of key nutrients of the dried mushroom (14, 15).

Compared with HAD, VFD can minimize degradation of the mushrooms' distinctive aroma (17, 18). However, due to its energy consumption, the promotion of the VFD technique is generally a problem (19). VFD can maintain the good appearance and nutritional value of mushrooms (20), and MVD has the greater capacity to produce more amino acids (9). However, the differential changes in nutrients and taste chemicals of mushrooms caused by HAD, VFD, and WVD remain largely unexplored,and there are few reports on the effects of drying on non-volatile taste compounds and metabolites in *S. rugosoannulata.*

In recent years, widely targeted metabolomics has been applied to the field of non-volatile compounds and nutrients in food (21). This technique combines the advantage of non-target and target metabolite detection technologies, thereby achieving high throughput while exhibiting high sensitivity and wide coverage of detection of metabolites in foods and plants (22). Zou et al. (23)used this technique to research the key taste components in two wild edible *Boletus* mushrooms. Therefore, we considered that widely targeted metabolomics could be applied to the comprehensive detection and analysis of nutrients and non-volatile taste components in *S. rugosoannulata* mushrooms.

The aim of this study was to better understand the changes in each category of main non-volatile taste metabolites of *S. rugosoannulata* in response to different drying methods. To do this, we used ultra performance liquid chromatography–tandem mass spectrometry (UPLC–MS/MS) combined with a widely targeted metabolomics technology to detect the non-volatile metabolites, including amino acids, nucleotides, organic acids, and sugars. Further, possible metabolic pathways were predicted through the transformation of metabolites. We anticipate our results will provide a theoretical reference and objective basis for the formation mechanism of the umami taste in dried mushrooms of *S. rugosoannulata* and perhaps similar ones.

MATERIALS AND METHODS

Raw Material

Stropharia rugosoannulata was collected in April 2021 from the Horticultural Institute of Guizhou (106°39′59″N, 26°30′20″E). All samples were immediately transferred to the lab for their pretreatment: surface mud and stipe root were wiped off.

Drying Methods

Microwave Vacuum Drying

Roughly 2,000 *g* of samples were dried inside the Sort Cleverly Inactive Microwave Vacuum Dryer (XINQI, Guiyang, Guizhou, China) with three progressive methods, as follows: Method 1, MW control was 2000 W for 30 min; Method 2, Mw control was 1000 W for 10 min; Method3, Mw control was 500 W for 10 min.

Hot Air Drying

The samples were spread on plates and these placed in a drying chambers (HT-KRZH-1IV Drier, Languanda, Guiyang, Guizhou, China)with modified humidifying and warming treatments applied as follows: Strategy 1, temperature of 55°C and 50% humidity for 6 h; Strategy 2, temperature of 45°C and 40% humidity for 8 h; Strategy 3, temperature of 35°C and 30%humidity for 12 h.

Vacuum Freeze Drying

The samples were quick-frozen at –40°C within the TDE400 ultra cold capacity freezer (ThermoFisher Logical, Beijing, China). Their solidification was halted after 12 h, then the pre-frozen tests were spread on plates and dried by a FD-1D-50 Vaccum Solidify Drier (BIOCOOL, Beijing, China).

Metabolites Analysis

Metabolites' Extraction

The freeze-dried samples were fragmented in a blender run for 30 s at 60 Hz. Then a 50-mg aliquot of individual samples were exactly weighed and put into an Eppendorf tube, after expansion of 700 μL of extricate arrangement (methanol/water = 3:1, precooled at –40°C, containing an internal standard). After 30 s of vortexing, the tests were homogenized at 40 Hz for 4 min and sonicated for 5 min in an ice-water shower. They were homogenized and sonicated again (three times), after which the

samples were extricated overnight at 4°C on a shaker. Next, they were centrifuged at 13,800 × *g* for 15 min at 4°C. The supernatant was carefully filtered through a 0.22 μm microporous membrane, then the resulting supernatants were diluted 20 times with extract solution containing internal standard and vortexed for 30 s and transferred to 2 mL glass vials, and take 30 μL from each sample and pooling as QC samples. Store at –80°C until the ultra performance liquid chromatography-tandem mass spectrometry (UHPLC-MS) analysis.

Ultra Performance Liquid Chromatography-Tandem Mass Spectrometry Analysis

The UHPLC separation was carried out using an EXIONLC System (Sciex Technologies, Framinghan, MA, United States). The mobile phase A was 0.1% formic acid in water, and the mobile phase B was acetonitrile. The column temperature was set to 40°C. The auto-sampler temperature was set at 4°C and the injection volume was 2 μ L.

A Sciex QTrap 6500 + LC-MS/MS system (Sciex Technologies, Framinghan, MA, United States) was used for the assay development. Typical ion source parameters were as follows: ionspray voltage: +5,500/–4,500 V, curtain gas: 35 psi, temperature: 400°C, ion source gas 1:60 psi, ion source gas 2: 60 psi, DP: ± 100 V.

MS Data and Statistical Analysis

SCIEX Analyst Work Station software (v1.6.3) (Sciex Technologies, Framinghan, MA, United States). was employed for the MRM data acquisition and processing. The MS raw data (.wiff) files were converted into the TXT format, using MSconventer. R program and database were applied to obtain peak detections and to carry out their annotation. The quantitative analysis of metabolites was performed using MRM analysis of QQQ mass spectrometry. After obtaining metabolite mass spectrometry data of different samples, peak area integration was performed on the mass spectrum peaks of all the substances, and the mass spectrum peaks of the same metabolite in different samples were integrated for correction.

The SIMCA (V16.0.2, Satorious Stedim Data Analytics AB, Umea, Sweden) software is used to perform Par format processing on the data, and then conduct automatic modeling and analysis to form PCA model In this project. We screened differential metabolites of *S. rugosoannulata* using the p-value of student's test is less than 0.05, and the threshold variable importance in projection (VIP) value (VIP $\geq$ 1) from the OPLS-DA model. The screening of different metabolites was visualized in the figure of the volcano plot. KEGG were used for enrichment analysis of differential metabolites and finding metabolic pathways.

RESULTS AND DISCUSSION

Metabolites Under Different Drying Methods of *Stropharia rugosoannulata*

To investigate the chemical composition profile in the stipe and pileus of *S. rugosoannulata* under different drying methods, the metabolites were identified by LC-MS/MS analysis. The overlay analysis of the QC-TIC diagram (**Figure 1A**) and the sample multi-peak detection of QC-EIC diagram (**Figure 1B**) showed that the obtained data had robust reliability and repeatability. As **Figure 1C** shows, we carried out a principal components analysis (PCA) on metabolites. Whether left fresh or treated with different drying methods, the pileus samples are positioned on the upper side of the figure, while those of stipe are on the bottom. This result indicates that pileus and stipe metabolites are quite different chemically. Similar observations were reported previously (2). Furthermore, samples of different treatments are located separately in the figure, indicating that the drying methods can affect the metabolites in *S. rugosoannulata*.

As seen in **Figure 1D**, 826 metabolites were divided into 25 classes, including 123 alkaloids,105 ketones, 63 phenols, 48 amino acids and derivatives, 30 benzenes, 29 fatty acyl class, 26 sesquiterpenes, 25 nucleotides and derivatives, 25 diterpenes, 20 triterpenes and triazines, 18 cumarins, 17 monoterpenes, 13 organic compounds, 10 anthraquinones, 9 aromatic compounds, 9 phytohormones, 9 lignans, 8 carbohydrate and derivatives, 8 organic acids and derivatives, 8 pyridines, 6 ketone acid and derivatives, 4 vitamins, 3 pyrimidine nucleosides, 3 purine nucleosides, and others. The main metabolites of *S. rugosoannulata* were differentially changed by the drying mode, including alkaloids, phenols, as well as some non-volatile flavor substances.

Key Non-volatile Taste Components Under Different Drying Methods of *Stropharia rugosoannulata*

To clarify the influence of drying methods on *S. rugosoannulata*'s non-volatile taste compounds, we focused on classes of metabolites likely to be major contributors to umami taste. In **Figure 2** are heat maps presenting the main components that affect umami taste, including amino acids and their derivatives, nucleotides and their derivatives, organic acids and their derivatives, carbohydrate and derivatives. These results are described below.

Amino Acids and Their Derivatives

This study detected 48 amino acids and their derivatives. As evinced by **Figure 2A**, their total amounts in stipe followed this trend in rank: HAD-S > F-S > MVD-S > VFD-S, which differed from that for pileus: HAD-P > MVD-P > VFD-P > F-P. Amino acids are one of the most important taste active compounds in mushrooms. Based on their taste characteristics, amino acids are chiefly divided into umami, sweet, bitter, and tasteless categories (24). We found greater quantities of 27 amino acids and their derivatives in stipe after HAD than either MVD or VFD, and likewise for 24 of them in pileus. In particular, the L-aspartic acid, L-glutamic acid, L-lysine, L-glutamine, L-threonine, L-serine, L-histidine, L-valine, and L-methionine content of the stipe and pileus after undergoing HAD are higher vis-à-vis MVD and VFD. Similar results were found in two previous studies (10, 14). Asp and Glu are typical MSG-like components in edible fungi, Thr and Ser are sweet components, and Val and Leu are bitter components (25). Our results show that hot air drying can improve both umami and sweet amino acids, but at the same

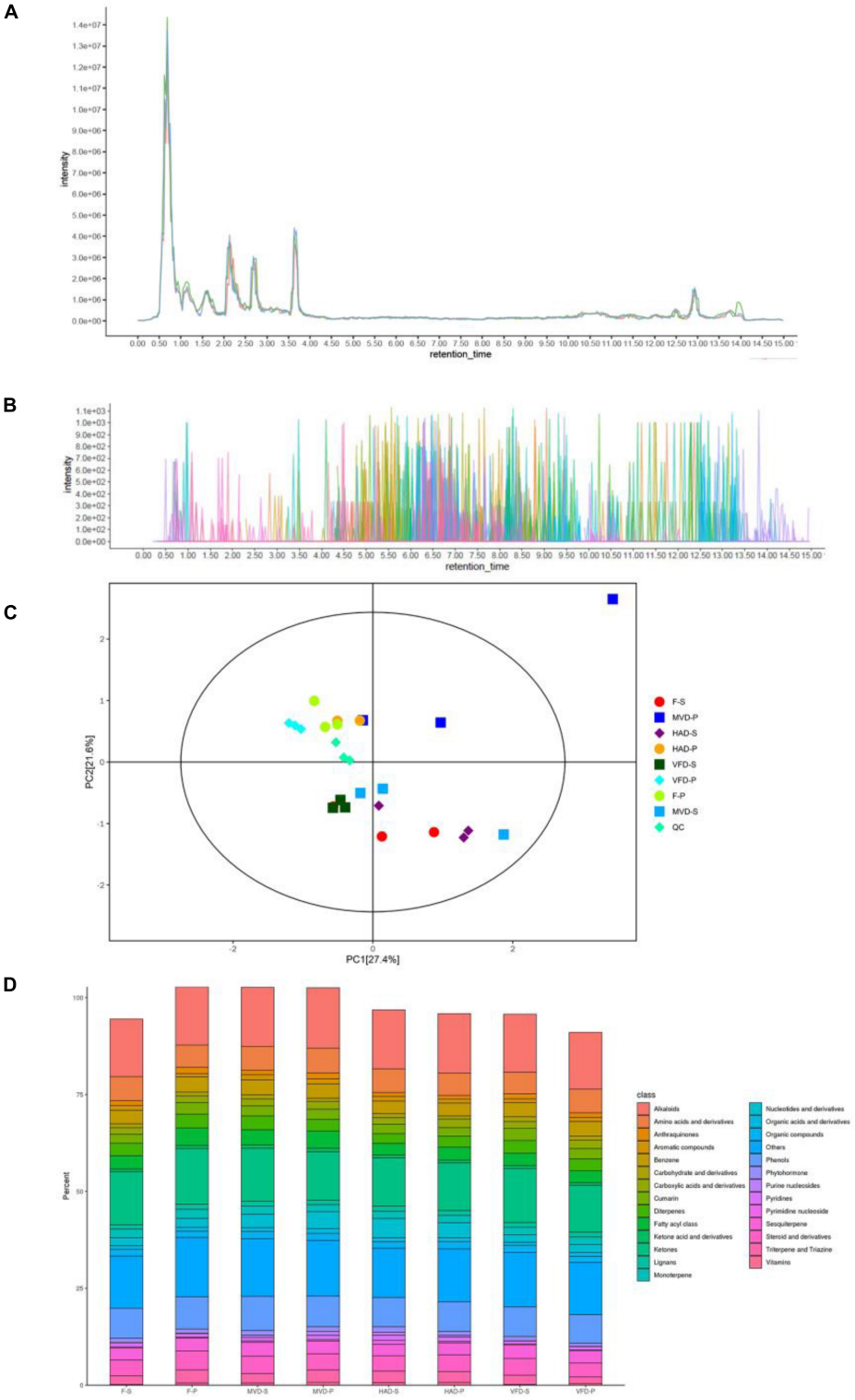

FIGURE 1 | (A) Total ion current of one quality control sample as revealed by mass spectrometry detection, and **(B)** a multi-peak detection plot of the sample metabolites in the multiple reaction monitoring mode. **(C)** PCA analysis of metabolites identified from the stipe and pileus of *S. rugosoannulata* mushrooms subjected to different drying methods. **(D)** Relative content of principal components. F-S, fresh stipe; F-P, fresh pileus; MVD-S, microwave vacuum drying of stipe; MVD-P, microwave vacuum drying of pileus; HAD-S, hot air drying of stipe; HAD-P, hot air drying of pileus; VFD-S, vacuum freeze drying of stipe; VFD-P, vacuum freeze drying of pileus.

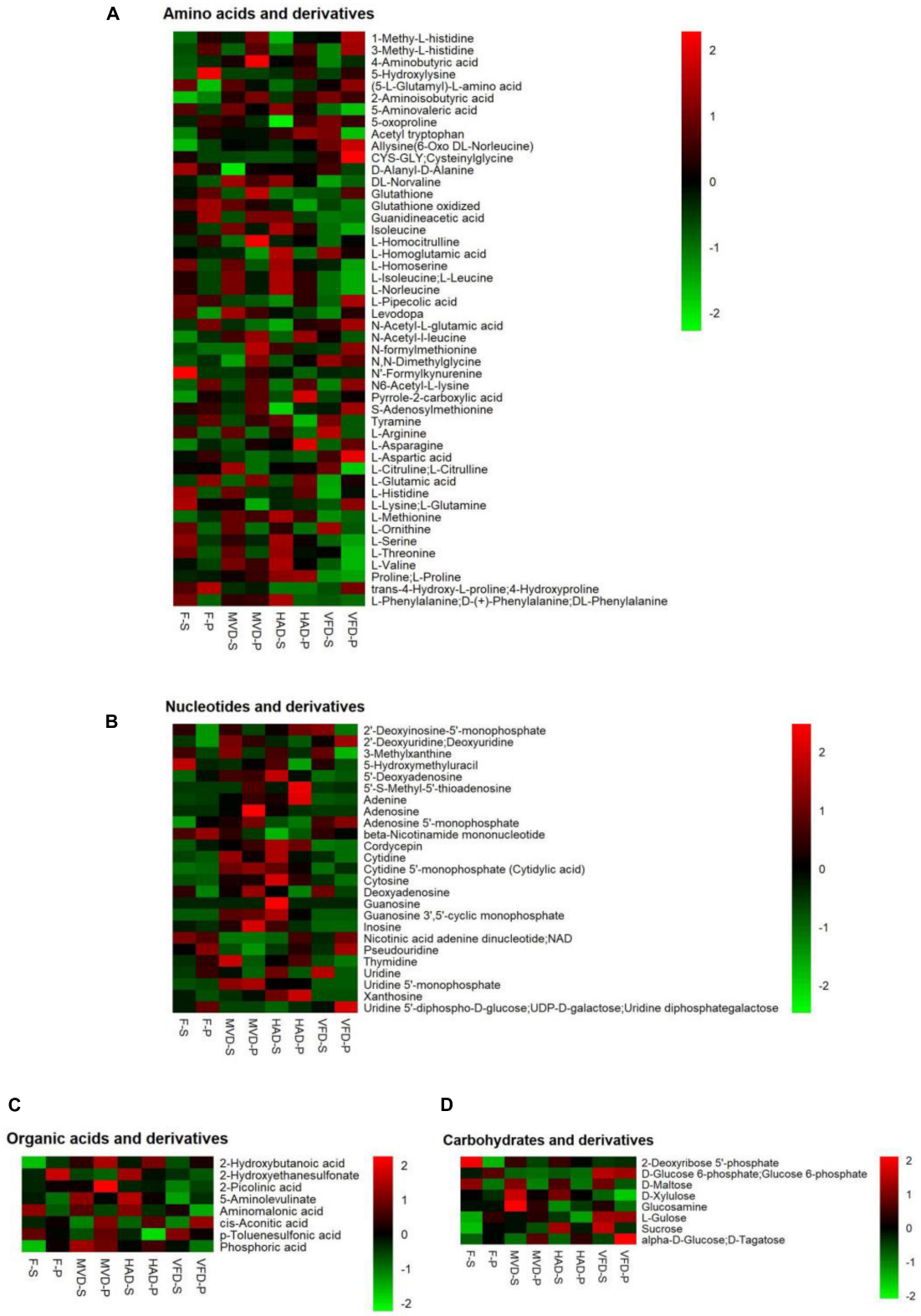

FIGURE 2 | Heat maps of the levels of the non-volatile metabolites under different drying methods. The abscissa represents different experimental groups, the ordinate represents the different metabolites compared by the group. The color indicates the relative expression of metabolites, from low (green) to high (red). **(A)** Amino acids and their derivatives, **(B)** nucleotides and their derivatives, **(C)** organic acid and their derivatives, and **(D)** carbohydrates and derivatives.

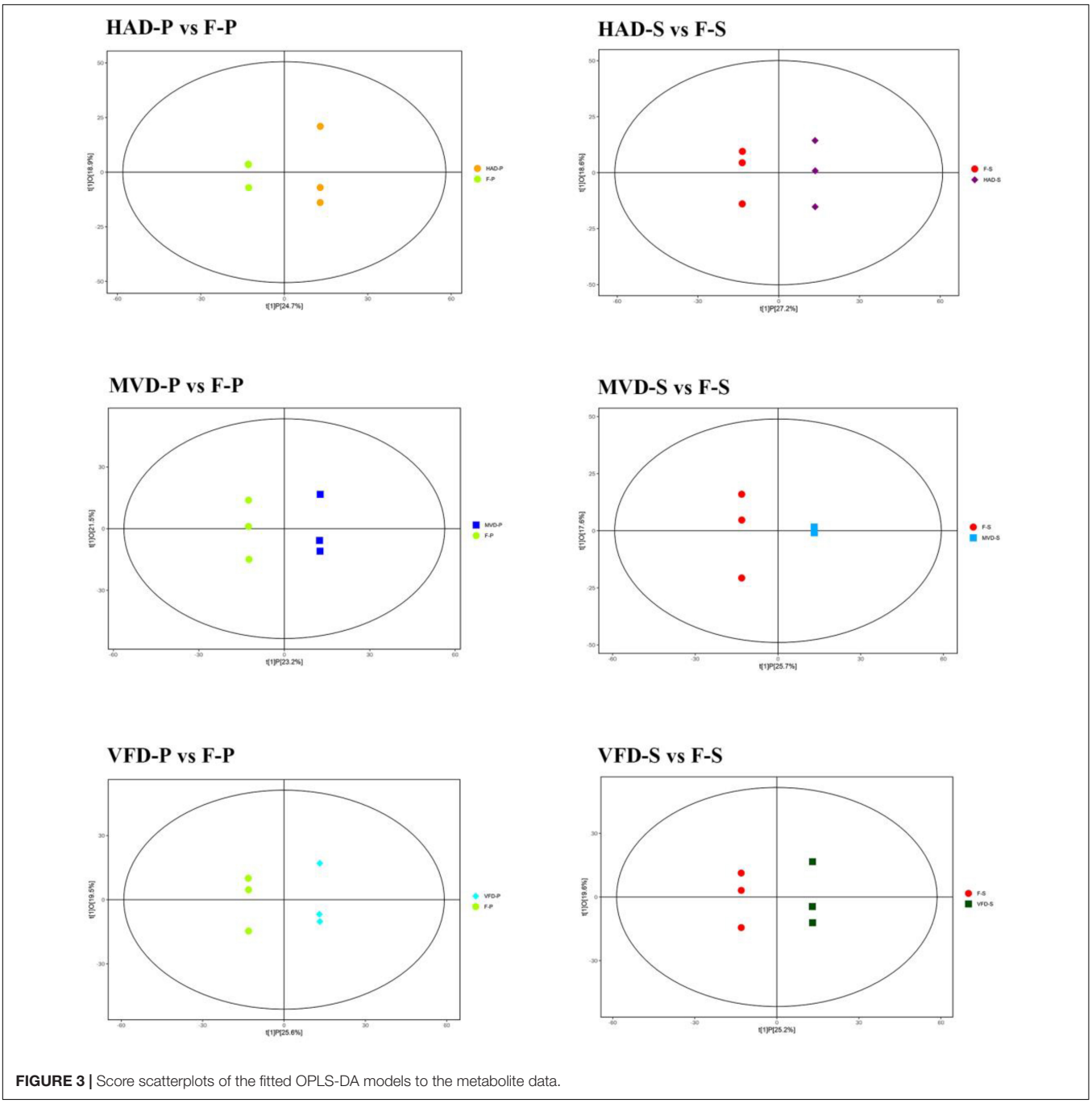

FIGURE 3 | Score scatterplots of the fitted OPLS-DA models to the metabolite data.

time it would also produce more bitter amino acids. Among the latter, 4-guanidinobutyric acid (GABA) has been reported in other research (23).

Nucleotides and Their Derivatives

Besides umami acids, the nucleotides in edible fungi also greatly influence their taste (26). Through research on fresh and dried stipe and pileus samples, we uncovered 25 nucleotides and their derivatives (**Figure 2B**). Among the three drying methods, after HAD the total content of nucleotides and their derivatives were highest by, even higher than those of fresh stipe and pileus samples of *S. rugosoannulata*. This result is not unlike that of a previously published study (18) and may be explained by thermal decomposition and enzymatic hydrolysis of ribonucleic acids or deoxyribonucleic acids during the hot air drying process (25).

Organic Acids and Their Derivatives

Organic acids impart sourness and astringency independently, hence they also contribute to edible fungi's complex and unique taste (27, 28). By determining the metabolites in *S. rugosoannulata*, eight kinds of organic acids and their derivatives were found. Unlike for its amino acids and

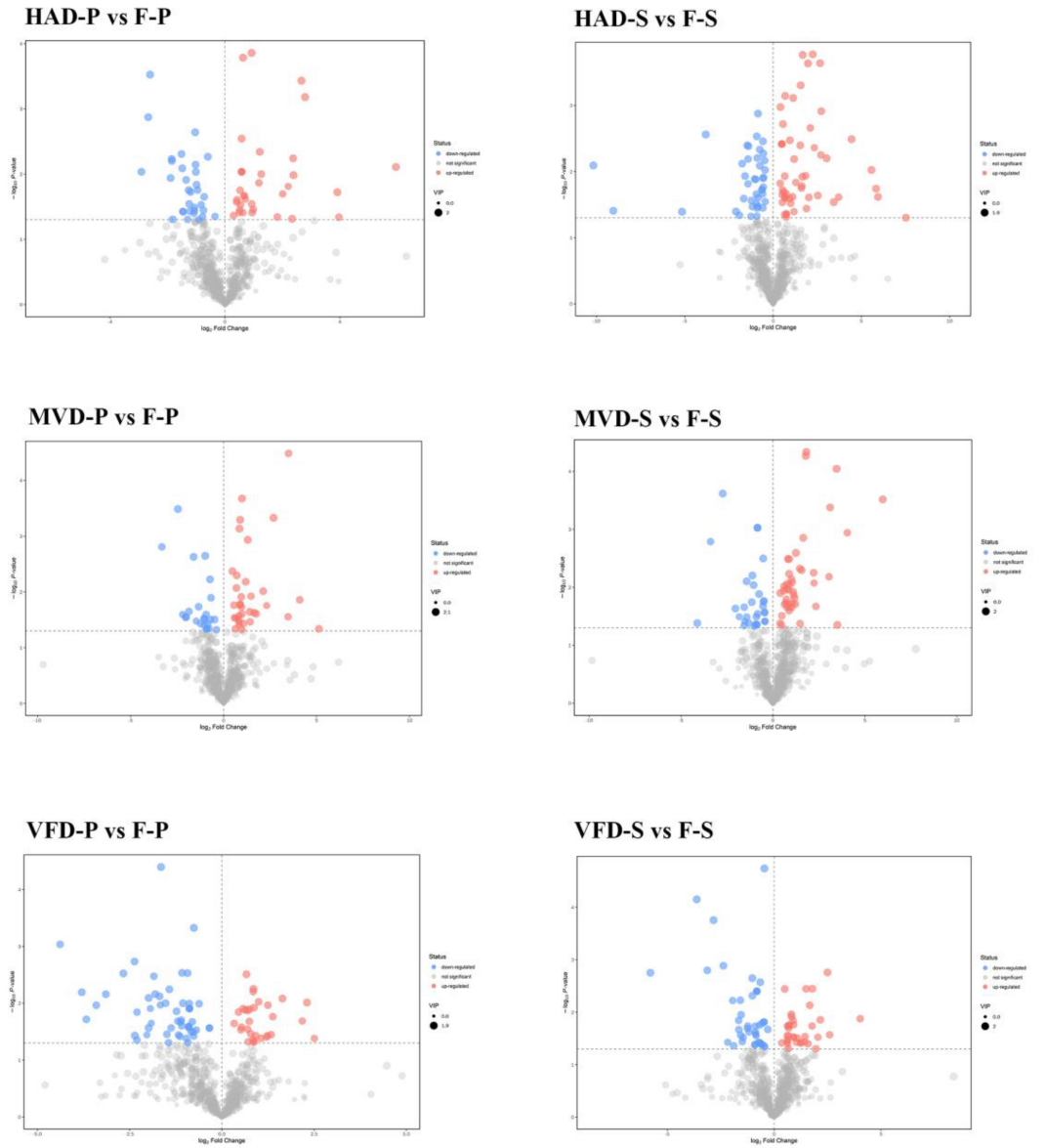

FIGURE 4 | Volcano plots of differential metabolites in different comparison samples.

nucleotides, the total amount of organic acids in the stipe and pileus was greatest after their MVD in comparison with the other treatments, showing this trend in rank: MVD > HAD > F > VFD.

Carbohydrates and Their Derivatives

Research has shown that sugars can produce sweetness and are the main ingredient that determines the taste of edible fungi (29). Here, eight carbohydrates and their derivatives, chiefly alpha-D-glucose, glucose 6-phosphate, D-maltose, L-gulose sucrose, were found (**Figure 2D**). The total content carbohydrates in VFD exceeded those in MVD, perhaps due to the Maillard reaction which may affect the carbohydrate content (30). But given that we found a higher carbohydrate content in HAD, this could instead be attributable to the increased dry matter content after HAD.

Screening and Analysis of Differential Metabolites

To better understand the effect of each drying method upon the metabolism of *S. rugosoannulata*, the orthogonal partial least squares discriminant analysis (OPLS-DA) model was used to compare the metabolic characteristics of different samples. The OPLS-DA scatterplot scores of HAD-S vs. F-S, VFD-S vs. F-S, MVD-S vs. F-S, HAD-P vs. F-P, VFD-P vs. F-P, MVD-P vs. F-P comparison groups are shown in **Figure 3**. These results show that all the samples were within the 95% confidence interval

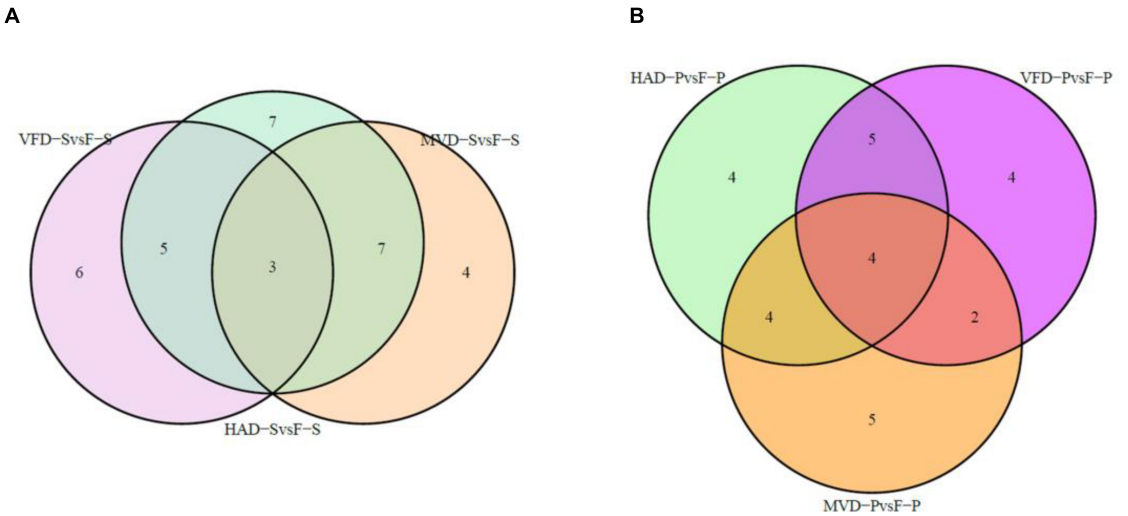

FIGURE 5 | Venn diagrams of overlapping and unique non-volatile taste metabolites screened for differential expression. In panels **(A,B)** are the comparisons in stipe and pileus, respectively.

(Hotelling's T-squared ellipse), suggesting that HAD, VFD, and MVD are all significantly different from fresh *S. rugosoannulata*.

The analysis of Volcano plots was further applied to visualize the differences in the metabolites. In these plots, each point represents a metabolite and the scattered dots represent the VIP (Variable Importance in the Projection) values of the fitted OPLS-DA model. Scattered colors represent the final screening results, with significantly up-regulated (UR) metabolites in red, significantly down-regulated (DR) metabolites in blue, and non-significantly different metabolites in gray. Significant differential metabolites were designated according to the criterion of VIP ≥ 1 and $P < 0.05$. In the pairwise comparisons (**Figure 4**), 94 metabolites in HAD-S vs. F-S (53 UP and 41 DR), 78 metabolites in VFD-S vs. F-S (35 UP and 43 DR), 75 metabolites in MVD-S vs. F-S (44 UP and 31 DR), 66 metabolites in HAD-P vs. F-P (35 UP and 31 DR), 84 metabolites in VFD-P vs. F-P (31 UP and 53 DR), 59 metabolites in MVD-P vs. F-P (35 UP and 24 DR) were designated as significantly differentiated. Whether in the stipe or pileus, the quantity of significant differential metabolites in the MVD vs. F group was lower than that in the HAD vs. F group or VFD vs. F group; hence, the influence on metabolites from microwave vacuum drying is lower than that from the hot air drying and vacuum freeze drying methods.

In order to further understand the impact of drying on flavor, we classified and compared the non-volatile flavor differential metabolites, including amino acid and derivatives, nucleotide and its derivatives, and organic acids and carbohydrates, produced under the different drying processes of *S. rugosoannulata*. **Figure 5** illustrates that HAD-S vs. F-S and HAD-P vs. F-P respectively had 22 and 17 differential non-volatile taste metabolites, VFD-S vs. F-S and VFD-P vs. F-P respectively had 14 and 15 non-volatile taste differential metabolites, as did MVD-S vs. F-S and MVD-P vs. F-P. This indicated HAD induced more non-volatile flavor changes than did VFD and MVD. Notably, there was some overlap occurring among non-volatile flavor differential metabolites in those comparison groups. As seen in **Table 1**, after comparing the fresh and dried edible fungi, the main changes in their non-volatile flavor differential metabolites are amino acids and their derivatives, some of which are up-regulated while others are down-regulated. Results from earlier studies have suggested that the reason for irregular changes in amino acid content with drying time is that the degradation and synthesis of amino acids both occur throughout the drying process (31). In the HAD-S vs. F-S group and HAD-P vs. F-P group, evidently over half of the differentially metabolized amino acids and their derivatives were up-regulated. Yet in the VFD-S vs. F-S group and VFD-P vs. F-P group, less than one third of the differentially metabolized amino acids and their derivatives were up-regulated. For example, L-isoleucine, L-norleucine, and L-proline were up-regulated in both HAD-S vs. F-S and HAD-P vs. F-P groups, but down-regulated in the VFD-S vs. F-S and VFD-P vs. F-P groups. This suggests high temperatures promote protein degradation, consistent with the findings of Ai et al. (32). Although there were only five and four differentially metabolized amino acids and their derivatives in the MVD-S vs. F-S group and MVD-P vs. F-P group, the numbers of them up-regulated and down-regulated was relatively uniform. The same pattern was found for differential metabolites of nucleotide and its derivatives, organic acids and carbohydrates, most of them being up-regulated in HAD-S vs. F-S, HAD-P vs. F-P, MVD-S vs. F-S, and MVD-P vs. F-P groups yet often down-regulated in the VFD-S vs. F-S and VFD-P vs. F-P groups. For instance, adenine, cordycepin, 5-aminolevulinate, and D-xylulose were up-regulated in HAD-S vs. F-S, HAD-P vs. F-P, MVD-S vs. F-S, and MVD-P vs. F-P groups, but in VFD-S vs. F-S and VFD-P vs. F-P groups they were either down-regulated or showed no significant difference.

These results indicated that the non-volatile flavor compounds of *S. rugosoannulata* underwent conversion during the different

TABLE 1 | Statistics for the differentially accumulated amino acid and derivatives, nucleotides and derivatives, carbohydrates, and organic acids during the different drying methods.

Class	Metabolites	HAD-S vs F-S				VFD-S vs F-S				MVD-S vs F-S				HAD-Pvs F-P				VFD-P vs F-P				MVD-P vs F-P			
		VIP	*p*	FC	Type	VIP	*p*	FC	Type	VIP	*p*	FC	Type	VIP	*p*	FC	Type	VIP	*p*	FC	Type	VIP	*p*	FC	Type
Amino acid and derivatives	2-Aminoisobutyric acid																	1.87	0.00	1.59	Up	2.01	0.00	1.81	Up
	4-Aminobutyric acid													1.04	0.10	2.21	Up					1.29	0.02	4.98	Up
	5-Aminovaleric acid					1.83	0.00	0.49	Down									1.76	0.02	0.47	Down				
	5-Oxoproline	1.77	0.01	0.73	Down																				
	Allysine(6-Oxo DL-Norleucine)																	1.78	0.01	1.37	Up				
	CYS-GLY;Cysteinyl glycine	1.90	0.04	0.03	Down					1.88	0.04	0.06	Down												
	DL-Norvaline	1.70	0.02	1.32	Up					1.63	0.04	1.37	Up												
	Glutathione oxidized													1.90	0.00	0.16	Down	1.32	0.01	0.26	Down				
	Guanidineacetic acid																	1.68	0.02	0.47	Down				
	Isoleucine	1.82	0.00	1.41	Up	1.88	0.00	0.57	Down					1.82	0.01	1.50	Up	1.83	0.01	0.54	Down				
	L-Aspartic acid	1.75	0.01	0.67	Down					1.70	0.03	0.73	Down	1.91	0.01	0.28	Down	1.81	0.01	1.81	Up	2.04	0.03	0.25	Down
	L-Glutamic acid					1.79	0.02	0.72	Down																
	L-Isoleucine; L-Leucine	1.82	0.00	1.41	Up	1.88	0.00	0.57	Down					1.82	0.01	1.50	Up	1.83	0.01	0.54	Down				
	L-Lysine; L-Glutamine	1.64	0.03	0.73	Down																				
	L-Norleucine	1.82	0.00	1.41	Up	1.88	0.00	0.57	Down					1.82	0.01	1.50	Up	1.83	0.01	0.54	Down				
	L-Pipecolic acid	1.72	0.02	0.65	Down					1.68	0.04	0.74	Down												
	L-Serine					1.78	0.04	0.67	Down									1.71	0.03	0.79	Down				
	L-Valine									1.65	0.04	1.31	Up												
	N,N-Dimethylglycine																	1.75	0.01	1.49	Up	1.89	0.01	1.62	Up
	Proline; L-Proline	1.65	0.03	1.60	Up	1.72	0.04	0.63	Down					1.72	0.02	1.59	Up	1.78	0.03	0.54	Down				
	S-Adenosyl-methionine	1.92	0.01	0.00	Down																				
Nucleotide and its derivates	5′-Deoxyadenosine									1.76	0.00	8.62	Up												
	5′-S-Methyl-5′-thioadenosine													1.88	0.01	62.00	Up								

(Continued)

TABLE 1 | (Continued)

Class	Metabolites	HAD-S vs F-S				VFD-S vs F-S				MVD-S vs F-S				HAD-Pvs F-P				VFD-P vs F-P				MVD-P vs F-P			
		VIP	*p*	FC	Type	VIP	*p*	FC	Type	VIP	*p*	FC	Type	VIP	*p*	FC	Type	VIP	*p*	FC	Type	VIP	*p*	FC	Type
	Adenine	1.79	0.01	3.15	Up					1.70	0.02	2.33	Up	2.00	0.00	6.34	Up	1.67	0.03	0.59	Down	1.92	0.02	3.12	Up
	Adenosine					1.57	0.03	4.13	Up																
	Adenosine 5′-monophosphate													1.54	0.04	0.47	Down								
	beta-Nicotinamide mononucleotide	1.86	0.04	0.23	Down									1.82	0.03	0.42	Down					1.86	0.04	0.49	Down
	Cordycepin	1.91	0.01	8.18	Up	1.90	0.00	0.19	Down	1.95	0.00	3.46	Up	1.86	0.00	2.32	Up	1.57	0.01	0.20	Down	1.72	0.04	1.80	Up
	Cytidine	1.91	0.00	3.92	Up									1.73	0.03	1.91	Up					1.96	0.00	2.46	Up
	Cytidine 5′-monophosphate (Cytidylic acid)	1.79	0.02	61.35	Up					1.85	0.00	62.75	Up									1.75	0.01	17.11	Up
	Cytosine	1.70	0.01	6.53	Up									1.52	0.02	4.03	Up								
	Guanosine					1.75	0.04	0.27	Down																
	Guanosine 3′,5′-cyclic monophosphate	1.80	0.02	57.07	Up																				
	Pseudouridine																					1.70	0.00	0.10	Down
	Uridine 5′-diphospho-D-glucose;UDP-D-galactose; Uridine diphosphategalactose	1.68	0.01	0.37	Down					1.71	0.02	0.69	Down	1.97	0.02	0.42	Down	1.70	0.03	1.45	Up	1.97	0.00	0.33	Down
	Uridine 5′-monophosphate									1.59	0.00	16.52	Up									1.76	0.00	11.26	Up
	Xanthosine													1.96	0.02	15.09	Up					1.92	0.01	4.37	Up
Organic acids	2-Hydroxybutanoic acid	1.78	0.01	1.58	Up					1.89	0.01	1.84	Up	1.67	0.04	1.43	Up								
	5-Aminolevulinate	1.87	0.00	1.61	Up	1.68	0.02	0.62	Down	1.83	0.01	1.49	Up	1.77	0.03	1.46	Up					1.94	0.00	1.39	Up
	Phosphoric acid	1.73	0.02	1.44	Up	1.91	0.00	1.41	Up	1.91	0.00	1.83	Up												
Carbohydrates	D-Xylulose																	1.91	0.03	0.54	Down				
	Sucrose	1.42	0.10	3.50	Up																				

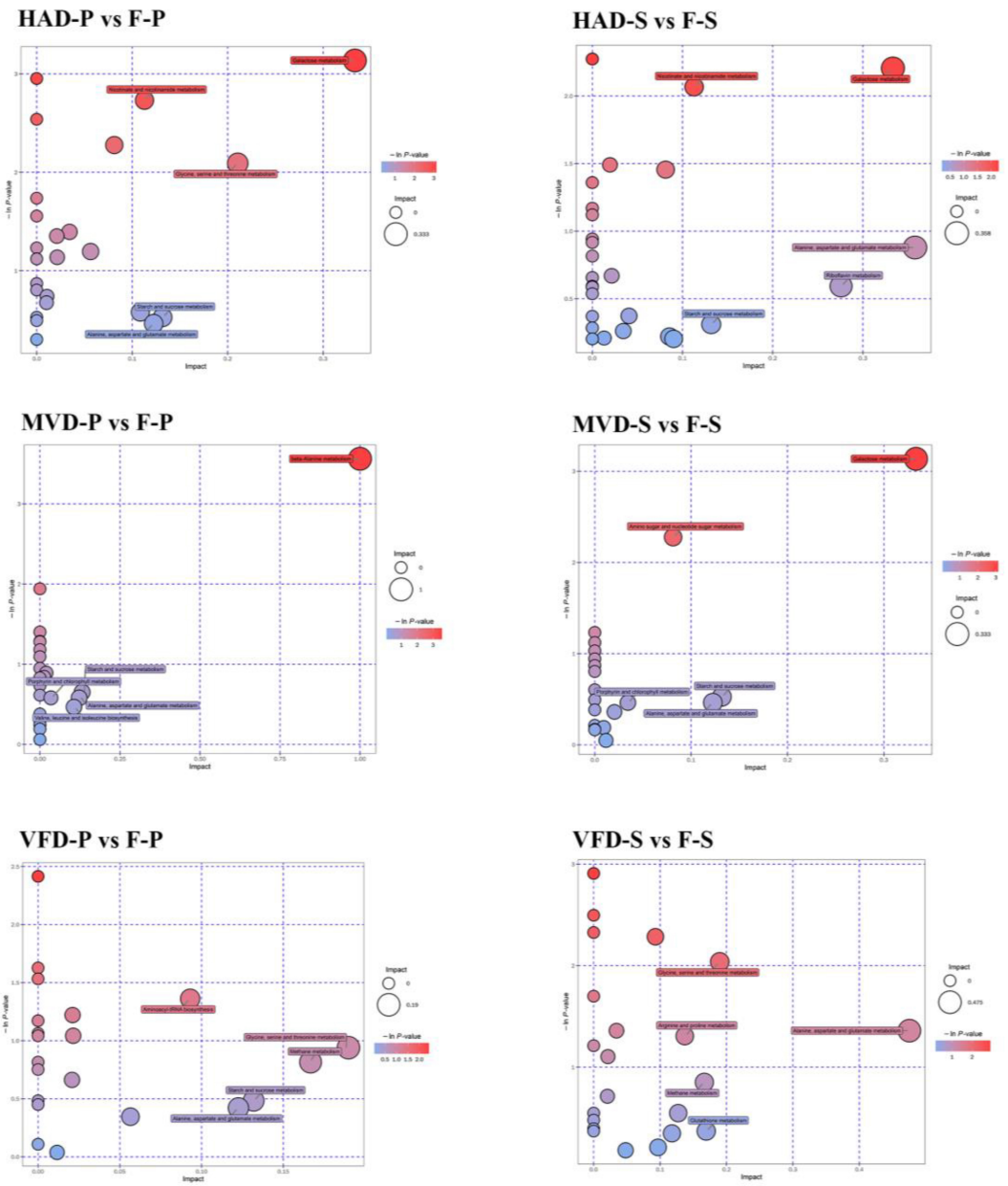

FIGURE 6 | Metabolic enrichment pathway analysis.

drying methods, especially in terms of differentially metabolized amino acids and nucleotides. Therefore, the non-volatile flavor of *S. rugosoannulata* after drying was probably related to the metabolism of amino acids and nucleotides. Sun et al. (7) argued that the umami taste of edible mushrooms is closely related to amino acid metabolism, nucleotide metabolism, and the Maillard reaction. Many umami amino acids and 5'-nucleotides in mushroom were investigated in numerous studies (25). This article not only focuses on these common non-volatile flavor substances, but also inferred the effects of related metabolites and derivatives, which is beneficial for comprehensively understanding the mechanism by a given drying method alters the metabolism of flavor-determining substances.

Enrichment Analysis and KEGG Pathway Analysis of the Differential Metabolites

Other researchers explored the main metabolic pathways of volatile flavor compounds in *shiitake* mushrooms through KEGG enrichment analysis: these being histidine metabolism, glutathione metabolism, and unsaturated fatty acid biosynthesis (33). However, only a few studies have investigated non-volatile flavors in mushrooms by conducting a widely targeted

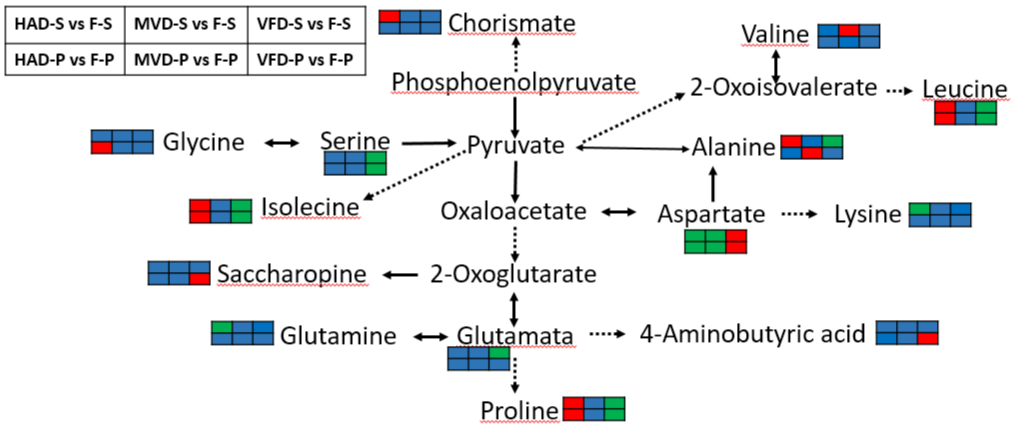

FIGURE 7 | Biosynthesis of amino acids. (The red color rectangle indicates that the metabolite content is significantly up-regulated; the green rectangle indicates that the metabolite content is significantly down-regulated; the blue rectangle indicates no significant difference in that metabolite content).

metabolomics analysis. In this study, the differential metabolites in fresh and dried samples were mapped to KEGG, PubChem, and HMDB online databases, and their enrichment results are shown in **Figure 6**. In it, metabolic pathway analyses are presented in bubble charts, in which each bubble denotes a metabolic pathway: the larger the bubble size, the greater the impact factor (based on a topological analysis); the darker the color, the smaller the *p*-value (enrichment analysis), and the more significant the degree of enrichment for that pathway.

The pathways of differential metabolites in the groups HAD-S and F-S were mainly concentrated in galactose metabolism; nicotinate and nicotinamide metabolism; alanine, aspartate, and glutamate metabolism; riboflavin metabolism; starch and sucrose metabolism. Those of the differential metabolites in the groups VFD-S and F-S were consisted chiefly of glycine, serine, and threonine metabolism; arginine and proline metabolism; alanine, aspartate, and glutamate metabolism; methane metabolism; glutathione metabolism. The pathways of differential metabolites in the groups MVD-S and F-S primarily comprised galactose metabolism; amino sugar and nucleotide sugar metabolism; starch and sucrose metabolism; porphyrin and chlorophyll metabolism; alanine, aspartate, and glutamate metabolism. Evidently, different drying methods can lead to disparate enrichment levels, whose difference also presented in the pileus. In this respect, pathway analysis revealed the enrichment in groups HAD-P and F-P being concentrated in galactose metabolism; nicotinate and nicotinamide metabolism; glycine, serine, and threonine metabolism; starch and sucrose metabolism; alanine, aspartate, and glutamate metabolism. By contrast, the metabolic pathways of differential metabolites in groups VFD-P and F-P mainly included aminoacyl-tRNA biosynthesis; glycine, serine, and threonine metabolism; methane metabolism; starch and sucrose metabolism; alanine, aspartate, and glutamate metabolism. The pathways of differential metabolites in groups MVD-P and F-P were principally involved in beta-alanine metabolism; starch and sucrose metabolism; porphyrin and chlorophyll metabolism; alanine, aspartate, and glutamate metabolism; valine, leucine, and isoleucine biosynthesis. Further, some metabolic pathways overlapped in these comparison groups, but their divergent enrichment levels provided compelling evidence that different modes of drying can produce differentially exclusive metabolites. Those changes in metabolic levels could be used to understand the impact of drying methods on *S. rugosoannulata*.

Although the drying method differs, we can see that amino acid metabolism was the main metabolic pathway affected in all treatments. To gain insight into the effects of drying methods on amino acid metabolism in *S. rugosoannulata,* see **Figure 7** based on the results from the KEGG annotation and enrichment analysis. Alanine, aspartate, and glutamate metabolism is clearly the common major metabolic pathway impacted by drying the stipe *via* hot air, freezing, or microwaves. Almost all amino acids take part in transamination reactions with pyruvate, oxaloacetate, or α-ketoglutarate to product alanine, aspartate, or glutamate, respectively (34). In addition, aspartate, glutamate, and alanine exert a great influence on both umami and sweetness of mushroom. **Figure 7** verified that drying, especially by hot air, substantially impacts the flavor amino acids of *S. rugosoannulata* at the metabolic level. Under the action of amino acid metabolism, proline, leucine, and isolecine in the groups HAD-S vs. F-S and HAD-P vs. F-P were all up-regulated.

4-Guanidinobutyric acid has the physiological effects of improving the body's sleep quality (35) and reducing blood pressure (36), had also been transformed in alanine, aspartate and glutamate metabolism. Notably, we found GABA up-regulated in groups VFD-P vs. F-P. It is known that GABA is a metabolic response to environmental stresses, for instance heat, cold and drought (37). Freeze-drying conditions could have up-regulated GABA in the pileus of *S. rugosoannulata*, probably due to glutamate being catalyzed by glutamate decarboxylase (EC:4.1.1.15) into GABA.

In the groups VFD-S vs. F-S and VFD-P vs. F-P, the common major metabolic pathway was that of glycine, serine, and threonine metabolism. Compared with hot air drying and microwave drying, the freeze drying mode has a greater impact on the metabolism of serine, and aspartate, which are the sweet

and umami components in the un-volatile flavor profile of mushrooms. Serine was down-regulated in groups VFD-S vs. F-S and VFD-P vs. F-P, perhaps because its synthesis rate is slowed in a low-temperature drying condition. Li et al. (14) found that temperature could alter the rate of protein degradation into amino acids in *Pleurotus eryngii*. Therefore, it may be that the enzymatic reaction related to serine production is impaired and limited by freeze-drying, while the high temperature of hot air drying promotes protein degradation. Still, we did find several down-regulated metabolites after HAD, such as aspartate and lysine. The Maillard reaction is considered the paramount non-enzymatic reaction in the late stage of drying (38), one which could use amino acids to react with sugars. Moreover, the loss of moisture after drying can promote the Strecker degradation that would convert an amino acid into an aldehyde containing the side chain (39). MVD caused changes in starch and sucrose metabolism of *S. rugosoannulata*, which suggests microwave drying can elicit changes to sugar flavor substances. Nevertheless, because of the complicated reactions caused under the three drying methods, a comprehensive evaluation of the non-volatile flavor profile in dried *S. rugosoannulata*, such as its amino acids, nucleotides, organic acids, and soluble sugars, must be further investigated.

CONCLUSION

In this study, a widely targeted metabolomics technology was applied to study the formation mechanism of non-volatile taste components obtained by different drying methods of the mushroom *S. rugosoannulata*. Overall, the results showed that the diversity of metabolites in the samples changed little in response to the three drying methods tested, but their relative content and metabolic pathways were significantly different. Comparing the three modes of drying, HAD is capable of improving both umami and sweetness by increasing the content of related amino acids and nucleotides, but the highest organic acid content is attained using MVD. We found the metabolite differences caused by microwave drying are less pronounced than those of HAD or VFD. Conversion of non-volatile taste compounds mainly occurs *via* the metabolism of amino acids and nucleotides. KEGG pathway analysis revealed that alanine, aspartate, and glutamate metabolism, these having a greater impact on umami, sweetness, and GABA, was the common major metabolic pathway affected after drying the stipe by HAD, VFD, and MVD. This study also shows that the metabolite differences caused by different drying methods are modulated by temperature, especially in that higher temperatures may cause protein degradation, the Strecker reaction, and the Maillard reaction. These findings indicate that in the actual production process, HAD, which is economical, convenient and better at improving the non-volatile taste components, could be given priority as a drying method. This study also advances our understanding of the transformation of nutrients and flavor substances in *S. rugosoannulata* caused by different drying methods. Nonetheless, further research is needed to elucidate the mechanisms underpinning these metabolism and molecular changes. Meanwhile, in order to fully explore the influence of drying methods on the flavor of *S. rugosoannulata*, the volatile flavor substances and other substances that may affect the flavor should also be analyzed qualitatively or quantitatively.

DATA AVAILABILITY STATEMENT

The data presented in the study are deposited in the MetaboLights repository, accession number MTBLS4460 (www.ebi.ac.uk/metabolights/MTBLS4460).

AUTHOR CONTRIBUTIONS

YL: conceptualization, methodology, formal analysis, writing—original draft, and writing—review and editing. FM: data curation and writing—original draft. PT: supervision and writing—review and editing. DH: software and project administration. QL: investigation and validation. ML: supervision, writing—review and editing, funding acquisition, and data curation. All authors contributed to the article and approved the submitted version.

FUNDING

This project was supported by Modern Agricultural Industrial Technology System of Edible Fungi in Guizhou Province, China (GZCYTX2022-05-02) and Guiyang Science and Technology Planning Project ([2020]-18-3).

REFERENCES

1. Yan Q, Huang M, Sun P, Cheng S, Zhang Q, Dai H. Steroids, fatty acids and ceramide from the mushroom *Stropharia rugosoannulata* Farlow apud Murrill. *Biochem Syst Ecol.* (2020) 88:103963. doi: 10.1016/j.bse.2019.103963
2. Hu S, Feng X, Huang W, Ibrahim SA, Liu Y. Effects of drying methods on non-volatile taste components of *Stropharia rugoso-annulata* mushrooms. *LWT-Food Sci Technol.* (2020) 127:109428. doi: 10.1016/j.lwt.2020.109428
3. Song Z, Jia L, Xu F, Meng F, Deng P, Fan K, et al. Characteristics of se-enriched mycelia by *Stropharia rugoso-annulata* and its antioxidant activities *in vivo*. *Biol Trace Element Res.* (2009) 131:81–9. doi: 10.1007/s12011-009-8343-8
4. He P, Geng L, Wang J, Xu C. Production, purfication, molecular characterization and bioactivities of exopolysaccharides produced by the wine cap culinary-medicinal mushroom, *Stropharia rugosoannulata* 2(#) (Higher Basidiomycetes). *Int J Med Mushrooms.* (2012) 14:365–76. doi: 10.1615/IntJMedMushr.v14.i4.40
5. Zhai X, Zhao A, Geng L, Xu C. Fermentation characteristics and hypoglycemic activity of an exopolysaccharide produced by submerged culture of *Stropharia rugosoannulata* #2. *Ann Microbiol.* (2013) 63:1013–20. doi: 10.1007/s13213-012-0555-z
6. Zhang W, Tian G, Geng X, Zhao Y, Tzi Bun N, Zhao L, et al. Isolation and characterization of a novel lectin from the edible mushroom *Stropharia rugosoannulata*. *Molecules.* (2014) 19:19880–91. doi: 10.3390/molecules191219880

7. Sun L, Zhang Z, Xin G, Sun B, Bao X, Wei Y, et al. Advances in umami taste and aroma of edible mushrooms. *Trends Food Sci Technol.* (2020) 96:176–87. doi: 10.1016/j.tifs.2019.12.018
8. Singh P, Langowski HC, Wani AA, Saengerlaub S. Recent advances in extending the shelf life of fresh *Agaricus* mushrooms: a review. *J Sci Food Agric.* (2010) 90:1393–402. doi: 10.1002/jsfa.3971
9. Pei F, Shi Y, Gao X, Wu F, Mariga AM, Yang W, et al. Changes in non-volatile taste components of button mushroom (*Agaricus bisporus*) during different stages of freeze drying and freeze drying combined with microwave vacuum drying. *Food Chem.* (2014) 165:547–54. doi: 10.1016/j.foodchem.2014.05.130
10. Tian Y, Zhao Y, Huang J, Zeng H, Zheng B. Effects of different drying methods on the product quality and volatile compounds of whole shiitake mushrooms. *Food Chem.* (2016) 197:714–22. doi: 10.1016/j.foodchem.2015.11.029
11. Ratseewo J, Meeso N, Siriamornpun S. Changes in amino acids and bioactive compounds of pigmented rice as affected by far-infrared radiation and hot air drying. *Food Chem.* (2020) 306:125644. doi: 10.1016/j.foodchem.2019.125644
12. Das I, Arora A. Alternate microwave and convective hot air application for rapid mushroom drying. *J Food Eng.* (2018) 223:208–19. doi: 10.1016/j.jfoodeng.2017.10.018
13. Politowicz J, Lech K, Sanchez-Rodriguez L, Figiel A, Szumny A, Grubor M, et al. Volatile composition and sensory profile of oyster mushroom as affected by drying method. *Drying Technol.* (2018) 36:685–96. doi: 10.1080/07373937.2016.1274903
14. Li X, Feng T, Zhou F, Zhou S, Liu Y, Li W, et al. Effects of drying methods on the tasty compounds of *Pleurotus eryngii*. *Food Chem.* (2015) 166:358–64. doi: 10.1016/j.foodchem.2014.06.049
15. Hou H, Liu C, Lu X, Fang D, Hu Q, Zhang Y, et al. Characterization of flavor frame in shiitake mushrooms (*Lentinula edodes*) detected by HS-GC-IMS coupled with electronic tongue and sensory analysis: influence of drying techniques. *LWT-Food Sci Technol.* (2021) 146:111402. doi: 10.1016/j.lwt.2021.111402
16. Zhou L, Li W, Pan W, Hussain S, Wang Y, Guo W, et al. Effects of thermal processing on nutritional characteristics and non-volatile flavor components from *Tricholoma lobayense*. *Emirates J Food Agric.* (2017) 29:285–92. doi: 10.9755/ejfa.2016-12-1815
17. Kompany E, Rene F. A note on the freeze-drying conditions for improced aroma retention in cultivated in mushrooms (*Agaticus-bisporus*). *LWT Food Sci Technol.* (1995) 28:238–40. doi: 10.1016/s0023-6438(95)91632-6
18. Luo D, Wu J, Ma Z, Tang P, Liao X, Lao F. Production of high sensory quality Shiitake mushroom (*Lentinus edodes*) by pulsed air-impingement jet drying (AID) technique. *Food Chem.* (2021) 341:128290. doi: 10.1016/j.foodchem.2020.128290
19. Wang H, Zhang M, Adhikari B. Drying of shiitake mushroom by combining freeze-drying and mid-infrared radiation. *Food Bioprod Process.* (2015) 94:507–17. doi: 10.1016/j.fbp.2014.07.008
20. Pei F, Yang W, Shi Y, Sun Y, Mariga AM, Zhao L, et al. Comparison of freeze-drying with three different combinations of drying methods and their influence on colour, texture, microstructure and nutrient retention of button mushroom (*Agaricus bisporus*) slices. *Food Bioprocess Technol.* (2014) 7:702–10. doi: 10.1007/s11947-013-1058-z
21. Fan F, Huang C, Tong Y, Guo H, Zhou S, Ye J, et al. Widely targeted metabolomics analysis of white peony teas with different storage time and association with sensory attributes. *Food Chem.* (2021) 362:130257. doi: 10.1016/j.foodchem.2021.130257
22. Wang H, Hua J, Yu Q, Li J, Wang J, Deng Y, et al. Widely targeted metabolomic analysis reveals dynamic changes in non-volatile and volatile metabolites during green tea processing. *Food Chem.* (2021) 363:130131–130131. doi: 10.1016/j.foodchem.2021.130131
23. Li J, Wu H, Wang L, Huang Y, Wang L. Key taste components in two wild edible Boletus mushrooms using widely targeted metabolomics. *Biochem Syst Ecol.* (2021) 96:104268. doi: 10.1016/j.bse.2021.104268
24. Yamaguchi S, Yoshikawa T, Ikeda S, Ninomiya T. Measurement of relative taste intensity of some L-alpha-amino acids and 5'-nucleotides. *J Food Sci.* (1971) 36:846–9. doi: 10.1111/j.1365-2621.1971.tb15541.x
25. Zhang Y, Venkitasamy C, Pan Z, Wang W. Recent developments on umami ingredients of edible mushrooms – A review. *Trends Food Sci Technol.* (2013) 33:78–92. doi: 10.1016/j.tifs.2013.08.002
26. Liuqing W, Qiuhui H, Fei P, Alfred Mugambi M, Wenjian Y. Influence of different storage conditions on physical and sensory properties of freeze-dried Agaricus bisporus slices. *LWT.* (2018) 97:164–71. doi: 10.1016/j.lwt.2018.06.052
27. Litchfield JH. Morel mushroom mycelium as a food-flavoring material. *Biotechnol Bioeng.* (1967) 9:289–304. doi: 10.1002/bit.260090303
28. Li B, Liu C, Fang D, Yuan B, Hu Q, Zhao L. Effect of boiling time on the contents of flavor and taste in *Lentinus edodes*. *Flavour Fragr J.* (2019) 34:506–13. doi: 10.1002/ffj.3532
29. Tsai SY, Tsai HL, Mau JL. Non-volatile taste components of *Agaricus blazei*, *Agrocybe cylindracea* and *Boletus edulis*. *Food Chem.* (2008) 107:977–83. doi: 10.1016/j.foodchem.2007.07.080
30. Jousse F, Jongen T, Agterof W, Russell S, Braat P. Simplified kinetic scheme of flavor formation by the Maillard reaction. *J Food Sci.* (2002) 67:2534–42. doi: 10.1111/j.1365-2621.2002.tb08772.x
31. Li W, Li R, Chen W, Feng J, Wu D, Zhang Z, et al. The anabolism of sulphur aroma volatiles responds to enzymatic and non-enzymatic reactions during the drying process of shiitake mushrooms. *Food Chem.* (2022) 371:131123. doi: 10.1016/j.foodchem.2021.131123
32. Ai Z, Zhang Y, Li X, Sun W, Liu Y. Widely targeted metabolomics analysis to reveal transformation mechanism of *Cistanche deserticola* active compounds during steaming and drying processes. *Front Nutr.* (2021) 8:742511. doi: 10.3389/fnut.2021.742511
33. Li W, Chen W, Wang J, Feng J, Wu D, Zhang Z, et al. Screening candidate genes related to volatile synthesis in shiitake mushrooms and construction of regulatory networks to effectively improve mushroom aroma. *J Sci Food Agric.* (2021) 101:5618–26. doi: 10.1002/jsfa.11213
34. Blanco A, Blanco G. Chapter 16 - Amino acid metabolism. In: Blanco A, Blanco G editors. *Medical Biochemistry*. Cambridge, MA: Academic Press (2017). p. 367–99.
35. Gottesmann C. GABA mechanisms and sleep. *Neuroscience.* (2002) 111:231–9. doi: 10.1016/S0306-4522(02)00034-9
36. Inoue K, Shirai T, Ochiai H, Kasao M, Hayakawa K, Kimura M, et al. Blood-pressure-lowering effect of a novel fermented milk containing gamma-aminobutyric acid (GABA) in mild hypertensives. *Eur J Clin Nutr.* (2003) 57:490–5. doi: 10.1038/sj.ejcn.1601555
37. Tian X, Wu X, Zhang S, Lou C. Functions of gamma-aminobutyric acid in higher plant responses to stress. [gamma-氨基丁酸在高等植物逆境反应中的作用]. *Life Sci.* (2002) 14:215–9.
38. Jiang W, Chen Y, He X, Hu S, Li S, Liu Y. A study of the tyramine/glucose Maillard reaction: variables, characterization, cytotoxicity and preliminary application. *Food Chem.* (2018) 239:377–84. doi: 10.1016/j.foodchem.2017.06.085
39. Schmidberger PC, Schieberle P. Changes in the key aroma compounds of raw Shiitake mushrooms (*Lentinula edodes*) induced by pan-frying as well as by rehydration of dry mushrooms. *J Agric Food Chem.* (2020) 68:4493–506. doi: 10.1021/acs.jafc.0c01101

Conflict of Interest: YL and ML were employed by Guizhou Characteristic Food Technology Co., Ltd.

The remaining authors declare that the research was conducted in the absence of any commercial or financial relationships that could be construed as a potential conflict of interest.

Advantages of publishing in Frontiers

OPEN ACCESS
Articles are free to read for greatest visibility and readership

FAST PUBLICATION
Around 90 days from submission to decision

HIGH QUALITY PEER-REVIEW
Rigorous, collaborative, and constructive peer-review

TRANSPARENT PEER-REVIEW
Editors and reviewers acknowledged by name on published articles

Frontiers
Avenue du Tribunal-Fédéral 34
1005 Lausanne | Switzerland

Visit us: www.frontiersin.org
Contact us: frontiersin.org/about/contact

REPRODUCIBILITY OF RESEARCH
Support open data and methods to enhance research reproducibility

DIGITAL PUBLISHING
Articles designed for optimal readership across devices

FOLLOW US
@frontiersin

IMPACT METRICS
Advanced article metrics track visibility across digital media

EXTENSIVE PROMOTION
Marketing and promotion of impactful research

LOOP RESEARCH NETWORK
Our network increases your article's readership